

GAS FLOW IN COMPACTED CLAYS

by

KRISTA SOPHIA GELMICH HALAYKO

A Thesis

**Submitted to the Faculty of Graduate Studies
in Partial Fulfillment of the Requirements for the Degree of**

MASTER OF SCIENCE

**Department of Civil and Geological Engineering
University of Manitoba**

Winnipeg, Manitoba

© September, 1998



National Library
of Canada

Acquisitions and
Bibliographic Services

395 Wellington Street
Ottawa ON K1A 0N4
Canada

Bibliothèque nationale
du Canada

Acquisitions et
services bibliographiques

395, rue Wellington
Ottawa ON K1A 0N4
Canada

Your file *Votre référence*

Our file *Notre référence*

The author has granted a non-exclusive licence allowing the National Library of Canada to reproduce, loan, distribute or sell copies of this thesis in microform, paper or electronic formats.

The author retains ownership of the copyright in this thesis. Neither the thesis nor substantial extracts from it may be printed or otherwise reproduced without the author's permission.

L'auteur a accordé une licence non exclusive permettant à la Bibliothèque nationale du Canada de reproduire, prêter, distribuer ou vendre des copies de cette thèse sous la forme de microfiche/film, de reproduction sur papier ou sur format électronique.

L'auteur conserve la propriété du droit d'auteur qui protège cette thèse. Ni la thèse ni des extraits substantiels de celle-ci ne doivent être imprimés ou autrement reproduits sans son autorisation.

0-612-32123-1

**THE UNIVERSITY OF MANITOBA
FACULTY OF GRADUATE STUDIES

COPYRIGHT PERMISSION PAGE**

GAS FLOW IN COMPACTED CLAYS

BY

KRISTA SOPHIA GELMICH HALAYKO

**A Thesis/Practicum submitted to the Faculty of Graduate Studies of The University
of Manitoba in partial fulfillment of the requirements of the degree**

of

MASTER OF SCIENCE

Krista Sophia Gelmich Halayko ©1998

**Permission has been granted to the Library of The University of Manitoba to lend or sell
copies of this thesis/practicum, to the National Library of Canada to microfilm this thesis
and to lend or sell copies of the film, and to Dissertations Abstracts International to publish
an abstract of this thesis/practicum.**

**The author reserves other publication rights, and neither this thesis/practicum nor
extensive extracts from it may be printed or otherwise reproduced without the author's
written permission.**

ABSTRACT

Compacted clays and clay-sand mixtures are being used increasingly to isolate wastes from the biosphere. Clay buffers are commonly used in landfills and are proposed for use in the Canadian nuclear fuel waste disposal concept. This study will investigate the effect of high gas pressures on gas migration through compacted clay materials.

Illite, illite/sand and bentonite specimens, 50mm in diameter and 24mm thick, were tested in a gas breakthrough apparatus with a capacity of 10 MPa. The inlet pressure was either increased in steps or was held constant. Gas breakthrough was said to occur when a response was noted at the outlet side of the specimen.

In the forty-two illite/sand specimens tested with effective clay dry densities, ρ_c , ranging from 1.30-2.10 Mg/m³, gas breakthrough was found to be between 0.2 and 6.4 MPa. For most of the fifty-six increasing pressure tests on bentonite ($\rho_c = 0.6-1.2$ Mg/m³) however, the upper capacity of the test equipment was reached before gas breakthrough was observed. The increased resistance to gas breakthrough is because of an increased proportion of bound water in bentonite which blocks all but the largest continuous pores. Below a certain degree of saturation, no resistance to gas flow was observed in either clay due to the fact that continuous gas pathways existed. This threshold was $\approx 85\%$ for illite and $\approx 93\%$ for bentonite. Capillary and advection theories were compared with the test data. The advection theories were found to provide a more realistic representation of the real system and an estimate of gas breakthrough pressure within an order of magnitude for increasing pressure tests.

ACKNOWLEDGMENTS

I would like to thank the following people for their assistance:

- My advisor, Dr. Malcolm Gray, for sharing with me his technical expertise, and for his encouragement.
- Dr. James Graham for being so generous with technical and personal advice throughout the course of my studies.
- Dr. Tee Boon Goh, for acting as an examiner of this thesis.

I would like to thank Harold Hume, fellow graduate student, for our many fruitful discussions, and for collaborating with me in our work on bentonite. In addition, I would like to thank T. Kirkham, K. Bannister, and the entire geotechnical group at the University of Manitoba for their assistance along with technical support from N. Piamsalee and K. Majury. The personnel at AECL, namely: D. Dixon, B. Shenton, A. Wan and B. Walker have provided me with technical and academic assistance, for which I am grateful.

The financial support of Natural Sciences and Engineering Research Council and the loan of the apparatus from Atomic Energy of Canada are gratefully acknowledged.

Most importantly, I am grateful to my family and friends who have provided me with encouragement throughout the course of my graduate studies. To my parents, Louise and Emie Gelmich, I am always grateful. Especially important has been the friendship and encouragement of my husband, Larry Halayko, who has never ceased to be patient and understanding throughout the course of my graduate studies.

TABLE OF CONTENTS

ABSTRACT.....	i
ACKNOWLEDGEMENTS	ii
TABLE OF CONTENTS	iii
LIST OF TABLES.....	viii
LIST OF FIGURES.....	ix
LIST OF SYMBOLS	xii
1. INTRODUCTION.....	1
1.1. CANADIAN NUCLEAR FUEL WASTE DISPOSAL CONCEPT	2
1.2. GAS GENERATION.....	3
1.2.1. Consequences of gas generation	4
1.3. OVERVIEW	5
2. LITERATURE REVIEW.....	7
2.1. INTRODUCTION.....	7
2.2. CLAY MINERALOGY	7
2.2.1. Clay minerals.....	7
2.2.1.1. <i>Illite</i>	10
2.2.1.2. <i>Montmorillonite</i>	11
2.2.2. Clay - water interaction.....	11
2.2.2.1. <i>Diffuse double layer models</i>	11
2.2.3. Soil fabric and pore structure	15
2.2.3.1. <i>Soil Fabric</i>	15

2.2.3.2. Pore size distribution	16
2.2.3.3. Effects of pore structure on flow phenomena	17
2.3. MERCURY INTRUSION POROSIMETRY	18
2.3.1. Limitations of mercury intrusion porosimetry testing	19
2.4. FLOW PHENOMENA	21
2.4.1. Capillarity	21
2.4.2. Permeability and hydraulic conductivity	22
2.4.3. Diffusion	27
2.4.4. Flow in soils with non-polar pore fluids	29
2.5. UNSATURATED FLOW	32
2.6. CURRENT STATE OF GAS MIGRATION RESEARCH	36
2.6.1. Current gas migration concepts	42
2.6.2. Outstanding issues in gas migration research	47
3. DEVELOPMENT OF RESEARCH PROGRAM	50
3.1. SCOPE OF RESEARCH	50
3.2. TESTING PROGRAM	51
3.2.1. Illite/sand mixtures	51
3.2.2. Bentonite	52
3.2.3. Bentonite and illite wetted with a non-polar fluid	53
3.2.4. Illite with modified pressure increment	53
4. TEST EQUIPMENT AND PROCEDURES	55
4.1. TEST EQUIPMENT	55
4.1.1. Gas breakthrough equipment	55
4.1.2. Data acquisition	56

4.1.2.1. Calibration of pressure transducers.....	58
4.1.3. Test cell.....	60
4.1.4. Compaction apparatus.....	60
4.2. SOIL MATERIALS.....	60
4.2.1. Illite.....	60
4.2.2. Bentonite.....	61
4.2.3. Sand.....	61
4.3. TEST PROCEDURES.....	62
4.3.1. Soil preparation.....	62
4.3.1.1. Soil-water mixtures.....	62
4.3.1.2. Soil-paraffin mixtures.....	63
4.3.2. Calculation of target parameters.....	64
4.3.3. Specimen preparation.....	66
4.3.4. Saturation procedure.....	67
4.3.5. Gas breakthrough test procedure.....	68
4.3.6. Post-breakthrough procedure.....	69
4.4. MERCURY INTRUSION POROSIMETRY PROCEDURES.....	70
4.4.1. Specimen preparation.....	70
4.4.2. Procedure for mercury intrusion porosimetry tests.....	71
5. TEST RESULTS.....	72
5.1. ILLITE.....	74
5.1.1. Illite/sand mixtures (ISU).....	74
5.1.1.1. Gas breakthrough response.....	75
5.1.1.2. Variations in water content.....	77

5.1.1.3. <i>Repeatability</i>	79
5.2. BENTONITE	80
5.2.1. Wetted (BW)	80
5.2.1.1. <i>Gas breakthrough response</i>	81
5.2.1.2. <i>Variations in water content</i>	82
5.2.1.3. <i>Repeatability</i>	82
5.2.2. Unsaturated (BU)	83
5.2.2.1. <i>Gas breakthrough response</i>	83
5.2.2.2. <i>Variations in water content</i>	85
5.2.2.3. <i>Repeatability</i>	85
5.3. SPECIALIZED TESTS	86
5.3.1. Bentonite and illite with non-polar fluids (NPFU)	86
5.3.2. Illite with modified time increments (ITU)	87
5.3.3. MIP tests on illite (MIP).....	89
6. DISCUSSION	91
6.1. DISCUSSION OF TEST RESULTS	91
6.1.1. Illite/sand mixtures.....	91
6.1.2. Wetted bentonite.....	93
6.1.3. Unsaturated bentonite.....	94
6.2. SYNTHESIS OF TEST RESULTS	95
6.2.1. Flow phenomena.....	95
6.2.1.1. <i>Effect of degree of saturation</i>	97
6.2.2. Illite conceptual model.....	98
6.2.2.1. <i>Pore structure</i>	98

6.2.2.2. <i>Clay - water system</i>	99
6.2.2.3. <i>Conceptual flow model</i>	100
6.2.3. Bentonite conceptual model.....	102
6.2.3.1. <i>Pore structure</i>	102
6.2.3.2. <i>Clay - water system</i>	103
6.2.3.3. <i>Conceptual flow model</i>	104
6.3. NUMERICAL MODELLING	106
6.3.1. Capillarity model.....	107
6.3.1.1. <i>Illite</i>	108
6.3.1.2. <i>Bentonite</i>	109
6.3.2. Advection models.....	111
6.3.2.1. <i>Poiseulle model</i>	111
6.3.2.2. <i>Kozeny-Carman model</i>	114
6.3.3. Summary.....	116
7. CONCLUSIONS AND RECOMMENDATIONS.....	118
7.1. CONCLUSIONS.....	118
7.2. RECOMMENDATIONS	121
8. BIBLIOGRAPHY.....	123
TABLES	129-144
FIGURES.....	145-185
APPENDIX A – GAS BREAKTHROUGH TEST RESULTS	186-244

LIST OF TABLES

Table 3.1	Test parameters for a standard test.....	129
Table 3.2	Target test parameters for illite sand (IS) series	129
Table 3.3	Target test parameters for bentonite tests (BU and BW).....	130
Table 3.4	Target test parameters for non-polar fluid (NPF) series.....	130
Table 3.5	Target test parameters for illite with modified time (IT) series	130
Table 4.1	Comparison of the properties of illite and bentonite.....	131
Table 4.2	Fractionated sand size comparison	132
Table 5.1	Summary of specimen conditions for the IS75 (75% illite/25%) sand test series	133
Table 5.2	Summary of specimen conditions for the IS50 (50% illite/50%) sand test series	134
Table 5.3	Summary of specimen conditions for the IS37.5 (37.5% illite/62.5%) sand test series	135
Table 5.4	Summary of specimen conditions for the IS25 (25% illite/75%) sand test series.....	136
Table 5.5	Summary of specimen conditions for the BW (bentonite wetted) test series	137
Table 5.6	Calculation of S_r from water inflow.....	138
Table 5.7	Summary of specimen conditions for the BU (bentonite unsaturated) test series	139
Table 5.8	Summary of specimen conditions for the NPF test series.....	140
Table 5.9	Summary of test performed on illite with water as a pore fluid.....	141
Table 5.10	Summary of specimen conditions for the ITU (illite-time) test series...	142

Table 6.1	Comparison of different models for gas breakthrough pressure in illite	143
Table 6.2	Comparison of different models for gas breakthrough pressure in bentonite.....	144

LIST OF FIGURES

Figure 1.1	Schematic diagram of the Canadian nuclear fuel waste repository concept.....	145
Figure 2.1	Silica tetrahedron.....	146
Figure 2.2	Alumina octahedron.....	146
Figure 2.3	Examples of clay structures.....	147
Figure 2.4	Conceptual ion concentrations for different DDL models.....	148
Figure 2.5	Two possible cation arrangements at the surface of a clay particle ...	149
Figure 2.6	Variation in double layer thickness with dielectric constant, D.....	150
Figure 2.7	Characteristic curve relative water content to pressure.....	151
Figure 2.8	Characteristic drainage curves for three hypothetical soils.....	152
Figure 4.1	Gas breakthrough test board and test cell.....	153
Figure 4.2	Schematic of gas breakthrough test equipment.....	154
Figure 4.3	Schematic of data acquisition system.....	155
Figure 4.4	Calibration data for pressure transducer 66544.....	156
Figure 4.5	Calibration data for pressure transducer 65842.....	157
Figure 4.6	Calibration data for pressure transducer 65843.....	158
Figure 4.7	Calibration data for pressure transducer 66542.....	159

Figure 4.8	Calibration data for pressure transducer 66543	160
Figure 4.9	Calibration data for pressure transducer 65841	161
Figure 4.10	Cross-section of test cell	162
Figure 4.11	Exploded view of test cell flange and filters	163
Figure 4.12	Division of specimen for water content tests	163
Figure 5.1	Increasing gas breakthrough pressure with increasing S_r	164
Figure 5.2	Increasing gas breakthrough pressure with increasing ρ_{dry}	165
Figure 5.3	Increasing gas breakthrough pressure with increasing $\rho_{clay\ dry}$	166
Figure 5.4	Decreasing rate of gas breakthrough with increasing ρ_{dry}	167
Figure 5.5(a)	Increasing gas breakthrough pressure with increasing S_r	168
Figure 5.5(b)	Increasing gas breakthrough pressure with increasing S_r	169
Figure 5.6(a)	Increasing gas breakthrough pressure with increasing ρ_{dry}	170
Figure 5.6(b)	Increasing gas breakthrough pressure with increasing ρ_{dry}	171
Figure 5.7	Pore size distributions for illite specimens compacted to $\rho_{dry}=2.04Mg/m^3$ at varying water contents	172
Figure 5.8	Pore size distributions for illite specimens compacted to $w=12\%$ with varying ρ_{dry}	173
Figure 5.9	Pore size distribution of illite with a single peak	174
Figure 6.1	Gas breakthrough pressure - effective clay dry density relationship for illite/sand specimens with $S_r = 85-90\%$	175
Figure 6.2	Gas breakthrough pressure - effective clay dry density relationship for illite/sand specimens with $S_r = 90-95\%$	176
Figure 6.3	Gas breakthrough pressure - effective clay dry density relationship for illite/sand specimens with $S_r = 95-100\%$	177

Figure 6.4	Summary of gas breakthrough pressure - effective clay dry density relationship for illite/sand specimens	178
Figure 6.5	Gas breakthrough pressure - saturation relationship for wetted bentonite specimens.....	179
Figure 6.6	Gas breakthrough pressure - saturation relationship for unsaturated bentonite specimens.....	180
Figure 6.7	Conceptual diagram showing flow paths within a compacted clay.....	181
Figure 6.8	Conceptual diagram showing factors used in advective models to represent the actual system.....	182
Figure 6.9	Conceptual diagram for flow in illite and bentonite during an increasing pressure test.....	183
Figure 6.10	Sample model calculations (illite).....	184-185

LIST OF SYMBOLS

A	- area
A_e	- effective area
AECL	- Atomic Energy of Canada Limited
AEV	- air entry value
C	- concentration
C_s	- shape factor
c	- constant
CANDU	- Canadian Deuterium Uranium nuclear reactors
D	- diffusion coefficient or dielectric constant
D_A	- apparent diffusion coefficient
d	- diameter
DL	- diffuse ion layer
DDL	- diffuse double layer
e	- unit electron charge
EDL	- electric double layer
f	- scale factor
G_s	- specific gravity
g	- gravitational acceleration
I_p	- plasticity index
i_h	- hydraulic gradient
K	- hydraulic conductivity
k	- porosity
L	- length

L_e	- effective length
MIP	- mercury intrusion porosimetry
n	- porosity
n_{eff}	- effective porosity
n_o	- electrolyte concentration
P	- pressure
P_c	- capillary pressure
P_b	- gas breakthrough pressure
P_g	- applied pressure
Pa	- Pascal
PSD	- pore size distribution
q	- flow
RBM	- reference buffer material
r	- radius
r^2	- coefficient of determination
S_r	- degree of saturation
S_T	- total surface area
s_D	- standard deviation
STP	- standard temperature and pressure
T	- temperature
T_s	- surface tension
u_a	- pore air pressure
u_w	- pore water pressure
V	- volume

V_v	- volume of voids
v	- velocity
V_{ave}	- average velocity
w	- water content
x	- thickness of DDL
α	- compressibility factor
θ	- contact angle
η	- absolute viscosity
μ	- dynamic viscosity
ρ	- density
ρ_d OR ρ_{dry}	- dry density
ρ_c OR $\rho_{clay\ dry}$	- effective clay dry density
σ	- total stress
τ	- tortuosity
Ψ_{mo}	- matric potential before loading
Ψ_{mo}	- matric potential after loading

1. INTRODUCTION

Barriers which consist of clays or clay-sand mixtures are becoming increasingly favoured as an engineering solution for the isolation of wastes from the biosphere. Compacted clay barriers are commonly used as liners for landfills. Clay-sand barriers are also a part of the Canadian nuclear fuel waste disposal concept for the permanent disposal of the radioactive waste. This concept is being proposed by Atomic Energy of Canada Limited; it is aimed at minimizing the burden on future generations of storing the nuclear waste produced today.

Engineered clay barriers commonly known as buffers are the focus of this research program. A bentonite-sand buffer has many desirable characteristics other than its low hydraulic conductivity. Bentonite swells significantly upon contact with water, and this characteristic is highly desirable for sealing any small cracks or fissures in the sub-grade or host rock, or any cracks which may develop in the buffer itself. Other desirable properties of the buffer include its low diffusion coefficient, and its tendency to increase the pH of the water in contact with it, thus inhibiting corrosion of metals. Buffer also has the capability to sorb radionuclides which might migrate from a container of radioactive waste.

In recent years, several researchers (Jeffries, 1991, Grogan et.al. 1992, Wikramaratna et.al. 1993, Agg et.al. 1996) have predicted that high gas pressures may develop through biological or chemical reactions within a nuclear waste disposal repository, significantly affecting flow of water and gas from it. Gases may also build up within

landfills, especially if there is an inadequate gas-release system. Studies have already been conducted on the hydraulic conductivity of bentonite and illite (Dixon, 1995) and on their diffusion coefficients (Cheung, 1989). However, the effect of increased gas pressures in clay buffers which could potentially damage the structure of the buffer and increase contaminant migration rates, is relatively unknown.

1.1. CANADIAN NUCLEAR FUEL WASTE DISPOSAL CONCEPT

Compacted clay buffers are employed in the Canadian nuclear fuel waste disposal concept. The concept consists of placing the nuclear fuel waste within a repository located in a deep geological formation, 500-1000m below the ground surface. Spent fuel bundles will be surrounded by a number of barriers which will retard the travel of radioactive substances to the biosphere. Since the radioactivity of the spent fuel will decrease with time, a low rate of flow from the repository to the biosphere is desirable. A schematic diagram of the Canadian nuclear fuel waste repository concept is shown in Figure 1.1. The most likely path by which radioactive isotopes could travel to the biosphere would be through contamination of groundwater. The barriers between the spent fuel bundle and the biosphere are as follows, (in order of increasing distance from the fuel bundle):

- container - the spent fuel bundles will be placed inside a corrosion-resistant titanium or copper container which would be designed to last at least 500 years

- **buffer** - a 50% Avonlea bentonite, 50% fractionated silica sand mixture will surround the container. Its low hydraulic conductivity will resist the movement of contaminated groundwater in the event that there was a breach in the container.
- **backfills** - backfills will be used to fill the emplacement rooms, tunnels, and shafts needed for the construction of the repository. The backfills will have characteristics similar to those of the buffer material.
- **host rock** - the plutonic rock of the Canadian Shield will isolate the waste from the surface, and will limit the effects of natural forces and human activity

1.2. GAS GENERATION

Gas will be produced within any sealed waste containment site. In landfills, decomposition of the organic fraction of the waste will produce quantities of gas larger than can be dissipated by diffusion. Since the landfill will be an anaerobic environment, the primary gases generated will be methane (CH₄) and carbon dioxide (CO₂) (Tchobanoglous et al., 1993).

Within a nuclear waste disposal repository, there will be a number of different mechanisms for the generation of gas. The controlling mechanisms depend upon time from emplacement. Gas can be generated in the repository upon biological degradation of organic materials, corrosion of metals left in the repository after construction, and by radiolysis (Agg et.al. 1996). For example, under the aerobic

conditions immediately following backfilling within a repository, carbon dioxide (CO₂) will form as a product of biological degradation of organics and will form the majority of gas in the repository (Grogan et.al.1992). It is estimated that it will take 8 to 300 years for all available oxygen to be spent (Johnson et.al. 1994a). After this, anaerobic conditions will occur and methane and carbon dioxide will be the principal gases formed.

Anaerobic corrosion of metals will produce hydrogen gas (H₂). In the short term, corrosion of ferrous concrete reinforcing bars and rock bolts will occur, and in the long term the canister itself will corrode. A review of the chemical reactions which produce these gases may be found in Jeffries (1991).

It is difficult to predict the amounts of gas that will be produced within a waste disposal repository. Since the repository will be sealed, any gas generation in excess of the small quantity that will be dissipated (through diffusion) will cause gas pressures to increase. This will likely be the case with the Canadian nuclear fuel waste disposal concept (Johnson et al. 1994a). For example, the oxidation of one kilogram of a ferrous metal will produce 580 litres of hydrogen gas at STP. This can clearly cause increases in pressure within the repository.

1.2.1. Consequences of gas generation

This thesis will study the effect of increased gas pressures on gas and water flow through compacted clay buffers. A bentonite-sand buffer is often chosen because it limits flow both by advection in response to a hydraulic gradient (as evidenced by its low hydraulic conductivity) and by diffusion in response to a concentration gradient (as evidenced by a low diffusion coefficient). Increased gas pressures will likely increase

hydraulic gradients and cause other flow mechanisms such as two-phase flow to occur. In two-phase flow, a buffer would be de-saturated by gases penetrating the pores and pushing the water out. Once a continuous pore from one side of the buffer to the other is established, it will provide a pathway for the flow of hazardous fluids. Increased gas pressures may also dilate existing pores or shear previously bound water, allowing greater rates of flow. Alternatively, high gas pressures may fracture the buffer and create completely new flow paths.

Some researchers (for example Grogan et.al. 1992) have suggested that venting of the excess gas pressure (as is done in some landfills) would alleviate the problems mentioned earlier for nuclear waste disposal repositories. If the container had already been breached however, the gases could become radioactive. A venting facility would also need to be staffed and maintained, putting a burden on future generations. Another difficulty that could result is fire or explosion in the venting facility (or in the repository) due to the highly flammable and explosive methane and hydrogen gases. Jeffries et al. (1991) and Grogan et al. (1992) both present detailed discussions of the fire and explosion hazards of gases generated in a repository and associated venting facilities.

1.3. OVERVIEW

The research program that forms the basis of this thesis report builds upon the work of Kirkham (1995) who performed gas breakthrough tests on illite. Work done in collaboration with Hume (1998) is also included in the report. The research program

investigated the effects of type of clay, sand content, pore fluid, and test duration on the gas breakthrough properties of compacted clay materials.

The literature review, Chapter 2, presents the current state of knowledge in the relevant areas of clay minerals and structure, flow phenomena in porous media, and gas migration research. Development of the research program and the scope of research are discussed in Chapter 3. A description of the test apparatus and procedures follows in Chapter 4. The test results are then presented in Chapter 5 and discussed in Chapter 6. Chapter 7 details conclusions that have been drawn from the research program and provides recommendations for future research.

2. LITERATURE REVIEW

2.1. INTRODUCTION

An understanding of the factors which affect gas flow in clay materials formed the foundation on which this research program was built. A review of pertinent literature is presented in this chapter. The review commences with a discussion of clay mineralogy and structure, specifically focusing on illite and bentonite, the clays which were used in this research program. The effect of the clay mineralogy and structure on flow of both water and gas in clay materials is then discussed. The final section of this chapter consists of a review of similar gas migration studies in clay materials by other researchers.

2.2. CLAY MINERALOGY

2.2.1. Clay minerals

There are two different usages of the word "clay". The first usage of "clay" refers to the size of a particle. By convention, any particle which has less than 2 μm equivalent diameter is referred to as a clay sized particle. This definition does not require that the composition of the particle be of any specific mineralogical species although a large proportion of clay sized particles are clay minerals (Bohn et al., 1985). In the second usage, the term 'clay mineral' is used to describe phyllosilicates, or layer silicates, which are a specific group of minerals. These may or may not be larger than 2 μm in equivalent diameter.

All clay minerals are made up of two types of structural units: tetrahedral sheets, and octahedral sheets. The following section is a brief summary of extended descriptions given for example, by Yong et al. (1992), and Mitchell (1976).

Tetrahedral sheets consist of silica tetrahedrons. In a silica tetrahedron, shown schematically in Figure 2.1, each silicon atom is covalently bonded to four oxygen atoms. In a tetrahedral sheet, three of the four oxygens are shared with neighboring silicon atoms, forming a hexagonal net (Mitchell, 1976). The three oxygen atoms which are shared form the basal plane. The one oxygen atom in a silica tetrahedron which is not shared with neighboring tetrahedrons is referred to as the apical atom. The structural unit of a tetrahedral sheet is $(\text{Si}_4\text{O}_{10})^{4-}$. It may repeat indefinitely in two dimensions.

Octahedral sheets are made up of octahedrons, as shown schematically in Figure 2.2. In an alumina or magnesia octahedron, cations (commonly Al^{3+} or Mg^{2+}) are in octahedral coordination with hydroxyl anions (Bohn, et al., 1985). Octahedral sheets can be split into two categories; dioctahedral and trioctahedral. In a dioctahedral sheet, a trivalent cation, such as aluminum occupies only two of the three possible cation positions within the sheet. In a trioctahedral sheet, a divalent cation such as magnesium must occupy all three cation positions within the sheet.

Clay layers are composed of multiple sheets, and can come in a number of different configurations. Within a layer, tetrahedral and octahedral sheets are bonded together by sharing the apical oxygen atoms of the tetrahedral sheet. A 1:1 layer silicate

consists of one tetrahedral sheet and one octahedral sheet. An example of a 1:1 layer silicate is kaolinite, shown in Figure 2.3. All the clays which will be discussed in this study are 2:1 layer silicates, in which an octahedral sheet is sandwiched between two tetrahedral sheets. Examples of 2:1 layer silicates are montmorillonite, illite (also referred to as hydrous mica), and vermiculite (Figure 2.3).

When a mineral is formed, certain cations are sometimes replaced by other cations of similar size but different valence. This replacement of cations is referred to as isomorphous substitution. For example, in a tetrahedral sheet, aluminum (3+) sometimes replaces silicon (4+). This gives the mineral a positive charge deficit, or a net negative charge. Isomorphous substitution can similarly happen in octahedral sheets. For example, in montmorillonite (a member of the smectite group), some of the aluminum atoms (3+) in the octahedral sheet are replaced by magnesium (2+). The result is again a net negative charge.

The layers described in previous paragraphs bond together to form clay mineral particles. The different types of 2:1 layer silicates differ mainly in the way the layers are held together (Mitchell, 1976, Craig, 1992). To satisfy the net negative charge created by isomorphous substitution, cations are attracted to the clay particles. The adsorbed cations are often held between the phyllosilicate layers by ionic bonds and in this way, help to bond the layers together.

The layer charge is defined as the amount of negative charge arising from isomorphous substitution which must be balanced by external cations, per structural unit. The

greater the layer charge, the stronger the ionic bond with the other layers will be (Bohn, et.al., 1985). In micas, the layer charge is quite high and cations between the layers are held very tightly. In contrast, smectites which have a low layer charge are weakly bonded to other layers. The layers are so weakly bonded that water (a polar molecule), can enter in between the layers and cause the clay to expand (or swell) under low applied stress levels. Electrochemical equilibrium is maintained in an expanding mineral.

The type of bonding between the layers of a clay can dictate its physical and chemical properties (Bohn, et.al., 1985). For example, the surface area of a clay affects many of its reactive properties. If the bonding between layers of a clay is very strong, the clay will form large crystals composed of many layers which will withstand considerable stresses. As a result, a clay with strong inter-layer bonds will have low specific surface area. If the bonding between layers is weak, however, the clay will fracture between the layers and will form many small flakes. This results in a very large specific surface area.

2.2.1.1. Illite

Illite is a 2:1 layer silicate which is also referred to as hydrous mica since it is a variation of the ideal mica structure. It has less interlayer fixed potassium ions and more structured water than a real mica (McBride, 1994). In illite, isomorphous substitution replaces one quarter of the silicon atoms in the tetrahedral sheets with aluminum. Potassium in the interlayer space satisfies the resulting positive charge deficit, as shown in Figure 2.3. The potassium ions are referred to as “fixed” because

they fit very tightly into the ditrigonal cavity which occurs between the basal oxygens of the tetrahedral sheet and are therefore unlikely to be replaced. The fixed potassium ions prevent water from getting into the inter-layer space and therefore restrict swelling of this type of clay. Illite has a relatively low specific surface area of $70 - 120 \times 10^3 \text{ m}^2/\text{kg}$ (McBride, 1994).

2.2.1.2. Montmorillonite

Montmorillonite is the main component of the natural bentonite material which was used in this research program. Montmorillonite is a 2:1 layer silicate which has isomorphous substitution predominantly in the octahedral sheet, as shown in Figure 2.3. In some montmorillonites, there is also some substitution of aluminum for silicon in the tetrahedral sheet. Since montmorillonite has a relatively low layer charge which occurs predominantly in the octahedral sheet, the layers are not tightly bound together by cations as in illite, and are much more likely to let water into the interlayer space. Swelling and shrinking properties exhibited by montmorillonite are a result of the water being able to occupy the interlayer space. Montmorillonite has a specific surface area of $600 - 800 \times 10^3 \text{ m}^2/\text{kg}$, due to the fact that the layers are not as tightly bound together as in illite and so the interlayer space is accessible surface area.

2.2.2. Clay - water interaction

2.2.2.1. Diffuse double layer models

In the pore fluid of a clay soil, cations are attracted to the negatively charged clay particles and tend to concentrate there. This concentration of cations at the surface of

the clay particle causes a concentration gradient, with the cation concentration away from the particle being lower than the average for the pore water. The cations will tend to diffuse away as a result of this concentration gradient. van Olphen (1963) describes this situation as being analogous to the Earth's atmosphere, where the gas molecules are attracted by the gravity of the earth but tend to diffuse away due to the low concentration of gases in the upper atmosphere. The two opposing forces will eventually result in an equilibrium where the concentration is quite high at the earth's surface (or at the surface of a clay particle) and decreases gradually with increasing distance.

Diffuse double layer (DDL) models are used to describe the concentration of cations near the surface of negatively charged clay particles. There are two components of the DDL. The first component is a dense layer of cations at the particle surface which is called the electric double layer (EDL). The second component is the diffuse ion layer (DL) where the ions gradually decrease in concentration with increasing distance from the clay particle.

The most common of the DDL models is the Gouy-Chapman model (Mitchell, 1976, van Olphen, 1963). The formula for calculating the thickness of the DDL (x), developed by Gouy and Chapman, is shown below.

$$x = \sqrt{\frac{DkT}{8\pi n_0 e^2 v^2}} \quad [2.1]$$

Where:

- D = dielectric constant
- k = Boltzmann constant (1.38×10^{-16} erg/K^o)
- T = temperature (°K)
- n_o = number of ions per unit volume
- e = unit electron charge (1.6×10^{-20} coulomb)
- v = valence of ions

A thorough discussion of the theory behind the Gouy-Chapman model is given in van Olphen (1963) and Mitchell (1976).

Equation [2.1] shows that the thickness, x, of the DDL:

- becomes larger as the dielectric constant, D increases
- becomes larger as the temperature, T, increases
- becomes smaller as concentration, n_o , increases
- becomes smaller as valence, v, increases

Several assumptions have been made in the Gouy-Chapman model which limit its actual representation of the real system. The assumptions are as follows (Mitchell, 1976).

1. Ions are treated as point charges with no size.
2. The clay particle has a uniform charge distribution on its surface.
3. The clay particle surface is a plate which is large in comparison to the thickness of the double layer.
4. The dielectric constant, D, is independent of position.

5. Plates are oriented in a parallel arrangement.

Stern presented a modification to the Gouy-Chapman model which addresses the problem of impossibly high cation concentrations at the clay particle surface (McBride, 1994). The differences between the two models are presented in Figure 2.4. The Gouy-Chapman model, as mentioned above, considers the ions as point charges with no size. In the Stern model, the concentration of cations at the particle surface is regulated by their size, or more simply, how many could 'fit' on the particle surface. This modification of the EDL is now referred to as the Stern layer. It can be seen on Figure 2.4 that with the Stern layer, the concentration of cations at the clay particle surface is much less than that predicted by the Gouy-Chapman model.

A modified diffuse double layer is presented by Yong, et al. (1992) in order to describe the interactions in a clay-water-ion system. In this model, the Stern layer is explained more fully by suggesting two possible arrangements of cations at the clay particle surface. The first possible arrangement is shown in Figure 2.5a, in which the hydrated cations interact with the clay particle through a layer of water molecules. The second configuration is shown in Figure 2.5b, where partially hydrated cations are in direct contact with the clay surface. Yong et al. (1992) state that the two configurations are not mutually exclusive and both conditions can occur at the same time at different locations. Both configurations will have diffuse swarms of hydrated ion clusters which extend outwards from the clay surface and decrease in concentration with distance (Dixon, 1995). Another similar model has also been developed by Güven (1992).

Water which is so strongly bound that it is not available for flow is generally considered to consist of the first layer of hydrated cations, which is approximately 0.1 - 0.4 nm thick (Yong and Warkentin, 1975). This bound water has been described by Dixon (1992) as a "non-porous solid", with respect to water flow. The effects of the DDL on the behaviour of water can extend up to 15 water layers (3.75 nm) from the particle surface in highly active clay particles such as bentonite (Yong et al., 1992).

Some researchers have found the DDL theory to less than fully explain the behaviour of montmorillonite-rich soils (Gens and Alonso, 1992). Pusch (1982), for example, found for sodium bentonites at high densities, that DDL theory did not adequately describe his experimental findings. He attributed the difference between his observations and the DDL calculations to the fact that at high densities, the DDL's do not have room to fully develop within the pores.

2.2.3. Soil fabric and pore structure

2.2.3.1. Soil Fabric

The structure of the layers of clay minerals was discussed in Section 2.2.1. These layers are the building blocks of the soil fabric. The structure of a soil fabric is commonly divided into four different levels. The first level is referred to as a 'domain'. A 'domain' (also referred to as a lamella by Güven, 1992) is comprised of several stacked layers and is generally 10×10^{-6} m (0.01mm) thick, (Kirkham, 1995). A 'cluster' is formed when several domains conglomerate. A 'cluster' is about 100×10^{-6} m (0.1mm) in size. A 'ped' is a group of several clusters and is about 1000×10^{-6} (1mm) in size.

The largest structural level is referred to as an 'aggregate'. It consists of a group of peds which is up to $10\ 000 \times 10^{-6}$ (10mm) in size.

2.2.3.2. Pore size distribution

All structure levels of the soil fabric affect the pore-size distribution (PSD) of a soil. The pores which exist between the peds or aggregates of a compacted soil are referred to as "macropores" (Yong et.al.,1992), "interaggregate pores" (Güven,1992 , Gens and Alonso, 1992) or as "inter-ped" pores, which will be used hereafter. The pores which exist within the peds themselves on the cluster and domain levels are referred to as micropores (Yong et.al., 1992), intraaggregate pores (Güven ,1992, Gens and Alonso, 1992) or intra-ped pores.

In a compacted clay, the water content of the soil at the time of compaction will greatly affect the size and quantity of the inter-ped pores (Garcia-Bengochea et al., 1979, Barden and Sides, 1970). When a soil is compacted, the ability of the peds and aggregates to resist the compaction forces becomes very important to the PSD of the soil after it is compacted. For example, in a soil which is drier than the optimum water content, the peds are quite strong and will be able to resist compaction pressures. (The optimum water content is defined as the water content at which the greatest dry density can be achieved for a given compactive effort, commonly determined as a result of the Modified Proctor compaction test). In soils with a water content below optimum, the resistance to compaction pressures will result in a network of pores between the peds. (These were previously referred to as inter-ped pores). In a soil which is on the wet side of the optimum water content, the peds will be soft and will not have much

resistance to the compaction forces. In these wet soils, the peds will deform easily and fill many of the inter-ped pores.

The water content of the soil at the time of compaction affects the intra-ped pores and controls soil suctions. The effects of compaction forces are concentrated on inter-ped pores (Wan, 1996, Delage and Graham, 1996). Within the peds, the intra-ped pores between domains and clusters are only slightly affected, if at all, by the compaction forces.

2.2.3.3. Effects of pore structure on flow phenomena

For a liquid or gas to be able to flow through a soil, the soil must have pores, and these pores must be connected to each other. The porosity, n , of a soil is defined as the ratio of the volume of voids in a soil to the total volume (Craig, 1992). A soil with a high porosity will have more pores, and generally, larger pores than a soil with a low porosity. In order for flow to occur however, the pores must be interconnected.

Effective porosity (n_{eff}) represents the portion of the total porosity that exists in interconnected pores which contribute to mass flow (Dixon, et.al 1985). Within the pores that make up the effective porosity of the soil, there is frequently a portion of the water which is bound to the soil particles and is not available for flow. The water not available for flow is within the DDL and is referred to as structured water (discussed in Section 2.2.2.1). The pore space which is available for flow is referred to as 'free pore space'. The free pore space can be occupied by water or a combination of water and gas, depending on whether the soil is saturated or unsaturated. Since flow phenomena

occur almost entirely within the free pore space, the term 'pore space' will be used hereafter to mean 'free pore space'.

A statistical network model has been used by Ruth (1995) to represent the pore structure of a porous medium. The network consists of two types of pores, tubes and vugs. The vugs represent the large pores and account for most of the porosity of the soil. These large pores represent the inter-ped and inter-aggregate pores. The tubes represent the pore throats or microtubes in between the vugs and they restrict the flow through the soil. The tubes represent the pores which occur between two peds when they are directly touching. The tubes control the flow in a soil, since they create a "bottleneck" effect.

2.3. MERCURY INTRUSION POROSIMETRY

One method of obtaining the PSD of a soil that has been used by many researchers (Diamond, 1971, Delage and Lefebvre, 1984, Juang and Holtz, 1986, Wan, 1996) is Mercury Intrusion Porosimetry (MIP) testing. The principle behind the test is that a non-wetting fluid (a fluid for which the contact angle is greater than 90° for the solid in question) will not intrude the pores of that solid until an external pressure is applied (Diamond, 1970). The pressure required to intrude the fluid into the soil is related to the size of the pores by the Washburn equation:

$$P = -4T_s \cos \frac{\theta}{d} \quad [2.2]$$

Where: P = pressure

T_s = surface tension of the liquid (mercury)

θ = contact angle of the liquid with the solid

d = diameter of the pore

In a MIP test, the chamber which holds the specimen is filled with mercury. The chamber is then pressurized to a selected pressure and held at that pressure while the specimen is intruded by mercury. When intrusion stops, this indicates that all of the pores which are large enough to be intruded at this pressure increment have been filled. A reading of the volume of mercury intruded is then taken. The pressure is then increased incrementally, and the volume of mercury intruded at each step is recorded. These data are then converted into a pore size distribution using equation [2.2].

2.3.1. Limitations of mercury intrusion porosimetry testing

While MIP testing can be a powerful tool for the investigation of the pore size distribution of a compacted clay soil, there are certain limitations of the test which should be noted. Diamond (1970) presents the following list of limitations of the test.

- a) The soil must be completely dry.
- b) Pores which are not accessible from the exterior of the specimen will not be included in the measurements.
- c) Pores which have entryways that are of a smaller diameter will only be intruded when the pressure becomes high enough to intrude the entryway. The pore size distribution obtained from the test will allocate the whole volume of such a pore under the diameter of the small entryway.

- d) The smallest pore size measured is regulated by the type of testing equipment. Depending on the type of soil and type of testing apparatus, the entire volume of pores of a given specimen may not be intruded.
- e) Specimen preparation may alter the PSD.

A method used to obtain a clearer understanding of the effect of pores with restricted entryways (limitation c), above) was presented by Delage, et al. (1984). The method consists of releasing the pressure after the porosimetry test, allowing some of the mercury to come out of the specimen. There will always be some mercury which does not come out of the specimen since it is trapped by constricted entryways or "bottlenecks". The specimen is then re-intruded and the new intrusion curve represents the free porosity only.

There are other limitations which were not presented by Diamond (1970) in the above list. Since the specimen must be dried before testing, this should be done with some care. Some clays can shrink significantly upon oven drying. Wan (1996) placed compacted clay specimens in a desiccator in close proximity to sulfuric acid which was used as a desiccant to dry the material. This desiccant reduced the amount of shrinkage upon drying as compared with other methods such as oven drying. Other methods such as accelerated freeze drying can also be used in an attempt to reduce shrinkage and the undesirable cracking which might occur. Care is also taken to avoid testing of specimens which have developed fissures during drying, since they will produce inaccurate results.

Results obtained from a MIP test are in terms of total porosity. Since the specimen is completely dry at the beginning of the test, there is no way to differentiate between porosity that was formerly occupied by structured water and that occupied by free water. This fact must be taken into account when interpreting MIP test results.

2.4. FLOW PHENOMENA

2.4.1. Capillarity

Capillarity is the tendency of a fluid to rise when it comes into contact with a solid surface. Associated with capillarity is the development of water pressure lower than atmospheric. This is referred to as matric suction by members of the geotechnical engineering community. Surface tension of a liquid is the force that causes the observed capillary action. Molecules in a liquid which are close to the surface have a greater attraction for one another than do molecules which are below the surface (Roberson et.al., 1990). This attraction of molecules for one another at the surface of a fluid produces a surface which is like a stretched membrane. This membrane is in tension and exerts forces on objects which are in contact with it. In an air-water system at room temperature, the surface tension of water, T_s , is 0.073 N/m.

When a capillary tube with a small diameter is inserted into a water bath, the water molecules are attracted to the glass tube and the water surface curves upward around the inner circumference of the tube. The angle at which the water surface intersects the glass tube, θ , is taken to be zero for most applications (Fredlund, 1993). The resulting upward force causes the water to rise in the tube. The capillary pressure which is exerted on the water in the tube is given by the following equation:

$$P_c = \frac{2T_s}{r} \quad [2.3]$$

where: P_c = capillary pressure
 T_s = surface tension
 r = radius of the tube.

2.4.2. Permeability and hydraulic conductivity

The hydraulic conductivity of a soil is defined as its ability to conduct a fluid (Craig, 1992). Darcy's law states that there is a direct relationship between the flow velocity through a soil and the hydraulic gradient acting on it, as shown in the following equation:

$$q = -AKi_h \quad [2.4]$$

Where: q = flow per unit time
 A = cross sectional area
 K = hydraulic conductivity (distance per unit time)
 i_h = hydraulic gradient.

The permeability, k , (or intrinsic permeability) is a function of the pore geometry alone where the hydraulic conductivity in the above equation, K , is a function of both the

pores and the pore fluid. The relationship between hydraulic conductivity, which takes into account the characteristics of the pore fluid, and permeability is shown in the equation below (Freeze and Cherry, 1979).

$$K = \frac{k\rho g}{\mu} \quad [2.5]$$

Where:

- K = hydraulic conductivity (m/s)
- k = permeability (m²)
- μ = dynamic viscosity of the pore fluid(kg/m*s)
- ρ = density of the pore fluid(kg/m³)
- g = gravitational acceleration (m/s²)

Darcy's law was derived from an empirical relationship discovered for the flow of water in sand and gravel. The hydraulic conductivity, K, varies over many orders of magnitude for different soils, from 10⁻² metres per second for sandy soil to 10⁻¹³ for unfissured clays. Darcy's law has been proven to have limitations, especially in dense clays.

There are upper and lower limits for which Darcy's law can be used. The law implies that there will be a linear relationship between the hydraulic gradient and the rate of flow. However, there is only a certain range for which this linear relationship will occur. Above and below this range the relationship between hydraulic gradient and flow rate becomes non-linear. Since Darcy's law assumes laminar flow, the upper limit of validity for the law is generally considered to be the threshold between laminar and turbulent

flow. Ruth (1995) states that the upper limit is not due to true turbulence since the Reynolds numbers observed are not high enough for a true transition to turbulent flow. He states that the non-linearity is actually due to laminar inertial effects caused by the tortuous path of the flow. This laminar inertial effect is called the Forchheimer effect.

Tortuosity, (τ), is a measure of how distorted the path of the fluid is. Tortuosity is defined as the actual distance which a fluid must pass through on a microscopic level per unit of linear displacement on a macroscopic level.

$$\tau = L_e/L \quad [2.6]$$

where: τ = tortuosity

L_e = effective length (length of actual flow path)

L = length of specimen

These distortions in the flow path cause laminar inertial effects. When flow in a pipe encounters a bend, the flow has a tendency to want to remain traveling in the same direction (this phenomenon is called inertia). As a result of the opposing forces of the bend in the pipe and inertia, secondary flow patterns are formed. These secondary flow patterns eventually dissipate due to viscosity but they also cause energy losses in the system (Ruth, 1995). These energy losses contribute to the non-linearity of the system.

The lower limit of Darcy's law is generally considered to be the point at which other effects or coupled flow processes become significant in comparison with the effect of hydraulic gradient (Dixon, 1995). Forces such as diffusion and osmosis can become significant in systems where the hydraulic gradient is very low (Dixon, 1995).

The starting point for most theoretical models for water flow through soils used today is the Poiseuille equation (Mitchell, 1976). Dixon (1995) has found that the Poiseuille equation predicts relatively accurately water flow within well characterized bentonite clay and bentonite-sand mixtures (with at least 25% bentonite content). The equation gives an average flow velocity for flow through a round capillary within the soil. It can be expressed:

$$v_{ave} = \frac{\gamma_w r^2}{8\eta} i_h \quad [2.7]$$

where: v_{ave} = average velocity (within a pore, microscopically)

γ_w = unit weight of water

r = capillary radius

η = viscosity

i_h = hydraulic gradient.

In equation [2.7], the smaller the capillary radius (analogous to the pore radius in a soil), the lower the velocity of flow through a soil. In the case of a soil with a large DDL, the radius term, r , would represent only the radius of the portion of the pore which consists of free water. As a result of this reduction in pore radius, the velocity would decrease.

The Kozeny-Carman equation is a combination of the Poiseuille equation and Darcy's Law. It builds upon the Poiseuille equation, and factors such as the shape factor, C_s , and tortuosity, τ , are introduced in an attempt to better model the actual system.

The starting point for the derivation of the Kozeny-Carman equation is the simple flow equation:

$$q = vA \text{ or } \frac{vV}{L} \quad [2.8]$$

where: v = superficial velocity (as observed externally)

V = volume.

or on a microscopic level:

$$q = v_{ave}A_e \text{ or } \frac{v_{ave}V_v}{L_e} \quad [2.9]$$

where: A_e = effective area,

V_v = volume of voids.

Using [2.8] and [2.9] and solving for v_{ave} gives:

$$v_{ave} = \frac{vVL_e}{V_vL} \quad [2.10]$$

Using the definitions of porosity, $n = V_v/V$ and tortuosity, equation [2.6], $\tau = L_e/L$ gives:

$$v = \frac{v_{ave}n}{\tau} \quad [2.11]$$

If the surface area is defined as, S_T = surface area/ m^3 of soil, then:

$$r = \frac{n}{[S_T(1-n)]} \quad [2.12]$$

Then substituting equations [2.11] and [2.12] into the Poiseuille equation, [2.7], and adding a shape factor C_s , to account for the pore shape within a clay gives:

$$v = \frac{n^3 C_s \gamma_w}{S_T^2 (1-n)^2 \tau \eta} i_h \quad [2.13]$$

If the effective length, L_e is then used to describe the hydraulic gradient, then the tortuosity must be squared, and the equation becomes:

$$v = \frac{n^3 C_s \gamma_w}{S_T^2 (1-n)^2 \tau^2 \eta} i_h \quad [2.14]$$

Substituting Darcy's Law, equation [2.4] ($v=Ki$), into [2.14] gives,

$$K = \frac{n^3 C_s \gamma_w}{S_T^2 (1-n)^2 \tau^2 \eta} \quad [2.15]$$

which is a form of the Kozeny-Carman equation.

Formulas for the flow of water within clay specimens, if altered, can be used to model gas flow. Gas breakthrough is assumed to occur in a saturated specimen when gas pressure pushes water out of a continuous pore (or de-saturates it). The time for pores to de-saturate under an applied pressure gradient can be found from the flow equations discussed above. Hume (1998) found that in constant pressure gas breakthrough tests on 100% bentonite, the Kozeny-Carman equation could be used to predict the time of gas breakthrough.

2.4.3. Diffusion

Flow of ions or molecules as a consequence of a concentration gradient is called diffusion. Diffusion can be a significant factor in dense clays where flow induced by a

hydraulic gradient is very low (Dixon, 1995). In very dense specimens or at low pressure gradients in long tests, diffusion of gas through pore water could be the predominant mechanism for gas flow. In the pore space of a soil, cations can diffuse through both the structured water and the free water although the diffusion rates will be slower in the structured water (Cheung, 1989b). Anions will diffuse only through the free water due to the fact that they are repelled from the surfaces of the negatively-charged clay particles where the structured water exists.

In a soil-water system, diffusion depends on many factors other than the primary mechanism of molecular diffusion in the water. Diffusion in a soil also depends on physicochemical processes like sorption, ion exchange, precipitation, and on properties of the soil itself like pore structure and tortuosity (Cheung, 1989). Fick's second law, shown below, is generally used to determine diffusion coefficients.

$$\frac{\partial C}{\partial t} = D \frac{\partial^2 C}{\partial x^2} \quad [2.16]$$

Where: C = concentration
 D = diffusion coefficient
 t = time.

Equation [2.16] is valid for a porous medium which is homogeneous, isotropic, isothermal, and has a continuous distribution of diffusion paths (Cheung, 1989). Due to the fact that the diffusion coefficient is affected by many different characteristics of the

soil-water system, the molecular diffusion coefficient measured from the tests is not a pure molecular diffusion coefficient in solution (Cheung, 1989). Therefore, the diffusion coefficient obtained from the tests is called the apparent diffusion coefficient, D_A .

In a repository environment, where gas generation rates will be slow, diffusion will likely become an important mechanism for gas transport. However, for the experiments carried out for studies described here, the pressure gradients are so large, and the test times for the gas breakthrough tests are generally short enough that diffusion was assumed to be negligible.

2.4.4. Flow in soils with non-polar pore fluids

The foregoing descriptions of flow in soils have been made assuming water as the pore fluid. In this section pore fluids other than water, specifically non-polar pore fluids, will be discussed. The study of soils with non-polar pore fluids in the engineering literature has arisen from the use of clays with low permeability such as bentonite to isolate wastes. In engineered barriers such as bentonite landfill liners, contamination with non-polar hydrocarbons could significantly increase the hydraulic conductivity of the liner and lead to unacceptable amounts of leakage. It is unlikely that the buffer used in a nuclear waste repository would be contaminated by hydrocarbons. It is useful, however, to use the study of non-polar fluids to gain insight on the effect of the DDL on flow within soil.

Mesri and Olson (1971) studied illite and smectite that were saturated with a non-polar fluid (benzene). For a smectite with a void ratio of 2, a water saturated specimen had a

hydraulic conductivity, K , of $\approx 10^{-11}$ cm/sec, whereas a specimen saturated with benzene had a $K \approx 10^{-5}$ cm/sec. The effect of the non-polar pore fluid was a little smaller for illite where the hydraulic conductivity (at a void ratio of 2) was $\approx 10^{-9}$ cm/sec when saturated with water, and $\approx 10^{-5}$ cm/sec when saturated with benzene. Mesri and Olson attribute the increase in hydraulic conductivity in both soils to the fact that non-polar fluids do not form DDL's, and therefore there was no bound water restricting the flow paths. The researchers further explain that with the small particles and small pores of a smectite clay, the DDL in a water-saturated specimen will take up almost all of the pore space resulting in a very low permeability. In an illitic clay, the pores are larger and in a water-saturated specimen the DDL will not fill the pores, so a larger proportion of the pore space will still be available for flow. The fact that clay particles in the domains will be more randomly arranged when a clay is saturated with a non-polar fluid is also presented as a cause of the increased permeability in these clays. The different viscosities of the fluids is mentioned only briefly.

Fernandez and Quigley (1985) conducted similar experiments on a natural Samia clay, which is primarily illitic with up to 15% smectite. They found that the hydraulic conductivity of this soil varied inversely with the dielectric constant, D , of the pore fluid. Water, with the highest dielectric constant ($D=80$), had the lowest hydraulic conductivity (of the pore fluids tested). The non-polar hydrocarbons, ($D\approx 2$) had the greatest hydraulic conductivity. Figure 2.6 shows the variation of the thickness of the double layer with the dielectric constant of the pore fluid. The increase in hydraulic conductivity can be explained by the fact that the reduction in DDL thickness with decreasing dielectric constant leaves more pore space available for flow. It is important

to note that both Mesri and Olson and Fernandez and Quigley presented their data in terms of hydraulic conductivity, K , which is a function of both the pore geometry and the pore fluid. However, Fernandez and Quigley note that the same trends were found using values calculated for permeability, k , since the effects of the different fluids on the DDL were so great that they “swamped” the effects of the fluid density and viscosity.

Fernandez and Quigley (1985) also attributed the difference in hydraulic conductivities to the fact that the clay structure observed under an electron microscope was also changed by the pore fluid. Benzene-saturated specimens were flocculated and had large inter-ped pores, whereas the water-saturated specimens were more dispersed, with smaller pores.

Jaynes and Boyd (1991a & 1991b), found that the hydrophilicity (affinity for water) of smectites (of which montmorillonite is a member) was “predominantly due to the exchangeable metal cations”. When metal cations are replaced with hydrophobic organic cations, the clay is referred to as an organo-clay. The organo-clay will also be hydrophobic, as opposed to the hydrophilic parent clay. If clays are purposeiy converted to organo-clays by exchanging the metal cations for small organic cations such as tetramethylammonium (TMA), the capacity of the clay to sorb hydrophobic organic contaminants will be increased. This is due to the fact that the hydrophilicity of the clay will be reduced, and hydrophobic organic cations will be sorbed in areas where previously water would exist. This would be an attractive attribute of clay barriers for the isolation of toxic hydrocarbons. However, the decreased hydrophilicity of the clay

may increase its hydraulic conductivity, possibly increasing flow rates through a clay buffer.

2.5. UNSATURATED FLOW

Flow processes in unsaturated soils are of concern in many different fields. In the area of waste isolation, clays with low hydraulic conductivity are often used as liners for landfills. During construction of these landfills, the clays are seldom in a saturated state. Groundwater will slowly saturate the clay following construction. The buffer surrounding the waste canister in the Canadian Repository Concept will also be placed in an unsaturated state and will be saturated over time by groundwater. The heat generated by the spent fuel will tend to dry the buffer in the immediate vicinity of the canister in the short term (Graham et al., 1997). It is therefore important to have an understanding of flow processes in unsaturated soils.

If a soil is initially saturated, it must be subjected to a certain pressure before any of the fluid will be driven out of the pores (Ruth, 1995, Fredlund and Rahardjo, 1993). This initial pressure required corresponds to the capillary pressure of the largest diameter pores which exist on the surface of the specimen. The pressure required to begin the drainage process of a saturated specimen is referred to as the threshold capillary pressure by Ruth (1995) and Dixon (1992), the air entry pressure by Freeze and Cherry (1979), and the air entry value by Fredlund and Rahardjo (1993).

The air entry value (AEV) is described by Fredlund and Rahardjo(1993) as “the matric suction which must be exceeded before air recedes into the soil pores”. Matric suction (capillarity) was previously discussed in Section 2.4.1. The smaller the pores in a soil are, the higher the capillary pressure which must be overcome in order to drive pore fluid out of the pores. The AEV can be described by the following equation, which is essentially the same equation that is used to describe matric suction.

$$AEV = (u_a - u_w) \quad [2.17]$$

where: AEV = air entry value
 u_a = pore air pressure
 u_w = pore water pressure

As pressure is increased above the AEV, the saturation of the specimen will decrease as smaller and smaller pores are drained of water. At a certain pressure, the drainage will cease. The pressure at which drainage stops is called the pendular capillary pressure by Ruth (1995) and the saturation of the specimen at that point is called the irreducible saturation. Pore fluid which exists in isolated pores that are not adjacent to any flow paths accounts for the fluid which makes up the irreducible saturation.

Figure 2.7 shows a characteristic drainage curve for a soil. A “characteristic drainage curve” for any given soil shows the capillary characteristics, and thus reflects the PSD of that soil. Dry and subsequent re-wetting behaviors are different. They will be described in the next paragraph. Characteristic drainage curves for three different types of soils are shown in Figure 2.8. The figure illustrates how their PSD’s affect the

manner in which soils de-saturate under increasing pressure. The uniform sand, curve c in Figure 2.8, has a relatively uniform pore size distribution. As a result, once the pressure reaches the capillary pressure of the uniform pores, all the pores will drain quickly. This rapid draining is evidenced by the sharply decreasing moisture content of this soil under applied pressure. In contrast, a silty clay (curve a) will have a wide range of pore sizes. Once the AEV is overcome, and the pressure increases, pores with smaller and smaller diameters will start to drain, this effect is shown in the sloped line which indicates a gradual decrease in moisture content with increasing pressure.

The previous paragraph describes how soils lose moisture as pressure is increased. When the pressure on the specimen is then decreased, fluid will begin to re-enter the pore space through capillary action, this is called the "wetting" or "imbibition" phase. A graph of degree of saturation versus pressure (Figure 2.7) illustrates the difference between drying and wetting curves. Although some researchers believe the hysteresis to be a result of a modification of the pore structure (Freeze and Cherry, 1979), Ruth (1995) states that the hysteresis is due to a bottleneck effect. Pores which are much larger than the entryway will not be intruded until the negative pressure (suction) is high enough to fill the pores. By the same process, drainage of pores with small entryways will not occur until the pressure is high enough to drain the entryway. Due to this 'bottleneck' effect, the saturation of the specimen will be different at the same pressure during the drainage and imbibition cycles.

Wheeler (1988) states that there are three different classifications of unsaturated soil with respect to air content:

- continuous gas phase, discontinuous water phase
- continuous gas phase, continuous water phase
- discontinuous gas phase, continuous water phase

Several researchers (Wheeler, 1988, Jeffries, 1991, Fredlund and Rahardjo, 1993) state that the gas phase will become continuous if the saturation is at or below a critical degree of saturation, which is approximately 85%, though this value will vary from soil to soil. When the air phase becomes continuous, water will fill primarily the smaller inter-ped pores where the peds are close to each other or are in contact with one another (Silverstein and Fort, 1997). Gens and Alonso (1992) state that the soil within the intra-ped pores can be considered to be saturated. It is when the air phase becomes continuous in the inter-ped pores that air will readily flow through a soil. Fredlund and Rahardjo (1993) reinforce this point by stating that a small change in the degree of saturation of a soil can significantly affect the hydraulic conductivity of an unsaturated soil. It is for this reason, that hydraulic conductivity of an unsaturated soil is often shown as a function of the degree of saturation.

Adaptations of Fick's and Darcy's laws have been used by researchers to describe the flow of air through an unsaturated soil. In these models, however, the driving force behind the flow is a pressure gradient instead of a hydraulic head difference. A detailed description of the formulation of these models, with experimental results may be found in Blight (1971).

2.6. CURRENT STATE OF GAS MIGRATION RESEARCH

A few groups of researchers have studied the concepts surrounding the flow of gas in engineered clay barriers for nuclear waste repositories with varying results. Only a small number of laboratory studies have been undertaken to provide data to prove the concepts. Since each country has its own repository concept, the laboratory studies are different due to the fact that the materials and methods used have generally been chosen solely for the concept in question. This difference in materials and methods of the laboratory studies has made the direct comparison of the results difficult.

Pusch et al. commenced their gas breakthrough research in 1983, by performing three gas breakthrough tests on compacted MX-80 bentonite (with bulk densities, ρ ranging from 1.88 - 2.05 Mg/m³) saturated with distilled water. The specimens were 50 mm in diameter and 15 mm in height. Two of the tests used nitrogen as the permeating gas, and in one test hydrogen was used. The major conclusion drawn from these experiments was that gas flow occurred through only a few selected flow paths. They drew this conclusion because the saturation of the specimens after the test was >95%, indicating that water had been forced out of only a small number of the pores.

Results of eight additional tests were reported by Pusch (1985). The tests were performed on MX-80 bentonite specimens with ρ of 1.88 -2.14 Mg/m³ saturated with a de-aired synthetic porewater. Nitrogen and hydrogen were again used as permeating gases. Most of the specimens were again 50 mm in diameter and 25 mm in height, although, one specimen was 300 mm in height. No specimens were directly comparable to the specimen with 300 mm height, since all specimens had different ρ .

Therefore, no positive statements could be made regarding the effect of specimen height. The major conclusion of Pusch's 1985 study was that there exists a critical gas pressure, above which gas will flow through the pores of a soil. Below this critical gas pressure, gas flow will occur only through diffusion. Pusch states that the capillary explanation for flow will only be valid for low densities ($\rho = 1.3\text{-}1.7 \text{ Mg/m}^3$), and correspondingly low critical gas pressures. At high densities, Pusch concludes that flow will occur through capillary action *and* by displacing aggregates and widening flow paths.

Pusch also generally found that a time effect was evident. Longer pressure increments produced breakthrough at lower pressures than did the short pressure increments. Pusch attributed this time effect to microstructural rearrangement and healing of pores by aggregates which are moved by the flowing gas to block previously-open pores. However, no comprehensive microstructural analysis is presented to support this hypothesis. Pusch also notes that empirically, the gas breakthrough pressure to swelling pressure ratio is from 0.2 - 0.9, although this concept is not discussed in detail.

Pusch (1987 and 1993) presents a micro structural model to explain the observations of gas breakthrough in compacted bentonite. When a compacted clay at a relatively low density is hydrated, gels emanate from the peds of soil and fill the large inter-ped voids of the soil fabric. These gels have a lower density than that of the specimen as a whole. Pusch explains that the mechanical resistance of these clay gels controls gas breakthrough. He suggests that as the dry density of the specimen increases, so also does the dry density of the gels and therefore the breakthrough pressure. Tests on

10% bentonite, 90% sand backfill mixtures are briefly discussed in Pusch (1993). These backfills had very low breakthrough pressures of 0.015 MPa (at $\rho_d \approx 1.9 \text{ Mg/m}^3$, and $\rho_c \approx 0.9 \text{ Mg/m}^3$), Pusch used these results to further support his hypothesis of the effects of clay gels, explaining that in materials with such a low clay dry density, the gels would not be homogenous and would be discontinuous.

Lineham (1989) studied intact specimens of London and Kimmeridge clays. Coming from natural deposits, the pore structure of these specimens is very different from those of engineered clay barriers for which clay is remolded and compacted. The London clay was described as a primarily illitic clay, with small amounts of kaolinite and smectite whereas the Kimmeridge clay was not described in detail except for the fact that it is very stiff to hard, and silty. Lineham performed two different types of gas breakthrough tests: low pressure, where the maximum pressure was 1.0 MPa, and high pressure, where the maximum pressure was 12.4 MPa. In these tests, an axial force was used to simulate the pressure at the burial depth of the specimen in the repository. Water-saturated nitrogen gas was then applied to one side of the specimen and increased in increments which ranged from 0.2 MPa to 1.0 MPa (generally ≈ 0.34 MPa). In the high pressure tests, gas breakthrough occurred from 3.45–6.21 MPa, and was correlated to the pore size distribution of the clay. Lineham found that the low pressure tests lasted about 4 months. Slow formation of a gas bubble on the outlet side was taken as a sign of diffusion of gas, as opposed to advection.

Volckaert et al. (1993) performed a number of different types of tests on Boom Clay, including one dimensional oedometer tests in which hydraulic conductivity and gas

breakthrough were measured. The hydraulic conductivity of a natural Boom clay was first determined. A gas pressure was then applied to one side of the specimen and increased step-wise until breakthrough occurred. After gas breakthrough, the specimen was re-saturated and subjected to another hydraulic conductivity and gas breakthrough cycle. It was found that the gas breakthrough pressure and hydraulic conductivities were quite reproducible. However, gas flow measurements were not as reproducible. Volckaert et al. concluded that the specimens were not permanently altered by the gas breakthrough process. The degree of saturation of the specimens after the gas breakthrough tests (prior to the re-saturation process) were also measured. Most degrees of saturation were found to be above 90%, leading the researchers to believe that the gas flow occurred through only a few paths, similar to Pusch's observation for MX-80 bentonite. A detailed conceptual model which combined concepts found in the literature with experimental observation was developed by the authors.

A radial gas flow test was also reported by Volckaert (1993) in which gas pressure was applied through a hollow needle installed in the centre of a specimen. These tests were meant to model radial gas flow from a breached canister inside a repository. Preliminary results were reported for Boom clay and a "more permeable" Pontida clay. The gas breakthrough pressures were of the same magnitude as the previous one-dimensional flow tests.

Horseman and Harrington (1994) performed gas breakthrough tests on natural Boom clay specimens with an average ρ_d of 1.63 Mg/m^3 . The effect of anisotropy was

examined by testing specimens with axes both parallel and normal to their bedding planes. Specimens were first saturated with synthetic pore fluid, and a hydraulic conductivity test was conducted. Then water-saturated helium gas was applied to one face of the specimen with steadily-increasing pressure until gas breakthrough. A confining pressure of 4.4 MPa was applied externally to the specimens throughout these tests. Gas breakthrough pressures were measured in terms of excess pressure (or deviator pressure) and ranged from 1.2 - 1.9 MPa for tests normal to their bedding planes to 0.5 - 1.0 MPa parallel to their bedding planes. Only a small number of tests (5) were performed for this study, so it is difficult to draw any positive conclusions from this work. However, each test was documented in great detail. The strength of this study lies primarily in the thorough review of pertinent theories and models. In a later study, Horseman and Harrington (1997) tested pure MX-80 bentonite with similar test procedures, however the confining pressure was 16 MPa. The results of a typical test with $\rho_d = 1.64 \text{ Mg/m}^3$ showed that excess pressure at breakthrough was $\approx 15.0 \text{ MPa}$. When the pressure was reduced and then increased again, the breakthrough pressure was reduced to $\approx 14.3 \text{ MPa}$. The authors suggested that this decrease in gas breakthrough pressure was due to the formation of preferential pathways. The results are so similar however that they may be taken to be normal variation in the data, and not a significant trend.

Tanai et al. (1997) performed gas breakthrough tests on three water saturated Kunigel (primarily bentonite) specimens and one Fo-Ca clay (primarily kaolinite) specimen at ρ_d from 1.6 - 1.8 Mg/m^3 . The specimens were 50 mm in diameter and 50 mm in height; the permeating gas used was argon. Gas breakthrough pressures (referred to as

threshold pressures) were between 1.4 and 4.0 MPa. The breakthrough pressures of the Kunigel were found to correlate well with their swelling pressures. Another group of Japanese researchers, Hokari et al. studied gas breakthrough pressures of unsaturated bentonite/sand mixtures at a very low bentonite content of 15 percent and a ρ_d of 1.8 Mg/m³. The gas breakthrough pressures were extremely low, 0.01 - 0.06 MPa, which was related to the low bentonite content. The effects of specimen size on hydraulic conductivity and gas breakthrough pressure were also investigated. Specimen height and diameter were both varied. Hydraulic conductivity was independent of specimen size, whereas gas breakthrough pressure was independent of height but decreased with increasing diameter. The number of tests (6), and scatter in the data suggest that more research in this area should be done before these tests are considered conclusive.

The experimental work described in Chapters 5 and 6 is a continuation of the work of Kirkham (1995) who tested compacted saturated and unsaturated illite specimens using distilled water as the pore fluid. The specimens were 50.7 mm in diameter and 24 mm in height and were compacted to ρ_d from 1.87 - 2.06 Mg/m³. The gas pressure (argon) was increased at a rate of 0.2 MPa every five minutes until gas breakthrough, which occurred from 0.4 - 6.4 MPa. A good correlation between the gas breakthrough pressure and the AEV derived from capillary theories was found for these tests. Kirkham also performed 6 tests on the reference buffer material (RBM) material, a 50% bentonite, 50% sand mixture at $\rho_d = 1.67$ Mg/m³ and $\rho_c = 1.22$ Mg/m³ at saturations from $S_r = 75 - 98\%$. However, in only one of these specimens was the gas

breakthrough pressure attained before the upper limit of the test equipment was reached at ≈ 9.5 MPa.

The testing on saturated and unsaturated bentonite described in Chapters 5 and 6 was carried out collaboratively by the author and Hume (1998). The test parameters were identical to those performed by Kirkham (1995), described above, except that bentonite at $\rho_d = 0.9 - 1.2 \text{ Mg/m}^3$ was used. Since gas breakthrough pressures in the tests on saturated bentonite were found to be higher than the upper limit of the test equipment (≈ 9.5 MPa), Hume went on to construct a higher pressure apparatus with an upper pressure limit of 50 MPa. He then performed increasing pressure tests on saturated and unsaturated bentonite at $\rho_d = 0.6 - 1.5 \text{ Mg/m}^3$ and $S_r = 75-100\%$, using a number of different saturation procedures. The gas breakthrough pressures for bentonite varied with ρ_d , S_r , and saturation procedure. Generally, for $\rho_d \geq 0.8 \text{ Mg/m}^3$ and $S_r > 75\%$ no breakthrough would be attained before the upper limit of the apparatus was reached at 50 MPa. However, the reproducibility of the tests was low. Hume also performed constant pressure tests on saturated bentonite with $\rho_d = 0.8 - 1.4 \text{ Mg/m}^3$ and applied pressure $P_g = 0.3 - 19.8$ MPa. Hume found that if the inlet pressure was held constant, gas breakthrough pressure was an inverse function of time for 100% bentonite specimens.

2.6.1. Current gas migration concepts

Although many different researchers have conducted gas breakthrough tests with different clays, gases, and test procedures, only a few basic hypotheses have been described by the researchers. Many of the researchers base their hypotheses on the

concept of capillarity (or the AEV) of the soil, as discussed in Section 2.5. Pusch uses a microstructural model to explain that as the clay becomes more dense, the frequency and size of continuous pores available for gas flow will decrease. When the external gas pressure is great enough to enter the throat of the largest continuous pore, it will push the water ahead of it until the gas reaches the opposite side of the specimen and breakthrough occurs. If the pressure is further increased, smaller and smaller pores will be intruded, and more and more gas pathways will be formed.

Pusch also relates the breakthrough pressure to the swelling pressure by explaining that clay gels of a lower density emanate from the peds and temporarily fill the larger continuous pores (upon uptake of water). The applied gas pressure must be great enough to overcome the mechanical strength of the clay gel before gas breakthrough will occur. Pusch states that the mechanical strength of these gels "is related to the bulk strength of the clay, of which the swelling pressure is a practical and relatively easily determined property." Pusch supports this statement by presenting empirical data showing that the gas breakthrough pressure is 50-90% of the swelling pressure.

Lineham (1989) also found the gas breakthrough pressure was dependent upon the AEV of the soil (at high pressures). In his low pressure tests, Lineham found that gas moved through diffusion.

Volckaert et.al.(1993) and Horseman and Harrington (1994) present a more detailed model for gas flow which builds upon the capillary model of Pusch. These researchers state that the matric potential of a soil arises from the interaction of the soil matrix with

water. The matric potential of a soil after loading, $\Psi_{m\sigma}$, will be equal to the pore water pressure of the soil, u_w , which is in turn equal to the matric potential of the soil before loading, Ψ_{m0} plus the total stress, σ , multiplied by a compressibility factor, α as shown in Equation 2.18:

$$\Psi_{m\sigma} = u_w = \Psi_{m0} + \alpha\sigma \quad [2.18]$$

where:

- $\Psi_{m\sigma}$ = matric potential after loading
- u_w = pore water pressure
- Ψ_{m0} = matric potential before loading
- σ = total stress
- α = compressibility factor, (from 0-1)

The compressibility factor ranges from 0.02 for sand to 1 for a pure clay such as bentonite. A compressibility factor of 1 represents the fact that in a pure clay, the application of an external pressure will be initially taken up by an increase in pore water pressure. (Conversely, for a sand the external pressure will result in an increase in the mineral-mineral contact stresses since the excess porewater pressure will rapidly dissipate due to drainage.) A drained condition is implicit in equation 2.18.

Building upon the above equation, the model states that there are four different conditions under which gas can flow in a clay:

1. When the applied gas pressure, P_g , is less than the difference between the pore water pressure and the matric potential before loading, then no flow of gas will occur except by diffusion in the pore fluid.

$$\text{diffusion: } P_g \leq u_w - \Psi_{mo}$$

2. When the applied gas pressure is greater than the difference between the pore water pressure and the matric potential before loading but less than the compressibility factor times the total stress, then flow will occur by two-phase flow (or by overcoming the AEV).

$$\text{two-phase flow: } u_w - \Psi_{mo} \leq P_g \leq \alpha\sigma$$

3. When the applied gas pressure is greater than the compressibility factor times the total stress, then flow will occur by pore dilation and flow along preferential pathways or microcracks. Note: since $\alpha=1$ in pure clays, there will be no two phase flow, only pore dilation.

$$\text{pore dilation: } P_g \geq \alpha\sigma$$

4. Tensile fracturing will occur when the applied gas pressure is much greater than the total stress.

$$\text{tensile fracturing: } P_g \gg \alpha\sigma$$

Later testing by Horseman and Harrington (1997) on pure MX-80 bentonite was used to support the concept (point number 3) that two phase flow cannot occur in pure clays. The observation that the gas breakthrough pressure was lower in repeat gas breakthrough tests on the same specimen was used to suggest that microcracks had formed in the first cycle of the test. However, the variation in the two gas breakthrough pressures was so small that it could have been simple variation in the data instead of a marked trend, as suggested. They also state that the increase in gas permeability on the virgin breakthrough line is an indication of the occurrence of pore dilation. Interestingly, the researchers state that "passage of a gas phase through the initially water-saturated buffer clay is only possible if the gas pressure slightly exceeds the sum of the external water pressure and the swelling pressure". This latter concept was not developed in detail.

Wikramaratna et al.(1993) and Wikramaratna and Goodfield (1994), present a simplified model which is similar to that of Volckaert et al.(1993) noted above, but instead of pore dilation, a concept of displacement of aggregates similar to that presented by Pusch, is used.

Jeffries (1991) conducted a theoretical study of the migration of gas within a repository. The concepts mentioned in the model of Wikramaratna et al. were discussed, along with a comprehensive study of factors which could affect gas migration including workmanship, fire and/or explosions, and tectonic movements which could detrimentally effect the buffer. This study provided a thorough review of all existing literature and

theory, however no conclusions can be drawn from it due to the absence of experimental work.

Kirkham (1995) found that the gas breakthrough pressure of compacted illite correlated well with the AEV for illite, but the correlation was not as good for bentonite, likely because of the large volume of bound water associated with bentonite's large specific surface areas. Kirkham found that gas breakthrough pressure increased with increasing p_d and S_r and that at $S_r < 80\%$, there was little resistance to gas breakthrough. This research program is a continuation of the work done by Kirkham.

Hume (1998) found that if the inlet pressure was held constant, gas breakthrough was related to time for bentonite specimens, and could be predicted well using the Kozeny-Carman equation, which describes viscous flow. Gas at high pressure would break through in a short time, while lower pressures would require longer times. This finding is different from the results of most other researchers who related gas breakthrough solely to the AEV of the clay. All of the constant pressure tests on bentonite led to breakthrough, even at pressures as low as 0.3 MPa (for a specimen with $\rho_c = 1.0 \text{ Mg/m}^3$). Hume states, however, that there might be an AEV below which no breakthrough would occur, but it must be lower than the range of pressures tested in his research program.

2.6.2. Outstanding issues in gas migration research

Due to the differences among the studies described in preceding sections, it is difficult to provide a summary and comparison of the research completed to date. Most of the

research is specific to the given country's repository concept. As a result, a number of inadequacies exist in the body of research to date. These inadequacies are listed below:

- Only a small number of clay materials have been studied, as each researcher focused generally on one material. Given the small range of test materials, differences in gas migration characteristics among different clay minerals have not been studied.
- The effect of sand in a clay/sand mixture has not been investigated and an "optimum" sand content has not been found.
- The state of saturation of the test materials has been inadequately studied, as most researchers assume saturated conditions, although evidence to support this fact is generally not given.
- Unsaturated materials have only been briefly studied (Hokari et al. 1997, Kirkham 1995).
- Effects of test parameters such as specimen size (Hokari et al. 1997, Kirkham, 1995), type of permeating gas, and rate of pressure application have only been briefly touched upon.
- Although many researchers state that gas flow occurs through microcracks in pure clays, a detailed microstructural investigation has not been performed to reinforce this theory.

The deficiencies which exist in the state of understanding of gas migration in clay buffers were examined. An experimental program was then constructed to address

some of these deficiencies. The development of this experimental research program is discussed in the following chapter.

3. DEVELOPMENT OF RESEARCH PROGRAM

3.1. SCOPE OF RESEARCH

This research program was undertaken to examine deficiencies in the body of gas migration research noted in Section 2.6.2. In the past five years, awareness of the importance of gas migration has been increasing within the community which researches and designs engineered clay barriers. A number of issues must be investigated before any positive statements can be made regarding gas flow within compacted clay buffers. This research program was undertaken in order to advance the level of understanding of gas flow within engineered clay buffers.

The review described in Chapter 2 has led to the following hypothesis:

Gas flow in compacted clays is controlled by pore structure, clay-water interaction, and pressure gradient.

To test this hypothesis, the following objectives have been formulated to define the scope of the research in this program.

1. to investigate and explain the effect of clay mineral type on gas migration through a compacted clay buffer.
2. to investigate and explain the effect of sand in a clay/sand material on gas migration through that material
3. to investigate the importance of test parameters such as rate of pressure application and their effect on test results

4. to produce test data which will provide support for the investigations described in points 1, 2, and 3.

3.2. TESTING PROGRAM

To allow direct comparisons, test parameters for "standard" tests were chosen to correspond with those used in previous tests in the Canadian research program (Kirkham, 1995). The standard test parameters are outlined in Table 3.1. The majority of the tests were done using step-wise pressure increments of 0.2 MPa every five minutes. In illite and illite/sand, the specimens had a range of effective clay dry density, ρ_c , of 1.23 - 2.08 Mg/m³ and a range of degree of saturation, S_r , of .45 - 1.00. In bentonite, specimens had a range of effective clay dry density ρ_c , of 0.60 - 1.20 Mg/m³ and a range of degree of saturation, S_r , of .60 - 1.00.

3.2.1. Illite/sand mixtures

It has been shown in previous studies on saturated clay/sand mixtures that sand in clay/sand mixture is a filler and that the clay content controls the properties of the mixture. Effective clay dry density, ρ_c , is defined as the mass of clay divided by the volume of the clay and the void space within a specimen. The sand is excluded and assumed to be an inert filler. The effective clay dry density of a clay/sand mixture has been shown to control hydraulic conductivity (Dixon et.al. 1987), and swelling pressures (Gray et.al.1985) provided that the clay content exceeds about 20% for bentonite.

It was hypothesized by the author that the effective clay dry density would also control the gas breakthrough pressures within a illite clay/sand mixture since advective processes would occur only in the clay portion of the mixture. Illite was chosen for this

study due to its relatively inactive character, and because a relatively large body of existing data for 100% illite was already available (Kirkham, 1995). Four different illite/sand test series (IS) were planned and executed, each with a different illite/sand ratio (25/75, 37.5/62.5, 50/50, and 75/25). For these tests, three parameters (ρ_c , ρ_d , and S_r) were taken into consideration when planning the program. The target ranges for these parameters are shown in Table 3.2. Using constant values of ρ_c , mixtures with different percentages of sand could be compared to each other. Table 3.2 shows that the ρ_d and ρ_c ranges for the series overlap.

3.2.2. Bentonite

A program of tests on both saturated and unsaturated bentonite was carried out collaboratively with H.B. Hume. Data collected by Hume are indicated clearly in subsequent sections. The maximum achievable dry densities for a given compactive effort for bentonite as obtained from the Modified Proctor test ($\rho_{d,max}(\text{bentonite}) = 1.3 \text{ Mg/m}^3$) are lower than for illite ($\rho_{d,max}(\text{illite}) = 2.0 \text{ Mg/m}^3$). As a result, the ρ_d values for both clay types were prepared within $\pm 0.2 \text{ Mg/m}^3$ of the $\rho_{d,max}$ for the specific clay so that results from tests on different clays could be compared. Another factor in the choice of ρ_d for the bentonite tests was the upper pressure limit of the apparatus ($\approx 9.5 \text{ MPa}$) since in the first few tests it was found that at $\rho_d > 1.0 \text{ Mg/m}^3$ the upper limit of the apparatus would be reached before gas breakthrough occurred.

Two test series were created, one where the tests were carried out directly after compaction without a saturation phase, and a second which included a saturation phase after compaction but prior to the gas breakthrough test. The tests that were

carried out directly after compaction are referred to as the bentonite “unsaturated” (or BU) test series. The test series that included a saturation phase will be referred to as the bentonite “wetted” (or BW) series, since full saturation was frequently not achieved. The target test parameters for both the unsaturated and wetted bentonite series are listed in Table 3.3.

3.2.3. Bentonite and illite wetted with a non-polar fluid

Early in the conduct of the bentonite test series, it was observed that bentonite exhibited a much higher gas breakthrough resistance than illite. Due to the clay-water interactions discussed in Chapter 2, it was hypothesized that the difference in the gas breakthrough resistance of illite and bentonite was due to bentonite’s tendency to form larger DDL’s which block flow paths. In order to test this hypothesis, a small testing program (the NPF series) was created using a non-polar pore fluid, paraffin oil. A non-polar fluid will not form DDL’s. These tests make it possible to observe flow behaviour in the absence of the DDL for both bentonite and illite. The ρ_d and S_r of these tests were chosen to directly correspond to tests that had already been carried out using water as a pore fluid. The target test parameters for the NPF series are outlined in Table 3.4.

3.2.4. Illite with modified pressure increment

A small testing program (series T) was created to investigate the rate of pressure application on the gas breakthrough response of illite specimens. This program used 100% illite at a ρ_d and S_r that had been repeated many times by the author and Kirkham (1995). The target parameters for this test series are outlined in Table 3.5. The only difference between the tests was the rate of pressure application. Some of

the tests had increasing pressure applied to them while others were conducted at constant pressure until gas breakthrough occurred.

4. TEST EQUIPMENT AND PROCEDURES

The equipment used for this testing program is located at the Geotechnical Laboratory of the University of Manitoba. Two identical sets of equipment were used. The equipment was originally assembled by T. Kirkham who provided a detailed description of the equipment and test procedures (Kirkham 1995). The following chapter outlines the equipment and procedures for gas breakthrough tests. Deviations from the equipment and procedures reported by Kirkham are noted.

4.1. TEST EQUIPMENT

4.1.1. Gas breakthrough equipment

The gas breakthrough test equipment consists of a test cell, a gas system and a water saturation system. Figure 4.1 shows a photograph of a test cell and the accompanying control board. A schematic diagram is shown in Figure 4.2. Pressure transducers and Bourdon gauges form the instrumentation component of the equipment. The gas system, water saturation system, and instrumentation will hereafter be referred to as the "test board". The test boards are described in detail in Kirkham (1995).

The test cell consists of a thick-walled stainless steel sleeve with two end flanges. The test cell attaches to the test board for testing, and is detached for specimen preparation and dismantling in a separate room. The specimen is compacted directly in the test cell to minimize specimen disturbance and to improve adhesion between the specimen and the cell wall.

The water saturation system (shown as dashed lines in Figure 4.2) was used to saturate specimens that were not at full saturation after compaction. The water saturation system consists of a water reservoir attached to a flow meter which is in turn attached to the specimen itself with stainless steel tubing and a number of valves. The flow meter measures water inflow to the specimen. In the sight burette of the flow meter, the movement of coloured paraffin oil indicates flow of water into the test cell. Changes in water inflow as small as 0.01 ml can be measured with the sight burette.

The gas system consists of a gas supply in the form of an argon gas cylinder, a gas collection tank (on the outlet side of the specimen) and associated tubing, valves, and gauges (shown as solid lines on Figure 4.2). The pressure in the argon cylinder (usually > 16 MPa) provided pressure for the purposes of this testing program. Argon was chosen because it is inert, and has low solubility in water (Kirkham, 1995). The actual gases that would be produced within a repository environment (among them methane and hydrogen), were not used due to the risk of fire or explosion. Since argon does not dissolve in water or alter the pH of the water, it is not expected to alter test results. Procedures for operating the equipment will be described later in this chapter.

4.1.2. Data acquisition

The data acquisition system consists of pressure transducers and data acquisition software. The latter is loaded on a personal computer adjacent to the test boards. A schematic diagram of the data acquisition system can be found in Figure 4.3. Each set of test equipment had three pressure transducers (1P, 2P and 3P in Figure 4.2) which measured the gas inlet pressure on the upstream side of the specimen, gas outlet

pressure on the downstream side of the specimen, and fluid pressure within the saturation system, respectively. On excitation from a constant voltage power supply, the transducers sent analog signals through to an analog-digital converter card. This card converted the signals into digital format which was converted into engineering units using the data acquisition software.

The data acquisition software used was LabTech Notebook v.7.3. The software allowed the tests to be monitored on the adjacent computer screen in real time, and also wrote the test data to a file which was stored for future analysis. The pressure transducers' signals are emitted as voltage (mV). The software was configured to convert this voltage to a pressure (in kPa) using the scale factor and offset constant obtained by calibration, using the following equation:

$$P = f(c + V) \quad [4.1]$$

where: P = pressure (kPa)

f = scale factor (a constant)

c = constant

V = voltage (mV)

Readings from the pressure transducers were taken by the data acquisition software ten times per second. These ten readings were then averaged for that second.

LabTech Notebook allows the user to input the frequency with which readings are sent to the screen or written to a file. Data were generally sent to the screen every second.

This rapid updating of the data allowed the pressures to be adjusted using the screen

as a guide. If there was a particularly long test, the data were written to the file less frequently to permit easier analyses. For example, for a constant pressure test spanning a number of weeks, data were written to the file only once every 240 seconds, whereas in faster tests, data were written to the file every 10 seconds. Time was also shown on the screen and written to the file using the computer's internal clock as a source. The excitation voltage was shown on the screen so that it could be monitored.

4.1.2.1. Calibration of pressure transducers

Pressure transducers were calibrated once when the test board was originally built, and then twice during the current testing program. The three calibrations produced closely similar results. Figures 4.4 through 4.9 show the three calibrations of the three transducers on each of the two test cells. Calibration was performed using a dead-load testing apparatus. Each pressure applied to the transducer registered voltage response. Using the known applied pressure of the dead load apparatus, a linear regression was performed on the results of the output from the transducers. The two variables: the scale factor (f) and an offset constant (c) were obtained from the regression.

Using the scale factors and offset constants from the three calibrations, graphs were plotted of transducer output (mV) versus reported pressure (kPa). Since the change in the offset constant among calibrations was proportionally larger than the change in scale factor, the difference between calibrations was generally constant throughout the whole pressure range. For example, a change in offset constant might cause every

reading of one set of calibration data to be 30 kPa higher than another set of calibration data. Due to this effect, the percentage difference between the calibrations was larger for lower pressures than for higher pressures.

The range of pressures for the gas breakthrough tests was approximately 0.2 - 9.0 MPa. For the lower pressure range, (0.2 - 2.0 MPa), the highest percentage difference among the calibrations was 23%, but the differences were generally less than 5%. For the higher pressure range (2.0 - 9.0 MPa), the highest difference was 2%, but the differences were generally less than 1.5%. Thus reported results are generally considered have an accuracy of $\pm 5\%$.

In most of the gas breakthrough tests reported, the pressure was increased in 0.2 MPa increments, each increment lasting 5 minutes. Breakthrough pressures have been reported in terms of these 0.2 MPa increments since it is impossible to know if or when breakthrough fell between increments. Because high precision in the measurement of breakthrough pressure was not possible, differences in the accuracy of the measurements were deemed to be acceptable. Pressures were double checked periodically using the Bourdon gauges mounted on the testing board. All data in this report were derived using the initial calibrations. This allowed a reference point from which to measure the largest possible error in the results.

Near the end of the testing program, the transducer with serial number 65841 malfunctioned due to damaged wires. The transducer was beyond repair and it was replaced by the transducer with serial number 65843.

4.1.3. Test cell

The cylindrical test cells were fabricated from stainless steel and consisted of a sleeve and two end flanges. The test cell is shown schematically in Figure 4.10. With the bottom flange attached to the sleeve, the specimen was compacted directly into the cell. The top and bottom flanges each had three orifices: two of which allowed the entry of water and gas, and the third vented to the atmosphere for flushing purposes. As shown in Figure 4.11, each orifice led to a series of grooves on the surface of the flange next to the specimen. These grooves allowed the fluid, whether it be gas or water, to flow over the entire surface of the filter stone. This facilitated permeation of the fluid into the specimen.

4.1.4. Compaction apparatus

The compaction apparatus consisted of a piston which was attached to a hand-operated hydraulic pump. A dial gauge mounted on the piston allowed for precision of up to 0.001" in the measurement of height of a given lift of soil. The piston of the compaction apparatus was also used to extrude the specimen upon completion of a test. Detailed description of the compaction apparatus was provided by Yarechewski (1993) and Kirkham (1995).

4.2. SOIL MATERIALS

4.2.1. Illite

The illite used for this testing program was marketed commercially by Canada Brick as "Sealbond", a mortar plasticizer. This illite is obtained from a Dundas shale member of the Georgian Bay Formation (Ordovician) that is described as a "soft, gray, illite-bearing

shale with moderate chlorite and no detectable expanding minerals, containing narrow, discontinuous limey and sandy interlayers” (Dixon and Woodcock, 1986). Properties of the illite are outlined in Table 4.1. The illite is of low plasticity, having a plasticity index (I_p) of 11.

4.2.2. Bentonite

Avonlea bentonite was used for part of the program. It is described as a greenish gray bentonite of the Upper Cretaceous Bearpaw Formation (Dixon and Woodcock, 1986). As shown in Table 4.1 Avonlea bentonite is a highly-plastic, swelling clay with a large specific surface area (because montmorillonite is the primary clay mineral). Bentonite is much different in character from the illite described in Section 4.2.1. Its plasticity index is 225.

4.2.3. Sand

The sand that was used for the tests was a fractionated silica sand or “frac sand”. Frac sand has been sieved so that all of the grains in a given category fall between two sieve sizes. For example, in 70 - 140 frac sand, all the sand will pass through a #70 U.S. Standard Sieve but will be retained on a #140 sieve.

Originally, it was thought that the same mixture of frac sand would be used for this testing program as was used for the Reference Buffer Material (RBM). It was found, however, that the two largest sizes of frac sand (8-12 and 12-20) caused scratching of the stainless steel material used for the test cells. To avoid damaging the cells, the two largest sand fractions from the RBM sand mixture were omitted in preparing specimens

for gas breakthrough tests. Table 4.2 shows the differences in particle size distribution between the sand used for RBM and the sand used for gas breakthrough tests.

4.3. TEST PROCEDURES

4.3.1. Soil preparation

4.3.1.1. Soil-water mixtures

Samples were mixed to a pre-determined water content and clay/sand ratio that provided the range of densities required by the test program. Clay and sand that had been oven-dried at 110°C were mixed with distilled, de-aired water (or paraffin in the case of a test series run with specimens using non-polar fluid). The quantities of soil and water required for a batch of soil were calculated using the equation:

$$w = \frac{M_w}{M_s} \quad [4.2]$$

Where: w = water content
 M_w = mass of water
 M_s = mass of soil, (for a clay/sand mixture, this value would be proportioned by weight as required, say 50/50 or 75/25)

The soil was then mixed with the water until the peds were as small as possible. To minimize water loss due to evaporation, mixing was done in a cool room where the temperature was held constant at 4°C. Generally, the largest peds which remained in

the mixture were about 2-4 mm in diameter. The soil mixture was then sealed in two plastic bags and placed in the cool room for three days to allow the water content throughout the entire batch to reach equilibrium.

4.3.1.2. Soil-paraffin mixtures

For specimens prepared using non-polar fluid, paraffin oil was mixed with the soil in place of water. The paraffin oil was of general laboratory grade, with chemical formula: C_nH_{2n} where $n= 14-24$. The specimens were made in such a way that it was possible to directly compare specimens that were prepared with paraffin with those prepared using water. That is, they were made at identical dry densities and degrees of saturation.

The clay that was used was oven-dried at 110°C for at least 24 hours, and then cooled in a desiccator prior to mixing with the paraffin. This was done in order to minimize the uptake of moisture from the air. It should be noted however, that a small amount of hygroscopic water (<5%) still remains when clay is dried in the above mentioned manner.

The mass of paraffin was calculated so that the volume of paraffin would be equivalent to the volume of water in the comparable water-based specimen. (Therefore, the degrees of saturation, specific volumes, and dry densities of both specimens would be the same.) Since the specific gravity of paraffin is less than 1, the mass of paraffin used to prepare such a specimen would therefore be less than the comparable water-saturated specimen. Due to the difference in specific gravities, the above formula for w , [4.2], was not appropriate for a paraffin-based specimen. The mass of paraffin required was calculated using the following equation:

$$M_{\text{paraffin}} = M_{\text{water}} \times G_{S(\text{paraffin})} \quad [4.3]$$

Where:

M_{paraffin} = mass of paraffin (g)

M_{water} = mass of water (in comparable specimen) (g)

G_s = specific gravity of paraffin (0.828)

4.3.2. Calculation of target parameters

Prior to preparation of a specimen, the “target” parameters for the test were evaluated from the experimental plan discussed in Chapter 3. There were three separate variables which were considered: water content (w), dry density (ρ_d), and degree of saturation (S_r). These variables are interrelated, so that if two are known, the third can be calculated.

The soil for a specimen was compacted in four lifts in order to achieve a constant dry density throughout. The mass of soil required for each of the four lifts was calculated using the following formula:

$$M_{\text{soil per lift}} = \frac{V_{\text{specimen}}}{4\rho_d(1+w)} \quad [4.4]$$

Where:

$V_{\text{specimen}} = \pi d^2 h / 4$ (cm^3)

ρ_d = target dry density (Mg/m^3)

w = target water content (as a fraction, e.g. 10% = 0.10)

The test volume inside the cell is 5.07 cm in diameter and 2.40 cm in height (for a volume of 48.45 cm³), so V_{specimen} is known.

The target water content (or the most recent water content test for a given batch) is used for the above calculation since the "initial" water content is not known at the time of compaction. Differences between the "target" and "initial" water contents sometimes result in a small difference between the "target" dry density and the "initial" dry density of the test.

For sand/illite mixtures, the effective clay dry density (ρ_c) of a specimen was also considered when determining the target parameters for a test. The effective clay dry density of a specimen is useful when examining the effect of the clay content on the behaviour of a specimen. Essentially, the sand within the specimen is assumed to be a filler which does not contribute to the behaviour of the specimen. In the calculation of ρ_c , the mass of clay is divided by the volume of the specimen minus the volume of the sand particles. Using ρ_c allowed specimens with different proportions of sand to be compared to one another. The effective clay dry density is calculated using the following equation:

$$\rho_c = \frac{M_{\text{clay}}}{V_{\text{specimen}} - V_{\text{sand}}} \quad [4.5]$$

Where: ρ_c = effective clay dry density (Mg/m³)
 M_{clay} = mass of clay (Mg)

V_{specimen} = volume of total specimen (m^3)

V_{sand} = volume of specimen occupied by sand particles (m^3)

4.3.3. Specimen preparation

Before soil that had already been mixed (as discussed in Section 4.3.1) was measured out for a specimen, it was warmed to room temperature while still sealed within two plastic bags. Three water content tests were then taken of the mixed soil. The results from these tests are referred to as the "initial" water content, and represent the state of the soil at the beginning of the test. The four lifts of soil needed to form the specimen were weighed out into small cups. The cups were covered to minimize the evaporation of water or paraffin.

Prior to specimen compaction, the bottom flange of the cell was attached using four small set screws. The cell was then placed open side up and a porous nickel filter stone was placed on the bottom of the cell. A filter paper was placed on top of the filter stone. The filter papers and stones were used to prevent migration of soil into the lines and valves. A cross-section of the test cell, specimen and filters was shown in Figure 4.10.

The first lift of soil was placed on top of the filter paper. The soil was compacted to a thickness of 6 mm (for a standard test) using a the compaction equipment described in Section 4.1.4. The top of the lift was then scored lightly using a pointed object in order to allow for better adhesion between successive lifts. On average, fourteen score lines

were used; seven in each of two perpendicular directions. The remaining three lifts were compacted in an identical manner. A filter paper was placed on top of the fourth lift, followed by a filter stone.

After the soil was compacted, the top flange of the cell was attached using four set screws. Six large threaded rods were then threaded through the sleeve and both flanges and tightened with nuts on each end. The cell was subsequently attached to the test board. A "quick coupler" arrangement was designed by the author to attach the leads from the test board to the cell. This simplified what was previously a difficult task. The leads to the test cell were fashioned in a way that they were readily accessible and could be easily attached.

4.3.4. Saturation procedure

Some of the specimens which had been initially compacted to less than 100% saturation were subsequently saturated within the test cell. The saturation procedure was used for only a limited number of tests. Specimens which did not include a saturation phase were said to be tested "as compacted".

The first step in saturation was to flush the leads and filter stones with water at atmospheric pressure. This was done with the flow meter isolated so that water used to saturate leads and filters would not be recorded as water inflow to the specimen. To accomplish the flushing procedure, the water inflow valve and bleed valve were opened simultaneously, allowing water to pass over the filter with minimal intrusion of water into the specimen. This was done at both ends of the specimen.

After flushing the leads and filters, the water system was pressurized to 0.2 MPa in order to expedite saturation of the specimen. Once the system was pressurized, the valve leading to the flow meter was opened. The principle used was one of dissolving air pockets into previously de-aired water at elevated pore back pressure. The valves connecting the water system to both ends of the specimen were then opened so that saturation could be achieved more quickly by allowing water uptake from both ends. Difficulties were encountered in achieving full saturation with a backpressure of 0.2 MPa, especially with specimens with low degrees of saturation at the time of compaction. This point will be discussed in more detail in Test Results, Chapter 5.

4.3.5. Gas breakthrough test procedure

Once the cell with its enclosed specimen was attached to the test board and the saturation phase had been completed (where required), the breakthrough portion of the test was commenced. First the data acquisition software was started, so that pressures could be monitored on the computer screen. The entire system was set to a backpressure of 0.2 MPa and the leads and filters were flushed with gas to remove any water and bring the whole system up to pressure. The gas outlet circuit was then isolated from the supply by closing a valve. With the gas outlet circuit isolated, any increase in pressure in the gas collection tank (Figure 4.2) was an indication of gas breakthrough, since this was the only way gas could get into the tank.

The gas pressure on the inlet side of the specimen was then increased in a series of pre-determined pressure increments. For standard tests, the inlet pressure was

increased by 0.2 MPa every 5 minutes. This pressure increment was chosen so that tests could be completed within one working day. For a test that went to the full capacity of the board (9.2 MPa), the gas breakthrough part of the test would take approximately 7 hours including installation, initial set-up, testing and decommissioning.

4.3.6. Post-breakthrough procedure

After a test was complete following breakthrough (or the upper pressure limit of the equipment was reached), all valves leading to the specimen were closed. The gas inlet and outlet circuits were brought back to atmospheric pressure by bleeding the lines. Any residual pressure in the test cell was then bled quickly. The cell was detached from the test board, and the clamping bolts and cell end flanges removed. The specimen was then extruded from the sleeve using the compaction ram and hydraulic pump described earlier. This procedure was performed as quickly as possible, since the removal of the end flanges exposed the specimen to air and potential loss of moisture through evaporation. The filter paper and stones prevented rapid evaporation.

The specimen was then cut into upper and lower halves, so that there was a disc of soil from the lower (inlet) side of the specimen, and one from the upper (outlet) side.

Division of the specimen into 4 separate zones for the purposes of water content tests is shown in Figure 4.12. The soil around the perimeter of each of these discs was removed. Water content tests were taken of these four specimens (gas inlet perimeter, gas inlet centre, gas outlet perimeter and gas outlet centre).

4.4. MERCURY INTRUSION POROSIMETRY PROCEDURES

4.4.1. Specimen preparation

Specimens for mercury intrusion porosimetry testing were prepared using similar procedures as for the gas breakthrough tests. Oven-dried illite and distilled, de-aired water were mixed and compacted in the manner described in section 4.3. However, the specimens were not tested in the breakthrough apparatus. The only difference from the standard compaction procedure was that some of the MIP specimens were compacted in one lift instead of four. There was concern that the interface between the lifts would become a fissure when the specimen was dried. This fissure would then fill prematurely with mercury during the intrusion process and would alter the test results.

Following compaction, the specimen was extruded from the cell without testing. It was broken into many small chunks, of about 2 grams each. A small chisel was used to break the specimen into chunks. Cutting the specimen with a knife would alter the pore size and shape at the surface of the specimen and was therefore avoided. The volume of the specimens was chosen to correspond with the chamber in the MIP testing apparatus, a Micromeritics "Auto Pore II - 9220" porosimeter at the laboratories of Atomic Energy of Canada Ltd., Pinawa, Manitoba. A specimen of 2 grams can be very nearly fully intruded with this apparatus and will produce the most meaningful results.

Two small "chunk" specimens were chosen from each large specimen. The chunks were selected to be free of visible fissures. Specimens were also chosen if they were

from the centre of the original large specimen where they would be least affected by the force of the compaction ram and cell walls.

The two small specimens were then carefully packaged and shipped to the AECL laboratory in Pinawa, where they were completely dried in a chamber in close proximity to sulfuric acid, a desiccant.

4.4.2. Procedure for mercury intrusion porosimetry tests

The MIP tests were performed by Mr. Brad Walker, technologist at the AECL laboratory. The dried specimen was placed in the chamber of the MIP testing apparatus and the chamber filled with mercury. The chamber was then pressurized incrementally. The pressure was held constant at each pressure increment until the intrusion of mercury had ceased. The termination of intrusion of mercury indicates that all pores large enough to be intruded at that particular pressure have been intruded. The cumulative volume of mercury intruded was then recorded before the pressure was increased again. Results of these tests will be described in Chapter 5.

5. TEST RESULTS

This chapter presents results of the testing program outlined in Chapter 3. Data for tests on illite/sand specimens will be discussed first, followed by results from tests on bentonite specimens and a number of specialized tests. A synthesis of the test results will be presented in Chapter 6. The gas breakthrough test results outlined in this chapter are for "standard" tests (with a pressure increment of 0.2MPa/5min), unless otherwise indicated.

In following sections and in the accompanying tables, the initial (or compaction) test parameters represent the state of the specimen at the time of compaction prior to the gas breakthrough test. Some of these parameters are measured (w , mass of soil compacted, volume of test cell), and others are calculated from the measured parameters (S_r , ρ_d , ρ_c). For the unsaturated tests, where no water inflow is permitted, the initial test parameters represent the state of the specimen at the beginning of the gas breakthrough test. Final parameters are those which were measured (w) and calculated (S_r) following the gas breakthrough test, after the specimen was extruded from the cell. A final dry density was not calculated from the final mass of soil, since losses of soil often occurred upon extrusion and slicing of the specimen. Therefore, the final mass used in calculating final dry density would produce inaccurate results.

For the purposes of this report, gas breakthrough pressure, P_b , is defined as the pressure level at which the first gas breakthrough response was noted. All gas breakthrough pressures are reported in terms of the pressure differential across the

specimen. Since the gas outlet backpressure is 0.2 MPa for all tests, the gas breakthrough pressure is the gas inlet pressure minus 0.2 MPa. Gas breakthrough was evidenced by an increase in the gas outlet pressure in excess of the backpressure and normal minor fluctuations, which were normally less than 5 kPa. Different tests had differing rates of gas breakthrough. In some specimens, gas breakthrough occurred rapidly, with the gas outlet pressure increasing by many MPa within a few seconds. In other tests, the gas outlet pressure would increase slowly, at a rate of only 10 kPa per minute. Systematic application of the above definition of gas breakthrough allows all tests to be evaluated, even with differing rates of gas breakthrough. The trends apparent in the different rates of gas breakthrough will be discussed later in this chapter.

A graph for each gas breakthrough test can be found in Appendix A. A representative sample of these graphs will be used to illustrate prominent trends in Figures 5.1 through 5.6. Some computer data files were accidentally overwritten or were not properly recorded. These graphs are identified with the words "data file not available". A manual backup record was kept for each test so the gas breakthrough pressure is still known even if the computer data file was lost. It should also be noted that several graphs show the gas collection line crossing the gas inflow line slightly following breakthrough. It is unlikely that the gasout pressure did actually exceed the gas inflow pressure. The minor variations in the calibrations of the pressure transducers, as discussed in Section 4.1.2.1 account for the phenomena.

5.1. ILLITE

5.1.1. Illite/sand mixtures (ISU)

Test specimens were prepared with varying ratios of illite to sand, degree of saturation, and dry densities. As described in Section 3.3.3, the target effective clay dry density, ρ_c , (or $\rho_{\text{clay dry}}$) was also taken into consideration when planning the initial test parameters. It should be noted that a number of tests are reported as having a degree of saturation slightly greater than 100 percent, which in theory is impossible. If an attempt was made to compact a specimen to a degree of saturation greater than 100%, a small amount of water could possibly have been driven out of the specimen into the lower filter paper and stone. It is also possible that there was slight variation in specific gravity which would result in a small error in the calculation of degree of saturation. Specific gravities, G_s , of 2.76 and 2.65 were used for illite and sand, respectively.

The following list outlines the number of tests carried out at each illite/sand ratio. The test ID names for this series begin with "ISU", meaning that these are illite/sand unsaturated tests. The number following these letters represents the illite content (i.e. ISU37.5-3 is the third test in the series which has 37.5% illite and 62.5% sand). The specimen conditions and gas breakthrough data for the illite/sand tests are shown in Tables 5.1 - 5.4.

- 75% illite / 25% sand - 10 tests (Table 5.1)
- 50% illite / 50% sand - 18 tests (Table 5.2)
- 37.5% illite / 62.5% sand - 10 tests (Table 5.3)
- 25% illite / 75% sand - 10 tests (Table 5.4)

5.1.1.1. Gas breakthrough response

Gas breakthrough pressure increased with increasing degree of saturation for all ratios of illite to sand. An example of this trend is illustrated in specimens ISU50-15 and ISU50-17, as shown in Figure 5.1. Each graph shows the gas inflow pressure being increased in 0.2 MPa increments every 5 minutes. When a response is noted in the gas collection pressure (the dashed line), gas breakthrough is said to occur. Arrows have been placed at the point of gas breakthrough. Both specimens have the same illite/sand ratio and dry density. However, ISU50-15 was compacted to a degree of saturation of 95.2% and had a gas breakthrough pressure of 3.2 MPa. The other specimen ISU50-17 had a lower degree of saturation of 80.6% and a lower breakthrough pressure of 1.0 MPa. This observation is similar to what Kirkham (1995) observed for 100% illite. He found that below a degree of saturation of about 80%, illite specimens did not exhibit any resistance to gas breakthrough. Of the five illite/sand specimens in this program that were compacted to a degree of saturation less than 80%, all broke through at the first pressure increment (0.2MPa). Six specimens were compacted to a degree of saturation between 80 and 85 percent; of these specimens three broke through at the first pressure increment (0.2 MPa) and the remainder broke through below 1.0 MPa. This finding is consistent with current hypotheses (Wheeler, 1988, Jeffries et al., 1991, Fredlund and Rahardjo, 1993) that state that the gas phase is continuous at a degree of saturation below about 85%, as discussed in Section 2.5. This would lead to very low or non-existent gas breakthrough pressures.

The gas breakthrough pressure also increased with increasing dry density. If saturation and illite/sand ratio were held constant, a specimen with the greater dry density would

have a higher gas breakthrough pressure. A typical illustration of this is shown in Figure 5.2, where the gas breakthrough graphs for specimens ISU50-5 and ISU50-14 are compared. Although they are both fully saturated, ISU-14 has a greater dry density and hence a greater gas breakthrough pressure. The specimen with a greater dry density would have lower porosity. A decrease in porosity would result in fewer, and likely smaller pores and hence an increase in gas breakthrough pressure.

The effective clay dry density, ρ_c , allows specimens of differing illite/sand ratios to be compared to one another by assuming sand is an inert filler. Gas breakthrough pressures of illite/sand mixtures show a greater dependence upon clay dry density than total dry density. This effect has been observed by other researchers for hydraulic conductivity and coefficients of diffusion (Gray et al. 1985, Dixon et al 1987). For example, specimens ISU50-12 and ISU37.5-8 shown in Figure 5.3 have closely similar dry densities, (2.15 and 2.14 Mg/m³, respectively) and degrees of saturation (93.7 and 93.6 %, respectively). However, their gas breakthrough pressures are different at 1.0 and 0.2 MPa, respectively. The difference in gas breakthrough pressure can be attributed to the fact that specimen ISU50-12 has a greater illite content (50% as opposed to 37.5% in specimen ISU37.5-8), and therefore has a higher effective clay dry density. The effective clay dry density of specimen ISU50-12 is 1.81 Mg/m³, whereas the effective clay dry density of specimen ISU37.5-8 is 1.65 Mg/m³.

Although gas breakthrough pressure did not show a strong correlation with the total dry density of the specimen, the rate of gas flow from the specimen following breakthrough generally decreased with increasing dry density. That is, specimens at the same

degree of saturation and clay dry density, but with different total dry densities due to their sand content would have approximately the same gas breakthrough pressures, but gas breakthrough response would be slower in the specimen with greater dry density. This effect can be seen in Figure 5.4, where the gas breakthrough responses of specimens ISU37.5-2 and ISU75-5 are compared. The specimens have almost identical degrees of saturation (84.6% and 84.8%) and effective clay dry densities (1.90 Mg/m^3), however, the specimen with 37.5% illite and 62.5% sand has a dry density of 2.30 Mg/m^3 as compared to the specimen with 75% illite and 25% sand which has a dry density of 2.02 Mg/m^3 . Specimen ISU37.5-2, which has the higher dry density, exhibits a slower rate of gas flow.

Generally, specimens with dry densities above 2.20 Mg/m^3 exhibited slow rates of breakthrough where those below 2.20 Mg/m^3 had relatively rapid gas breakthrough and rate increased with decreasing dry density. However, if the effective clay dry density was extremely low, as with the tests in the ISU25 series, gas breakthrough was rapid, regardless of dry density. In these specimens with very low effective clay dry densities, ($< 1.50 \text{ Mg/m}^3$) there appears to be a shift from a clay-dominated to a sand-dominated material. If materials that have a very low effective clay dry density are indeed sand-dominated, then it follows that gas breakthrough resistance would be minimal.

5.1.1.2. Variations in water content

Water content tests were taken following completion of gas breakthrough. As described in Chapter 4 and as shown in Figure 4.12, each specimen was divided into four for purposes of measuring water content (gas inlet perimeter, gas inlet centre, gas

outlet perimeter, gas outlet center). The ASTM standard for water content tests, D2216, states that a minimum of 20g of moist soil should be used per test. Almost all water content tests were performed using 20-30g of moist soil. There were a few tests, however, that had slightly less than 20g of moist soil.

A 95% confidence interval was used to determine whether differences in water content were significant or not. Generally, the difference is taken to be significant if zero is not a part of the 95% confidence interval. A 95% confidence interval is determined by the following equation:

$$\bar{d} \pm t_{\alpha/2, n-1} \cdot \frac{s_D}{\sqrt{n}}$$

Where: \bar{d} = the average of the differences

α = 100 - desired confidence interval (i.e. for a 95% interval, $\alpha = 100-95=5$)

n = the number of observations

s_D = the standard deviation of the differences

$t_{\alpha/2, n-1}$ = the value on the x axis of the t-distribution curve (with $n-1$ degrees of freedom) for which the area under the t curve to the right of t is $\alpha/2$. (the $t_{\alpha/2, n-1}$ values were obtained from Devore (1991)).

It would be expected that if gas was bypassing the specimen by traveling along the cell walls that the water content at the perimeter of the specimen would be significantly lower. However, the difference between the centre and perimeter water contents was not significant ($0.03 \pm 0.05\%$). As a result, the average of the two inlet and two outlet values was used to obtain the difference between the inlet and outlet sides of the

specimen. The difference between inlet and outlet water content was significant, with the inlet being less ($-0.30 \pm 0.12\%$) than the outlet. This is supported by the observation that the gas outlet side was visibly wetter (as evidenced by a darker colour) for many of the specimens upon extrusion from the test cell. If continuous gas pathways had formed by pushing water out of the pores, from the gas inlet to the gas outlet side, then this observation is also consistent with what would be expected. This observation is contrary however to researchers such as Pusch (1985) who took the absence of a difference in water contents between the gas inlet and outlet sides of bentonite specimens to mean that gas had traveled through only a small number of pathways. It is also contrary to the observations of Hume (1998) who observed a higher water content on the inlet side of bentonite specimens which were subjected to very high pressures of up to 50 MPa. This matter will be discussed further in Chapter 6.

5.1.1.3.Repeatability

Repeatability of these tests was good throughout all illite/sand ratios and ranges of dry density and degree of saturation . A few examples are given below:

Test	ρ_d (Mg/m ³)	S_r (%)	P_b (MPa)
ISU50-3	2.03	100.8	0.4
ISU50-4	2.04	100.1	0.6
ISU75-1	2.11	97.3	2.8
ISU75-2	2.10	95.3	2.8

5.2. BENTONITE

5.2.1. Wetted (BW)

This series of tests was performed on 100% Avonlea bentonite. The specimens were subjected to a saturation phase following compaction. They are referred to as “wetted” rather than “saturated” because full saturation was not achieved. Tests BW-1 through BW-6C (11 tests) are the work of the author, whereas tests BW-7 through BW-23 (16 tests) are the collaborative work of the author and H.B. Hume. These collaborative tests are also reported in Hume 1998.

The intent of this series of tests was to compact soil at varying water contents and saturate them by uptake of water. The effect of differing soil structures at the time of compaction could then be investigated. The results of these tests are shown in Table 5.5. Wetted specimens were saturated at a backpressure of 0.2 MPa until movement in the water inflow burette ceased, usually after about two days, as described in Chapter 3. In theory, the final degree of saturation calculated from the water inflow measurements should correlate well with the measured final degree of saturation. Table 5.6 shows calculations of final degree of saturation from water inflow measurements. Generally, the measured final degree of saturation was much higher than that calculated from the water inflow measurements. The possible explanation for this observation involves test procedures. The water inflow burette is isolated during the flushing of the filters, prior to the saturation phase so that water used to saturate the filters will not be measured as inflow to the specimen. It is possible however that water was traveling through the filters into the specimen during this flushing procedure,

especially for specimens compacted to low degrees of saturation with high levels of suction. This results in the inflow measurements underestimating the quantity of water that has entered the specimen.

Although all of the specimens reached 85-98% saturation, none were fully saturated. This is possibly due to the lack of an applied vacuum to remove air from the specimen. Some of the specimens were compacted to very low degrees of saturation of less than 60 percent. These specimens contained large amounts of air which would have to be displaced if true saturation was to occur. Work by Hume (1998) also suggested a backpressure of greater than 0.2 MPa is needed to saturate bentonite specimens within the time frame used for these tests.

5.2.1.1. Gas breakthrough response

For tests compacted to dry densities greater than 0.95 Mg/m^3 , there was no gas breakthrough before the upper limit of the test board, $\approx 9.2 \text{ MPa}$, was reached. Below 0.75 Mg/m^3 , the gas breakthrough pressures were generally very low, $< 1.0 \text{ MPa}$. All tests that did breakthrough showed rapid rates of breakthrough. In the threshold area between $0.75\text{-}0.95 \text{ Mg/m}^3$ the gas breakthrough pressure varied widely and did not seem to show strong correlation with either dry density or initial or final degree of saturation. The lack of correlation between gas breakthrough pressure and either initial or final degree of saturation might be because after the saturation phase, all tests have relatively high degrees of saturation (85-98%) resulting in a continuous water phase. Moreover, it is likely that the face of the specimen that was in contact with water was fully saturated. Gas would have to push water out of the pores at the gas

inlet face in order to enter the specimen. A further discussion of this phenomenon will be included in Section 5.2.2.

5.2.1.2. Variations in water content

The lateral variation in water content ($5.6 \pm 1.0\%$) was significant, with the perimeter water content being higher. This is different from what was found for illite specimens and is possibly due to the saturation procedure. Variation between the gas inlet and gas outlet sides ($3.2 \pm 4.5\%$), was not significant, also contrary to what was found for illite.

5.2.1.3. Repeatability

Repeatability was inconsistent in this test series. As discussed in the Section 5.2.1.1, for dry densities above 0.95 or below 0.75 Mg/m^3 , the tests were very repeatable. However, for dry densities in the threshold range, $0.75\text{-}0.95 \text{ Mg/m}^3$, the tests were not repeatable. For example, it would be expected that a specimen (BW-6) compacted to a dry density of 0.90 Mg/m^3 and having initial and final degrees of saturation of 60.3 and 94.4 , respectively, would have a higher gas breakthrough pressure than for a test which had lower dry density and degrees of saturation (BW-5B, $\rho_d=0.86 \text{ Mg/m}^3$, $S_{r(\text{compaction})}=54.7\%$, $S_{r(\text{final})}=87.1\%$). However, the opposite was true. Specimen BW-6 has a gas breakthrough pressure of 0.6 MPa , whereas the value for BW-5B was greater than 9.2 MPa .

5.2.2. Unsaturated (BU)

The testing on unsaturated bentonite was carried out collaboratively with H.B.Hume (1998). Twenty-nine tests were performed with dry densities ranging from 0.9-1.2 Mg/m³ and degrees of saturation from 60-99%. Since these specimens were to be tested in an unsaturated state, the saturation portion of the test was excluded. Table 5.7 contains the test data for this series. Some of the tests were carried out with wet filters in order to replicate test procedures and conditions used previously for the saturated tests. However, the majority of these tests (24) were carried out using dry filters. Wet filters made the data difficult to interpret, since the exact water uptake from the filters (and hence specimen saturation at the time of the gas breakthrough test) was not known.

5.2.2.1. Gas breakthrough response

The gas breakthrough pressure of these specimens showed a strong correlation with degree of saturation. Below a degree of saturation of about 90%, the specimens exhibited little gas breakthrough resistance. Above a degree of saturation of 90%, the gas breakthrough pressures rose sharply. For example, specimens BU-15, BU-11B and BU-19 (as shown in Figures 5.5 (a) and (b)) have dry densities of 1.10 or 1.11 Mg/m³. As the degree of saturation of the specimens increases, (82.2, 91.1, 97.6, respectively), so also does the gas breakthrough pressure (0.2, 0.6 and 5.4 MPa, respectively).

Gas breakthrough pressure also increased with increasing dry density, if water content was held constant. This also represented an increase in degree of saturation. For

example, the gas breakthrough pressure increased from 0.2 to >9.2 MPa in tests BU-6, BU-18 and BU-10 (as shown in Figures 5.6 (a) and (b)), where the water content was relatively constant within the range of 52.7-54.3% but the dry density increased from 0.90 to 1.13 Mg/m³.

Tests with wet filters seemed to have a significantly higher gas breakthrough pressure than those with dry filters. Tests BU-11 and BU-11B were compacted at a dry density of 1.11 Mg/m³ and water contents between 48.1 and 49.1% (for degrees of saturation of 90.1 and 91.0, respectively). Specimen BU-11 was compacted on wet filters and had a gas breakthrough pressure greater than 9.2 MPa. Specimen BU-11B, compacted using dry filters, had gas breakthrough pressure of 0.6 MPa. Furthermore, the average $w_{\text{gas inlet}}$ for specimen BU-11 had increased by 4.8% to 52.9% due to water uptake from the wet filters. Evidently, the gas inlet face of the specimen had a higher degree of saturation than the average for the specimen as a whole. This high degree of saturation on the face likely reduced the number of continuous gas pathways which explains the greater resistance to gas breakthrough of specimen BU-11.

All tests in which gas breakthrough was achieved exhibited rapid rates of gas breakthrough. This observation is opposite to that observed for illite. In bentonite, even specimens with high dry densities and degrees of saturation and correspondingly high gas breakthrough pressures show a rapid rate of breakthrough.

5.2.2.2. Variations in water content

The lateral variation in water content, between the perimeter and centre of the specimen ($0.4 \pm 0.6\%$) was not significant. The difference between the inlet side and outlet side of the specimen ($0.04 \pm 0.74\%$) was also not significant if the specimens compacted on wet filters were excluded. The specimens compacted on wet filters showed an elevated water content on the gas inlet side of the specimen. This is due to the fact that the specimens were compacted on a wet filter (on the gas inlet side) which increased the water content.

5.2.2.3. Repeatability

The tests were quite repeatable. Five of the six sets of repeat tests at similar dry densities and degrees of saturation had gas breakthrough pressures within 0.2 MPa of each other. The sixth repeat series of tests, BU-7, BU-7B and BU-7C, had closely similar conditions at the time of compaction, however the gas breakthrough pressures varied widely, 1.4, 4.8, and 3.6 MPa, respectively. These specimens had the highest degree of saturation of any of the repeat tests (98.5, 98.8, 97.8, respectively). These tests seem very sensitive to variations in either dry density or degree of saturation. Since the gas breakthrough response of the unsaturated bentonite tests as a whole increases sharply with degree of saturation, this might be the cause for these variations.

5.3. SPECIALIZED TESTS

5.3.1. Bentonite and illite with non-polar fluids (NPFU)

A small number of tests were carried out on illite and bentonite specimens which were prepared using a non-polar pore fluid, paraffin oil. The test ID's for these specimens start with either "INPFU" or "BNPFU", signifying either illite (or bentonite) non-polar fluid-unsaturated. Table 5.8 shows the specimen conditions and gas breakthrough results for this series.

Illite was mixed with paraffin oil to an effective water content of 12.0% (as discussed in Section 4.3.1.2) and was compacted to a dry density of 2.05 Mg/m^3 for an effective degree of saturation of 95.6%. These test parameters were chosen because they had been repeated as standard tests (using water) several times by the author with highly repeatable results. These four tests that have been performed on illite at similar dry densities and degrees of saturation are outlined in Table 5.9. The four standard illite tests had an average gas breakthrough pressure of 3.75 MPa. The two tests on illite which were mixed with paraffin had an average breakthrough pressure of 2.2 MPa, which is 59% of the standard test value.

Three tests were performed on bentonite, two mixed with water and one with paraffin. The two tests with water had quite different breakthrough pressures at 3.6 and 5.4 MPa. Repeatability of unsaturated bentonite tests in this range of degree of saturation is relatively low, as discussed in Section 5.2.2.2. However, for the purposes of this comparison, the average of the two standard bentonite tests is 4.5 MPa. The test

performed on bentonite that was mixed with paraffin broke through at the first pressure increment (0.2 MPa), which is 4% of the gas breakthrough pressure for a standard test. Moreover, the texture of bentonite that was mixed with paraffin was markedly different from that mixed with water. Bentonite mixed with paraffin did not form into peds and was “clumpy”, somewhat like flour mixed with oil. Bentonite mixed with water forms peds and has a dry “crumblike” appearance. In contrast, illite mixed with paraffin looked similar, if not drier, than that mixed with water.

5.3.2. Illite with modified time increments (ITU)

A small set of tests was performed on illite in which the rate of pressure application was varied. The name for this series is “ITU”, which signifies illite-time, unsaturated. The gas breakthrough pressures and specimen conditions for this series are shown in Table 5.10. Two “standard” tests were conducted on illite at a dry density of 2.04 Mg/m³ and a degree of saturation of 98.3%. These tests acted as the control specimens. Both standard tests had a gas breakthrough pressure of 3.6 MPa.

Two tests, ITU-1 and ITU-1B with dry densities and degrees of saturation closely similar to the standard were carried out using a pressure increment of 0.2 MPa per hour (as opposed to 0.2 MPa every five minutes for the standard tests). These tests broke through at 2.2 and 1.8 MPa, respectively. The average of these two tests, 2.0 MPa, is 56% of the standard value.

Six tests were then conducted where the pressure was constant. The time to breakthrough t_b was then measured. Tests ITU-3, ITU-4, ITU-4B, and ITU-5 were all

compacted to a dry density of 2.04 Mg/m^3 , and closely similar degrees of saturation (97.2, 96.9, 96.9, 97.2%, respectively). The results of these tests are outlined below:

Test ID	P_b (MPa)	t_b (hours)
ITU-5	0.8	>336 hours
ITU-3	1.8	22.7
ITU-4	2.8	0.3
ITU-4B	2.8	0.2

This data are interesting in that they suggest an inverse relationship between applied pressure and the time to gas breakthrough. In this set of data, the time to gas breakthrough increases exponentially with decreasing applied pressure. Tests ITU-1 and ITU-1B, where the average breakthrough pressure was 2.0 MPa ($t_b=8 \text{ h}$) can be compared to test ITU-3, where the pressure was constant at 1.8 MPa and the time to gas breakthrough was 22.7 hours. It would be expected that if the pressure were raised suddenly at the beginning of a test, that breakthrough would occur more quickly than a gradual increase in pressure. It is possible that some sort of occlusion of pores occurs due to the rapid application of pressure.

Two other tests, ITU-6 and ITU-7 were carried out at a lower degree of saturation, 94.1% but a higher dry density (2.06 Mg/m^3) than the others in this series. Test ITU-6 had a constant applied pressure of 1.8 MPa and broke through at 0.64 hours. Test ITU-7 had a constant applied pressure of 0.8 MPa and broke through in 0.5 hours. These test results seem counter-intuitive, since the test with the lower applied pressure broke through in a shorter period of time. Also, in tests ITU-3 and ITU-5, the times to

gas breakthrough were much higher than in comparable tests ITU-6 and ITU-7, even though the dry densities and degrees of saturation of the specimens were relatively close. It is very difficult to interpret the data from tests ITU-6 and ITU-7, however, since the illite used for these tests was from a different batch than that used for the rest of the testing program. The Atterberg limits, specific gravity, and particle size distributions for this new batch of illite were investigated, and they are closely similar to the old batch. The mineralogical composition might differ somewhat between the batches. However this has not been investigated.

5.3.3. MIP tests on illite (MIP)

Seven MIP tests were carried out on illite. The testing program was planned and the specimens were prepared by the author. They were then sent to AECL's Whiteshell Laboratories for MIP testing. The data presented for these MIP tests has been previously reported by the author in Gelmich (1994), and by Kirkham (1995). Most of the specimens show an incremental intrusion graph (or PSD) with two distinct peaks which can be interpreted as the inter and intra-ped pores. Figure 5.7 shows a series of tests that were compacted to a dry density of 2.04 Mg/m^3 , but at four different water contents. The specimen compacted at a water content of 10% had the highest peak at the 1 micron pore size which is the inter-ped level and the lowest peak at the 0.1 micron size which is the intra-ped level. Conversely, the specimen compacted at $w=13\%$ has the lowest peak at the 1micron size and the highest peak at the 0.1micron size. This illustrates the fact that as water content increases, the number of inter-ped pores decrease as the soil is able to deform and fill these pores. Soil with a lower

water content does not deform as much and hence does not fill as many of the inter-ped pores.

Figure 5.8 shows two different specimens that were compacted at the same water content, but to different dry densities. The specimen with the higher dry density has fewer pores, as would be expected from the resulting decrease in porosity. The lines have essentially the same peaks. However, the line that represents the higher density specimen is shifted downwards. In Figure 5.9 an example of a single-peaked incremental intrusion graph is shown. This specimen was compacted at a low dry density of 1.95 Mg/m^3 and a water content of 15% (which is wet of optimum). Even though the dry density is low and many pores would be expected, there is no second peak at the 1 micron level. The soil, which was at a high water content at the time of compaction, deformed to fill almost all of the inter-ped voids. The foregoing observations are consistent with those found by other researchers (Wan 1996, Delage and Graham, 1996) as discussed in Section 2.2.3.2.

6. DISCUSSION

6.1. DISCUSSION OF TEST RESULTS

6.1.1. Illite/sand mixtures

As discussed in Chapter 5, the gas breakthrough pressures of illite/sand mixtures depend on the effective clay dry density of the specimen. The gas breakthrough pressure also depends on the degree of saturation of the specimen. Figures 6.1 through 6.3 show gas breakthrough pressure as a function of effective clay dry density for different ranges of saturation for illite/sand specimens.

Figure 6.1 shows the relationship between gas breakthrough pressure and effective clay dry density for specimens with degrees of saturation from 85 to 90 percent. It should be noted that specimens of all illite/sand ratios that were tested (25/75, 37.5/62.5, 50/50, and 75/25) are included as points on this graph. The specimens with varying illite to sand ratios can be placed on the same graph because the effective clay dry density, not the total dry density, is used. The best fit line for the data points is shown as a dashed line. The coefficient of determination, r^2 , for this best-fit line is low at 0.478. Upon close inspection, it looks as if there might be a threshold effective clay dry density of approximately 1.8 Mg/m^3 below which the specimens will not have any resistance to gas breakthrough in this range of saturation. For specimens with effective clay dry density greater than 1.8 Mg/m^3 , the gas breakthrough pressure appears to increase linearly with increasing effective clay dry density.

For sake of comparison, best-fit lines for Kirkham's (1995) data for 100% illite were included in Figures 6.1 to 6.4 as solid lines. Kirkham divided his data into degrees of saturation of above 80% and below 80%. For 100% illite, the effective clay dry density and the total dry density would be identical. Since Kirkham reported his gas breakthrough pressures as total pressure (not pressure difference across the specimen as in this study), the illite/sand gas breakthrough pressures will also be reported as total pressure so that they can be directly compared. The backpressure was 0.2 MPa for all tests, so the gas breakthrough pressures reported here will be 0.2 MPa higher than those in the rest of this thesis. The best-fit line for the illite/sand mixtures at degrees of saturation between 85 and 90 percent falls between the >80% and <80% degree of saturation lines for 100% illite, as would be expected.

For specimens with degrees of saturation between 90 and 95 percent, the best-fit line has a very high coefficient of determination of 0.9368, as shown in Figure 6.2. This means that the best-fit line represents the data very well. This line also falls between the >80% and <80% lines for 100% illite, as would be expected.

Figure 6.3 shows the data for specimens with a degree of saturation between 95 and 100 percent. The best-fit line fits the data very well, with a coefficient of determination of 0.8807. This line is above the >80% line for 100% illite. This is expected since the average saturation of the data points included in the 95-100% line for illite/sand mixtures would be higher than the >80% line for 100% illite. It follows that at the same effective dry density, a population of specimens with a higher average degree of saturation would also have a higher average gas breakthrough pressure.

Figure 6.4 is a summary of all the best-fit lines for each group of data points. This graph clearly shows that illite/sand mixtures of differing clay/sand ratios can be compared with each other, as well as with 100% illite specimens on the basis of effective clay dry densities. All else equal, an increase in effective clay dry density will result in an increase in gas breakthrough pressure. The increases are substantial for effective clay dry densities of greater than 1.6 Mg/m^3 . If sand in a clay/sand system behaves as an inert filler, then the porosity in the clay portion of the structure would control its behaviour. All else equal, an increase in effective clay dry density would result in a decrease in porosity, which would result in a decrease in pore frequency. A reduction in the size of the pores would also be expected. It follows that this reduction in both the frequency and size of pores would result in a decrease in paths available for flow, and ultimately an increased gas breakthrough pressure in tests using incremental loading procedures.

6.1.2. Wetted bentonite

A summary graph of the test data for wetted bentonite is presented in Figure 6.5. The figure shows the test data in a three-dimensional dry density/water content/gas breakthrough pressure space. Tests in which gas breakthrough was achieved are denoted as white triangles. Tests in which the upper limit of the testing apparatus was reached before gas breakthrough are shown as black triangles. It is apparent from the graph that there is a threshold dry density of approximately 0.90 Mg/m^3 , above which no gas breakthrough was achieved before the upper limit of the testing apparatus was reached (9.2 MPa). This threshold dry density was regardless of degree of saturation.

Below a dry density of approximately 0.70 Mg/m^3 , the specimens exhibited little resistance to gas breakthrough, regardless of degree of saturation. In the range of dry density between $0.70 - 0.90 \text{ Mg/m}^3$, the gas breakthrough pressures were highly variable, ranging from 0.2 MPa, to greater than 9.2 MPa. This set of test data is difficult to interpret since each specimen was unsaturated upon compaction and an attempt was made to saturate it within the test cell. Although none of the specimens were fully saturated at the time of testing (as shown in Table 5.5), possible saturation at the faces of the specimen might have impeded gas flow. Since the final water content tests are closer to the actual state of the specimen at the time of testing, the final water contents were used for this graph.

6.1.3. Unsaturated bentonite

The test data for the unsaturated bentonite series is shown in a three-dimensional space in Figure 6.6. Since these specimens were tested as compacted (without a saturation phase), the complicating factors of incomplete saturation, or saturation gradients throughout the specimen are not a factor as they were with the "wetted" series. With the unsaturated specimens, the gas breakthrough pressure depends highly on the degree of saturation. In Figure 6.6, it can be seen that below a degree of saturation of about 93%, there is very little resistance to gas breakthrough. Above a degree of saturation of 93%, as full saturation is approached, the gas breakthrough pressures increase sharply. As the degree of saturation approaches 100%, more and more pores are filled with water, and the continuous gas pathways become occluded. When a specimen is fully saturated, gas must push water out of continuous pores from the inlet side of the specimen to the outlet side in order to initiate gas breakthrough. If

the gas inlet pressure is not great enough, or the time of the test is not long enough, then no breakthrough will be observed for that test. It is interesting to note that gas breakthrough pressures increase much more sharply as full saturation is approached in bentonite than in illite. This difference can be attributed to the different chemical reactions within the pore water - clay mineral systems. This point will be discussed further in following sections.

6.2. SYNTHESIS OF TEST RESULTS

After examining the test data, a conceptual model was devised to explain the flow phenomena in illite and bentonite. In many instances, the experimental observations for illite were very different from bentonite. The model presented in the following sections will explain the differences in flow behaviour between the different clays through use of theories of soil structure and flow phenomena.

6.2.1. Flow phenomena

Various flow phenomena were discussed previously in Section 2.4. Capillarity was discussed first, since it is the simplest model for flow. Essentially, the capillary model (or Air Entry Value model), states that if the applied pressure is great enough to overcome the capillary forces within a pore, then the pore will drain. In real systems, however, there are other factors which impede pore drainage. Factors such as viscosity of the pore fluid, and magnitude of the applied pressure were included in the Poiseuille model. A representation of the pores within a real system is presented in Figure 6.7. The diagram shows the inter-ped pores on an exaggerated scale for the sake of demonstration. As shown on this figure, flow paths (a) and (b), are continuous, while flow path (c) is not continuous and will not contribute to flow. From this diagram,

it can be shown that flow paths are tortuous, pores are not perfectly circular, and pore diameter varies within the flow path of a real system. The Kozeny-Carman model introduced factors which accounted for tortuosity of the flow path, and the fact that pores within a soil are generally not perfectly cylindrical capillaries. A visual representation of the factors used to approximate a real system is shown in Figure 6.8. It is important to note, however that none of the flow models take into account the variation in diameter among the flow paths, or within a single flow path. This is represented in Figure 6.8, which shows all flow paths are identical.

If the pressure applied to a soil simply is not great enough to overcome the capillary forces in even the largest possible continuous flow channel, then no flow will occur. This is rarely the case, however. Using the capillary model, it can be calculated that pore sizes of $0.3 \mu\text{m}$ and larger will have AEV's of less than 1.0 MPa. Pore size distributions for illite obtained from MIP tests indicate that the average of the large pore mode is approximately $0.3 \mu\text{m}$. The average large pore mode in bentonite is approximately $20 \mu\text{m}$. These values do not take electro-chemical effects into account. Clearly, if pore size distribution was the only factor affecting gas flow, then gas breakthrough would be expected to occur at pressures below 1.0 MPa (for any test duration). In laboratory tests, gas breakthrough pressures for both illite and bentonite were found to be frequently higher than 1.0 MPa in increasing pressure tests.

If gas pressure is great enough to overcome the capillary forces at the entrance to a continuous pore, then various factors will come into effect which will control the rate of gas flow (or de-saturation) in the pore. Pore diameters in a real system will vary, if the

diameter narrows significantly in an area of ped-ped contact, then no further flow will occur until the pressure is great enough to overcome the capillary forces at this pore "throat". As previously mentioned, other factors include viscosity of pore fluid, shape of pores, tortuosity of flow path, and applied pressure in excess of the AEV. All of these factors combined will determine the rate of de-saturation of the pore. Once a pore is fully de-saturated, from one end of the specimen to the other, then gas breakthrough is said to occur since gas can flow freely.

6.2.1.1.Effect of degree of saturation

In the above discussion, full saturation of the specimen has been implied. For unsaturated soils however, there is a lower threshold of saturation below which gas will flow freely through the pores. This threshold saturation corresponds with the degree of saturation at which continuous gas pathways exist within the soil. The threshold degree of saturation found in this study was approximately 85% for illite and illite/sand mixtures, and 93% for bentonite. This observation agrees with the findings of Wheeler (1988), Jeffries (1991) and Fredlund and Rahardjo (1993) who stated that a threshold pressure exists, below which there exist continuous pathways available for gas flow. In the literature, this threshold degree of saturation was reported as approximately 85%.

In the range of 85-100% saturation in both illite and illite/sand mixtures, gas breakthrough pressure at a given clay density increases with increasing degree of saturation, as discussed in Chapter 5. This can be explained by the hypothesis that as the degree of saturation increases, fewer and fewer continuous gas-filled paths are available for flow. In bentonite this effect was much more noticeable than in illite. As

the degree of saturation increased in bentonite, the gas breakthrough pressure increased sharply as the degree of saturation approached 100% (Figures 6.5 and 6.6). In fact, in fully saturated bentonite specimens, there was no breakthrough before the upper limit of the test boards were reached (9.2 MPa), even at low dry densities of 1.00 Mg/m³. The reasons for the differences in gas breakthrough responses of illite and bentonite will be discussed in the following section.

6.2.2. Illite conceptual model

6.2.2.1. Pore structure

Illite's pore structure depends somewhat on the water content at the time of compaction and the dry density to which the material is compacted. MIP tests that were performed on illite were discussed in Section 5.3.3. Generally, illite has a bimodal pore structure when prepared and compacted to the water contents and dry densities used for this study. Illite has a wide range of pore sizes though few pores are larger than approximately 3 μm . Below 3 μm , the pore size distributions (Figure 5.7) show that there are pores at almost every diameter, all the way down to the lower limit of the equipment, 0.003 μm . The larger pores in the distribution can be assumed to be the inter-ped pores whereas the smaller ones are the intra-ped pores (Wan, 1995). The limitations of MIP testing outlined in Section 2.3.1 should be noted. An important limitation is that pores reported from MIP testing are a measure of total porosity and do not account for reduced pore sizes due to structured water.

6.2.2.2. Clay - water system

Illite is a relatively inactive clay. Most of the positive charge deficit brought about by isomorphous substitution is satisfied by "fixed" potassium ions in the ditrigonal cavity. As a result, illite does not form large DDL's by using hydrated cations to satisfy a positive charge deficit. The extent of structured water in illite will be small as compared with bentonite. In illite there was only a 40% reduction in gas breakthrough pressure when a non-polar pore fluid was used. This is a significant decrease, although not as severe as in bentonite. If the DDL effects were ignored and the viscosity of water and paraffin oil were compared, it would be expected that specimens with paraffin oil pore fluid would have a higher gas breakthrough pressure. This is because paraffin is more viscous than water at room temperature and should take longer to flow. The viscosity of paraffin oil is $1.9 \times 10^{-2} \text{ N}\cdot\text{s}/\text{m}^2$, as compared to water which has a viscosity of $1.0 \times 10^{-3} \text{ N}\cdot\text{s}/\text{m}^2$. Clearly, some other mechanism associated with electro-chemical surface effects on water must be affecting gas breakthrough behaviour.

In comparison, the gas breakthrough pressure decreased by 95% when a non-polar pore fluid was used with bentonite. It is important to note that structural effects of mixing clay with a non-polar fluid were not investigated. This should be undertaken before final conclusions are drawn. Nevertheless, the qualitative observations from these tests add insight into fundamental differences between illite and bentonite behaviour.

6.2.2.3. Conceptual flow model

A simplified schematic diagram of the pore structure of illite is shown in Figure 6.9. The various pore sizes of illite are represented in the figure. No structured water has been shown for illite. Although DDL's do form in illite as discussed previously, they are small as compared with bentonite and will be assumed to be so small that they do not appreciably affect flow phenomena for this simple example. In the standard test procedure used in this project, the gas inlet pressure is increased in step-wise fashion by 0.2 MPa every five minutes. As the pressure applied to a specimen increases, more and more pores will begin to de-saturate and participate in the flow process as their AEV is reached and exceeded. In Figure 6.9, at pressure P_2 , the largest pore begins to de-saturate and at pressure P_3 the second largest pore de-saturates. It will take time for water to be extruded from even the largest pores which first started de-saturating. At the end of this period, breakthrough will commence and some gas pressure increase will be observed on the outflow side. For the conceptual example, breakthrough would occur at t_3 , when the largest pore becomes de-saturated. After breakthrough occurred at P_3 , the pressure was further increased. The participation of more and more pores in the flow process accounts in part for the observation that the gas collection line on the gas breakthrough graph is concave upward for illite specimens, indicating an increasing rate of flow. It is possible however, that this effect is also due to increasing gradient across the specimen, which will also increase the flow rate.

The observation that the water content on the gas outlet side of illite specimens at the end of testing was significantly higher than at the gas inlet side is evidence that many pores participate in the flow process in illite. If the gas is pushing water through a

relatively large number of pores as is hypothesized, then water would be expected to be pushed to the gas outlet side of the specimen, and this was observed in these tests. As mentioned in Section 5.1.1.1, illite/sand specimens with identical effective clay dry densities but different total dry densities had the same gas breakthrough pressure. However, the rate of gas breakthrough was slower in the specimen with higher total dry density. This decreased rate of flow can be attributed to increased tortuosity of the flow path in a denser clay system. Even though the sand is an inert filler, the greater tortuosity of the flow path would retard flow.

As discussed in Section 5.3.2 breakthrough pressures of illite exhibit time dependence, as they do also in bentonite (Hume, 1998). However, in illite the effect is not as marked. For example, tests ITU-2 and ITU-2B in which a standard increment was used (0.2 MPa/5 minutes) broke through in 1.3 hours at 3.6 MPa. When the pressure was incremented 0.2 MPa every hour in tests ITU-1 and ITU-1B (that is, twelve times more slowly), the gas breakthrough took 8 hours, and breakthrough occurred at a pressure of 2.0 MPa. Similar observations were found for illite tested at a single constant pressure. It should be noted that since gas breakthrough in illite exhibits time dependence, test procedures will affect the gas breakthrough pressure observed. For a test in which the pressure was increased more slowly, the gas breakthrough pressure was lower because the gas had more time to travel through the pores. The question then arises whether there is any pressure below which no gas flow will take place.

In constant pressure tests, the gas collection pressure graph after breakthrough was generally a straight line with a shallow slope, indicating gas inflow was very slow. If

only a limited range of pores were participating in the flow process (because the pressure was constant and the AEV value of only a certain number of pores was reached), then a constant rate of flow would be expected.

One interesting experimental observation is that test ITU-5 on illite at a dry density of 2.04 Mg/m^3 , degree of saturation of 97.2% and at a constant pressure of 0.8 MPa did not break through in 336 hours at which time the test was stopped. This suggests there may be a lower pressure limit below which no flow will occur since the pressure is not large enough to overcome the capillary forces in even the largest pore channel. The average pore size of the large pore mode from the MIP tests (Figure 5.7) for this dry density and water content is approximately $0.3 \text{ }\mu\text{m}$. If two layers of structured water (not available for flow) is assumed, then the pressure required would be 1.0 MPa, which is greater than the applied 0.8 MPa. Since this result comes from only a single test, further testing should be done before positive conclusions can be made.

6.2.3. Bentonite conceptual model

6.2.3.1. Pore structure

In Avonlea bentonite, the pore distribution is generally bi-modal, with a peak frequency of inter-ped pores in the 10-100 μm range, and intra-ped pores in the 0.025-0.1 μm range (Dixon et al., 1998). The number of inter-ped pores with diameters in the 10-100 μm range depends upon both the water content at the time of compaction, and the dry density to which the specimen is compacted. The specimens used for this study were compacted to water contents on the wet side of optimum, which would reduce the

number of inter-ped pores (Barden and Sides, 1970, Delage and Graham, 1996). However, the specimens were compacted to low dry densities generally less than 1.00 Mg/m³. At these relatively low densities, the large pore mode would still be clearly evident.

Since the size and frequency of the inter-ped pores will control flow phenomena, it follows that the dry density to which a soil is compacted will have a direct effect on flow. Far more total pore volume exists at the smaller, intra-ped pore size than the inter-ped pore size in bentonite specimens (Wan, 1995). It should be noted that the pore size distribution (PSD) of bentonite is different than that of illite. In bentonite there are very few pores whose diameters fall between the large and small sizes. In illite, as mentioned previously, there are many pores of a variety of sizes.

6.2.3.2. Clay - water system

In contrast to illite, bentonite is a highly active clay which uses hydrated cations to satisfy some of its positive charge deficit. In bentonites, the diffuse double layers can be up to 4 nm thick (approximately 15 water layers) (Yong et al., 1992). However, in the compacted clays of this study, the pores (especially the intra-ped pores) are not large enough to allow for the full formation of such a large DDL (Mesri and Olson, 1971, Dixon et al., 1998). The small pore mode does not change markedly with different methods of specimen preparation, water content or dry density to which the specimen is compacted (Wan, 1995). This is due to the theory that the small pore mode reflects the basic interaction between water and the clay minerals (Garcia-Bengochia et al., 1979). With the large proportion of small pores, and the understanding that much of

the water in bentonite is in the form of structured diffuse double layers, most flow phenomena can be expected to occur through the larger inter-ped pores.

6.2.3.3. Conceptual flow model

Figure 6.9 is a simplified representation of bentonite pore structure compared with that of illite. In bentonite, most of the pores are small, and are filled with structured water. There are few larger pores, which are only partially filled with structured water. Once the pressure is great enough to overcome the AEV of the effective diameter of the larger pores, de-saturation will commence (shown in Figure 6.9 at pressure P_4). Some time later gas breakthrough will take place.

A measurement which supports the hypothesis is the observation that there was no statistically significant difference between the water contents at the bottom (gas inlet) and top (gas outlet) of bentonite specimens. If gas flow occurs by de-saturating only a small number of the larger diameter pores, then it can be expected that the water content will not change appreciably from one end of the specimen to the other. Pusch (1993), made the same observation for his experimental work on MX-80 bentonite.

It was noted previously that in bentonite specimens gas breakthrough pressure increased sharply above a degree of saturation of approximately 93%. At degrees of saturation below 90%, there is little resistance to gas breakthrough in bentonite. As previously mentioned, the majority of the water in bentonite occupies the intra-ped spaces. The intra-ped spaces are always saturated, except at very low degrees of saturation (Wan, 1995). Generally, changes in degree of saturation are taken up by

the inter-ped pores. It is for this reason that bentonite can have seemingly high degrees of saturation of about 90%, with no resistance to gas breakthrough since there are still continuous gas pathways in the inter-ped pores. If we consider that the last 10% saturation is the portion that saturates the large inter-ped pores, then the rapid increase in gas breakthrough pressure occurs due to occlusion of the larger pores.

Many of the incremental pressure tests on bentonite did not produce gas breakthrough. Initially it was thought that the upper pressure limit of the apparatus (9.2 MPa) was not great enough to overcome the AEV of even the largest pores in bentonite specimens. Hume (1998), however found that in saturated bentonite specimens, gas breakthrough depended on the duration of the pressure increment. For example, in increasing pressure tests specimens compacted to a dry density of 1.00 Mg/m^3 gas did not break through before the upper limit of his specially designed testing apparatus (50 MPa) was reached. Hume then conducted a number of constant pressure tests ranging from 0.3 to 19.8 MPa in which the time to gas breakthrough was recorded. All specimens he tested broke through, and the time to gas breakthrough was found to be inversely proportional to the constant applied pressure. If left long enough, specimens would break through even at very low applied pressures. For example, in a constant pressure test at 0.3 MPa, a specimen with a dry density of 1.00 Mg/m^3 broke through in 120.5 hours. It is evident, therefore, that the duration of the increasing pressure tests of this study was not long enough to allow the pores to de-saturate. This discovery was made only after the majority of the present program had been completed.

The observation that flow in bentonite was found to be highly time-dependent presents interesting questions about the behaviour of structured pore water in a water-bentonite system. Dixon et al. (1998) suggest that structured water may shear and become available for advective flow within a bentonite if densities are low enough and applied pressure is high enough. Structured water has up to this point been described as being "unavailable for flow". However, it is possible that only the Stern layer is unavailable for flow, whereas the rest of the DDL exhibit significantly increased viscosities which impede flow but do not make it impossible. Dixon also found that at densities greater than 1.05 Mg/m^3 , the high dissolved salt content of bentonite may disrupt water structuring within the pores. The majority of specimens used in this study have dry densities less than 1.00 Mg/m^3 , so no such effect was observed in this study.

6.3. NUMERICAL MODELLING

Numerical models outlined in Chapter 2 for water flow through saturated soil can be adapted to predict gas breakthrough pressures. As defined previously, once a continuous pathway for gas is established from one side of the specimen to the other, gas breakthrough is said to occur. The following models will predict the pressure at which the pores will de-saturate and gas breakthrough will occur. The models were described in detail in Dixon (1995), Kirkham (1995), and Hume (1998).

For both illite and bentonite, one set of experimental gas breakthrough values was chosen to be compared with the models. The test values were chosen because they were representative of the testing program as a whole. Since the theoretical models

are essentially for fully saturated specimens, and most of the tests in this study are unsaturated, specimens that were closest to full saturation were chosen. Test parameters for the illite comparative specimen are shown in Table 6.1. An average of two tests (ITU-2 and ITU-2B) were used. These tests had a dry density of 2.04 Mg/m^3 , a degree of saturation of 98.3 percent, and a gas breakthrough pressure (in an increasing pressure test) of 3.6 MPa. The test parameters for the bentonite comparative specimen are shown in Table 6.2. The test ID was BW-11; it had a dry density of 1.00 Mg/m^3 , a degree of saturation of 96.7 percent, and a gas breakthrough pressure of greater than 9.2 MPa since no gas breakthrough was observed before the upper limit of the test apparatus was reached.

In the models a number of assumptions must be made with regards to average pore size, tortuosity, shape factor and viscosity of pore fluid. Variation in these assumptions will change the output from the models significantly. While there is no "correct" assumption for each of these values, the rationale behind each assumption will be explained. Since the variation in the input parameters for each model is so great, an approximation of the observed gas breakthrough pressure within an order of magnitude is generally considered a good "fit".

6.3.1. Capillarity model

The first model is the capillarity model, equation [2.3] below. The gas breakthrough pressure is calculated from the pore size observed from MIP tests. A number of water layers are assumed to reduce the pore diameter available for flow. This is a very basic model which corresponds with the simplified system in Figure 6.7. Only one pore size

is taken into account, and complicating factors such as tortuosity and viscosity are not included in this model. For the capillarity model, the predicted gas breakthrough pressure is independent of time and the same for both increasing and constant pressure tests.

$$P_b = \frac{2T_s}{r} \quad [2.3]$$

One assumption implicit in this model is that the average pore radius can be used to represent the whole system. In illite this might be an adequate approximation since there is a normal distribution of pores. In bentonite, however, since the large and small pore modes are significantly different in size and the standard deviation of the pore sizes is large, this assumption is less reasonable. The average pore size of the large pore mode observed from the MIP tests for bentonite was therefore used. The diameter available for flow was then reduced to account for water which was bound or had increased viscosity due to the effects of the diffuse double layer. An assumed thickness of 0.5 nm in illite (2 water layers) and 2 nm (10 water layers) in bentonite, was then used to constrict flow.

6.3.1.1. Illite

Observed test results for the representative illite tests are compared with the model predictions in Tables 6.1. Sample calculations for the capillarity model, which use the same method used by Kirkham (1995) are shown in Figure 6.10. For illite, the gas breakthrough pressure from the capillarity model (1.0 MPa) is relatively close to the observed gas breakthrough pressure (3.6 MPa) for an increasing pressure test.

Since the capillarity model assumes gas breakthrough is independent of time, rate of pressure increase cannot be accounted for. Gas breakthrough pressure of illite was found in the ITU test series (Table 5.10) to be dependent on time. In tests on specimens with identical parameters, gas breakthrough pressure was found to range from 1.8 MPa (longest gas breakthrough time) to 3.6 MPa (shortest gas breakthrough time). However, in a constant pressure test at 0.8 MPa, no gas breakthrough was observed in 336 hours. It is possible that the gas breakthrough pressure predicted by the capillarity model of 1.0 MPa corresponds with the AEV of the largest continuous pore. It therefore follows that a constant pressure test at 0.8 MPa, which is below the AEV value, would never breakthrough. In illite which is a relatively inactive clay, results obtained from simplified models such as the capillarity model can approximate the system reasonably well.

6.3.1.2. Bentonite

For bentonite, two different capillarity calculations were performed, one for the average diameter of the large pore mode ($20 \times 10^{-6} \text{m}$) and one for the average diameter of the small pore mode ($0.01 \times 10^{-6} \text{m}$) (Dixon et al., 1998). A 2 nm thick layer of bound water was used to restrict the flow for both calculations. Using the large pore mode, the model predicted a gas breakthrough pressure (0.02 MPa) significantly smaller than that observed in incremental pressure tests in which the gas breakthrough pressure was greater than 9.2 MPa. This discrepancy might be due to an overestimation of large pore size because of small cracks picked up by the MIP test. The layer of bound water was possibly conservative since the effects of the DDL in terms of increased viscosity may extend further than this (Yong et al, 1992). The gas breakthrough pressure

predicted when the average of the small pore mode was used (73.0 MPa) was much larger than the test results, especially for the constant pressure tests (discussed below).

For saturated specimens at the same dry density (1.00 Mg/m^3), Hume found that in constant pressure tests breakthrough was achieved at pressures as low as 0.3 MPa, given a long enough time increment. Using the small pore mode in the capillarity model predicts a gas breakthrough pressure of 73 MPa, which is clearly an overestimate of gas breakthrough pressure. It is expected that use of the small pore mode would overestimate the gas breakthrough pressure since flow phenomena are assumed to occur in the large pore mode, as previously discussed.

Gas breakthrough pressures obtained from the capillarity model are independent of time. Therefore, the capillarity model and the tests are incompatible, especially in clays with highly time-dependent gas breakthrough behaviour such as bentonite. In many of the standard increasing pressure tests of this study where gas pressure was increased quickly (0.2 MPa every five minutes), water did not have time to fully leave the pore spaces and therefore no gas breakthrough was observed. However, due to the time dependence of the gas breakthrough process in bentonite discovered by Hume (1998), this does not mean that no breakthrough would occur if the test was conducted with a longer time increment.

6.3.2. Advection models

To include time-dependence of flow, two advection models, (Poiseulle and Kozeny-Carman) were used to estimate the gas breakthrough pressure. Essentially, the time to de-saturate a continuous pore in a specimen of the correct length was calculated.

6.3.2.1. Poiseulle model

The Poiseulle model expands upon the simple capillary system by considering viscosity and pore length. Following the work of Hume (1998), equation [2.7] below, was adapted to predict the time to gas breakthrough in constant pressure tests.

$$v_{ave} = \frac{\gamma_w r^2}{8\eta} i_h \quad [2.7]$$

First, the hydraulic gradient, was converted into $\Delta P/\Delta L$, since both pressure and specimen length are constant, the equation can be written as:

$$v_{ave} = \frac{r^2 P}{8\eta L} \quad [6.1]$$

Since velocity is in units of length per unit time, this equation can be integrated with respect to time to obtain a gas breakthrough time for a constant pressure test, shown in equation [6.2].

$$t_c = \frac{4L^2 \eta}{Pr^2} \quad [6.2]$$

where: t_c = time to breakthrough in a constant pressure test

L = length of flow path

η = viscosity

P = pressure (constant, Pa)

r = pore radius

For constant pressure tests, the estimation of time to gas breakthrough was relatively straightforward, as the pressure could be directly input into the equation. However, for increasing pressure tests which formed the majority of this study, an alternate model had to be formed. As Hume (1998) had previously done, the step-wise increase in pressure was assumed to be constantly increasing in order to simplify the equation. The pressure term P , from equation [6.1] was replaced by $p \times t$ in equation [6.3], where p is the rate of pressure increase (in units of pressure per second) and t is the time from commencement of the test.

$$v_{avo} = \frac{r^2 p t}{8 \eta L} \quad [6.3]$$

This equation was then integrated with respect to time to obtain a time to gas breakthrough [6.4].

$$t_i = \sqrt{\frac{8L^2 \eta}{p r^2}} \quad [6.4]$$

where: t_i = time to breakthrough in an increasing pressure test
 p = rate of pressure increase for an increasing pressure test (Pa/sec)

The known rate of pressure increase was then used to back calculate the gas breakthrough pressure at the time of breakthrough. The gas breakthrough pressure was then compared with gas breakthrough pressures obtained from increasing pressure tests.

The following assumptions are implicit in these equations. It is assumed that the viscosity of pore water is constant, and that it is identical to that of free water at the same temperature. This assumption is questionable since the formation of DDL's and dissolved salts, especially in bentonite may have a significant effect on the viscosity of the pore fluid. An average pore radius is also used in this equation. For this model, the average pore radius will be calculated in two ways; from MIP test data, and from measured specific surface area (SSA). The specific surface area method was found by Dixon (1995) to produce results closest to those observed for hydraulic conductivity. (Calculation of pore radius from specific surface area is implicit in the form of the Kozeny-Carman equations used in Section 6.3.2.2).

6.3.2.1.1. Illite

The two different pore radius calculations were entered into the Poiseuille model with significantly different results. The first pore radius used was the MIP value that was used for the capillarity model. The gas breakthrough pressure predicted using the MIP method (0.4 MPa) was significantly less than the observed value (3.6 MPa). This is possibly due to an underestimation of the proportion of water that was structured. The second value for pore radius was calculated from the measured specific surface area. This calculation is shown in Figure 6.10. When these pore radius values were entered into the Poiseuille model, the gas breakthrough pressure was significantly overestimated (20.0 MPa) likely due to the very small predicted pore radius, which corresponds to the smallest of pores observed on the MIP graph. It would be expected that the test specimen, which is not fully saturated, would have slightly lower breakthrough pressures than predicted by a model which assumes full saturation. The

gas breakthrough pressure observed from the tests (3.6 MPa) lies within the range between the two Poiseuille model values (0.4 and 20.0 MPa), however they are both within an order of magnitude of the observed pressure.

6.3.2.1.2. Bentonite

In bentonite, the representative test specimen did not exhibit breakthrough in increasing pressure tests before the upper limit of the apparatus was reached (9.2 MPa). The predicted gas breakthrough pressures obtained from the Poiseuille model ranged from 0.2 MPa for the MIP method, to 24.6 MPa for the SSA method. It is evident that the MIP method underestimates the gas breakthrough value. Again, this underestimation is possibly due to the underestimation of the proportion of bound water, or small cracks being included in the MIP test data.

6.3.2.2. Kozeny-Carman model

The Kozeny-Carman equations for gas breakthrough were derived by the author in much the same way as those for the Poiseuille equation, discussed in the previous section. These equations introduce a shape factor C_s and a tortuosity factor τ ; these factors are defined in the literature and are assumed to be 0.4 and $\sqrt{2}$, respectively (Mitchell, 1976). The starting point for the derivation was a form of the Kozeny-Carman, equation [2.14]:

$$v = \frac{n^3 C_s \gamma_w}{S_r^2 (1-n)^2 \tau^2 \eta} i_h \quad [2.14]$$

The hydraulic gradient was converted to pressure differential per unit length,

$$v = \frac{n^3 C_s P}{S_T^2 (1-n)^2 \tau^2 \eta L} \quad [6.5]$$

Equation [6.5] was integrated with respect to time to obtain:

$$t_c = \frac{L^2 S_T^2 (1-n)^2 \tau^2 \eta}{2n^3 C_s P} \quad [6.6]$$

where: S_T = total surface area
 C_s = pore shape factor (0.4)
 τ = tortuosity ($\sqrt{2}$)

which is the Kozeny-Carman model for constant pressure tests.

In much the same way as in equation [6.3], P was replaced by $p \times t$ to represent the rate of pressure increase in an increasing pressure test.

$$v = \frac{n^3 C_s p t}{S_T^2 (1-n)^2 \tau^2 \eta L} \quad [6.7]$$

Equation [6.7] was integrated with respect to time to obtain the time to gas breakthrough for an increasing pressure test.

$$t_c = \sqrt{\frac{L^2 S_T^2 (1-n)^2 \tau^2 \eta}{n^3 C_s p}} \quad [6.8]$$

The known rate of pressure increase was again used to calculate the gas breakthrough pressure at the time of breakthrough. The gas breakthrough pressure was then compared with gas breakthrough pressures obtained from increasing pressure tests.

6.3.2.2.1. Illite

For illite, the gas breakthrough pressure obtained from the Kozeny-Carman model was the highest of the models at 31.5 MPa. Dixon (1995), observed that for illitic clay, the Kozeny-Carman model consistently predicted lower hydraulic conductivities than the Poiseuille equation, which is in agreement with this finding. Possible explanations for the overestimation of the gas breakthrough pressure include underestimation of the inter-ped pore sizes in a compacted clay when using the SSA method. It is also possible that the assumed tortuosity is too great, or the shape factor is too small.

6.3.2.2.2. Bentonite

For bentonite, the Kozeny-Carman model predicted a pressure of 24.0 MPa, which is very close to the Poiseuille model (24.6 MPa). This model would likely provide the best prediction gas breakthrough pressures upon careful study of each parameter, calibration and verification. The model is the most sophisticated in terms of approximating the actual system.

6.3.3. Summary

Advection models can be used to approximate gas breakthrough pressures in increasing pressure tests within an order of magnitude. Advection models however include many parameters with wide ranges of possible values. In order to construct a viable advection model, a comprehensive calibration and verification which is beyond the scope of this study, would be required. The Kozeny-Carman model would likely result in the best approximation of the real system. It includes a number of factors which increase the degree to which the real system is modelled such as tortuosity of flow path and non-cylindrical pores.

The capillarity model is of restricted usefulness for predicting the gas breakthrough pressure due to the fact that flow in compacted clays is a time dependent process, and this model does not take that factor into account. The capillarity model can possibly be useful, however in predicting the lower threshold, or AEV value of a clay, below which no gas breakthrough will occur.

7. CONCLUSIONS AND RECOMMENDATIONS

7.1. CONCLUSIONS

The following hypothesis was given in Chapter 3:

Gas flow in compacted clays is controlled by pore structure, clay-water interaction, and pressure gradient.

The conclusions outlined in this chapter will show that this hypothesis has been proven.

The objectives of this research program, listed below, were stated in Section 3.1,

Scope of Research.

1. to investigate and explain the effect of clay mineral type on gas migration through a compacted clay buffer.
2. to investigate and explain the effect of sand in a clay/sand material on gas migration through that material
3. to investigate the importance of test parameters such as rate of pressure application and their effect on test results
4. to produce test data which will provide support for the investigations described in points 1, 2, and 3.

These four objectives have been achieved.

After inspecting the test data, the following conclusions have been drawn.

- For illite, illite/sand, and bentonite specimens, there is a threshold degree of saturation below which there is virtually no resistance to gas breakthrough.

In illite this threshold degree of saturation is approximately 85%. In bentonite it is approximately 93%. The difference in threshold degree of saturation can be attributed to the fact that the continuous pores used for gas flow are made up of the large (inter-ped) pore mode. In bentonite, the fraction of pore volume which exists in large pores is relatively small. The large pores will be the last to fill with water as the specimen approaches full saturation. The degree of saturation must therefore be high before the large pores will start to fill with water (occlude) and provide resistance to gas flow.

- Gas breakthrough pressure in illite/sand specimens depends on the effective clay dry density of the specimen. For the purposes of gas breakthrough in illite materials, sand can be considered an inert filler. Inter-ped pores decrease in size and frequency as dry density increases and therefore control flow. The following equations describe the relationship between effective clay dry density and gas breakthrough pressure in illite/sand specimens for the increasing pressure test procedures used in this study:
 - $P_b = 1.08 \times 10^{-2} e^{2.3668\rho_c}$ for $S_r = 85-90\%$
 - $P_b = 1.0 \times 10^{-4} e^{5.8043\rho_c}$ for $S_r = 90-95\%$
 - $P_b = 9.0 \times 10^{-4} e^{4.094\rho_c}$ for $S_r = 95-100\%$
- Illite specimens exhibit time dependence of flow. That is, long test durations will permit breakthrough at low pressures. Short time durations require high pressures. Due to this fact, the gas breakthrough pressure from increasing pressure tests is unique to this type of test. Tests with differing rates of pressure application will have different gas breakthrough pressures. The rate of pressure increase used in these tests was relatively high, and therefore

the gas breakthrough pressures reported here are higher than would be found with lower rates of pressure increase.

- Advection models, using reasonable assumptions, can be used to approximate gas breakthrough pressure of illite and bentonite specimens within one order of magnitude for increasing pressure tests. The capillarity model does not give a good prediction of gas breakthrough pressure, due to the fact that time-dependence of flow is not taken into account. The capillarity model might be useful however, for determining the AEV pressure for a clay below which no gas flow will occur.

The following conceptual models were constructed in order to explain the test observations with support from microstructural investigations, and pertinent theories in the literature:

- In increasing pressure tests, flow in illite occurs in many pores. The pore size distribution obtained from MIP tests shows that there are a wide variety of pore sizes in illite. As pressure increases, more and more pores become available for flow as their AEV is exceeded. Gas breakthrough will occur when the largest pore, which first commenced de-saturation has fully drained from the gas inlet to the gas outlet side of the specimen.
- In bentonite, flow is controlled by the large pore mode. The pore size distribution of bentonite is strongly bi-modal, with very few pores with intermediate size. In bentonite, large DDL's form which result in thick layers of structured water at the clay particle surface. This structured water

probably completely blocks the small pores. The flow diameters of the large pores are also reduced by structured water.

7.2. RECOMMENDATIONS

After completion of this testing program, and upon analysis of the test data, a number of outstanding issues arose. A number of recommendations for future research are presented below which would increase the level of understanding of gas flow in compacted clays. Some of the recommendations would also increase the understanding of the effect that specific testing procedures will have on the test data.

- Further studies should be done on illite and bentonite specimens which would prove or disprove the existence of an AEV below which no breakthrough will occur.
- Further studies on the effects of non-polar pore fluids would likely give insight into the effect and formation of DDL's. A thorough microstructural analysis of specimens that had been prepared with non-polar fluids would give insight into the extent to which the clay structure itself is altered.
- An investigation of gradient effects should be undertaken. Tests could be performed in which specimen length, gas inflow pressure, and/or backpressure were varied.
- Variation of specimen diameter would give insight into the effect of cross-sectional area and number of flow paths.

- Measurement of volumes of both gas and water on the outlet side of the specimen would give insight into the flow processes occurring within the specimen.
- Use of a tracer to mark the actual paths of gas flow would show which pores the gas is traveling through and would indicate the presence of any fissures. A tracer could also be used to ensure that no gas is bypassing the specimen by traveling along the cell walls.
- A thorough investigation of the various parameters used in advective flow models such as tortuosity and shape factor would increase confidence in the model output. A sensitivity analysis, calibration, and verification should also be performed on the models.
- The type of permeating gas should be varied to determine if such parameters affect test results.

8. BIBLIOGRAPHY

Agg, P.J., Cummings, R.W., Rees, J.H., Rodwell, W.R., Wikramaratna, R., (1996). Gas Generation and Migration Research. Nirex Science Report No. 96-002.

Barden, L., Sides, G., (1970). Engineering Behaviour and Structure of Compacted Clay, ASCE Journal of the Soil Mechanics and Foundations Division. July 1970, p.1171-1199.

Blight, G.E., (1971). Flow of air through soils. ASCE Journal of Soil Mechanics. vol.97, pp.607-624.

Bohn, McNeal, O'Connor, (1985). Soil Chemistry (Second Edition). John Wiley & Sons Inc., New York, New York.

Cheung, S.C.H. (1989). Methods to measure apparent diffusion coefficients in compacted bentonite clays and data interpretation. Canadian Journal of Civil Engineering, vol.16, pp.434-443.

Craig, R.F., (1992). Soil Mechanics (Fifth edition). Chapman & Hall, London.

Davies, P.B. (1991). Evaluation of the Role of Threshold Pressure in Controlling Flow of Waste-Generated Gas into Bedded Salt at the Waste Isolation Pilot Plant. Sandia National Laboratories. Albuquerque, NM, Sandia Report SAND90-3246.

Delage, P., Graham, J., (1996). Understanding the behaviour of unsaturated soils requires reliable conceptual models, General Report on Session 1, Soil Properties. First International Conference on Unsaturated Soils, Paris, France, September 1995. (eds. E.E. Alonso, and P. Delage). Balkema, Rotterdam, vol.3, pp.1223-1256.

Delage, P., Lefebvre, G. (1984). Study of the structure of a sensitive Champlain clay and of its evolution during consolidation, Canadian Geotechnical Journal, vol.21, pp.21-35.

Devore, J.L. (1991). Probability and Statistics for Engineering and the Sciences (3rd edition). Brooks/Cole, Pacific Grove, California.

Diamond, S. (1970). Pore Size Distributions in Clays, Clays and Clay Minerals, vol.18, pp.7-23, Pergamon Press, UK.

Diamond, S. (1971). Microstructure and Pore Structure of Impact-Compacted Clays, Clays and Clay Minerals, vol.19, pp.239-249.

Dixon, D.A., Gray M.N., Thomas, A.W., (1985). A Study of the Compaction Properties of Potential Clay-Sand Buffer Mixtures for Use in Nuclear Fuel Waste Disposal, Engineering Geology, vol.21, pp.247-255, Elsevier Science Publishers, Amsterdam.

- Dixon, D.A. , Woodcock, D. R., (1986). Physical and Engineering Properties of Candidate Buffer Materials. Atomic Energy of Canada Limited, Pinawa, Manitoba. Technical Record - 352.
- Dixon, D.A., Gray, M.N., Hnatiw, D., (1992). Critical gradients and pressures in dense swelling clays. Canadian Geotechnical Journal, vol.29, no.6, pp.1113-1119.
- Dixon, D.A., (1995). Towards an Understanding of Water Structure and Water Movement Through Dense Clays. Doctor of Philosophy Thesis, University of Manitoba, Winnipeg, Manitoba.
- Dixon, D.A., Graham, J., Gray, M.N., (1998). Hydraulic conductivity of clays under low hydraulic gradients. Article submitted to the Canadian Geotechnical Journal for possible publication.
- Evet, J.B., Liu, C. (1989). Fluid Mechanics and Hydraulics. McGraw-Hill, New York.
- Fernandez, F., Quigley, R.M., (1985). Hydraulic conductivity of natural clays permeated with simple liquid hydrocarbons. Canadian Geotechnical Journal, vol.22, pp.205-214.
- Fredlund, D.G., Rahardjo, H., (1993). Soil Mechanics for Unsaturated Soils. Wiley-Interscience. New York.
- Freeze, R.A., Cherry, J.A., (1979). Groundwater. Prentice-Hall Inc. Englewood Cliffs, New Jersey.
- Garcia-Bengochea, I., Lovell, W.C., Altschaeffl, A. (1979). Pore Distribution and Permeability of Silty Clays. ASCE Journal of the Geotechnical Engineering Division, vol. 105, no. GT7, pp.839-856.
- Gelmich, K.S., (1994). Gas Breakthrough and Mercury Porosimetry Testing on Illite. unpublished report for AECL Research, Vault Sealing Section and the University of Manitoba Geotechnical Engineering Group, Winnipeg, Manitoba.
- Gens, A., Alonso, E.E. (1992). A framework for the behaviour of unsaturated expansive clays. Canadian Geotechnical Journal. vol.29. pp.1013-1032.
- Goh, T.B. (1996). Soil Chemistry and Mineralogy Course Notes. Unpublished. Department of Soil Science, University of Manitoba, Winnipeg, Manitoba.
- Graham, J., Chandler, N.A., Dixon, D.A., Roach, P.J., To, T., Wan, A.W.L. (1997). The buffer/container experiment: results, synthesis, issues. Atomic Energy of Canada Limited, Whiteshell Laboratories, Pinawa, Manitoba. Report no. AECL-11746, COG-97-46-I.

Grogan, H. A., Worgan, K. J., Smith, G. M., Hodkinson, D. P., (1992). Post-Disposal Implications of Gas Generated from a Repository for Low and Intermediate Level Wastes. INTERA, Environmental Division, Henley-on-Thames, UK. Technical Report NAGRA-NTB-92-07.

Guven, N., (1992). Molecular aspects of clay-water interactions. in CMS Workshop Lectures, vol.4, Clay-water interface and its rheological implications, eds. Guven, N., Pollastro, R.M., Clay Minerals Society Publishing.

Hensley, P.J., Schofield, A.N., (1991). Accelerated physical modelling of hazardous-waste transport. *Geotechnique*. vol.41, pp.447-465.

Hokari, T., Okihara, M., Ishii, T., Ishii, T., Ikuse, H., (1997) Experimental Study on Scale Effects of Bentonite/Sand Mixtures on Gas Migration Properties. *Materials Research Society Proceedings* vol. 465. pp. 1019-1026.

Horseman, S.T., Harrington, J. (1994). Migration of repository gases in an overconsolidated clay. *British Geological Survey*. Report No.WE/94/7.

Horseman, S.T., Harrington, J.F., Sellin, P. (1997). Gas Migration in MX80 Buffer Bentonite. *Materials Research Society Proceedings* vol. 465. pp. 1003-1010.

Hume, H.B. (1998). Gas breakthrough in compacted Avonlea bentonite. Master of Science thesis, University of Manitoba, Winnipeg, Manitoba.

Hume, H.B., (1997a). Gas breakthrough in unsaturated Avonlea bentonite plugs. Ontario Hydro, Toronto. Report no. 06819-REP-01200-0014 R00.

Hume, H.B., (1997b). High pressure gas-breakthrough apparatus and a procedure for determining the gas-breakthrough pressure of compacted clay. Atomic Energy of Canada Limited, Whiteshell Laboratories, Pinawa, Manitoba. Report no. AECL-11827, COG-97-303-I.

Impey, M.D., Takase, H. (1995). International Gas Assessment Workshop and Design Review for the Rokkasho Phase II Shallow Land Burial Facility. INTERA Report no. IE4421-2

Jaynes, W.F., Boyd, S.A. (1991a). Hydrophobicity of Siloxane Surfaces in Smectites as Revealed by Aromatic Hydrocarbon Adsorption from Water. *Clays and Clay Minerals*. vol. 39, pp.428-436.

Jaynes, W.F., Boyd, S.A. (1991b). Clay Mineral Type and Organic Compound Sorption by Hexadecyltrimethylammonium-exchanged Clays. *Soil Science Society of America Journal*. vol.55, pp.43-48.

Jeffries, R.M., Liew, S.K., Thomas, J.B. (1991). Gas Migration in Deep Radioactive Waste Repositories; A review of Processes, Data, and Models. United Kingdom Department of Environment. Report No. DOE/HMIP/RR/91/029.

Johnson, L.H., LeNeveu, D.M., Shoesmith, D.W., Oscarson, D.W., Gray, M.N., Lemire, R.J., Garisto, N.C., (1994a). The Disposal of Canada's Nuclear Fuel Waste: The Vault Model for Postclosure Assessment. AECL Research Document No. AECL-10714, COG-93-8.

Johnson, L.H., Tait, J.C., Shoesmith, D.W., Crosthwaite, J.L., Gray, M.N. (1994b). The Disposal of Canada's Nuclear Fuel Waste: Engineered Barriers Alternatives. AECL Research Document No. AECL-10718, COG-93-8.

Juang, C.H., Holtz, R.D., (1986). Fabric, Pore Size Distribution, and Permeability of Sandy Soils. ASCE Journal of Geotechnical Engineering. vol.112, no.9, pp.855-868

Kirkham, T., (1995). Development of test equipment and procedures for determination of the gas-breakthrough pressure of compacted clay materials with preliminary results. Master of Science thesis, University of Manitoba, Winnipeg, Manitoba.

Lineham, T.R. (1989). A Laboratory Study of Gas Transport Through Intact Clay Samples. United Kingdom Atomic Energy Authority. NSS/R115.

McBride, M.B., (1994). Environmental Chemistry of Soils. Oxford University Press, New York, New York.

Mesri, G., Olson, R.E., (1971). Mechanisms controlling the permeability of clays. Clays and Clay Minerals, vol.19, pp.151-158, Pergamon Press, London.

Mitchell, J.K. (1976). Fundamentals of Soil Behaviour. (eds. Lambe, T.W., Whitman, R.V.). John Wiley and Sons, Inc. New York, New York.

Mitchell, J.K. (1991). Conduction Phenomena: from Theory to Geotechnical Practice. Geotechnique, vol.41, no.3, pp.299-340.

Oscarson, D.W., Dixon, D.A., (1989). The Effect of Steam on Montmorillonite. Applied Clay Science, vol.4, pp. 279-292.

Oswell, J.M., (1991). Elastic plastic behaviour of a sand-bentonite mixture. Doctor of Philosophy Thesis, University of Manitoba, Winnipeg, Manitoba.

Pusch, R. (1982). Mineral-water interactions and their influence on the physical behaviour of highly compacted Na bentonite. Canadian Geotechnical Journal. vol. 19, pp. 381-387.

Pusch, R., Forsberg, T. (1983). Gas migration through bentonite clay. University of Lulea, Lulea, Sweden. Swedish Nuclear Fuel and Waste Management Co., Technical Report 83-71.

Pusch, R. Ranhagen, L., Nilsson, K., (1985). Gas Migration Through MX-80 Bentonite. Swedish Geological, Lund, Sweden, Technical Report NAGRA NTB 85-36.

Pusch, R., Hokmark, H., Borgesson, L., (1987). Outline of Models of Water and Gas Flow Through Smectite Clay Buffers. Swedish Nuclear Fuel and Waste Management Co., Technical Report 87-10, Stockholm, Sweden.

Pusch, R. (1993). Current Status and Future Plans for R&D on Gas Penetration and Release Through Buffer Materials. Reprinted from International Workshop on Research and Development of Geological Disposal, PNC Tokai, Japan.

Roberson, J.A., Crowe, C.T. (1990). Engineering Fluid Mechanics. Houghton Mifflin Company, Dallas, Texas.

Silverstein, D.L., Fort, T. (1997). Studies in Air-Water Interfacial Area for Wet Unsaturated Particulate Porous Media Systems. Langmuir. V.13, pp.4756-4761.

Tanai, K., Kanno, T., Galle, C. (1997). Experimental Study of Gas Permeabilities and Breakthrough Pressures in Clays. Materials Research Society Proceedings vol. 465. pp. 995-1001.

Tchobanoglous, G., Theisen, H., Vigil, S. (1993). Integrated Solid Waste Management. McGraw Hill, New York.

Theng, B.K.G. (1974). The Chemistry of Clay-Organic Reactions. John Wiley and Sons, New York.

Troeh, F.R., Jabro, J.D., Kirkham, D., (1982). Gaseous Diffusion Equations for Porous Materials. Geoderma, vol.27, pp.239-253.

van Olphen, H., (1963) An Introduction to Clay Colloid Chemistry. Interscience Publishers (John Wiley and Sons), New York, New York.

Volckaert, G., Put, M., Ortiz, L., De Canniere, P., Horseman, S., Harrington, J., Fioravante, V., Impey, M., Worgan, K. (1993) MEGAS - Modelling and Experiments on Gas Migration in Repository Host Rocks. Pegasus Meeting, CRS Koln.

Wan, A.W.L., (1996). The use of thermocouple psychrometers to measure in situ suctions and water contents in compacted clays. Doctor of Philosophy thesis, University of Manitoba, Winnipeg, Manitoba.

Wheeler, S.J., Sham, W.K., (1990). Gas pressure in unsaturated offshore soils. Canadian Geotechnical Journal. vol.27, pp.79-89.

Wheeler, S.J., (1988). A conceptual model for soils containing large gas bubbles. Geotechnique. vol.38, pp.389-397.

Wikramaratna, R.S., Goodfield, M., (1994). A proposed programme of experimental and theoretical modelling studies of gas migration through bentonite. AEA Technology Report No. AEA-ESD-0033. Oxfordshire, UK.

Wikramaratna, R.S., Goodfield, M., Rodwell, W.R., Nash, P.J., Agg, P.J., (1993). A Preliminary Assessment of Gas Migration from the Copper/Steel Canister. Swedish Nuclear Fuel and Waste Management Co. SKB Technical Report 93-31, Stockholm, Sweden.

Yarechewski, D., (1993). Constant Mean Effective Stress Tests on Sand Bentonite Specimens at Elevated Temperature. Master of Science Thesis, University of Manitoba, Winnipeg, Manitoba.

Yariv, S., Cross, H., (1979). Geochemistry of Colloid Systems. Springer-Verlag, Berlin.

Yong, R.N., Warkentin, B.P., (1975). Soil Properties and Behaviour, Developments in Geotechnical Engineering, Elsevier Scientific Publishing Company, New York.

Yong, R.N., Mohamed, A.M.O., Warkentin, B.P., (1992). Principles of Contaminant Transport in Soils. Elsevier Scientific Publishing Company. New York.

Table 3.1: Test parameters for a standard test

Parameter	Value
<i>specimen dimensions</i>	height = 24 mm diameter = 50.7 mm
<i>pressure increment</i>	0.2 MPa/5 minutes
<i>backpressure for saturation</i> (in tests which include a saturation phase)	0.2 MPa
<i>permeating gas</i>	argon
<i>pore fluid</i>	distilled, de-aired water

Table 3.2: Target test parameters for illite/sand (IS) series

	Illite/sand mixtures			
	25/75	37.5/62.5	50/50	75/25
<i>number of tests</i>	6	8	18	10
ρ_c (Mg/m^3)	1.23-1.51	1.65-1.90	1.57-2.04	1.85-2.08
ρ_d (Mg/m^3)	2.12-2.23	2.14-2.30	1.97-2.30	2.00-2.20
S_r	0.45-0.96	0.85-1.00	0.72-1.00	0.85-0.97

Table 3.3: Target test parameters for bentonite tests (BU and BW)

	unsaturated (BU)	wetted (BW)
<i>number of tests</i>	29	27
ρ_d (Mg/m ³)	0.9-1.2	0.6-1.0
S_r	0.60-0.99	1.00

Table 3.4: Target test parameters for non-polar fluid (NPF) series

	illite	bentonite
<i>number of tests</i>	2	2
ρ_d (Mg/m ³)	2.05	1.15
S_r	0.96	0.99

Table 3.5: Target test parameters for modified time increment (T) series

<i>number of tests</i>	8
ρ_d (Mg/m ³)	2.04
S_r	0.98
<i>pressure increments</i>	0.2MPa/5 min 0.2MPa/hr 1.0MPa (constant) 2.0MPa (constant) 3.0MPa (constant)

Table 4.1: Comparison of the properties of illite and bentonite

PROPERTY	ILLITE	BENTONITE
Primary clay mineral	hydrous mica	montmorillonite
Plasticity Index (I_p)	11	208
Liquid Limit (w_L)	31	257
Plastic Limit (w_P)	20	49
Unified Soil Classification	CL	CH
Specific Gravity	2.76	2.75
Specific surface area (m^2/g)	43-81	519-631
Free swell volume (cm^3/g)	<1	>9
Optimum moisture content (%) (from Modified Proctor test)	12	10**

(after Kirkham, 1995 and Dixon, 1995)

****Note:** *The results from a Modified Proctor Test on bentonite do not show a defined "peak" as is the case with illite. For bentonite, almost the same dry density can be achieved with water contents ranging from 10 to 40 percent.*

Table 4.2: Frac sand size comparison

Frac Sand Size (U.S. Standard Sieve No.)	% of total mixture (by weight) for RBM	% of total mixture (by weight) for gas breakthrough
8 - 12	5	0
12 - 20	10	0
16 - 30	10	20
20 - 40	24	29
40 - 70	22	22
70 - 140	29	29

Table 5.1: Summary of specimen conditions for the ISU75 (75% illite / 25% sand) test series

Test ID	P _b (MPa)	INITIAL(compaction)				FINAL				
		ρ _d (Mg/m ³)	ρ _c (Mg/m ³)	S _r (%)	w (%)	S _r (%)	W _{average} (%)	W _{gas inlet} (%)	W _{gas outlet} (%)	W _{centre} ¹ (%)
ISU75-1	2.8	2.11	1.98	97.3	10.43	87.5	9.38	9.42	9.34	
ISU75-2	2.8	2.10	1.97	95.3	10.43	85.6	9.37	9.40	9.35	
ISU75-3	1.8	2.14	2.01	90.3	9.20	83.0	8.45	8.12	8.78	
ISU75-4	3.2	2.17	2.05	96.5	9.20	90.6	8.84	8.09	9.20	
ISU75-5	0.2	2.02	1.90	84.6	10.83	82.2	10.52	10.49	10.44	10.64
ISU75-6	1.2	2.06	1.95	91.5	10.83	86.9	10.28	10.09	10.50	10.26
ISU75-7	2.2	2.20	2.08	**90.7	*8.00	83.9	7.40	7.34	7.46	
ISU75-8	1.2	2.17	2.05	**84.6	*8.00	78.8	7.45	7.42	7.49	
ISU75-9	1.2	2.05	1.91	97.9	11.83	90.7	10.95	10.68	11.21	
ISU75-10	0.2	2.00	1.85	89.0	11.83	84.8	11.27	11.28	11.27	

* The initial w was not available, so the target value was used.

** The initial saturation has been calculated from the target water content.

¹ Specimens ISU75-5 and ISU75-6 were cut into three disks, gas inlet, centre, and gas outlet.

**Table 5.2: Summary of specimen conditions for the
ISU50 (50% illite / 50% sand) test series**

Test ID	INITIAL(compaction)					FINAL			
	P _b (MPa)	ρ _d (Mg/m ³)	ρ _c (Mg/m ³)	S _r (%)	w (%)	S _r (%)	W _{average} (%)	W _{gas inlet} (%)	W _{gas outlet} (%)
ISU50-1	0.2	1.97	1.58	71.9	9.91	67.1	9.25	9.29	9.20
ISU50-2	0.2	1.98	1.58	82.0	11.20	75.2	10.27	10.34	10.19
ISU50-3	0.2	2.00	1.60	93.3	12.32	88.4	11.67	11.82	11.52
ISU50-4	0.6	2.03	1.66	100.8	12.32	91.5	11.19	10.80	11.57
ISU50-5	0.4	2.04	1.66	100.1	12.00	90.6	10.95	10.70	11.19
ISU50-6	0.6	2.00	1.60	100.3	13.00	90.7	11.84	11.60	12.09
ISU50-7	5.4	2.30	2.02	**	10.28	87.2	5.80	5.15	6.44
ISU50-8	6.2	2.30	2.03	**	11.21	91.9	6.09	5.49	6.68
ISU50-9	0.2	2.08	1.72	84.2	9.29	75.5	8.33	8.29	8.38
ISU50-10	0.2	2.03	1.66	76.1	9.29	67.3	8.22	8.16	8.28
ISU50-11	1.6	2.17	1.84	98.1	8.94	88.4	8.08	7.78	8.36
ISU50-12	1.0	2.15	1.81	93.7	8.94	87.2	8.32	8.10	8.55
ISU50-13	1.2	2.20	1.88	92.8	7.83	88.2	7.45	7.34	7.56
ISU50-14	2.4	2.23	1.92	100.0	7.83	92.8	7.27	7.21	7.33
ISU50-15	3.2	2.28	2.00	95.2	6.65	82.5	5.75	5.83	5.68
ISU50-16	2.0	2.25	1.95	87.8	6.63	76.7	5.80	5.81	5.79
ISU50-17	1.0	2.29	2.02	80.6	5.38	68.3	4.56	4.52	4.60
ISU50-18	0.8	2.21	1.90	88.9	7.32	81.6	6.72	6.73	6.70

**During compaction water flowed out of the specimen, since an attempt was made to compact it to a S_r >100%.

Table 5.3: Summary of specimen conditions for the IS37.5 (37.5% illite / 62.5% sand) test series

Test ID	P _b (MPa)	INITIAL(compaction)				FINAL				
		ρ _d (Mg/m ³)	ρ _c (Mg/m ³)	S _r (%)	w (%)	S _r (%)	Waverage (%)	W _{gas Inlet} (%)	W _{gas outlet} (%)	W _{centre} (%)
ISU37.5-1	2.0	2.30	1.90	101.30	6.30	81.60	5.08	4.94	5.22	4.27
ISU37.5-2	0.4	2.31	1.90	84.80	5.26	74.30	4.61	4.69	4.86	
ISU37.5-3	1.0	2.24	1.79	99.00	7.32	90.40	6.68	6.21	7.15	
ISU37.5-4	0.2	2.24	1.79	85.80	6.36	78.80	5.84	5.78	5.90	
ISU37.5-5	0.6	2.17	1.70	100.90	8.98	89.30	7.94	7.68	8.21	
ISU37.5-6	0.6	2.18	1.70	92.10	8.02	85.00	7.40	7.04	7.75	
ISU37.5-7	0.6	2.15	1.65	102.10	9.57	87.00	8.14	7.81	8.48	
ISU37.5-8	0.2	2.14	1.65	93.60	8.89	86.70	8.24	8.10	8.38	

¹ This specimen was cut into three disks: gas inlet, centre, and gas outlet.

**Table 5.4: Summary of specimen conditions for the
IS25 (25% illite / 75% sand) test series**

Test ID	P_b (MPa)	INITIAL(compaction)				FINAL			
		ρ_d (Mg/m ³)	ρ_c (Mg/m ³)	S_r (%)	w (%)	S_r (%)	$W_{average}$ (%)	$W_{gas\ inlet}$ (%)	$W_{gas\ outlet}$ (%)
ISU25-1	0.2	2.23	1.49	46.1	3.48	41.40	3.10	3.06	3.15
ISU25-2	0.2	2.07	1.23	31.5	3.48	n/a	n/a	n/a	n/a
ISU25-3	0.2	2.23	1.51	86.5	6.52	77.00	5.81	5.78	5.84
ISU25-4	0.2	2.19	1.44	78.0	6.52	71.20	5.95	5.96	5.94
ISU25-5	0.2	2.15	1.37	97.0	8.87	85.10	7.78	7.62	7.94
ISU25-6	0.2	2.12	1.32	90.5	8.87	81.90	8.03	7.86	8.19

Table 5.5: Summary of specimen conditions for the
BW (bentonite wetted) test series

Test ID	P _b (MPa)	INITIAL(compaction)				FINAL			
		ρ _d (Mg/m ³)	S _r (%)	w (%)	Inflow (ml)	W _{average} (%)	W _{gas inlet} (%)	W _{gas outlet} (%)	S _r (%)
BW-1	>4.8	1.00	97.7	62.4	0.29	61.5	58.5	64.4	96.4
BW-2	>9.2	0.99	71.6	46.1	3.17	56.7	60.4	53.0	88.1
BW-2B	>9.2	0.99	71.6	46.1	3.62	57.7	63.5	51.8	89.6
BW-3	0.2	0.79	51.4	46.1	1.37	81.5	80.7	82.2	91.0
BW-4	0.2	0.60	35.0	46.1	1.92	116.7	¹	¹	88.7
BW-5	>9.2	0.85	55.5	45.2	1.66	70.0	78.0	62.0	86.0
BW-5B	>9.2	0.86	54.7	44.0	1.45	70.1	75.7	64.4	87.1
BW-5C	>9.2	0.86	54.7	44.0	**	70.4	80.4	60.4	87.5
BW-6	0.6	0.90	60.3	45.2	2.36	70.7	69.7	71.7	94.4
BW-6B	0.6	0.92	58.4	42.6	2.20	68.3	67.8	68.8	93.7
BW-6C	1.0	0.92	58.4	42.6	1.86	67.9	67.7	68.0	93.1
BW-7	1.0	0.60	42.0	54.6	0.92	114.2	115.2	113.3	88.0
BW-8	>9.2	1.00	78.2	49.5	5.01	59.4	65.5	53.3	93.8
BW-10	>9.2	0.88	82.2	63.4	1.86	70.2	76.3	64.1	91.0
BW-11	>9.2	0.98	96.7	63.5	0.28	61.5	67.5	55.6	93.7
BW-12	>9.2	0.78	69.1	63.5	1.27	76.7	80.3	73.2	83.5
BW-13	>9.2	0.81	55.5	48.3	2.65	78.6	86.5	70.6	90.2
BW-14	>9.2	0.71	46.3	48.3	1.30	93.1	79.7	106.5	89.1
BW-15	>9.2	1.00	85.5	54.4	2.09	60.4	64.2	56.5	94.9
BW-16	2.6	0.80	61.4	54.4	1.17	78.9	83.1	74.7	89.0
BW-17	1.0	0.70	51.0	54.3	1.81	96.1	97.2	95.0	90.2
BW-18	0.4	0.70	56.5	60.2	1.14	98.3	97.6	98.9	92.3
BW-19	0.4	0.76	60.9	58.1	1.57	87.1	86.9	87.3	91.2
BW-20	0.2	0.66	50.3	58.1	1.17	108.2	104.4	112.0	93.5
BW-21	0.4	0.91	73.0	53.7	2.96	68.7	69.2	68.1	93.4
BW-22	0.2	0.61	36.8	46.9	1.20	111.9	111.6	112.2	87.7
BW-23	>9.2	0.98	61.5	40.3	3.27	59.4	66.2	52.7	90.8

¹ Specimen was crushed on extrusion from the test cell.

Table 5.6: Calculation of S_r from water inflow

(A) Test ID	(B) Mass of water before sat. (g)	(C) Measured inflow (ml)	(D) Mass of water after saturation (g)	(E) Water content after saturation (%)	(F) S_r calculated from inflow (%)	(G) S_r measured (%)	(H) Diff. between (G)-(F) (%)
BW-1	30.23	0.29	30.52	63.00	99.0	97.4	-2.7
BW-2	22.11	3.17	25.28	52.71	81.5	89.1	7.5
BW-2B	22.11	3.62	25.73	53.65	83.0	90.5	7.4
BW-3	17.65	1.37	19.02	49.68	55.1	91.6	39.5
BW-4	13.40	1.92	15.32	52.70	40.4	89.2	54.4
BW-5	18.61	1.66	20.27	49.23	60.6	86.7	29.6
BW-5B	18.33	1.45	19.78	47.48	59.4	87.8	31.8
BW-5C	n/a	n/a	n/a	n/a	n/a	88.3	n/a
BW-6	19.71	2.36	22.07	50.61	67.7	95.3	28.3
BW-6B	18.99	2.20	21.19	47.54	65.7	94.6	29.9
BW-6C	18.99	1.86	20.85	46.77	64.7	94.0	30.5
BW-7	15.87	0.92	16.79	57.76	44.3	88.4	49.6
BW-8	23.98	5.01	28.99	59.84	94.0	94.8	-0.3
BW-10	27.03	1.86	28.89	67.76	87.7	91.8	3.6
BW-11	30.15	0.28	30.43	64.09	97.6	94.5	-4.1
BW-12	24.00	1.27	25.27	66.86	72.8	84.6	12.8
BW-13	18.96	2.65	21.61	55.05	63.2	90.7	29.9
BW-14	16.61	1.30	17.91	52.08	49.8	89.3	44.1
BW-15	26.36	2.09	28.45	58.71	92.3	96.5	2.8
BW-16	21.09	1.17	22.26	57.42	64.8	90.2	27.2
BW-17	18.42	1.81	20.23	59.64	56.0	91.4	37.9
BW-18	20.42	1.14	21.56	63.56	59.7	92.7	35.3
BW-19	21.39	1.57	22.96	62.36	65.5	91.9	28.2
BW-20	18.58	1.17	19.75	61.76	53.6	94.1	42.6
BW-21	23.68	2.96	26.64	60.41	82.2	93.9	12.0
BW-22	13.86	1.20	15.06	50.96	39.9	88.7	54.5
BW-23	19.13	3.27	22.40	47.19	71.8	90.8	20.9

Table 5.7: Summary of specimen conditions for the BU (bentonite unsaturated) test series

Test ID	INITIAL(compaction)					FINAL			
	P _b (MPa)	p _d (Mg/m ³)	S _r (%)	w (%)	Filters	W _{average} (%)	W _{gas inlet} (%)	W _{gas outlet} (%)	S _r (%)
BU-1	>9.2	1.02	92.7	57.6	WET	59.5	65.6	53.3	95.7
BU-2	0.2	0.90	**80.3	*60.0	WET	60.7	62.5	58.9	81.2
BU-3	0.2	1.00	93.9	59.4	DRY	56.8	56.7	56.9	89.7
BU-3B	0.6	1.02	92.1	56.7	DRY	58.5	58.1	58.9	95.1
BU-4	7.8	1.04	98.5	57.9	DRY	55.2	52.3	58.2	93.9
BU-5	0.6	1.00	85.9	54.3	WET	58.4	59.2	57.6	92.4
BU-6	0.2	0.90	73.1	54.3	DRY	53.5	53.0	54.0	72.0
BU-7	1.2	1.07	98.5	56.0	DRY	52.8	54.9	51.8	92.9
BU-7B	4.6	1.07	98.8	56.4	DRY	53.9	52.8	54.9	94.4
BU-7C	3.6	1.08	97.8	54.9	DRY	53.3	53.1	53.4	94.8
BU-8	0.6	1.04	94.1	55.9	DRY	56.1	56.2	56.0	94.4
BU-8B	0.8	1.04	94.2	56.1	DRY	54.2	54.1	54.4	91.0
BU-9	0.2	1.00	78.1	49.4	WET	52.8	53.0	52.5	83.5
BU-10	>9.2	1.13	101.5	53.3	DRY	48.9	50.5	47.3	93.1
BU-11	>9.2	1.11	90.1	48.1	WET	49.4	52.9	46.0	92.6
BU-11B	0.6	1.11	91.0	49.1	DRY	49.6	49.2	50.0	91.8
BU-11C	0.6	1.09	92.3	50.8	DRY	50.5	50.3	50.8	91.8
BU-12	0.2	0.91	66.3	49.1	DRY	48.2	48.5	47.9	65.0
BU-13	0.2	1.00	**70.7	*45.0	WET	48.7	48.9	48.4	76.5
BU-13B	0.2	1.00	70.4	44.7	DRY	44.4	44.6	44.2	70.0
BU-14	0.2	0.89	61.5	46.8	DRY	46.3	46.2	46.5	60.9
BU-15	0.2	1.10	82.2	44.7	DRY	46.7	47.0	46.3	85.9
BU-16	6.8	1.17	99.2	48.7	DRY	47.0	48.0	46.0	95.7
BU-17	0.8	1.13	91.8	48.2	DRY	47.9	47.5	48.2	91.2
BU-18	0.4	1.03	86.9	52.7	DRY	51.7	51.9	51.6	85.4
BU-18B	0.2	1.06	84.2	49.1	DRY	49.4	49.4	49.4	84.8
BU-18C	0.2	1.04	85.5	50.8	DRY	50.3	50.5	50.2	84.8
BU-19	5.4	1.11	97.6	52.0	DRY	50.8	51.5	50.1	95.2
BU-20	0.2	0.99	79.7	51.5	DRY	49.9	50.2	49.6	77.2

* The initial w is not available, therefore the target value was used.

** The initial saturation has been calculated from the target water content.

**Table 5.8: Summary of specimen conditions for
NPF (non-polar fluid) test series**

Test ID	P _b (MPa)	Clay type	INITIAL(compaction)				FINAL			
			Pore fluid	ρ _d (Mg/m ³)	S _r (%)	W _{eff} (%)	S _r (%)	W _{average} (%)	W _{gas inlet} (%)	W _{gas outlet} (%)
INPFU-1A	2.0	illite	paraffin	2.05	95.6	12.00	**	**	**	**
INPFU-1B	2.4	illite	paraffin	2.05	95.6	12.00	**	**	**	**
BNPFU-2	0.2	bentonite	paraffin	1.15	98.8	50.00	**	**	**	**
BNPFU-3A	3.6	bentonite	water	1.15	99.3	50.59	101.4	51.63	51.62	51.63
BNPFU-3B	5.4	bentonite	water	1.15	99.3	50.59	96.1	48.97	49.42	48.52

Table 5.9: Summary of tests performed on illite with water as a pore fluid

Test ID	ρ_d (Mg/m ³)	w (%)	S_r	P_b
T40(Kirkham, 1995)	2.05	12.3	96.9	¹ 3.8
T50	2.04	12.0	94.1	4.0
ITU-2	2.04	12.6	98.3	3.6
ITU-2B	2.04	12.6	98.3	3.6
			Avg.	3.75

¹ Kirkham reported this as 4.0 MPa, since he used absolute breakthrough pressure instead of pressure difference across the specimen.

Table 5.10: Summary of specimen conditions for the ITU (illite-time) test series

Test ID	P _b (MPa)	t _b (hrs)	Pressure Increment	INITIAL(compaction)					FINAL			
				P _d (Mg/m ³)	S _r (%)	W (%)	S _r (%)	W _{average} (%)	W _{gas inlet} (%)	W _{gas outlet} (%)		
ITU-1	2.2	9.00	200 kPa/hr	2.04	98.4	12.60	93.3	11.95	10.87	13.03		
ITU-1B	1.8	7.00	200 kPa/hr	2.04	98.4	12.60	94.3	12.09	12.63	11.54		
ITU-2	3.6	1.33	200 kPa/5min	2.04	98.3	12.58	91.4	11.70	11.61	11.79		
ITU-2B	3.6	1.33	200 kPa/5min	2.04	98.3	12.58	91.6	11.73	11.89	11.56		
ITU-3	1.8	22.70	1.8 MPa (const.)	2.04	97.2	12.34	92.8	11.79	11.12	12.45		
ITU-4	2.8	0.30	2.8 MPa (const.)	2.04	96.9	12.29	91.8	11.63	11.35	11.91		
ITU-4B	2.8	0.20	2.8 MPa (const.)	2.04	96.9	12.29	90.1	11.41	11.45	11.38		
ITU-5	0.8	none (in 336 hrs)	0.8 MPa (const.)	2.04	97.2	12.34	92.8	11.78	11.47	12.09		
ITU-6	1.8	0.64	1.8 MPa (const.)	2.06	94.1	11.67	91.4	11.33	11.02	11.65		
ITU-7	0.8	0.50	0.8 MPa (const.)	2.06	94.1	11.67	91.9	11.40	11.34	11.47		

Table 6.1: Comparison of different models for gas breakthrough pressure in illite 143

Model	P _b (MPa)
Observed (laboratory experiment)	3.6
Capillarity model (pore size observed from MIP)	1.0
Poiseuille model (pore radius observed from MIP)	0.4
Poiseuille model (pore radius calculated from surface area)	20.0
Kozeny-Carman model (pore radius calculated from surface area)	31.5

Assumptions:

- Average pore diameter from MIP: 0.3×10^{-6} m
- Assumed thickness of bound water at the clay surface: 0.5×10^{-9} m
- Specific surface area 60 000 m²/kg

Test parameters for observed data:

- $\rho_d = 2.04$ Mg/m³
- $S_r = 98.3$ %
- Water content = 12.5 %

Table 6.2: Comparison of different models for gas breakthrough pressure in bentonite

Model	P_b (MPa)
Observed (laboratory experiment)	>9.2
Capillarity model (pore size observed from MIP – large pore mode)	0.02
Capillarity model (pore size observed from MIP – small pore mode)	73.0
Poiseuille model (pore radius observed from MIP)	0.2
Poiseuille model (pore radius calculated from surface area)	24.6
Kozeny-Carman model (pore radius calculated from surface area)	24.0

Assumptions:

- Average pore diameter from MIP (large pore mode): 20×10^{-6} m
- Average pore diameter from MIP (small pore mode): 0.01×10^{-6} m
- Assumed thickness of bound water at the clay surface: 2.0×10^{-9} m
- Specific surface area 750 000 m^2/kg

Test parameters for observed data:

- $\rho_d = 1.00 \text{ Mg/m}^3$
- $S_r = 96.7 \%$
- Water content = 62.5 %

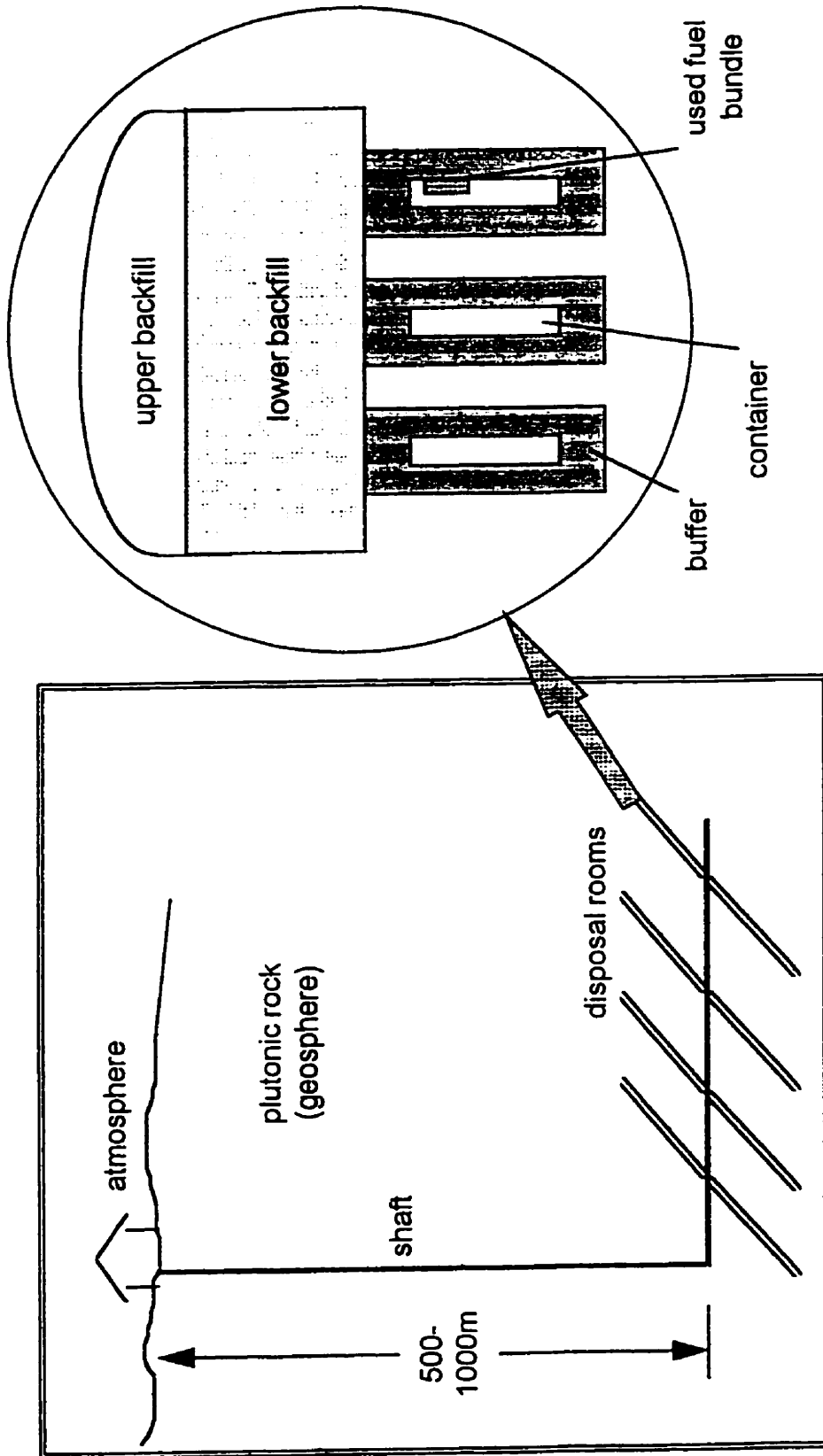


Figure 1.1: Schematic diagram of the Canadian nuclear fuel waste repository concept

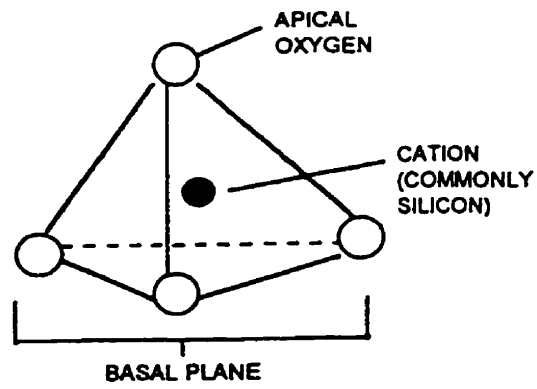


Figure 2.1: Silica tetrahedron

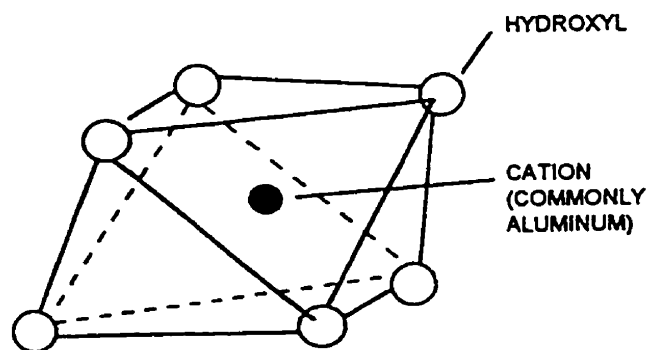


Figure 2.2: Alumina octahedron

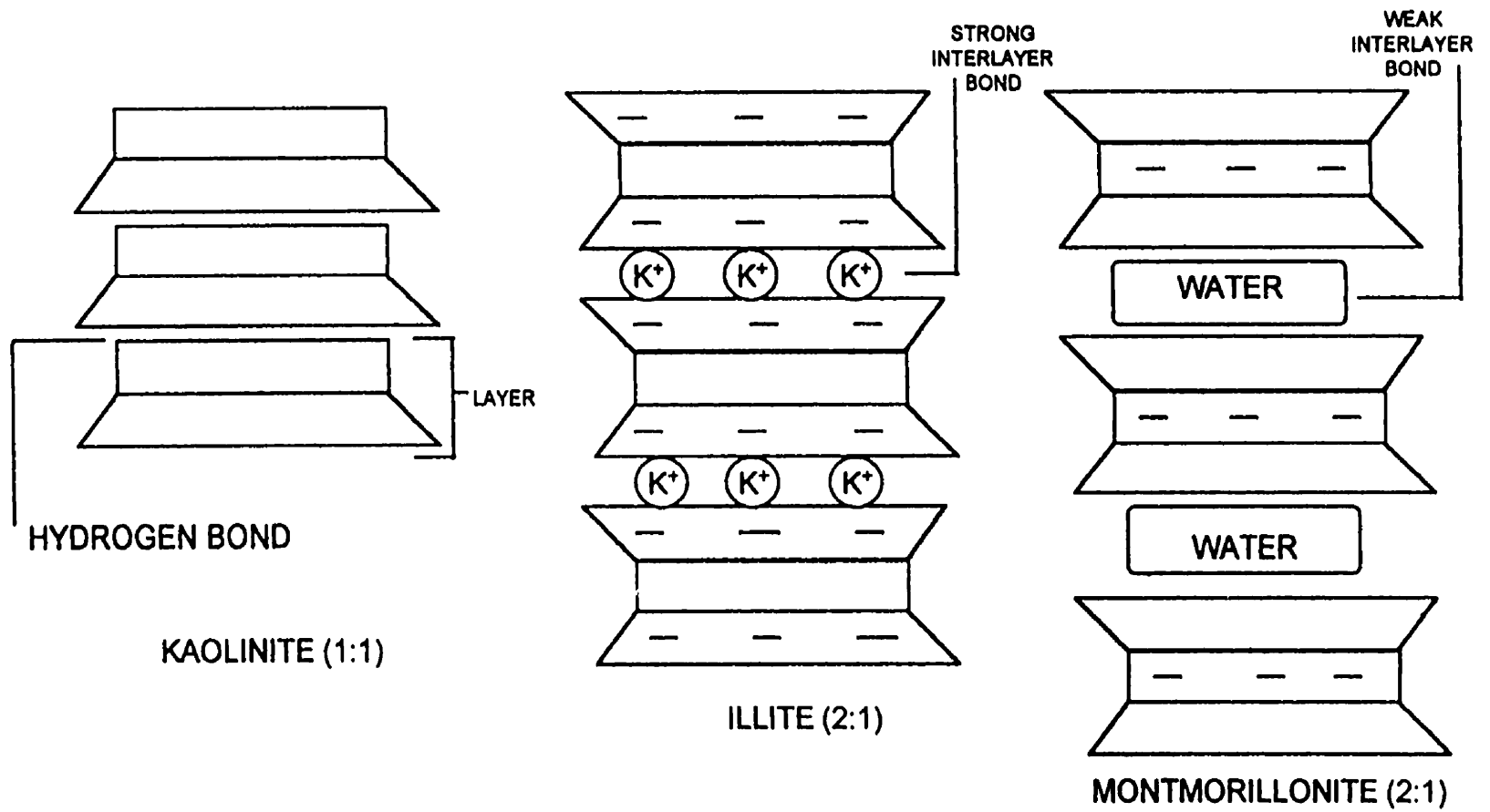
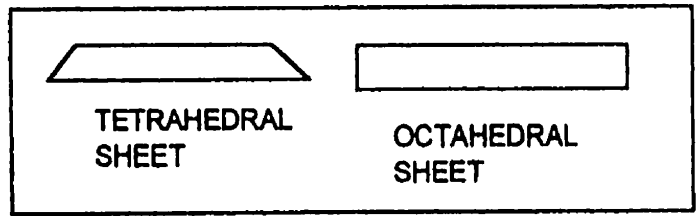


Figure 2.3: Examples of clay structures

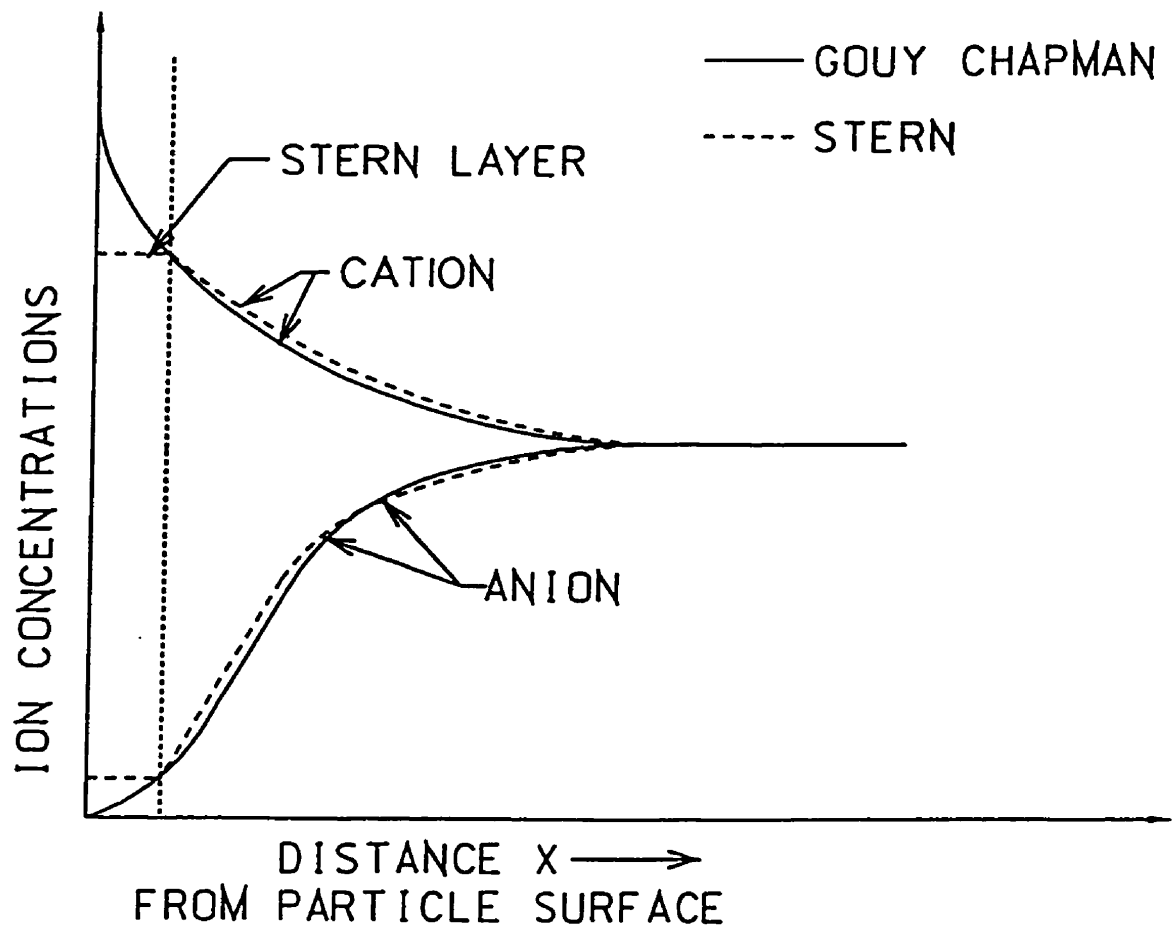


Figure 2.4: Conceptual concentrations for different DDL models

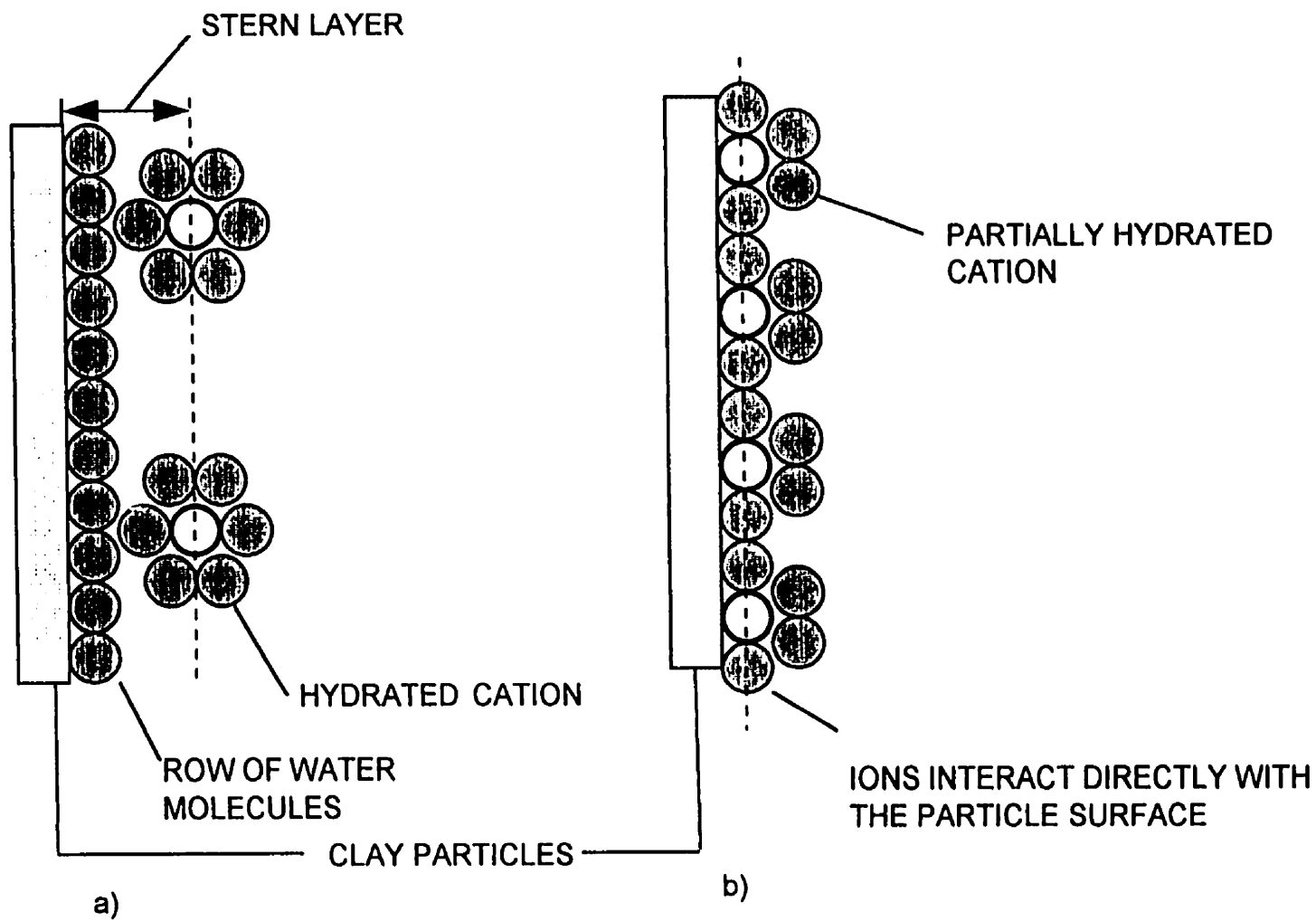


Figure 2.5: Two possible cation arrangements at the surface of a clay particle (after Yong, 1992)

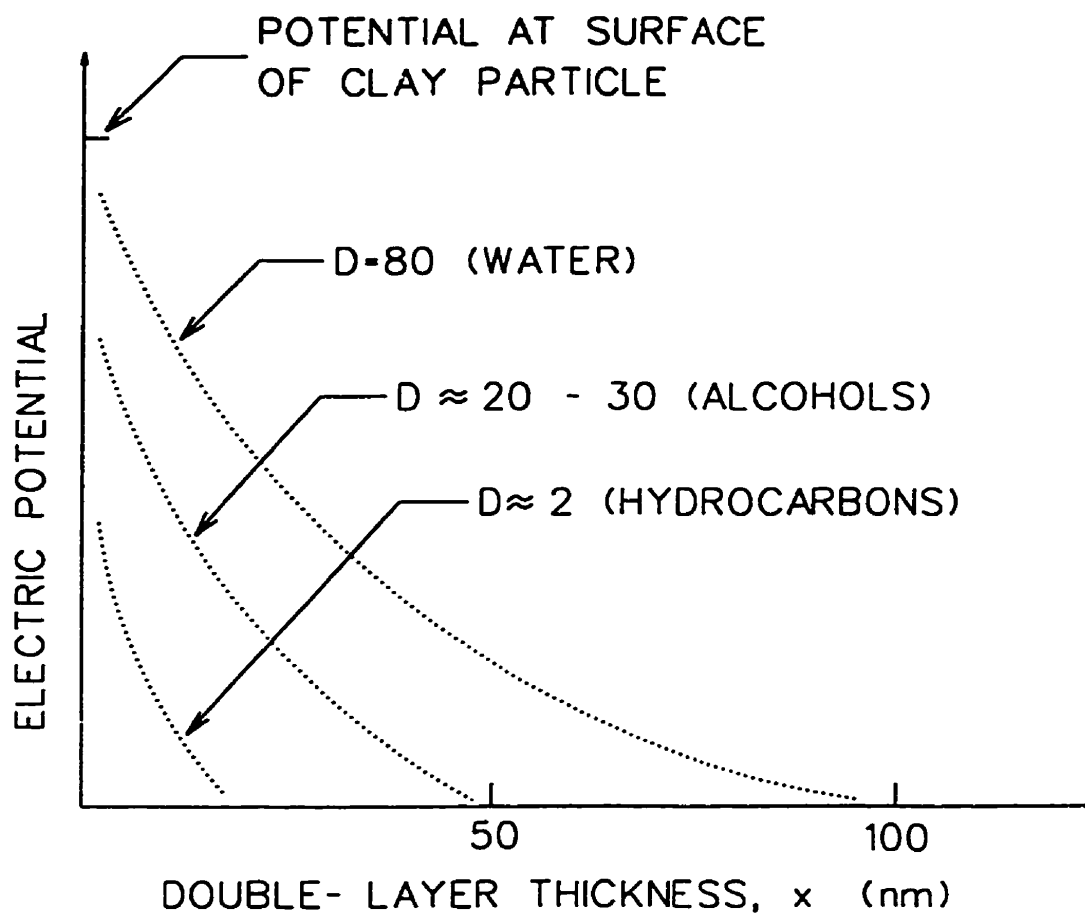


Figure 2.6: Variation in double layer thickness with dielectric constant, D (after Fernandez and Quigley, 1985)

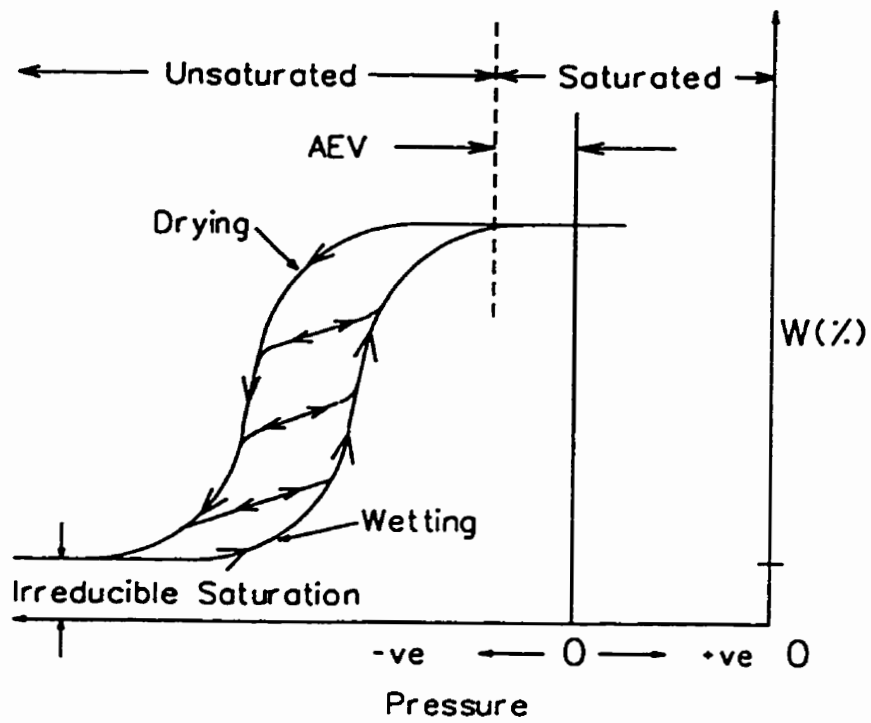


Figure 2.7: Characteristic curve relating water content to pressure (after Freeze and Cherry, 1979)

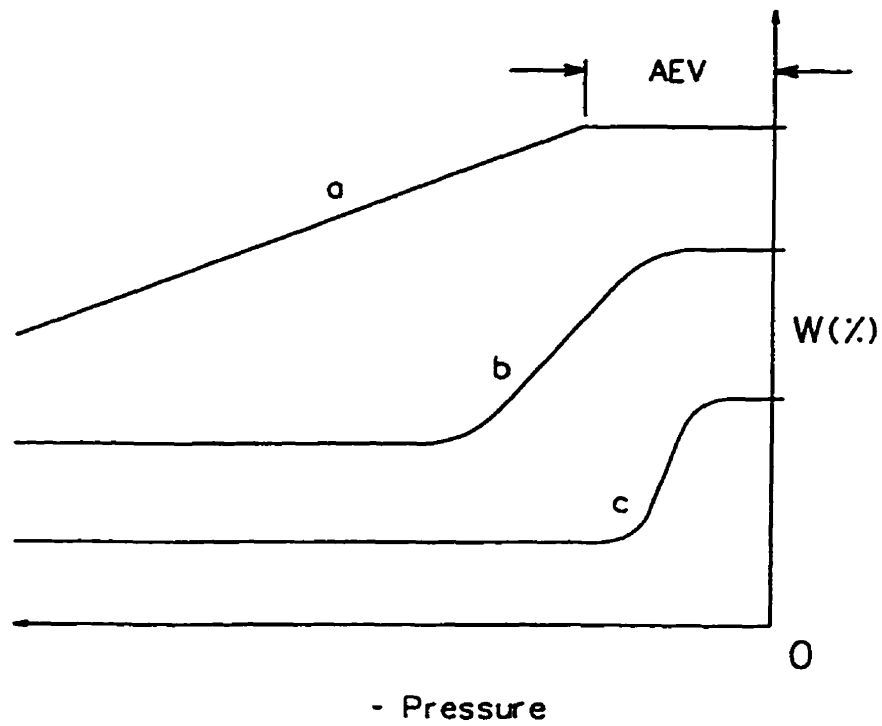


Figure 2.8: Characteristic drainage curves for three hypothetical soils
a) silty clay, b) silty sand, c) uniform sand
(after Freeze and Cherry, 1979)

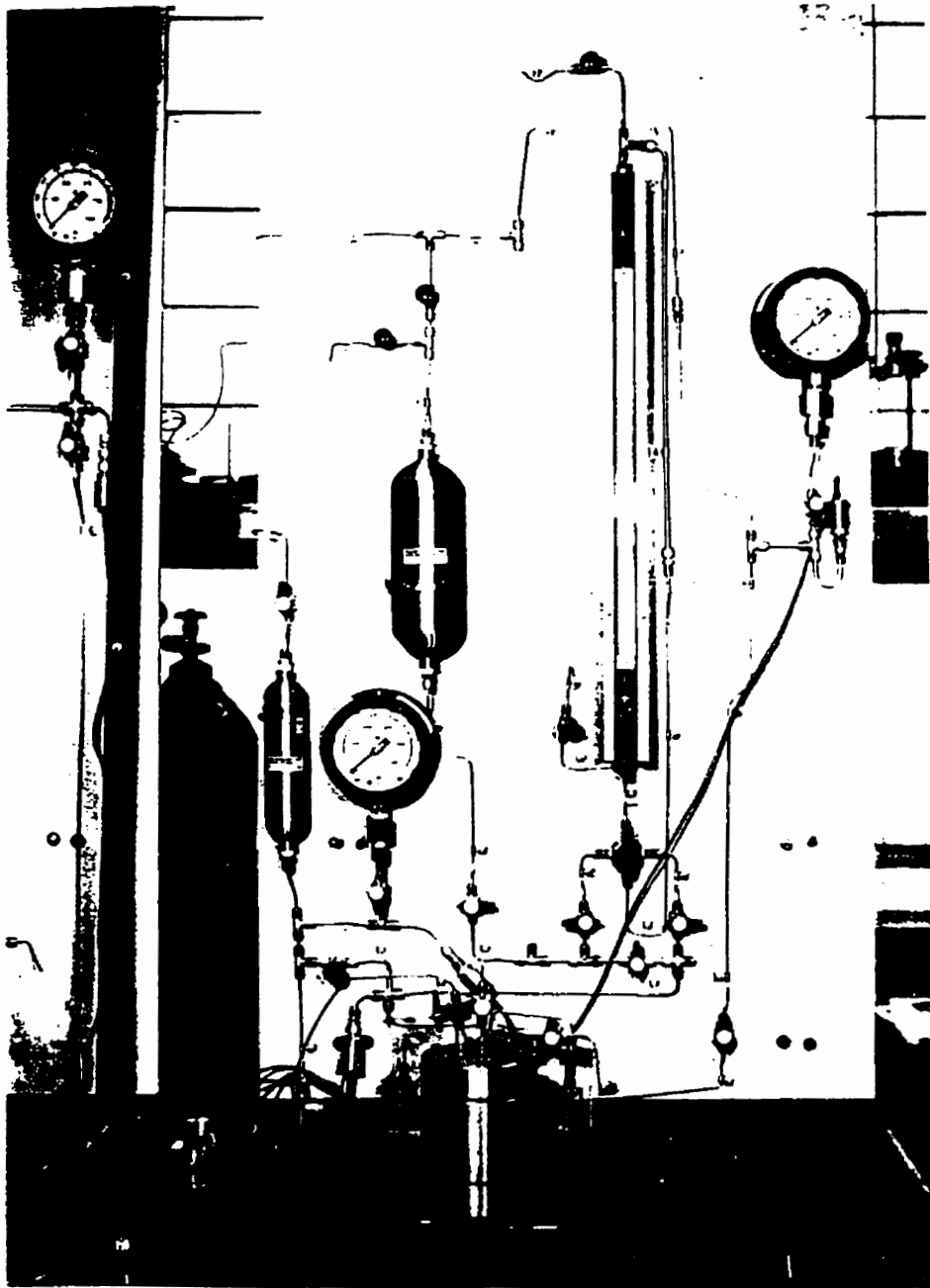


Figure 4.1: Gas breakthrough test board and test cell (after Kirkham, 1995)

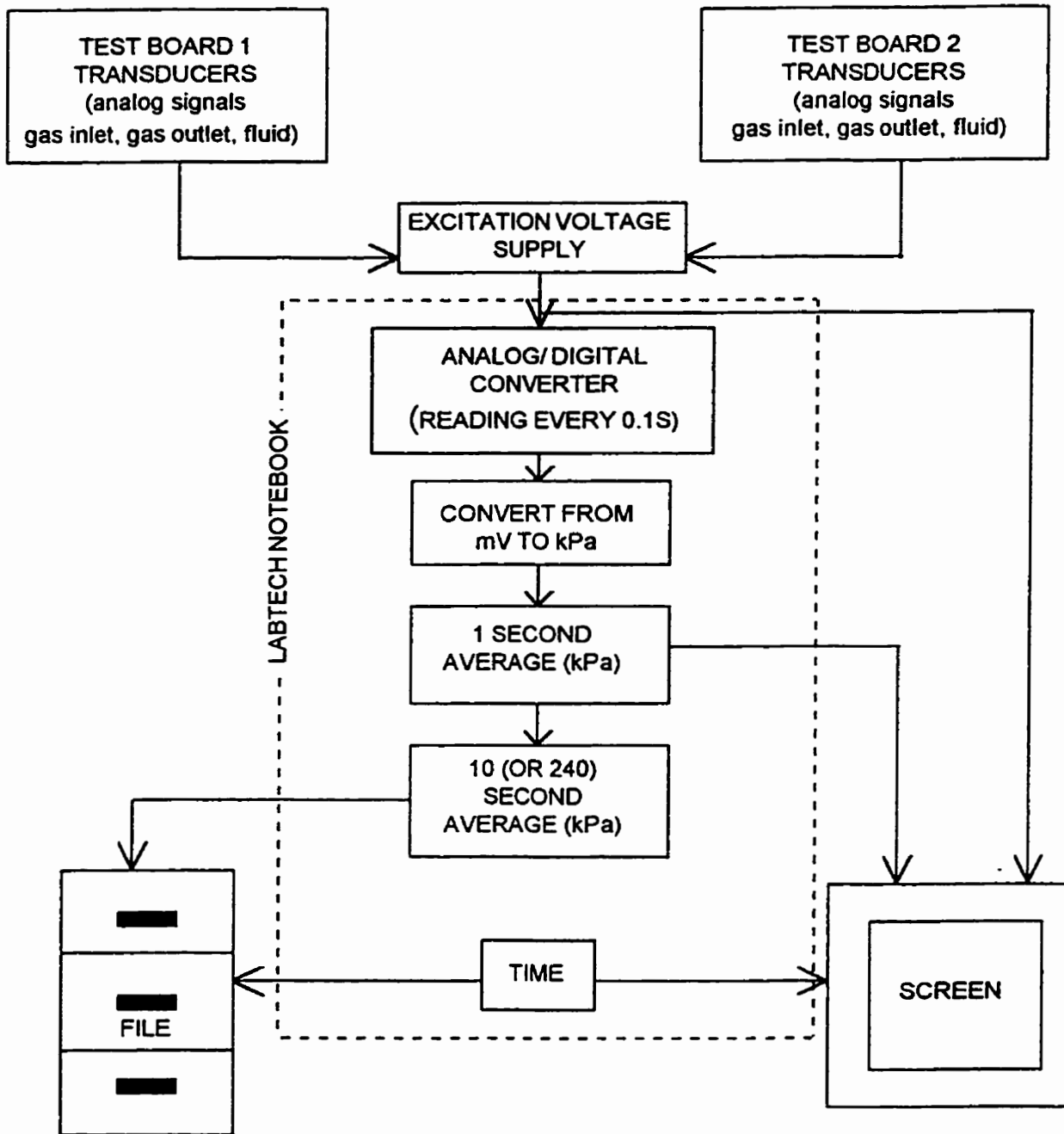


Figure 4.3: Schematic of data acquisition system

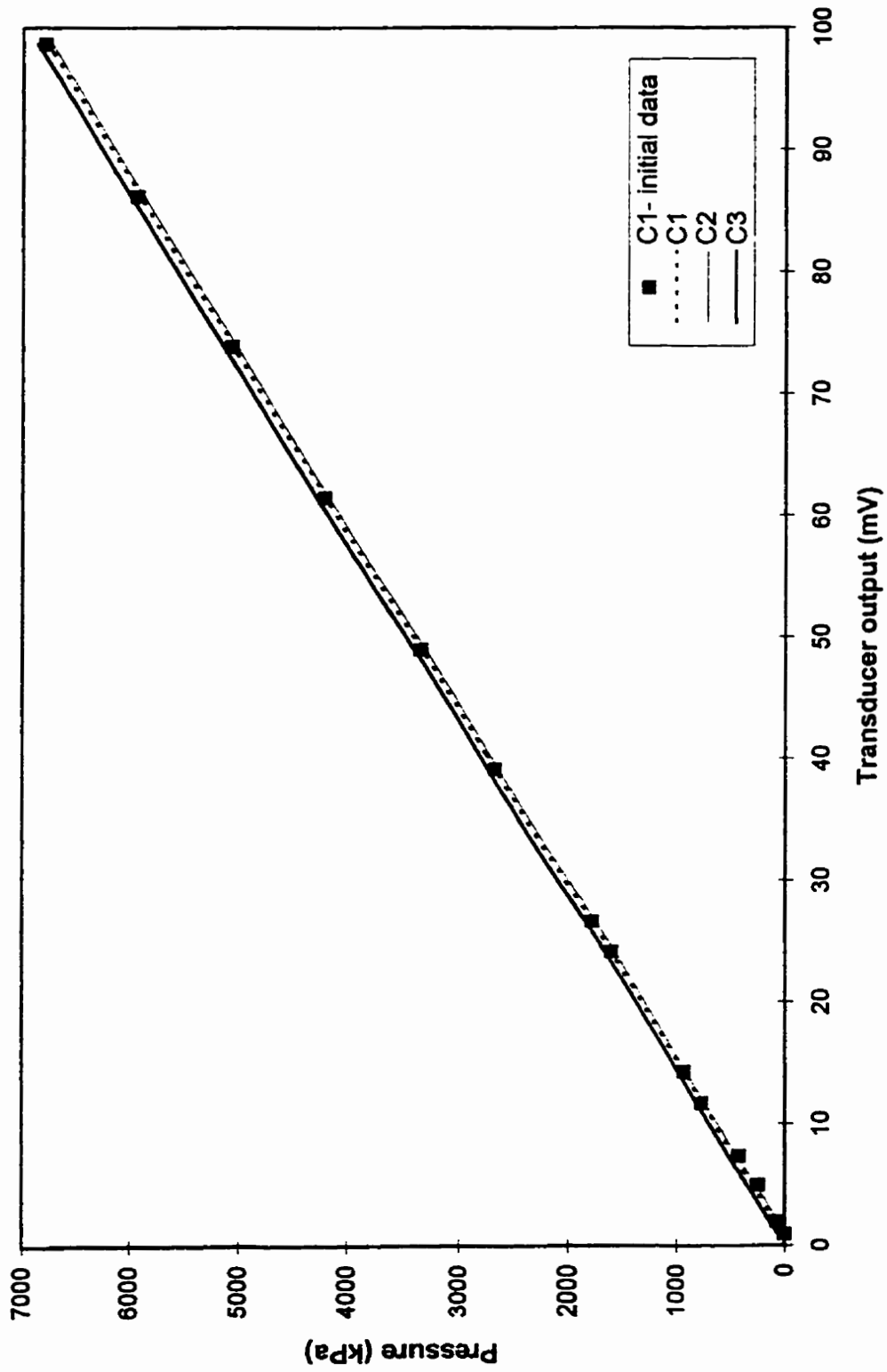


Figure 4.4 - Calibration data for pressure transducer 66544

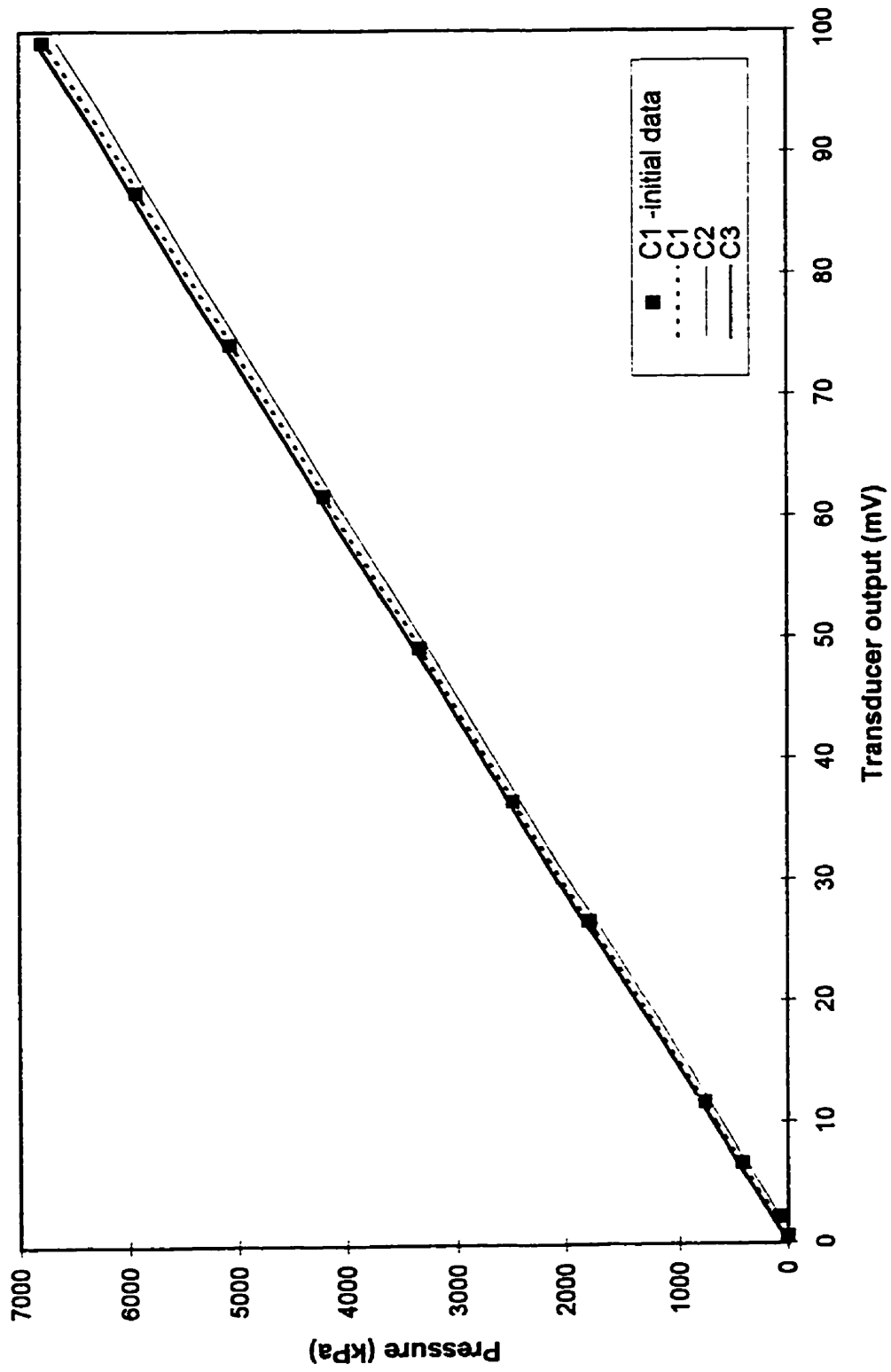


Figure 4.5 - Calibration data for pressure transducer 65842

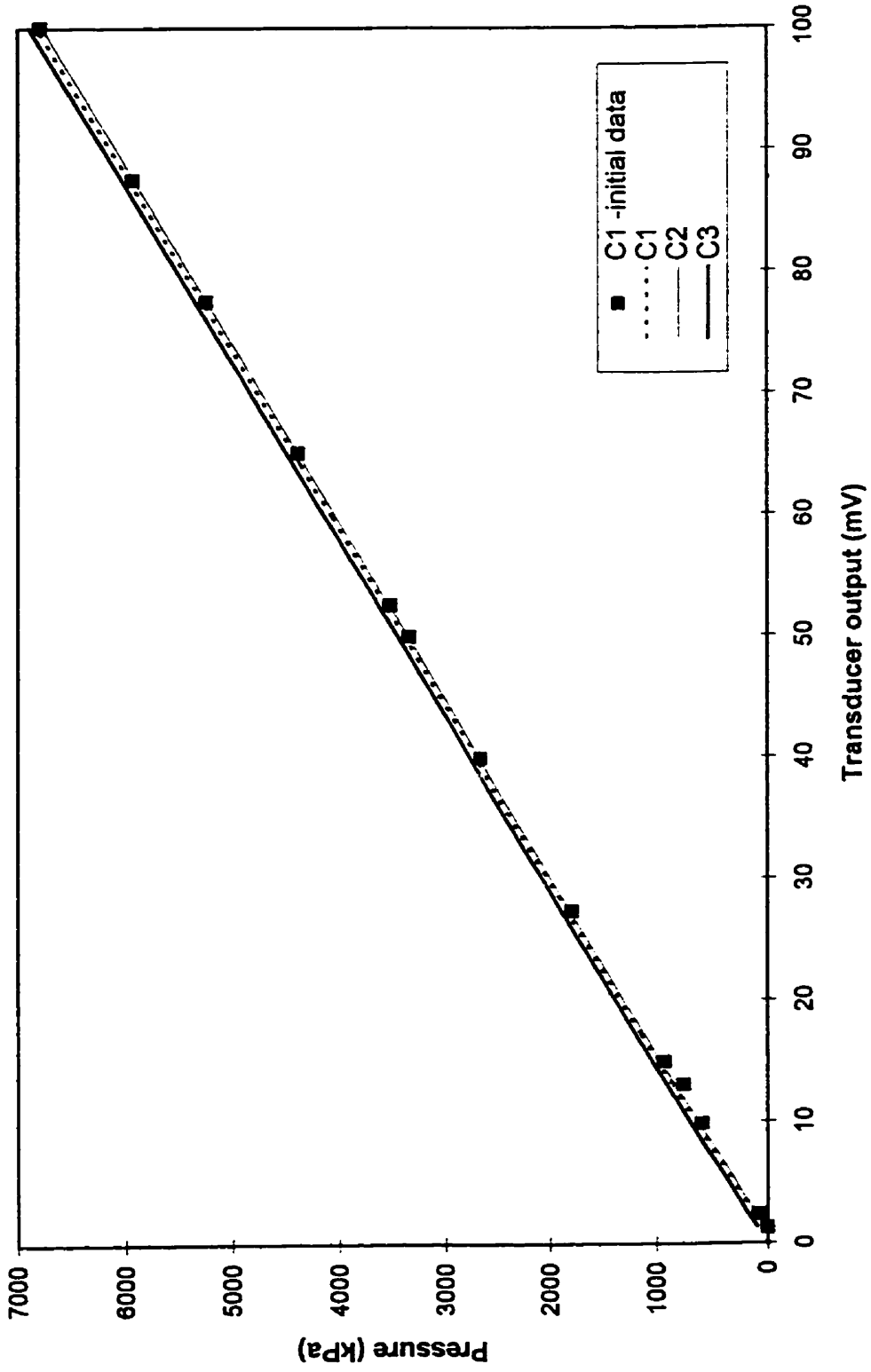


Figure 4.6 - Calibration data for pressure transducer 65843

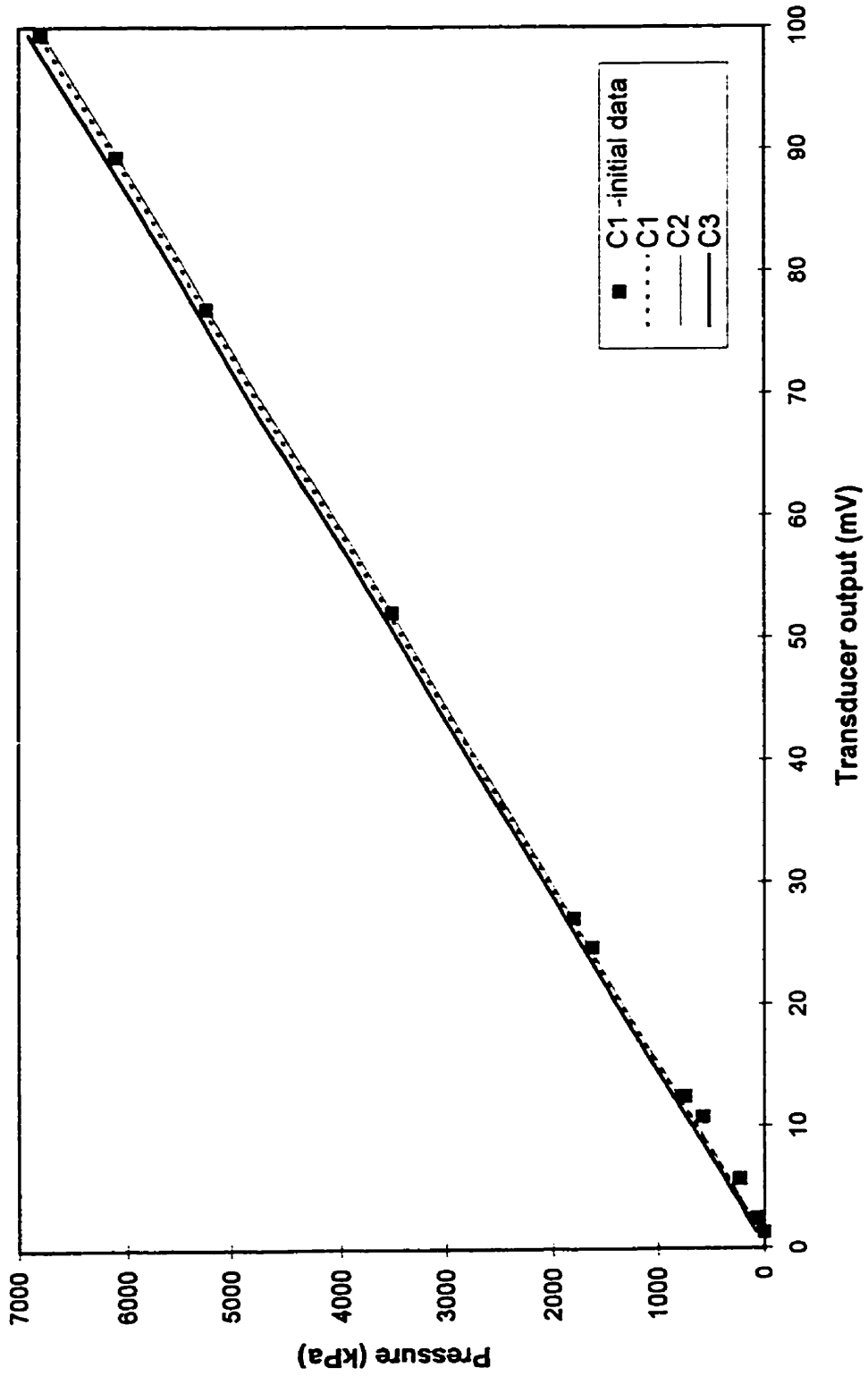


Figure 4.7 - Calibration data for pressure transducer 66542

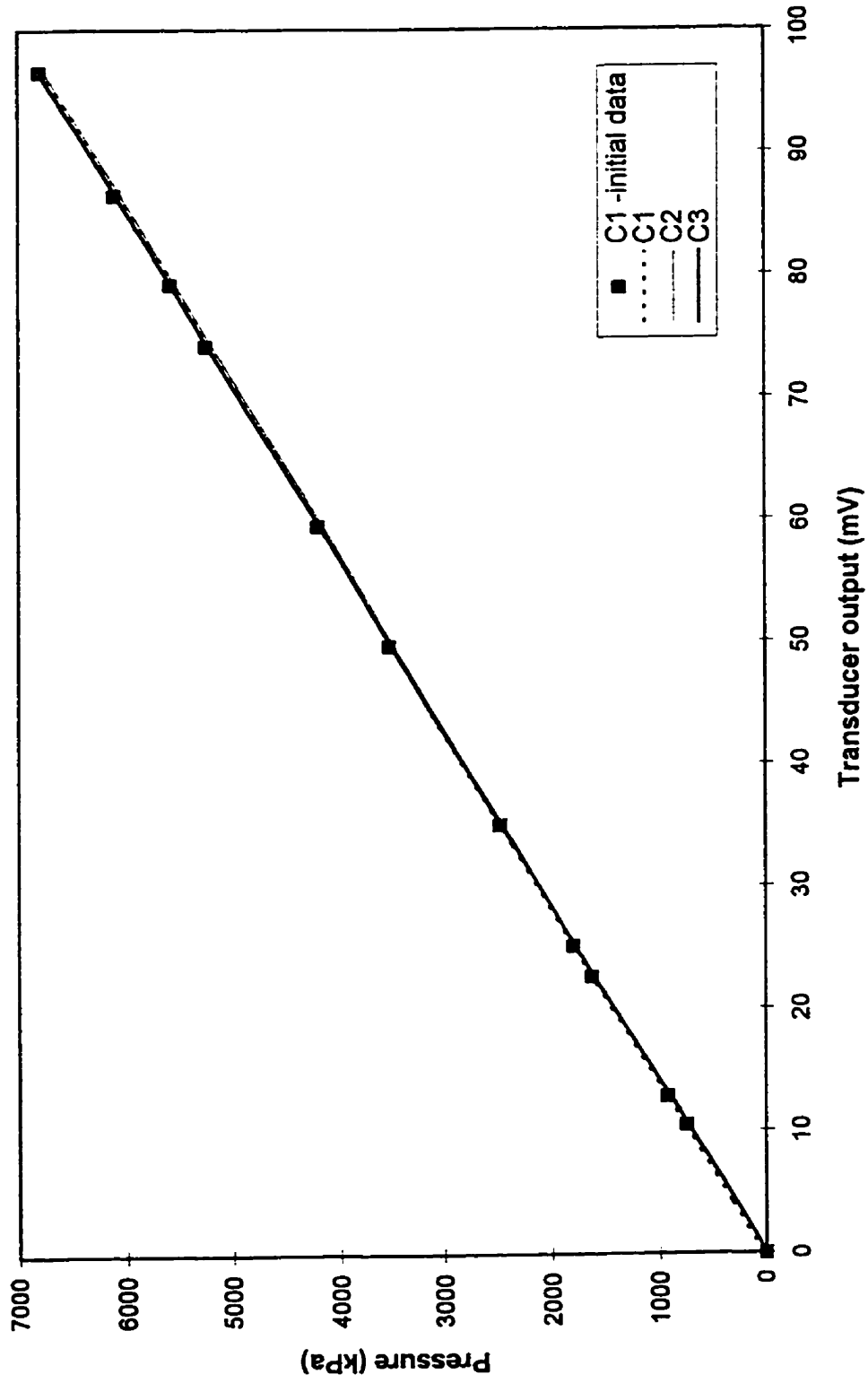


Figure 4.8 - Calibration data for pressure transducer 66543

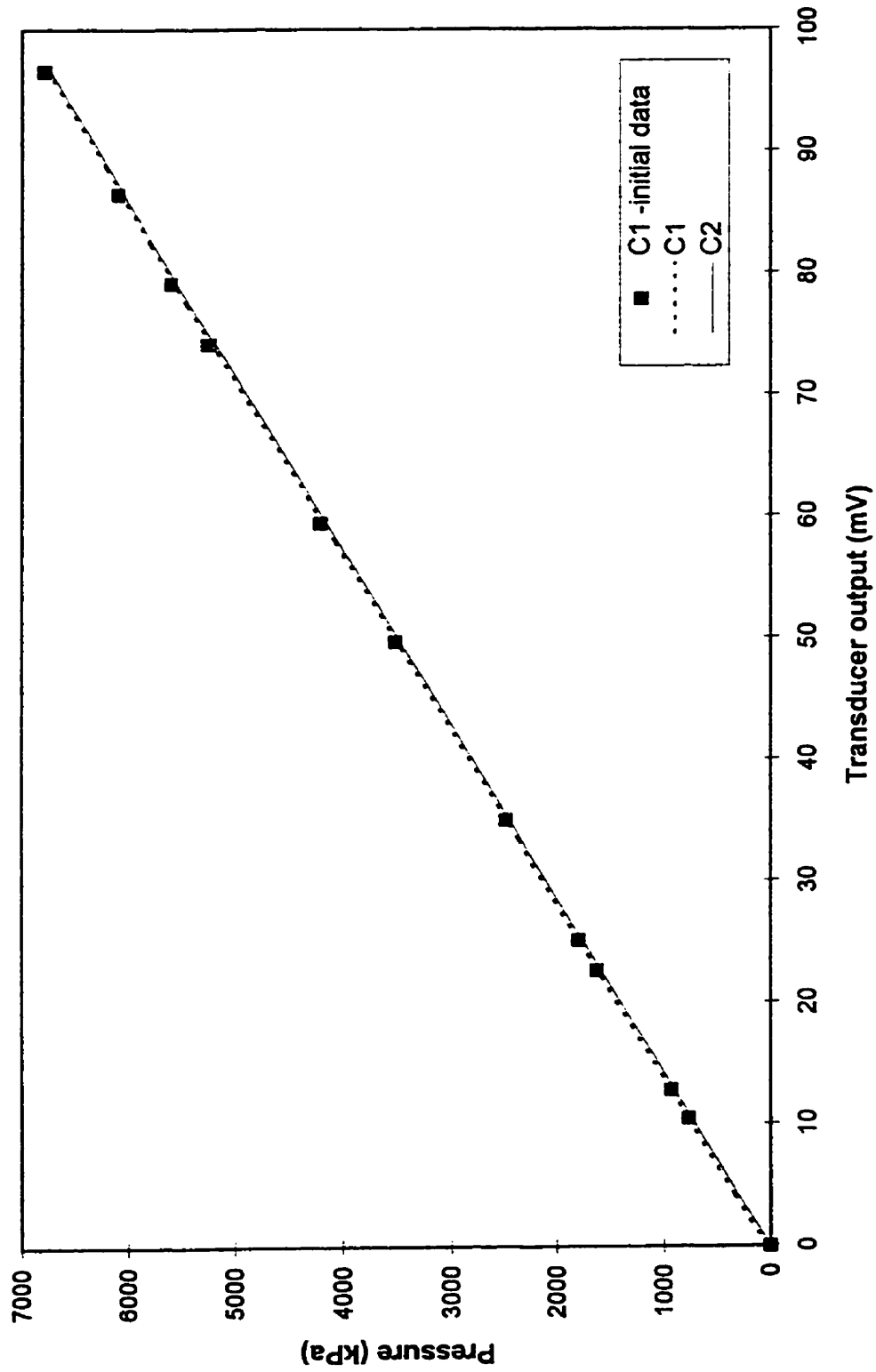


Figure 4.9 - Calibration data for pressure transducer 65841

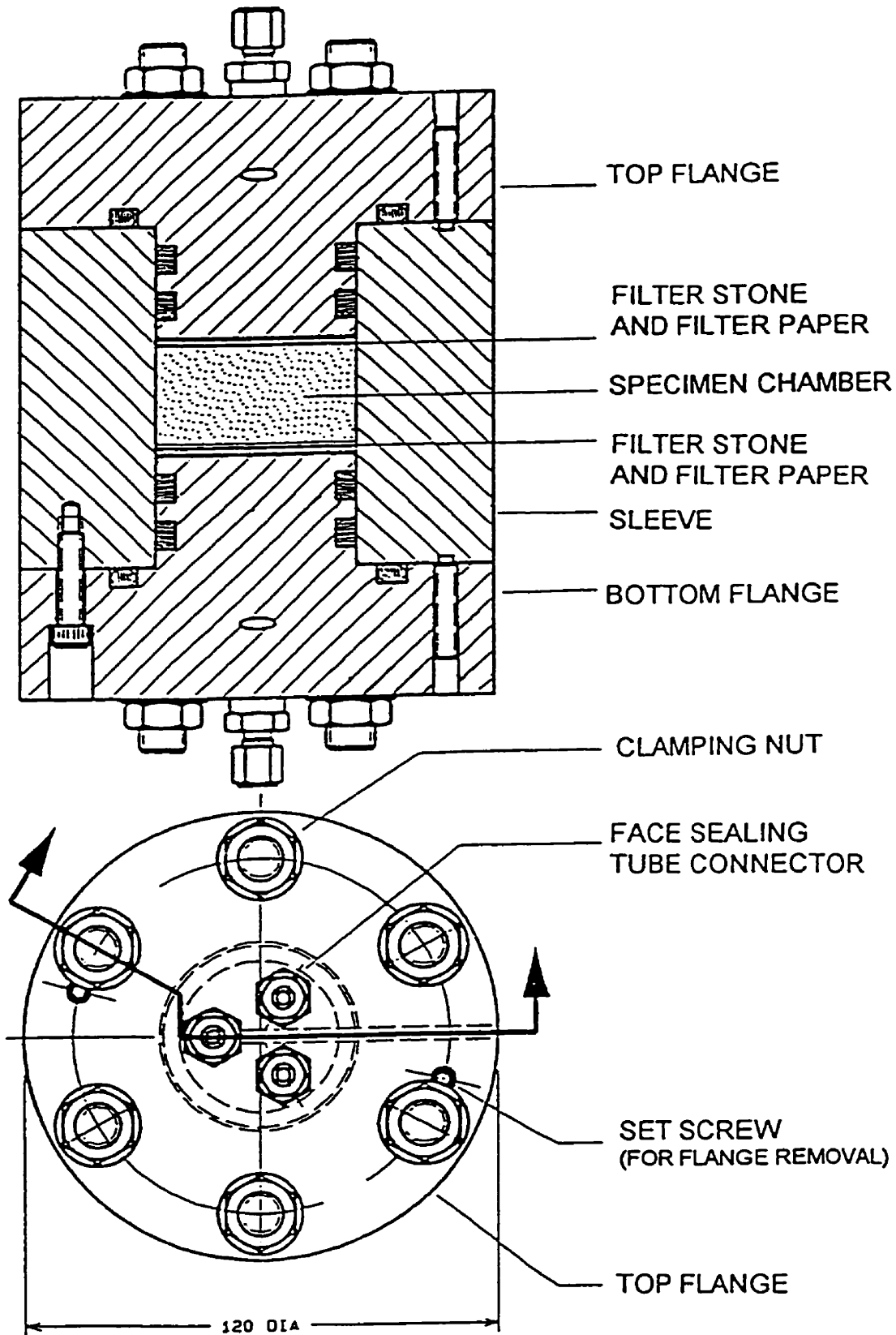


Figure 4.10: Cross-section of test cell (after Kirkham, 1995)

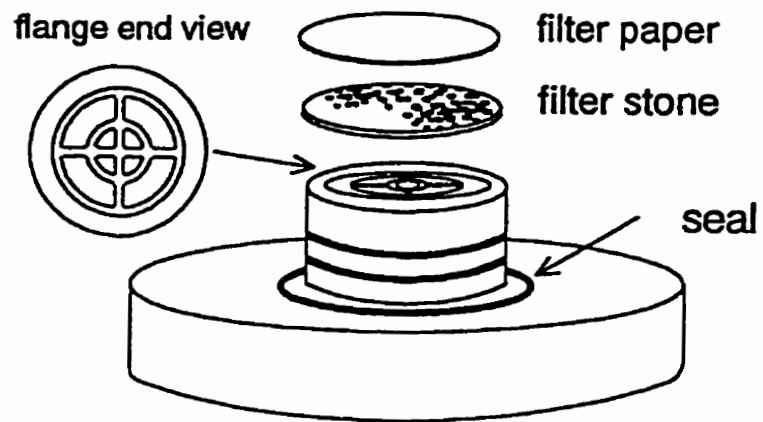


Figure 4.11: Exploded view of test cell flange and filters (after Kirkham, 1995)

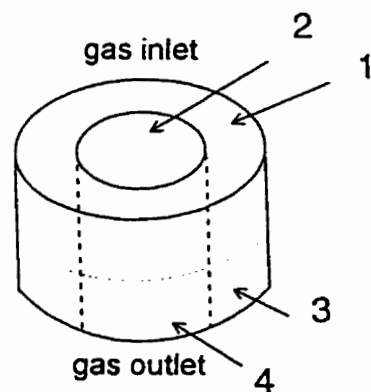


Figure 4.12: Division of specimen for water content tests

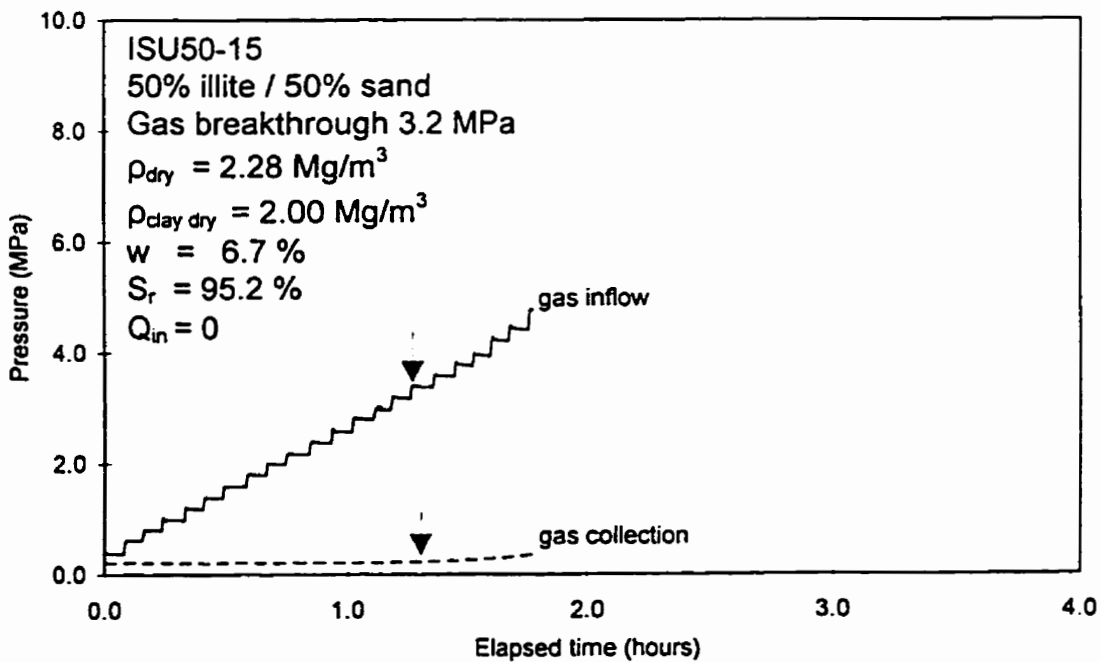
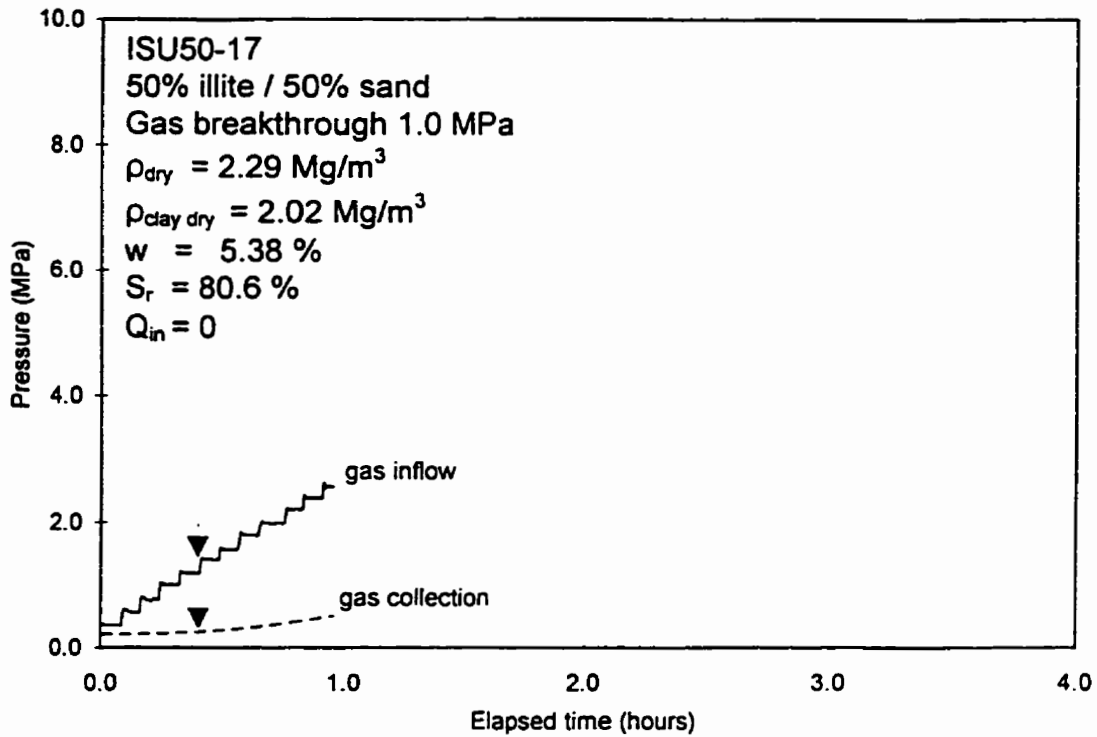


Figure 5.1: Increasing gas breakthrough pressure with increasing S_r

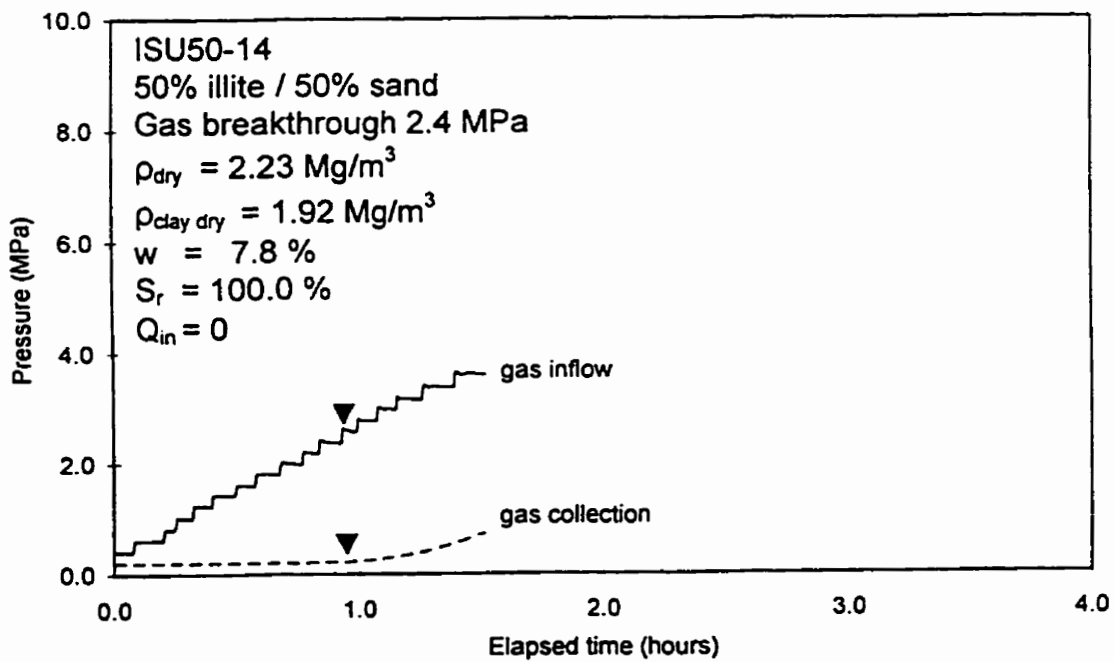
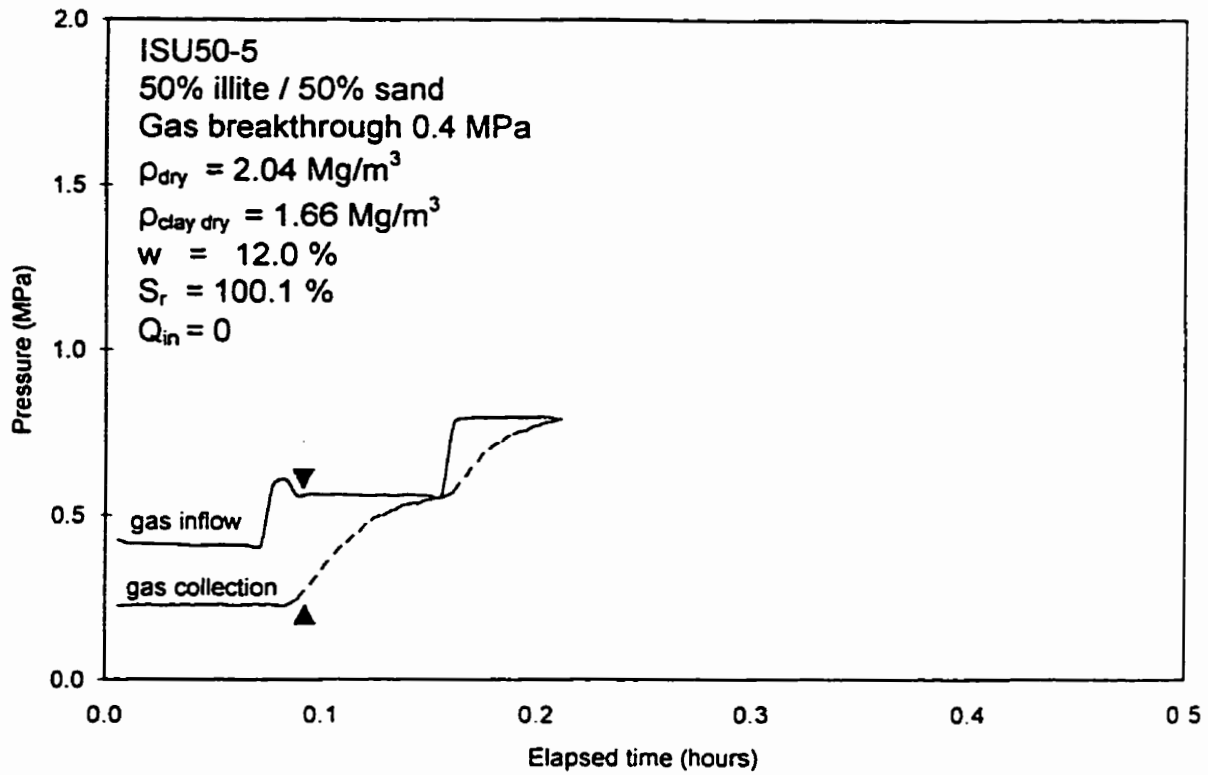


Figure 5.2: Increasing gas breakthrough pressure with increasing ρ_{dry}

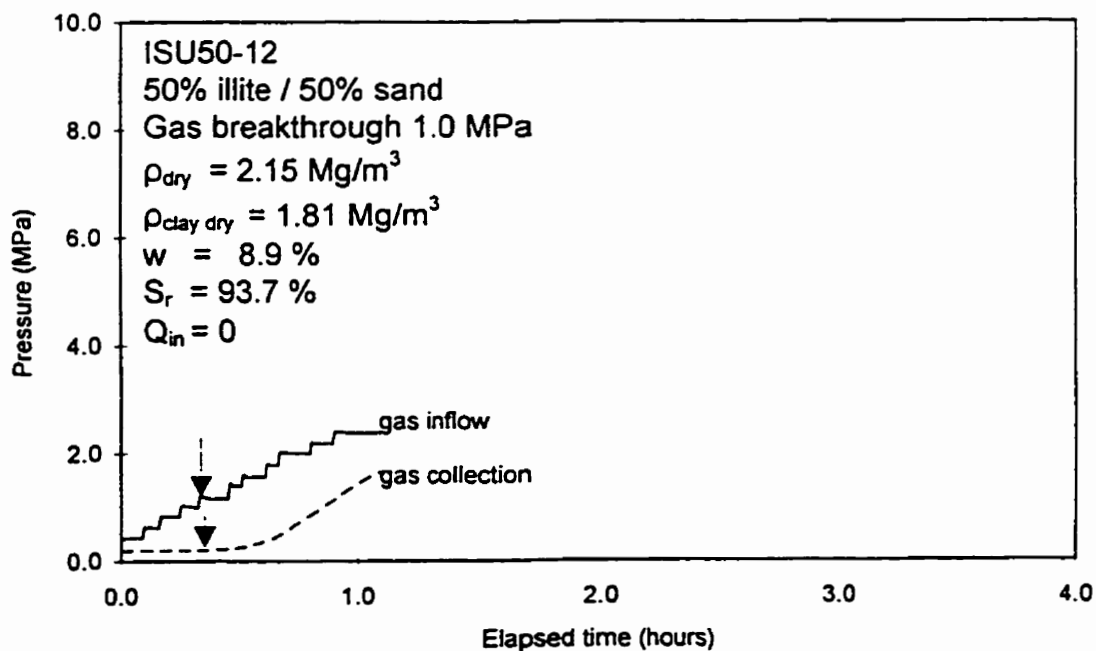
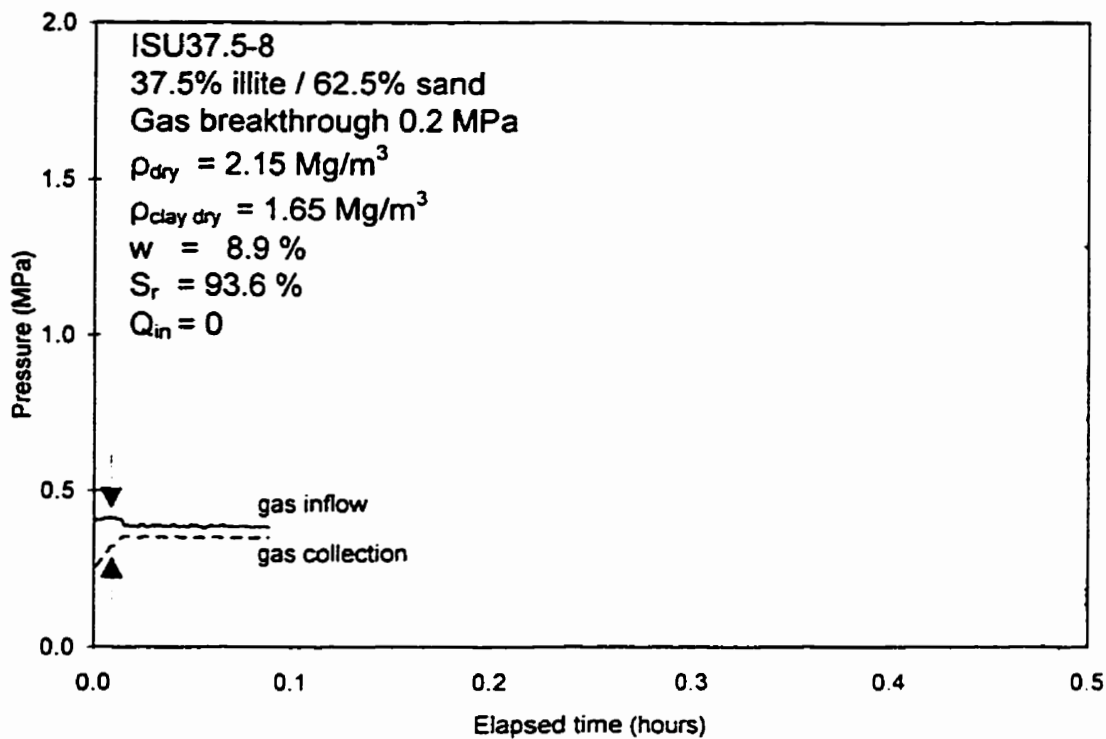


Figure 5.3: Increasing gas breakthrough pressure with increasing $\rho_{clay\ dry}$

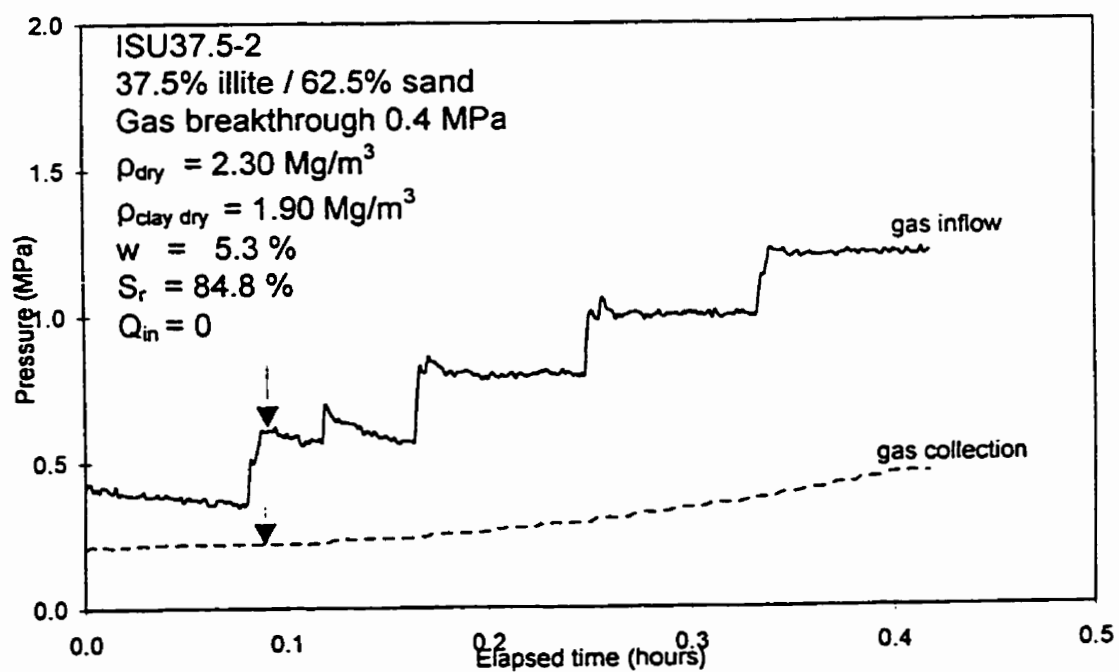
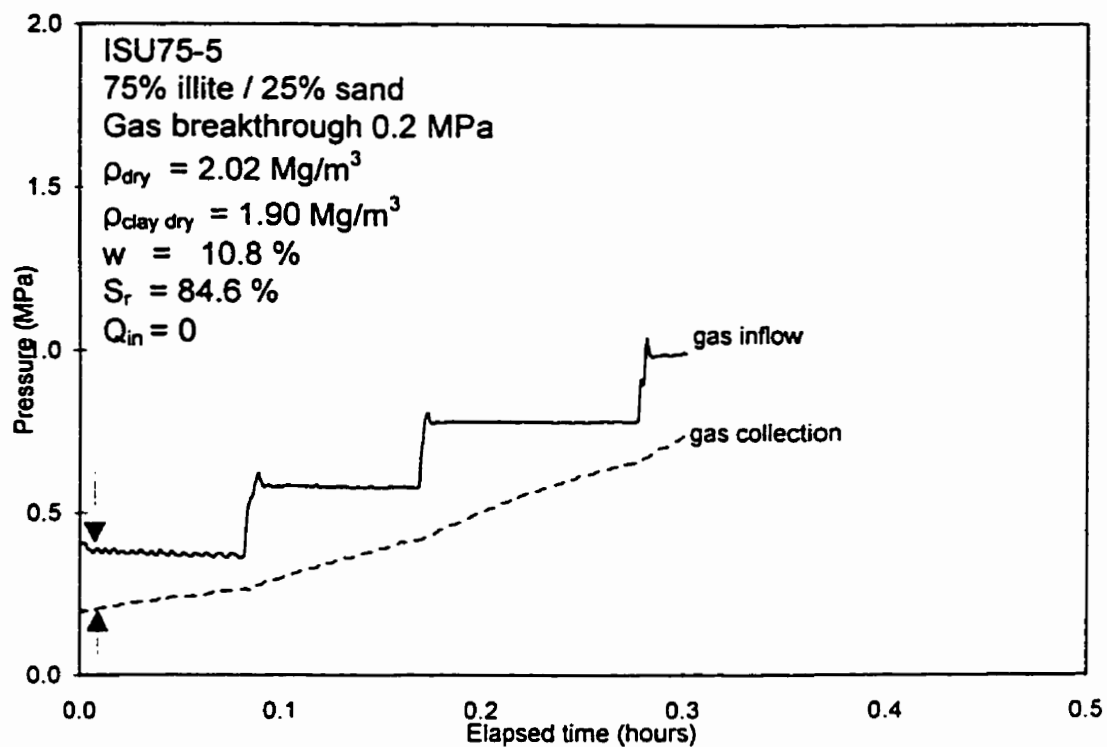


Figure 5.4: Decreasing rate of gas breakthrough with increasing ρ_{dry}

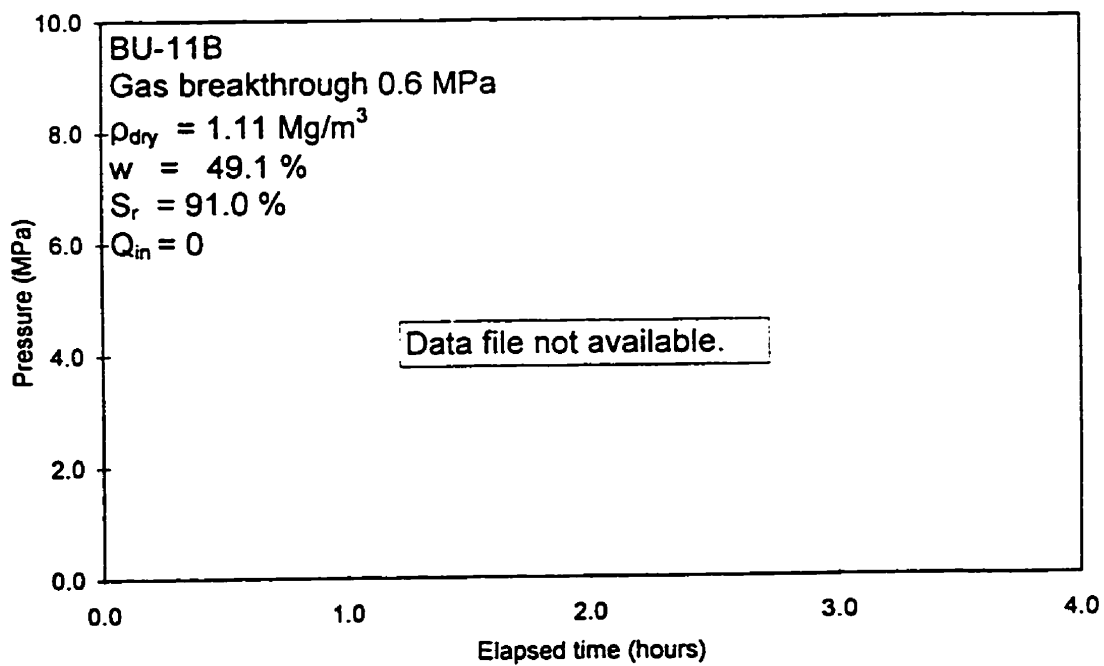
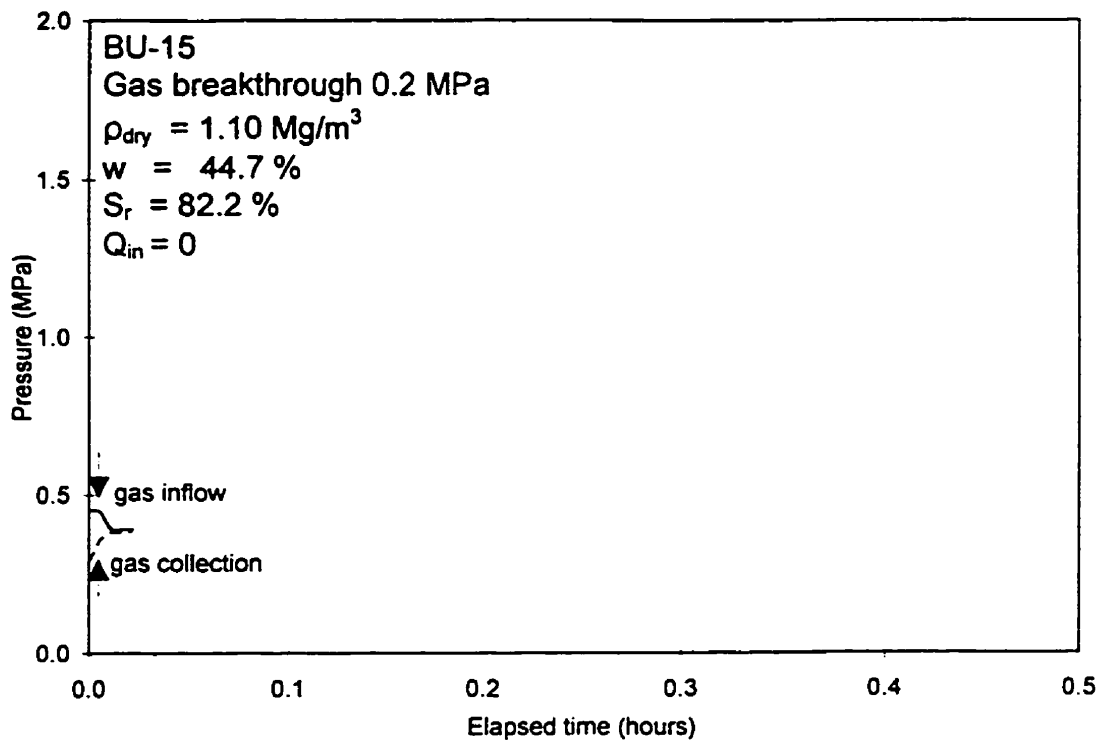


Figure 5.5(a): Increasing gas breakthrough with increasing S_r

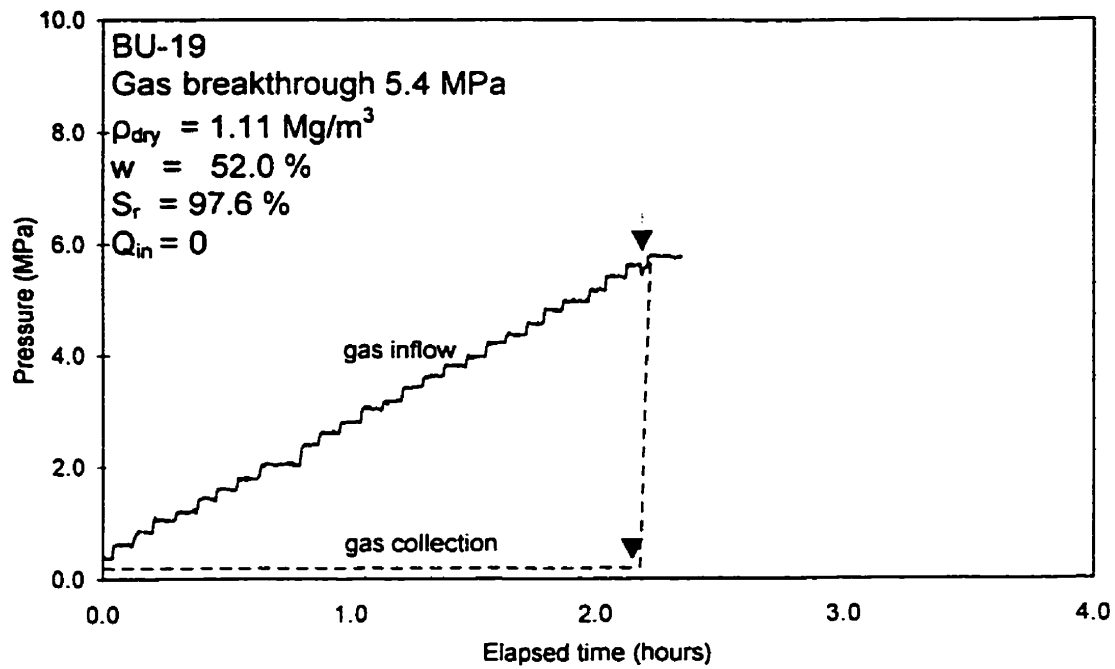


Figure 5.5(b): Increasing gas breakthrough with increasing S_r

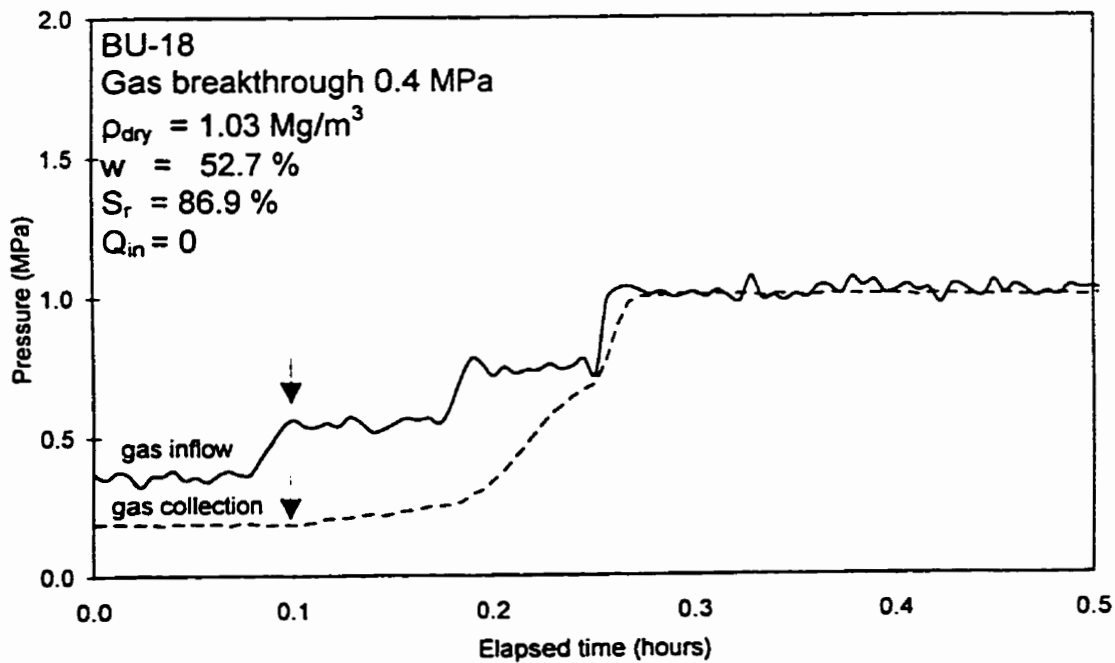
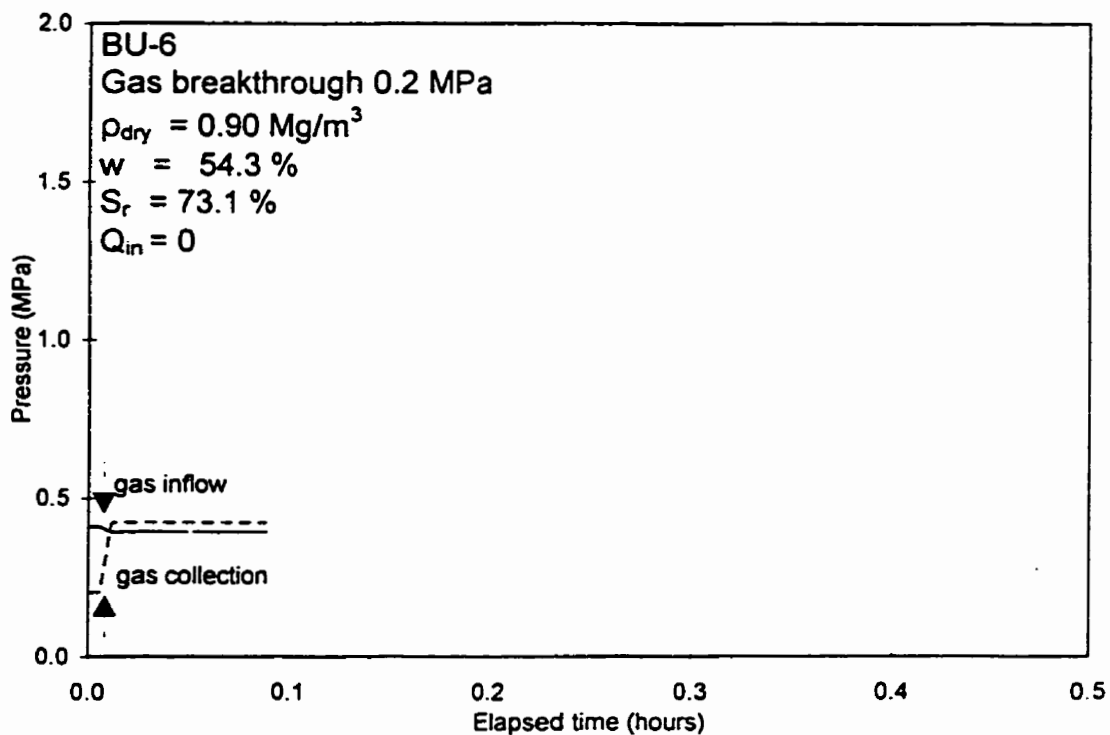


Figure 5.6(a): Increasing gas breakthrough pressure with increasing ρ_{dry}

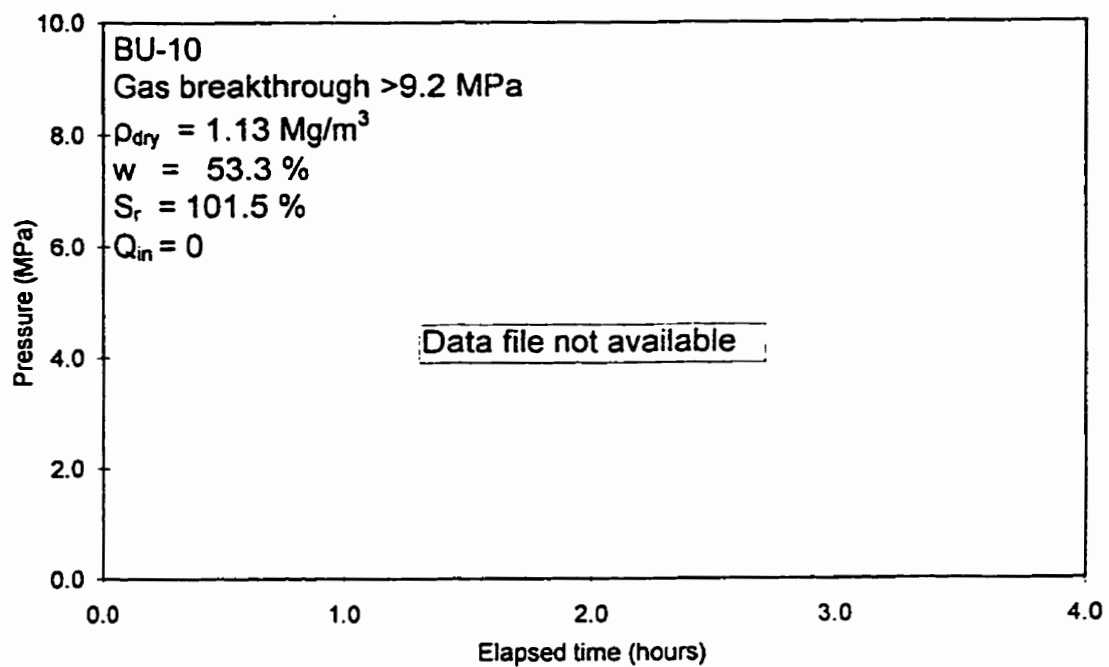


Figure 5.6(b): Increasing gas breakthrough pressure with increasing ρ_{dry}

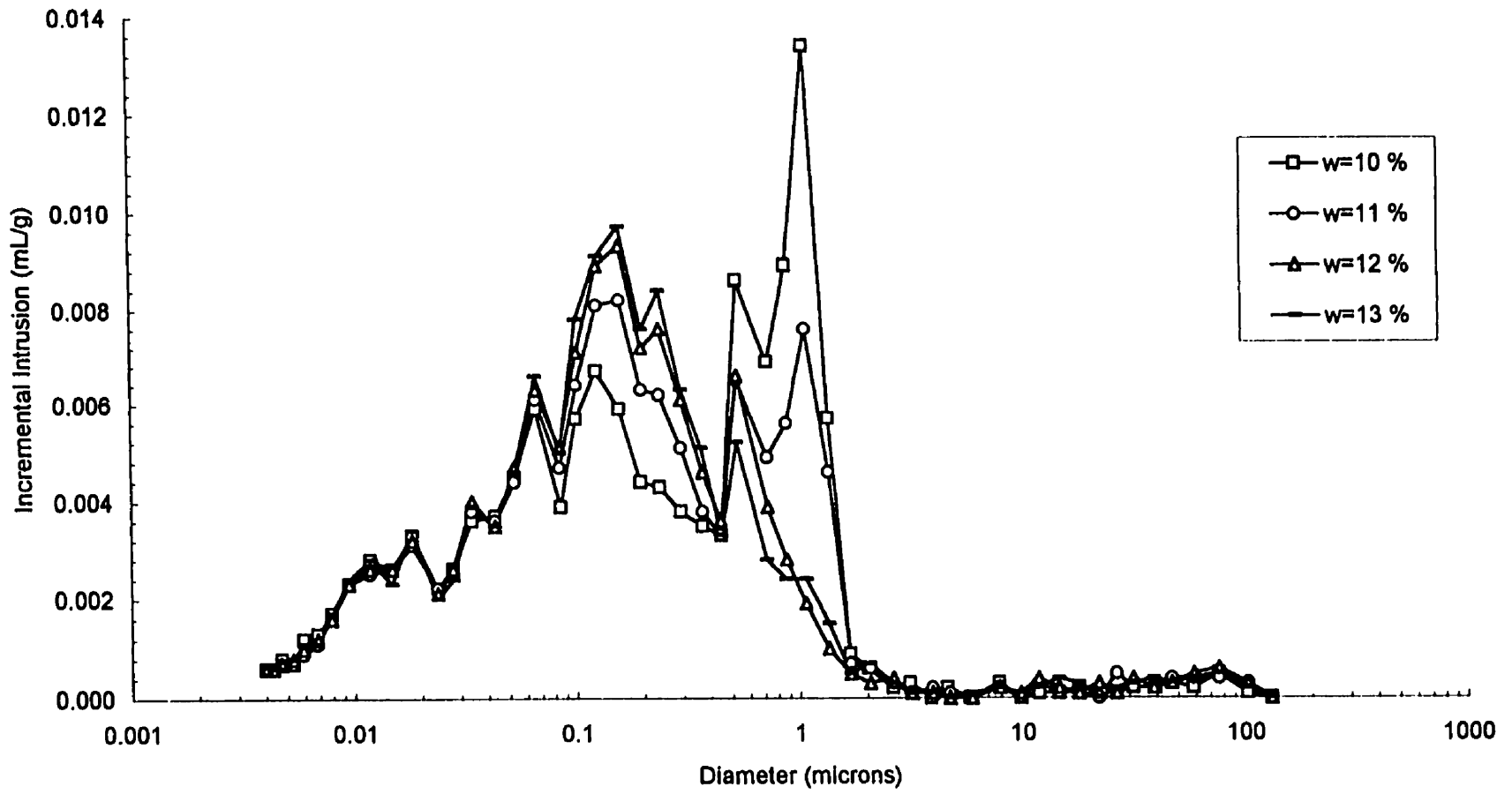


Figure 5.7: Pore size distributions for illite specimens compacted to $\rho_d = 2.04 \text{ Mg/m}^3$ at varying water content

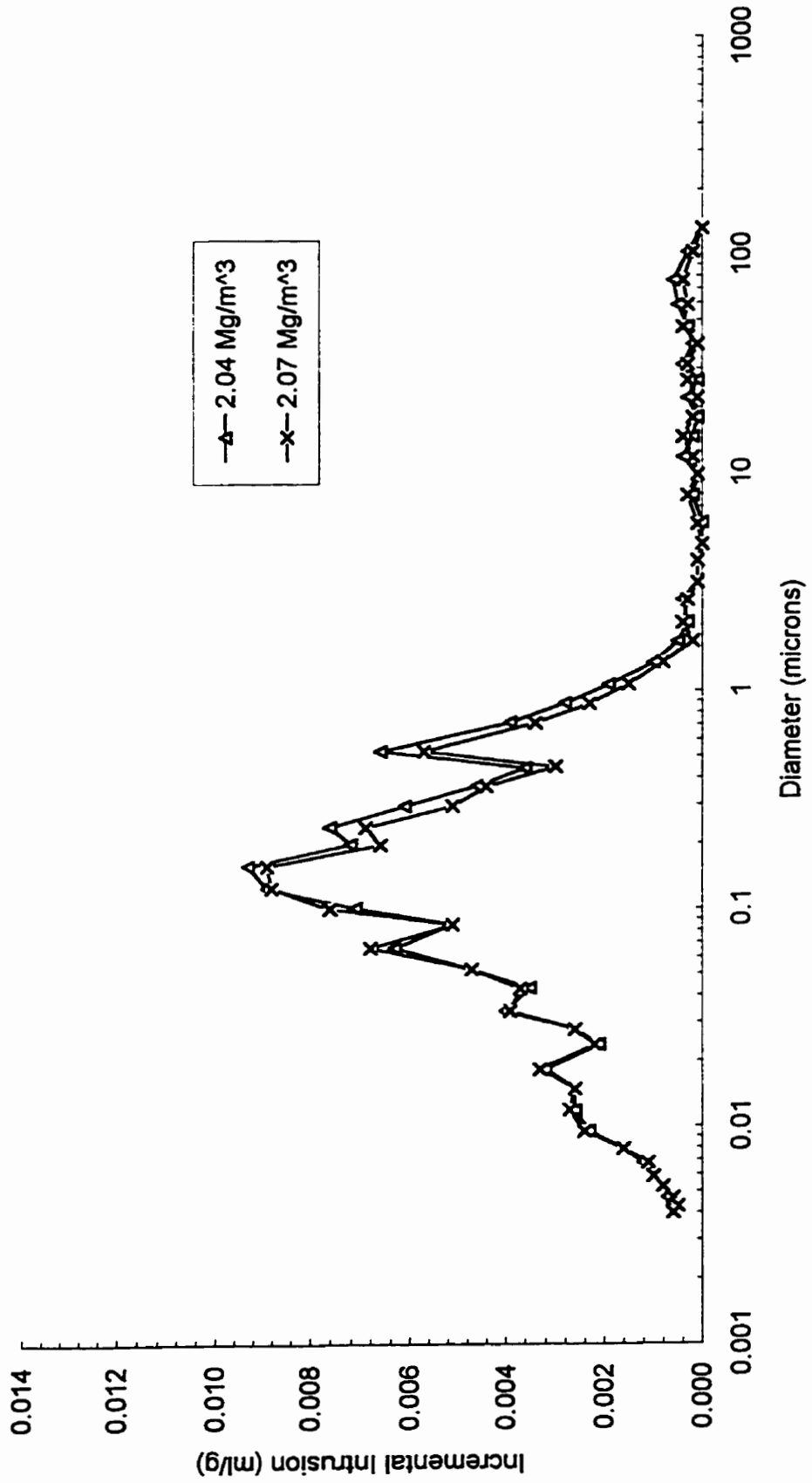


Figure 5.8: Pore size distributions for illite specimens compacted to $w = 12\%$ with varying p_d

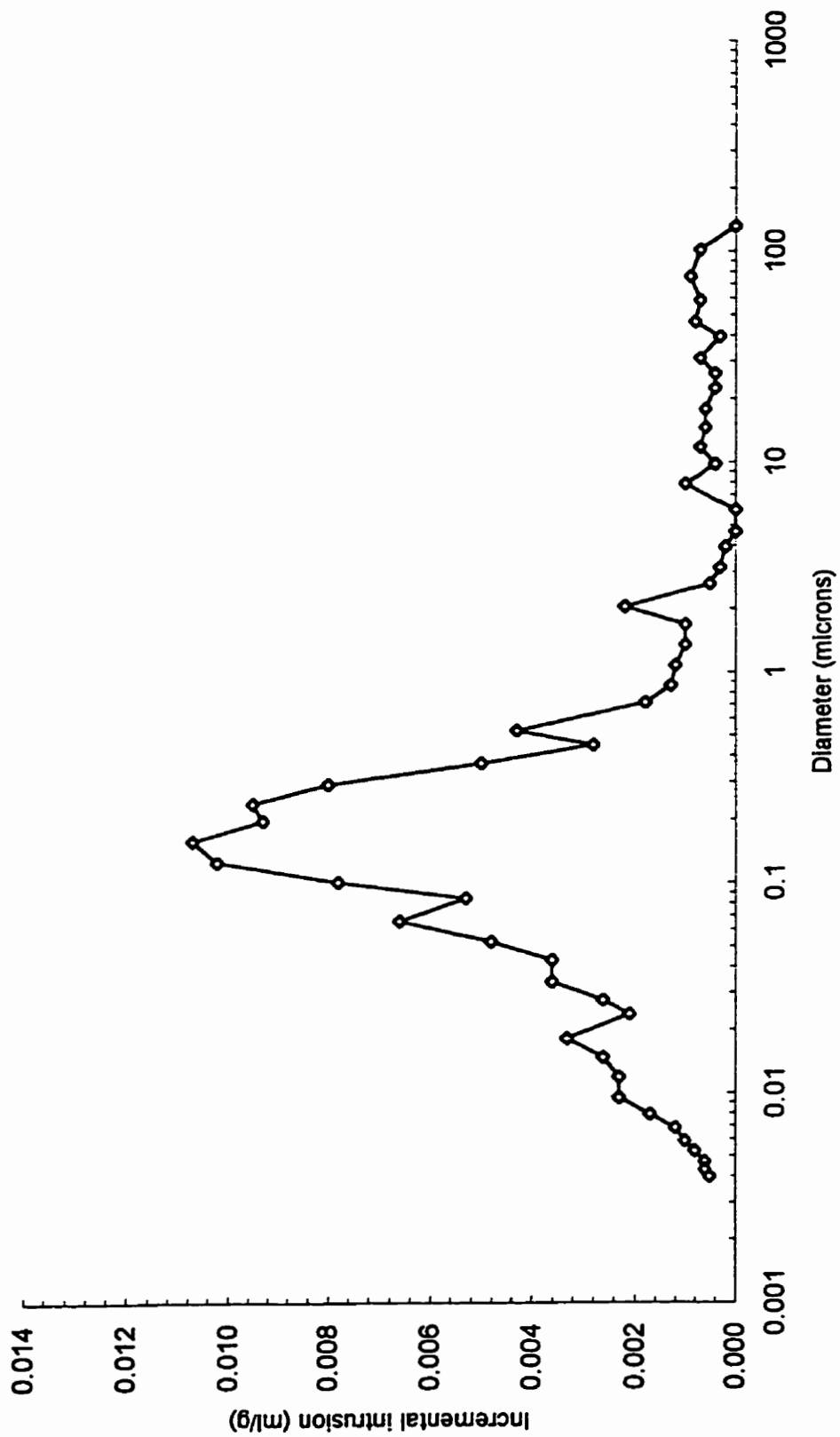


Figure 5.9 : Pore size distribution of illite with a single peak, $\rho_d = 1.95 \text{ Mg/m}^3$, $w = 15\%$

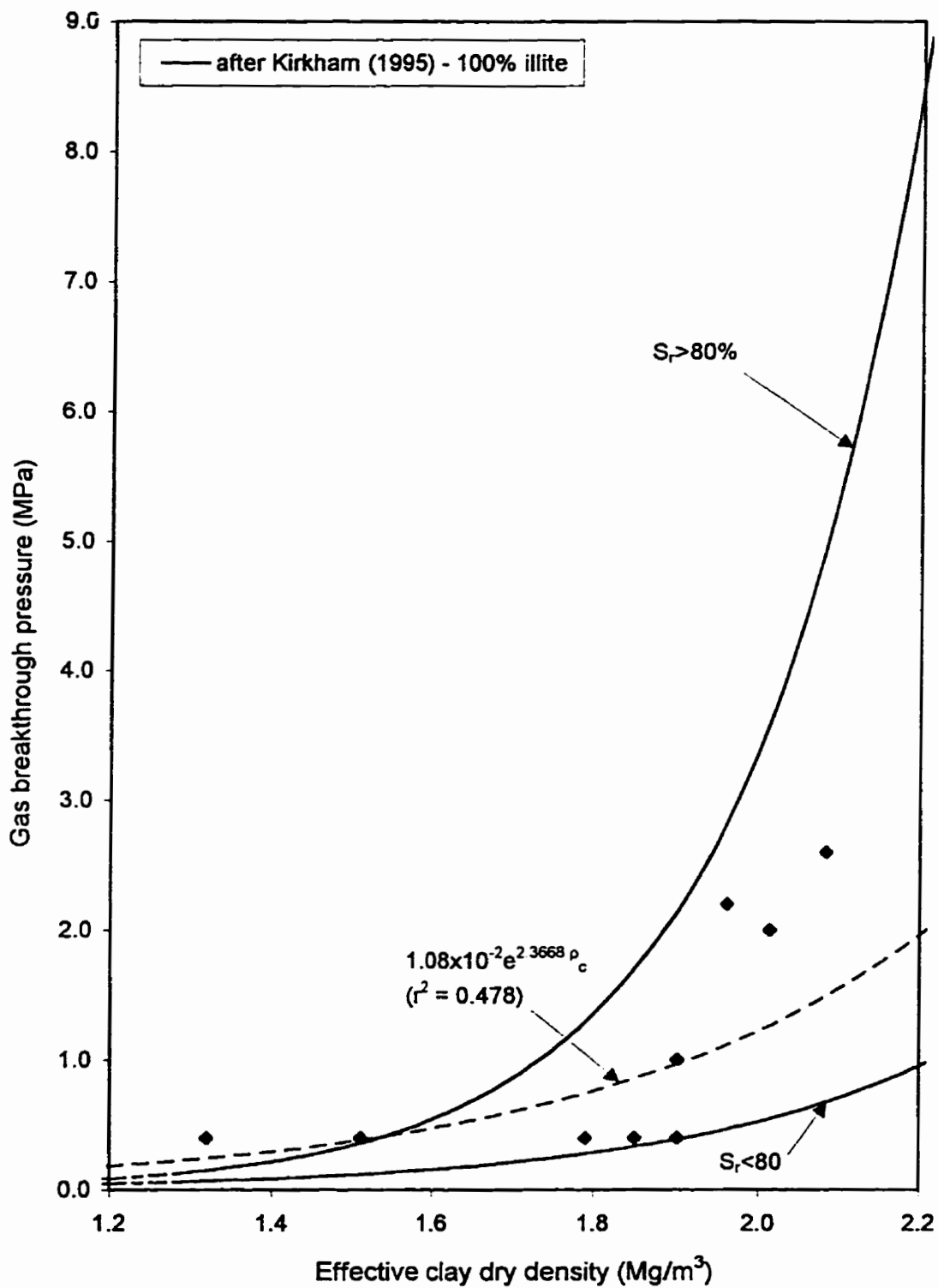


Figure 6.1: Gas breakthrough pressure - effective clay dry density relationship for illite/sand specimens with $S_r = 85-90\%$

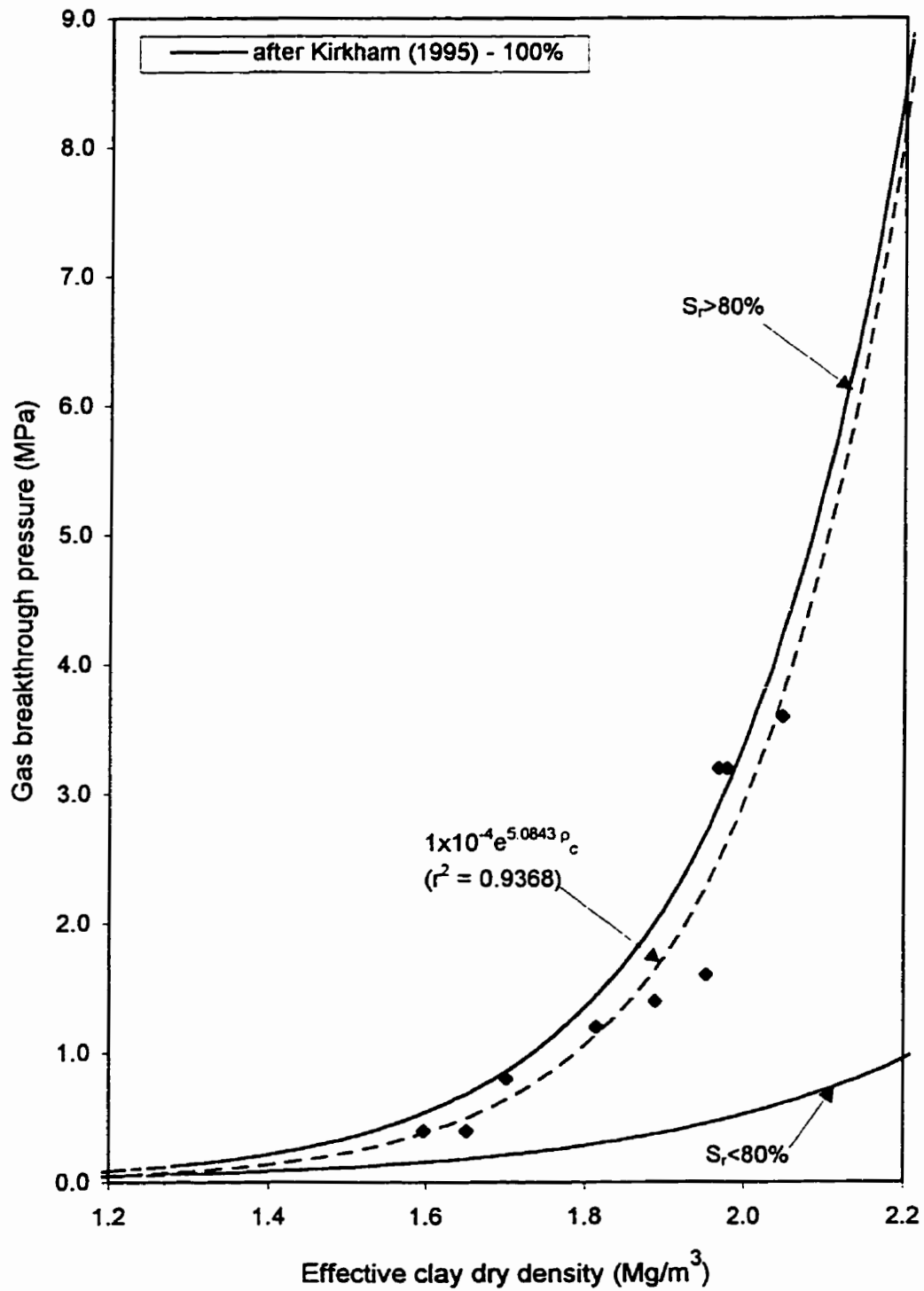


Figure 6.2: Gas breakthrough pressure - effective clay dry density relationship for illite/sand specimens with $S_r = 90-95\%$

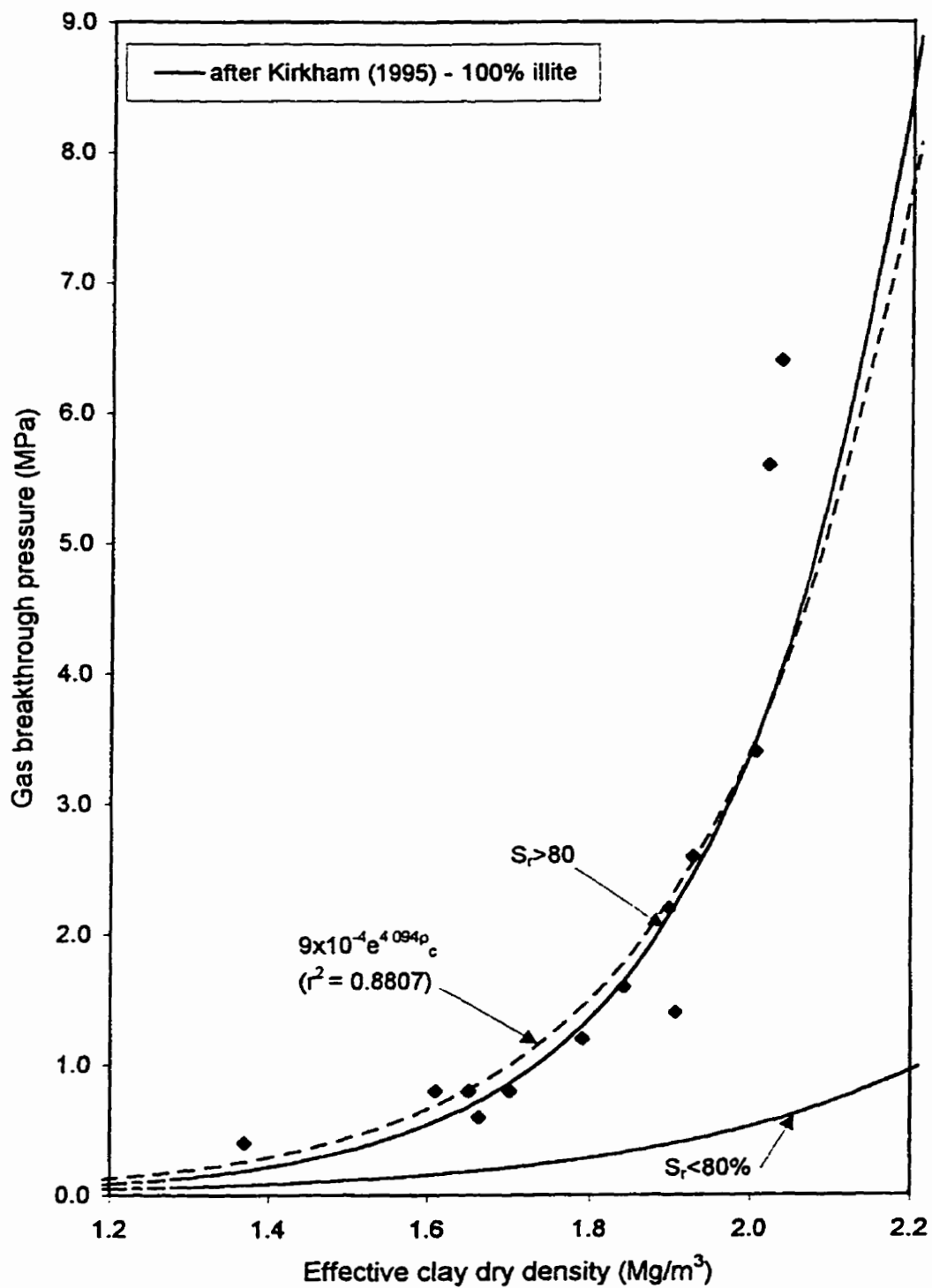


Figure 6.3: Gas breakthrough pressure - effective clay dry density relationship for illite/sand specimens with $S_r = 95-100\%$

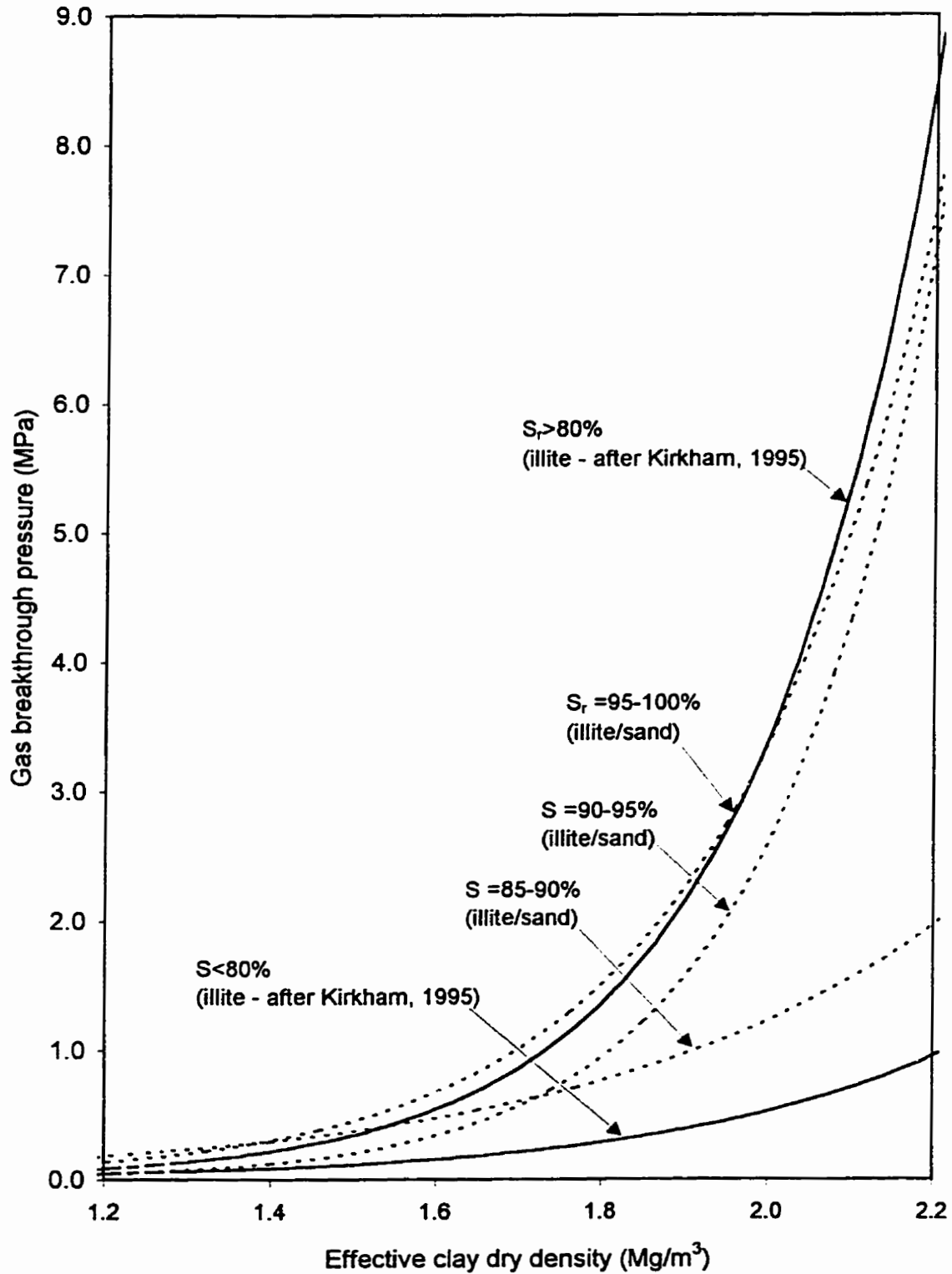
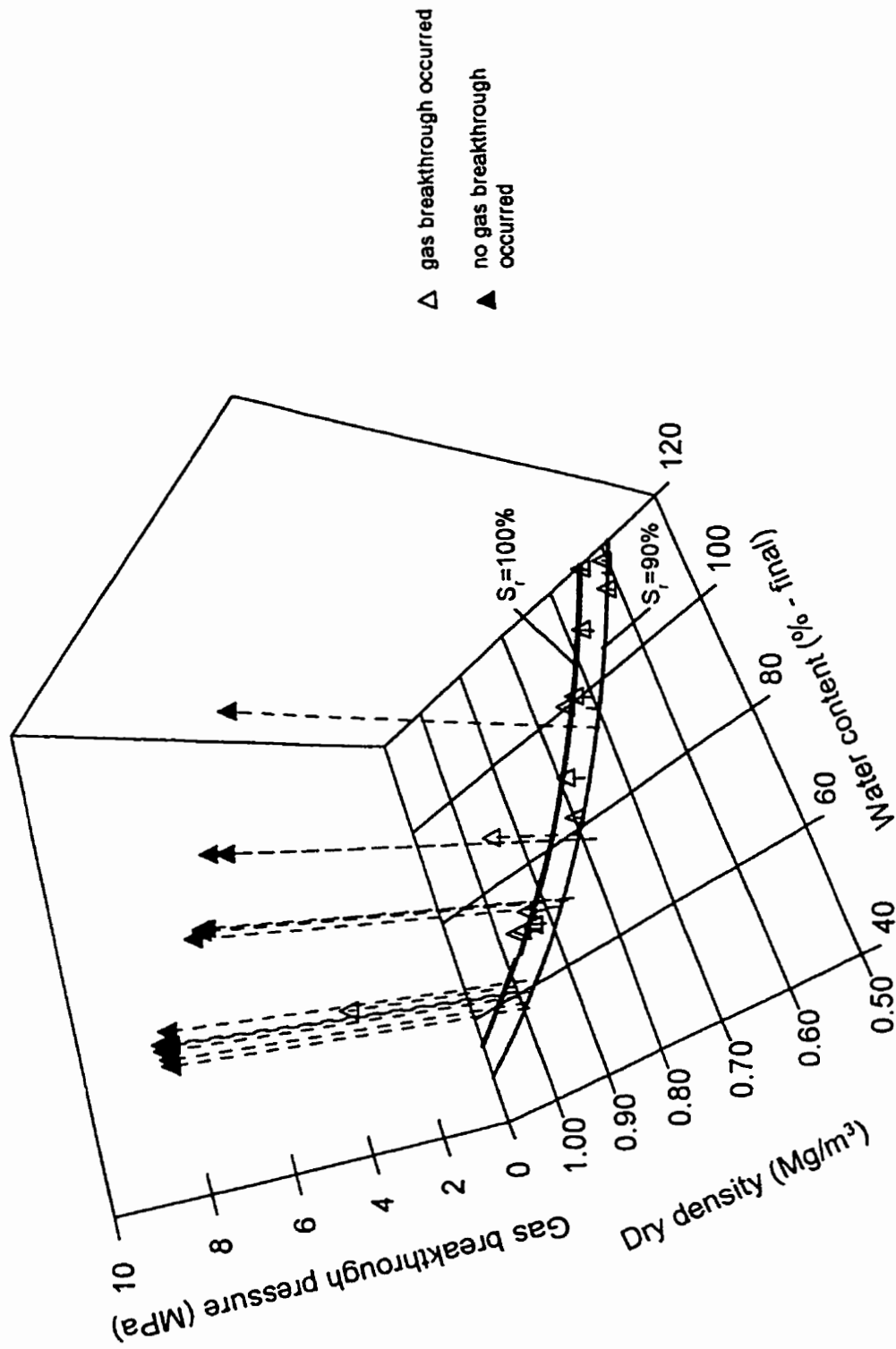


Figure 6.4: Summary of gas breakthrough pressure - effective clay dry density relationship for illite/sand specimens



Δ gas breakthrough occurred
 \blacktriangle no gas breakthrough occurred

Figure 6.5: Gas breakthrough pressure - dry density - water content relationship for wetted bentonite

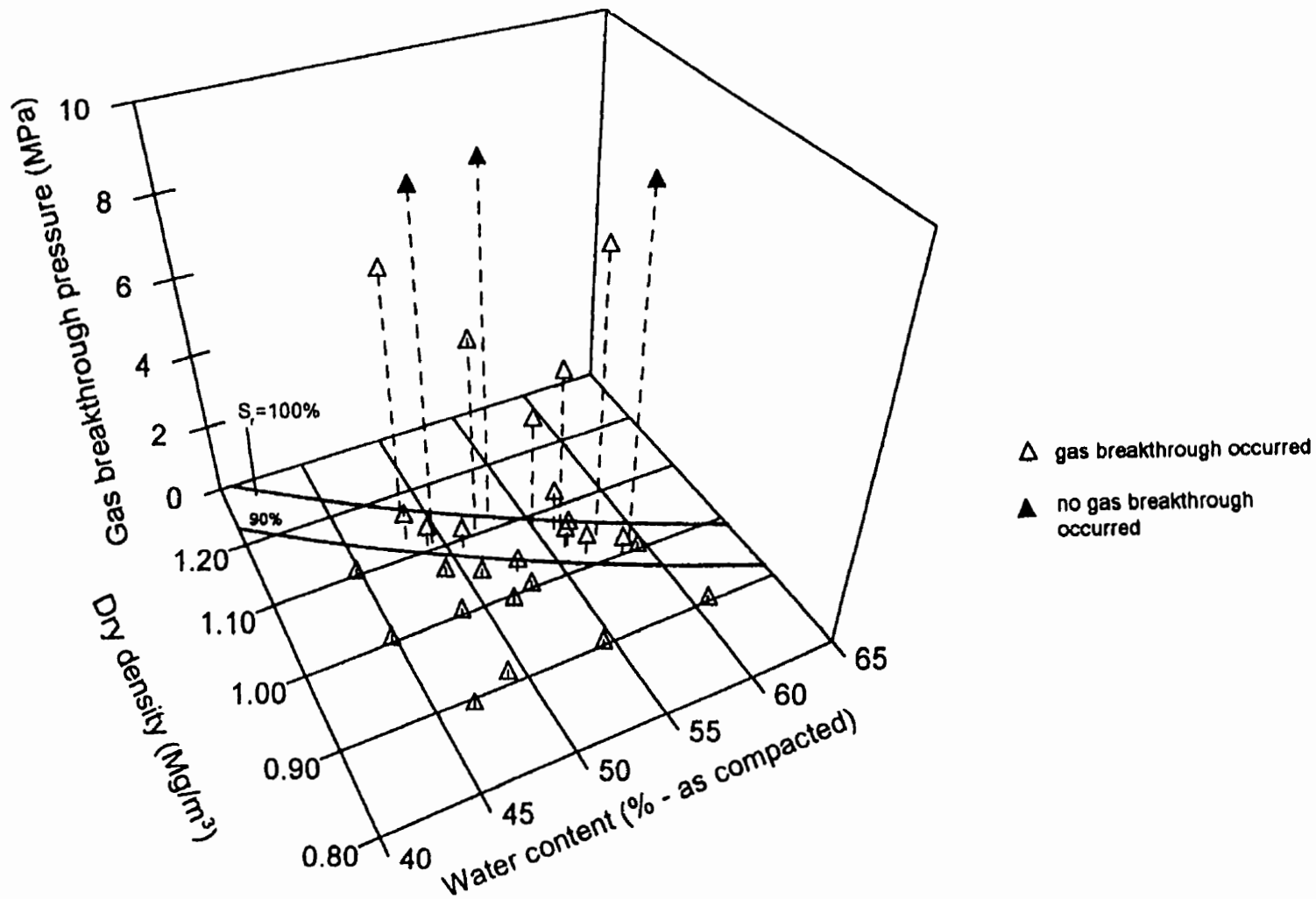


Figure 6.6: Gas breakthrough pressure - dry density - water content relationship for unsaturated bentonite

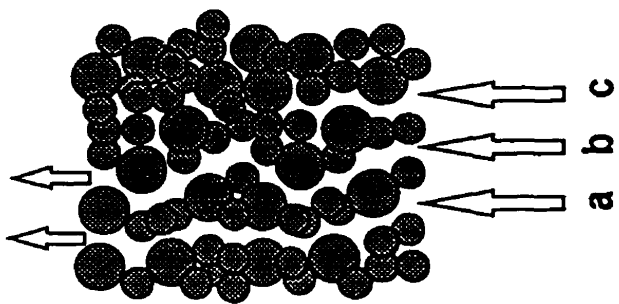


Figure 6.7: Conceptual diagram showing flow paths within a compacted clay

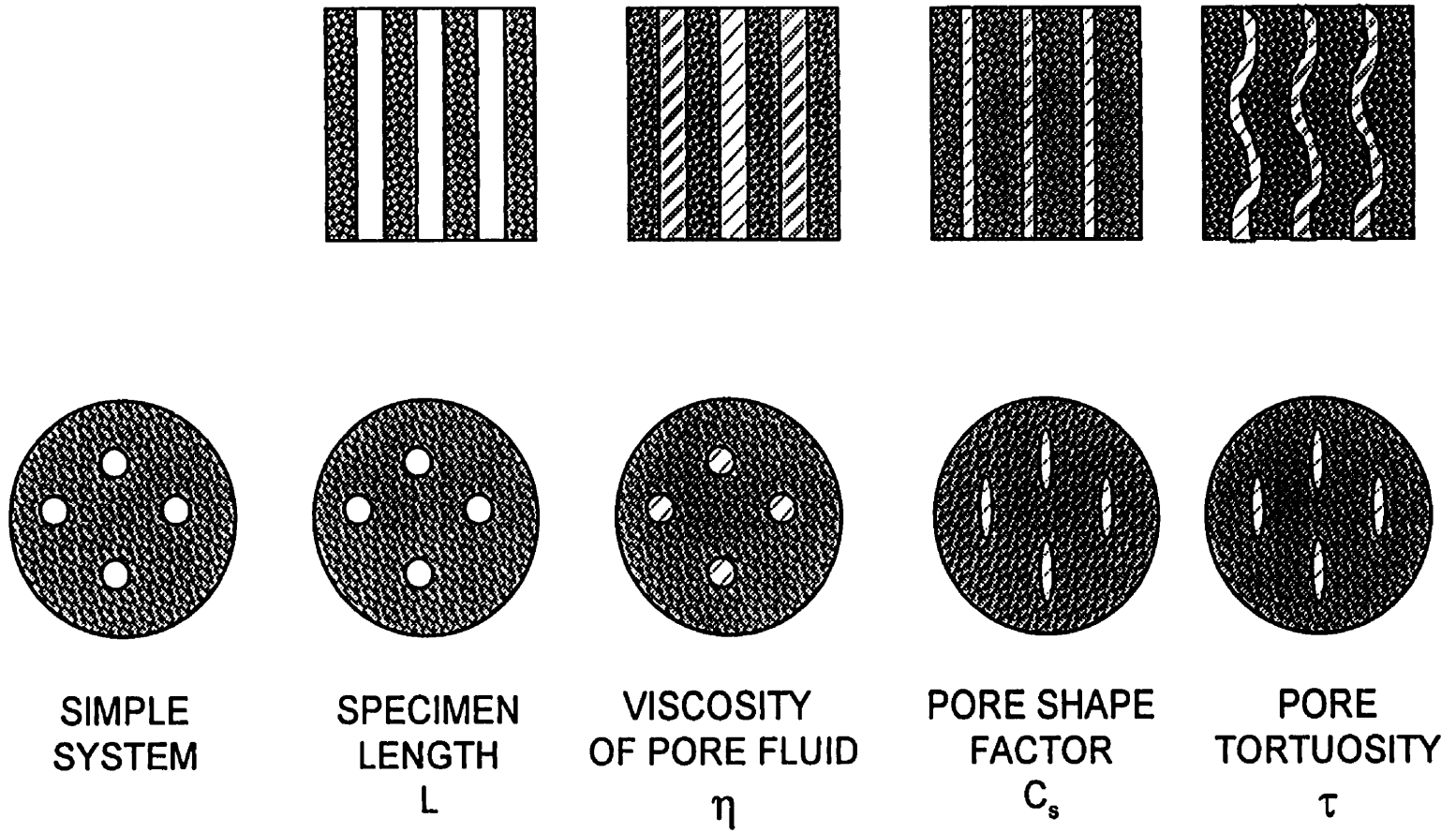


Figure 6.8: Conceptual diagram showing factors used in advective models to represent the actual system

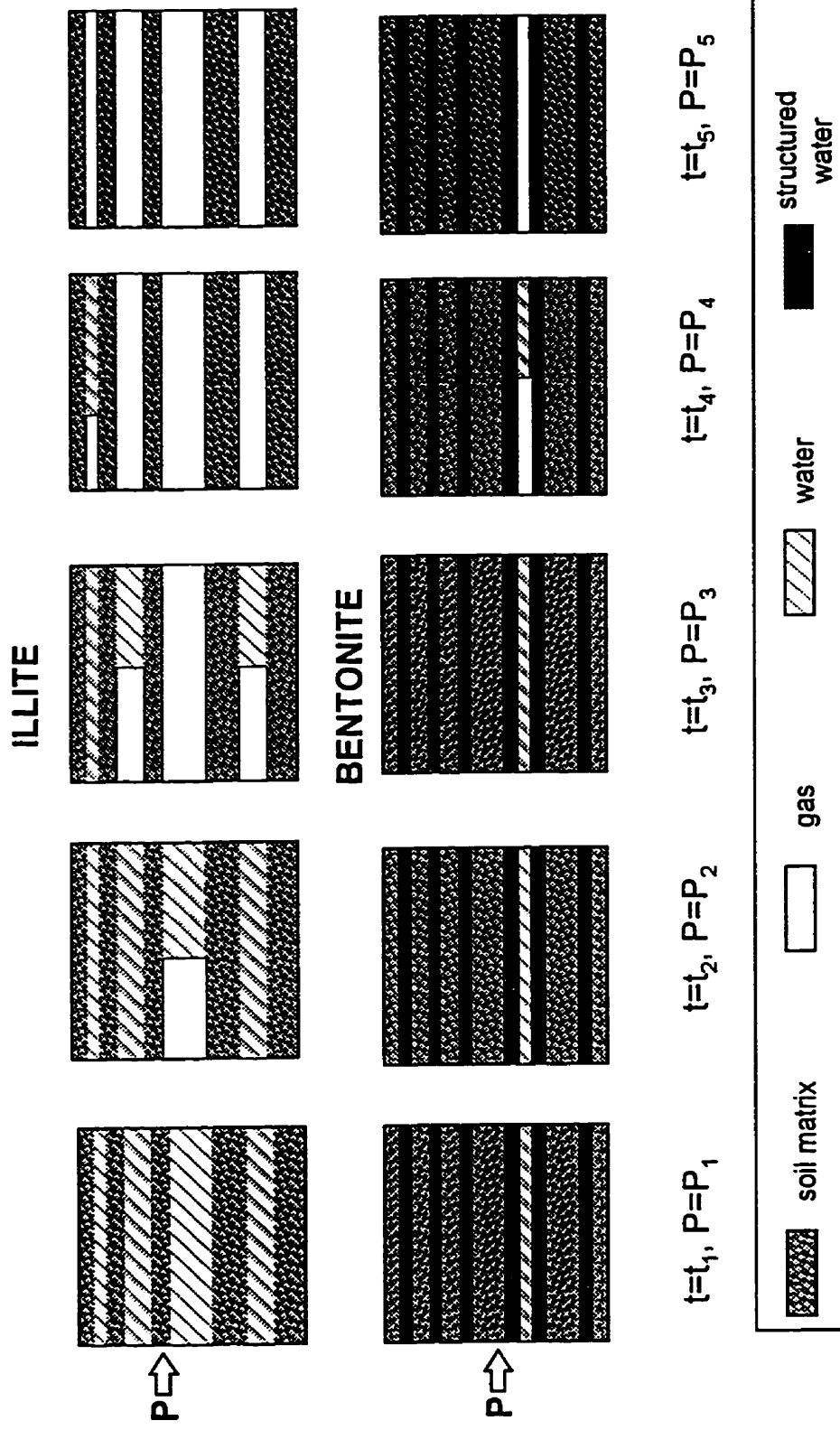


Figure 6.9: Conceptual diagram for flow in illite and bentonite during an increasing pressure test

Calculate pore radius from MIP tests:

$r = \frac{\text{diameter from MIP} - (2 \times \text{thickness of bound water})}{2}$

$$r = \frac{0.3 \times 10^{-6} - (2 \times 0.5 \times 10^{-9})}{2} = 1.495 \times 10^{-7} \text{ m}$$

Calculate pore radius from specific surface area:

$$\text{SSA} = 60\,000 \text{ m}^2/\text{kg}$$

$$S_T = 2040 \text{ kg/m}^3 \times 60\,000 \text{ m}^2/\text{kg} = 1.224 \times 10^8 \text{ m}^{-1}$$

$$r = n/S_T(1-n) = .26/1.224 \times 10^8(1-.26) = 2.87 \times 10^{-9} \text{ m}$$

Capillarity:

$$P_b = 2T/r$$

$$P_b = 2(0.073)/1.495 \times 10^{-7}$$

$$P_b = 1.0 \text{ MPa}$$

Poiseulle:

$$t = \sqrt{\frac{8L^2\eta}{pr^2}}$$

$$L = 0.025 \text{ m}$$

$$\eta = 1.02 \times 10^{-3} \text{ Pa}\cdot\text{sec}$$

$$p = 200\,000 \text{ Pa} / 5 \text{ minutes}$$

$$= 667 \text{ Pa/second}$$

$$t = \sqrt{\frac{8(0.025)^2 1.02 \times 10^{-3}}{667(2.87 \times 10^{-9})^2}} = 30467 \text{ sec.}$$

$$t = 8.5 \text{ hours}, P_b = 20.0 \text{ MPa}$$

Figure 6.10(a) : Sample model calculations (illite)

$$t = \sqrt{\frac{L^2 S_r^2 (1-n)^2 \tau^2 \eta}{n^3 C_s \rho}}$$

$$\tau = 2$$

$$C_s = 0.4$$

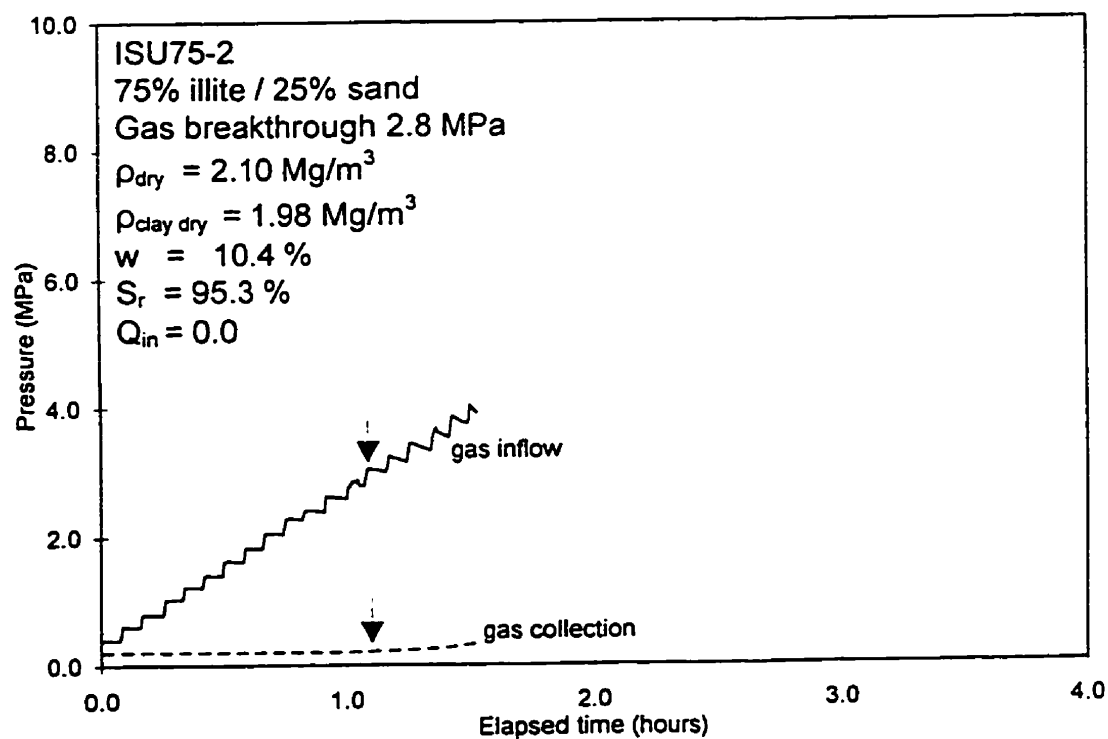
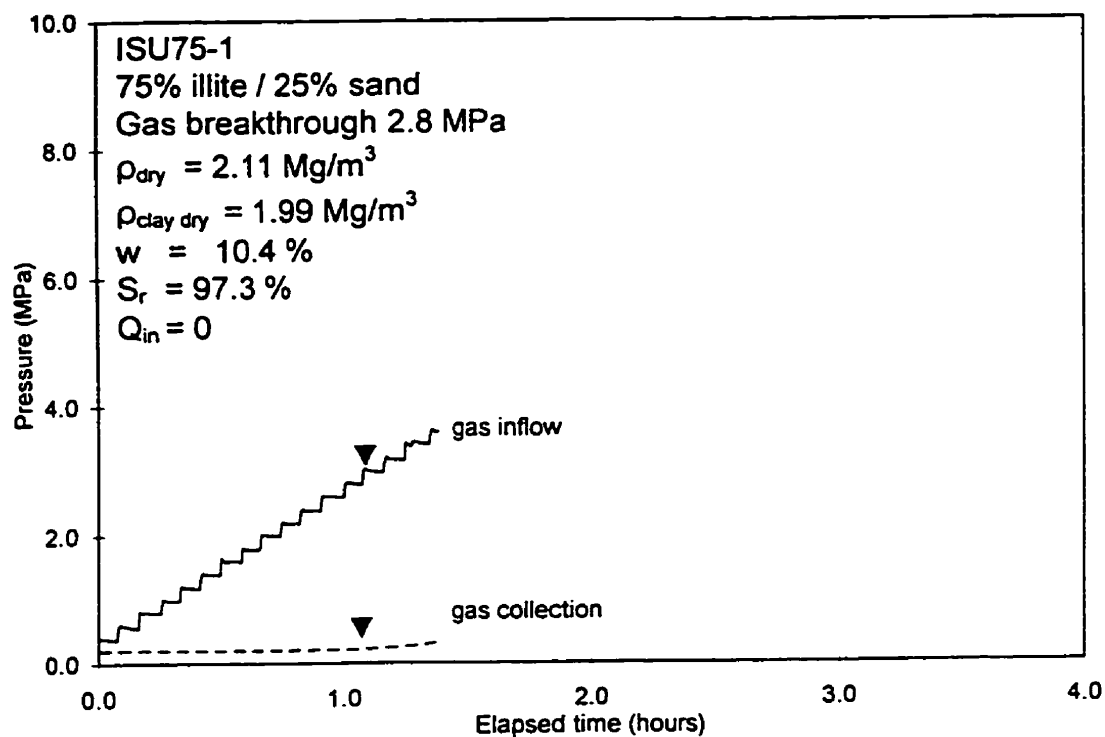
$$t = \sqrt{\frac{(0.025)^2 (1.224 \times 10^8)^2 (1 - .26)^2 \sqrt{2}^2 (1.02 \times 10^{-3})}{(0.26)^3 (0.4) (667)}} = 47230 \text{ sec.}$$

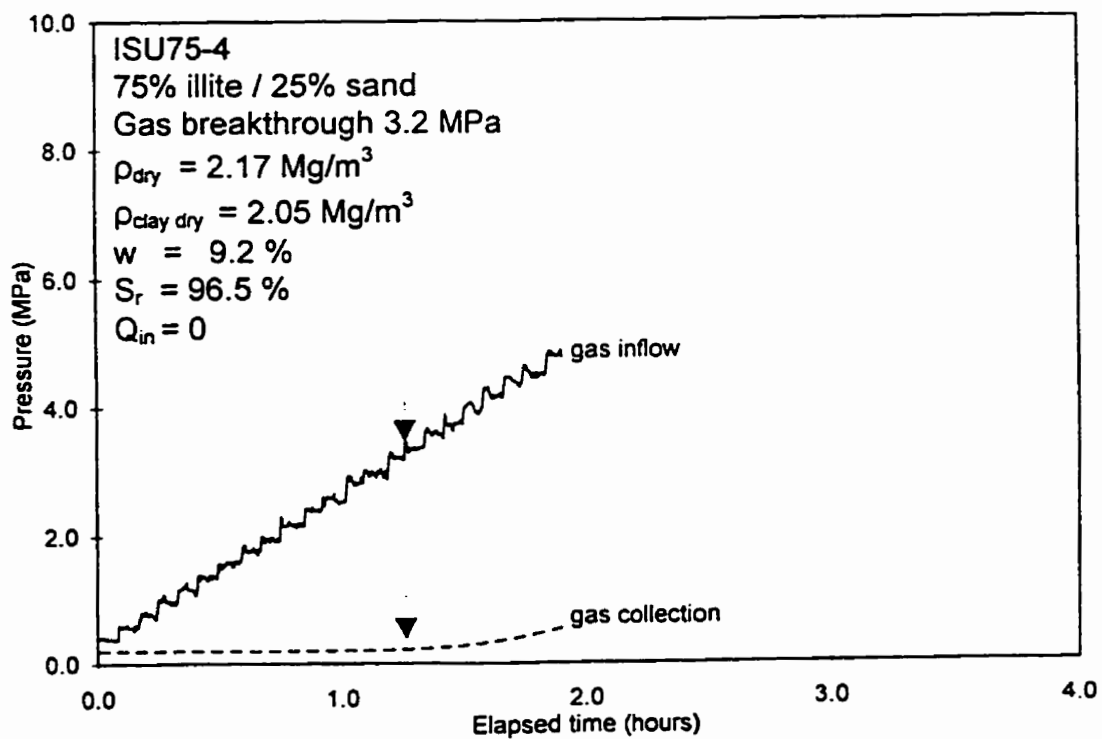
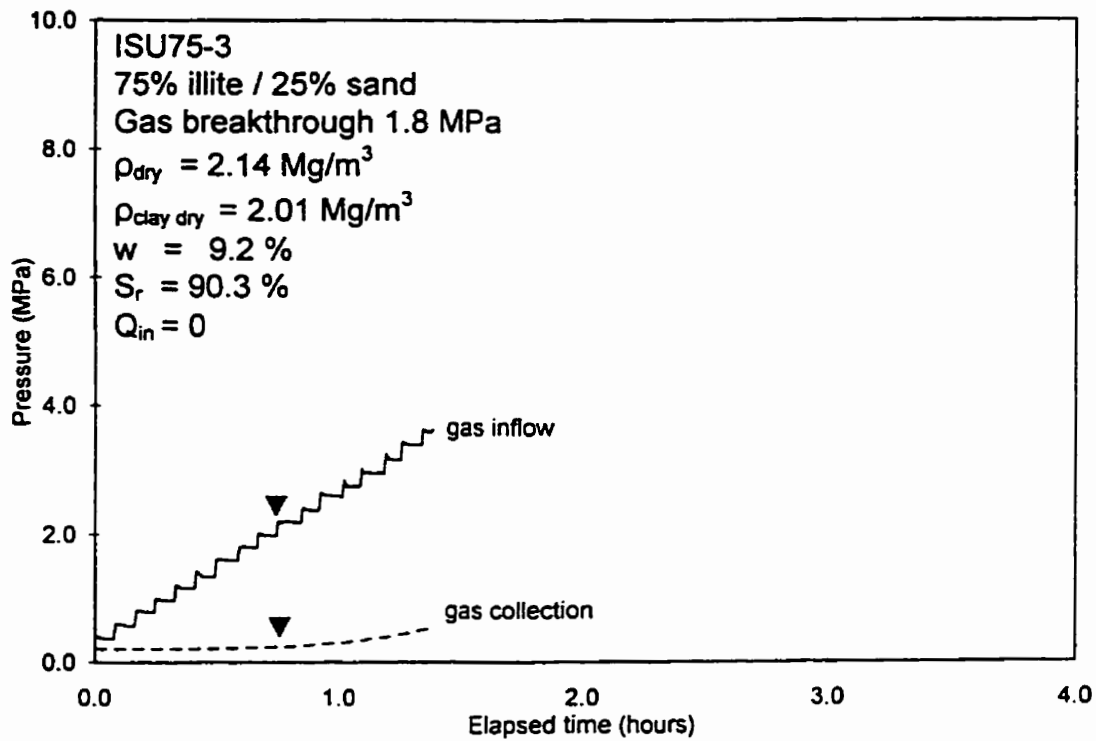
$$t = 13.0 \text{ hours, } P_b = 31.5 \text{ MPa}$$

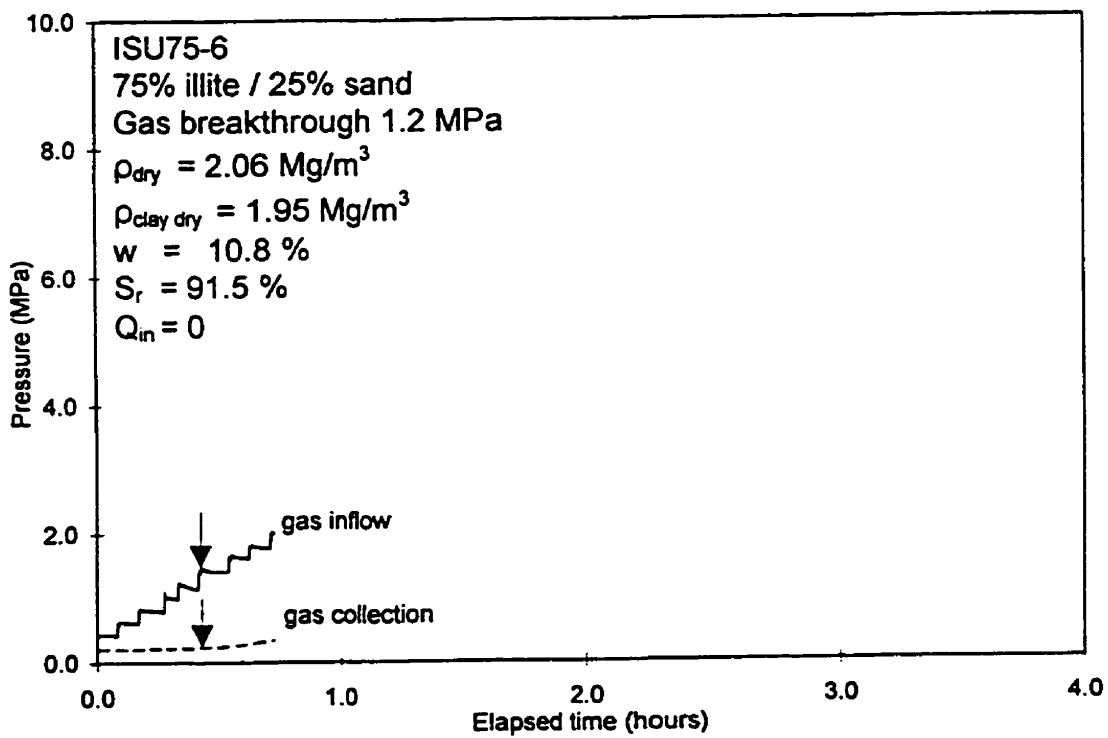
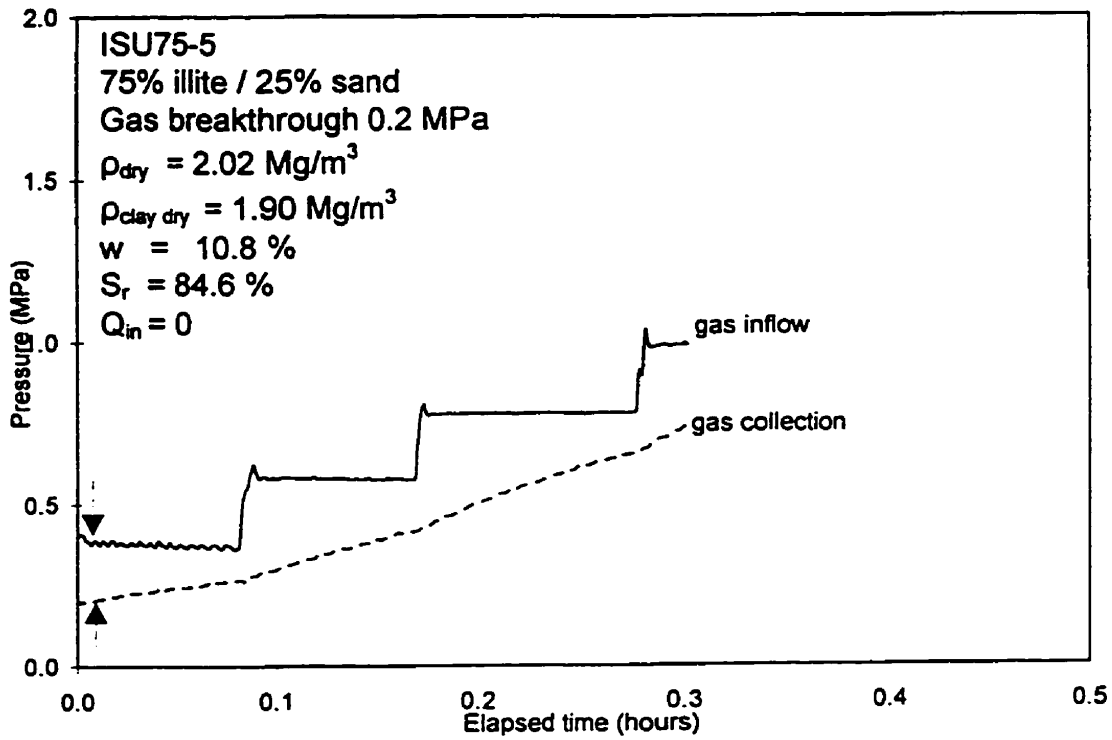
Figure 6.10(b) : Sample model calculations (illite)

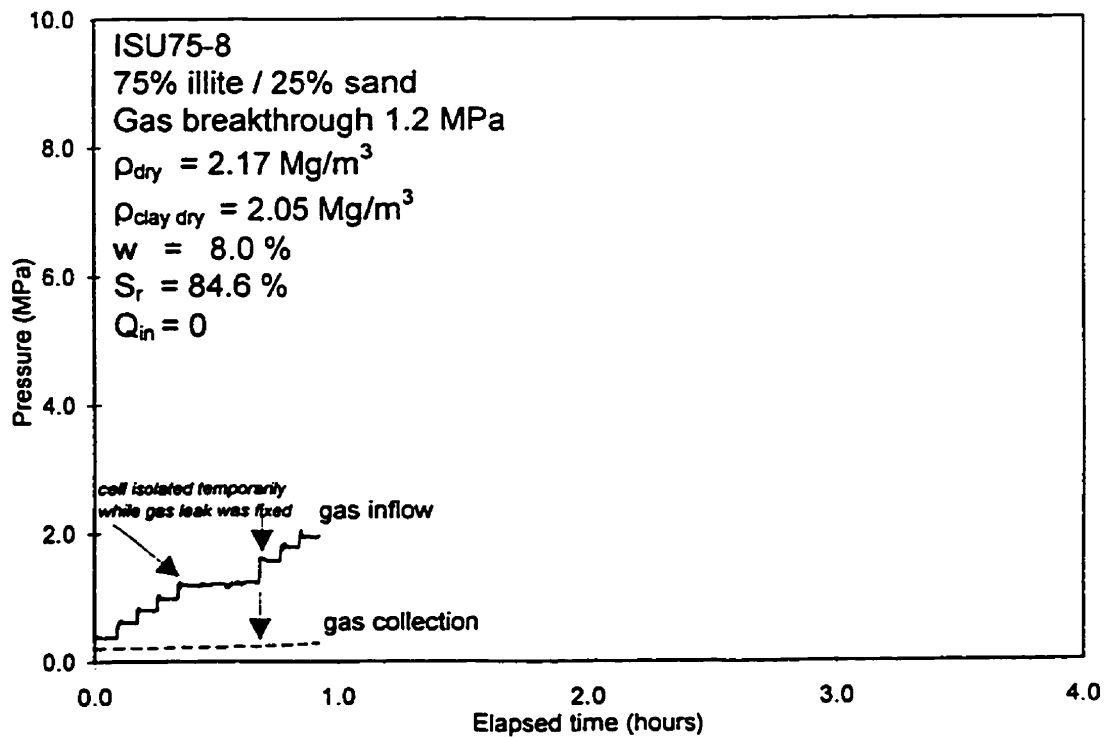
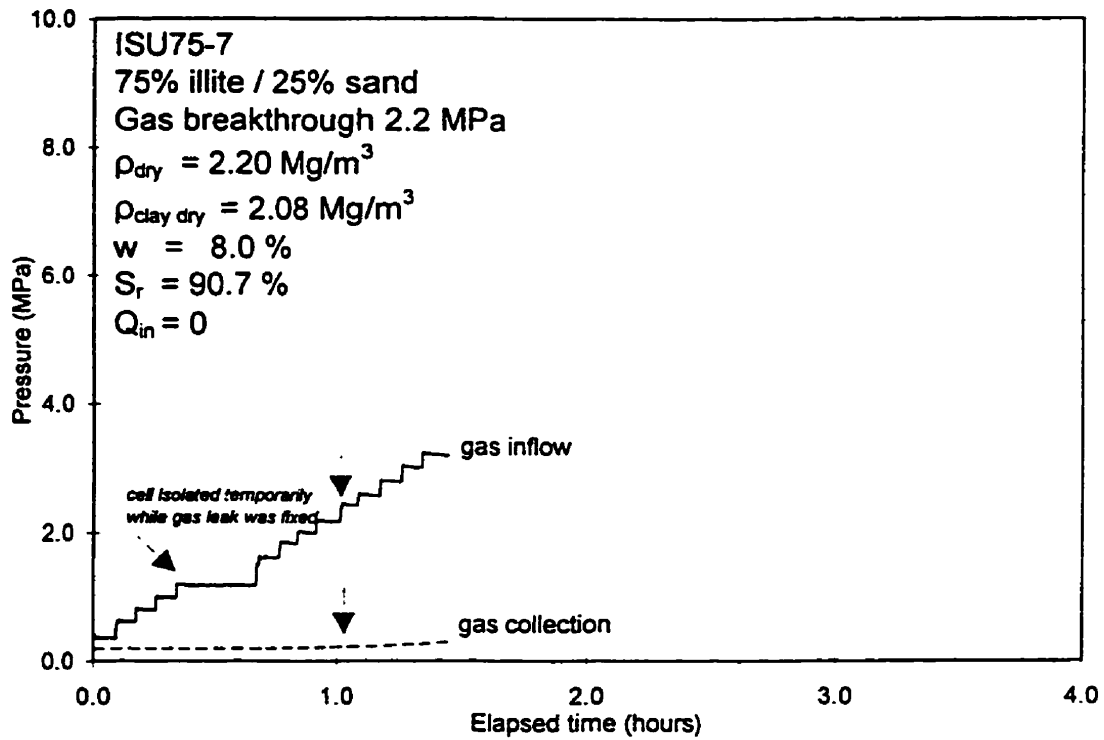
APPENDIX A

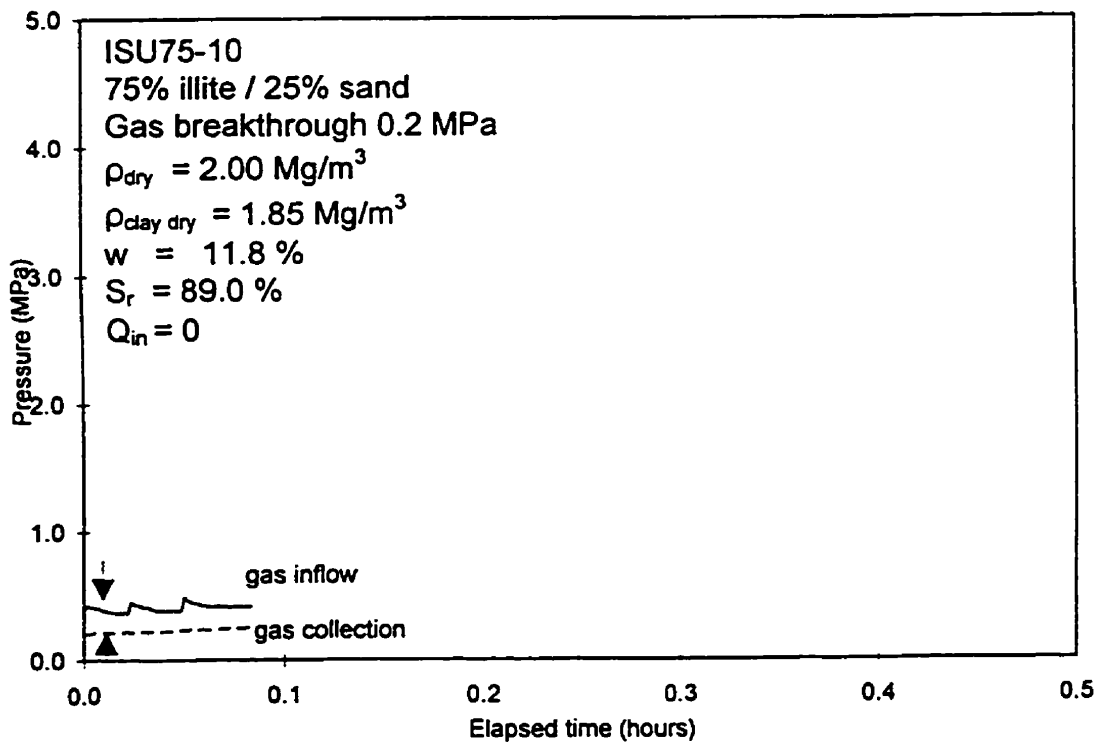
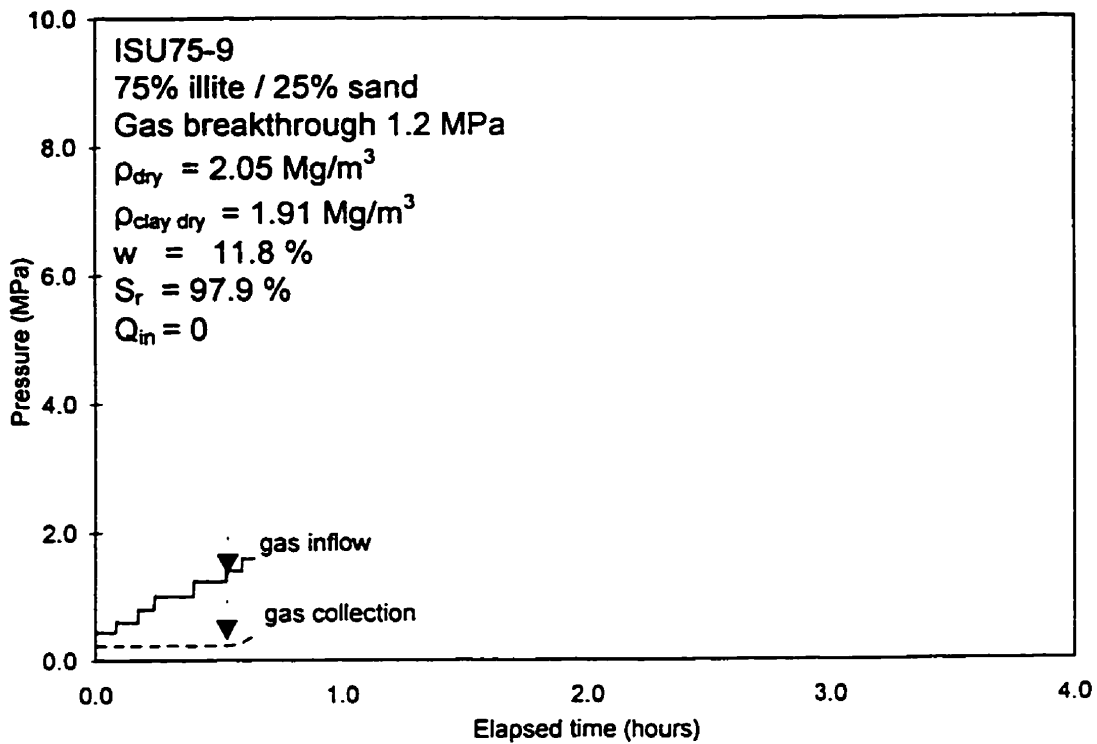
GAS BREAKTHROUGH TEST RESULTS

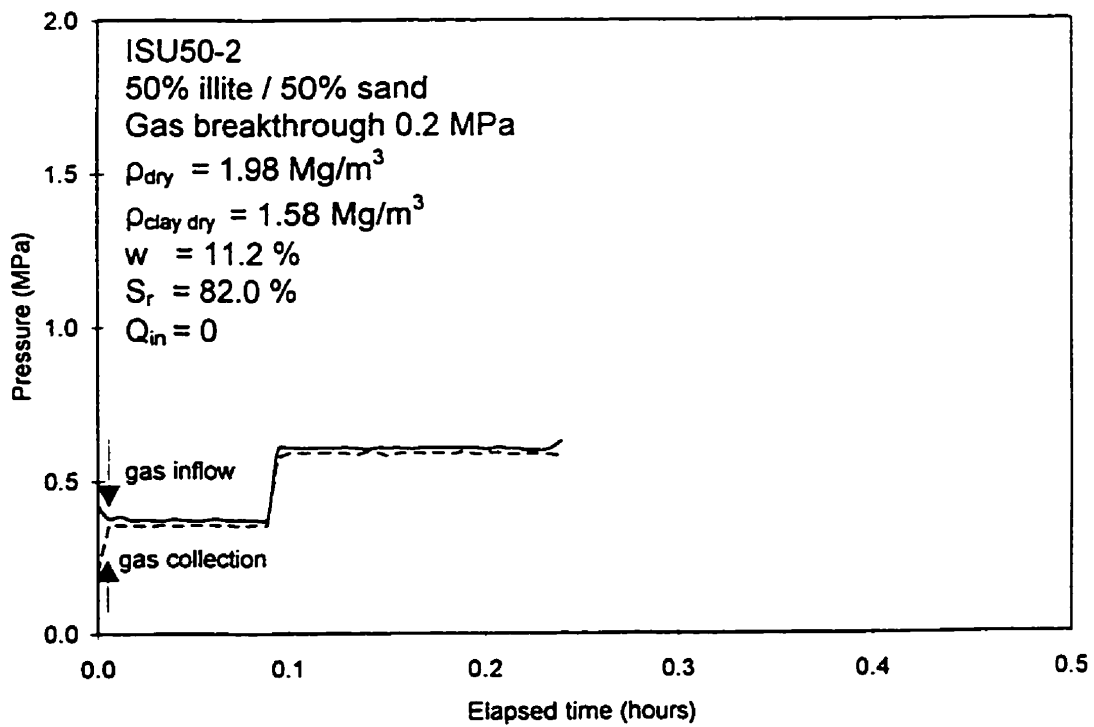
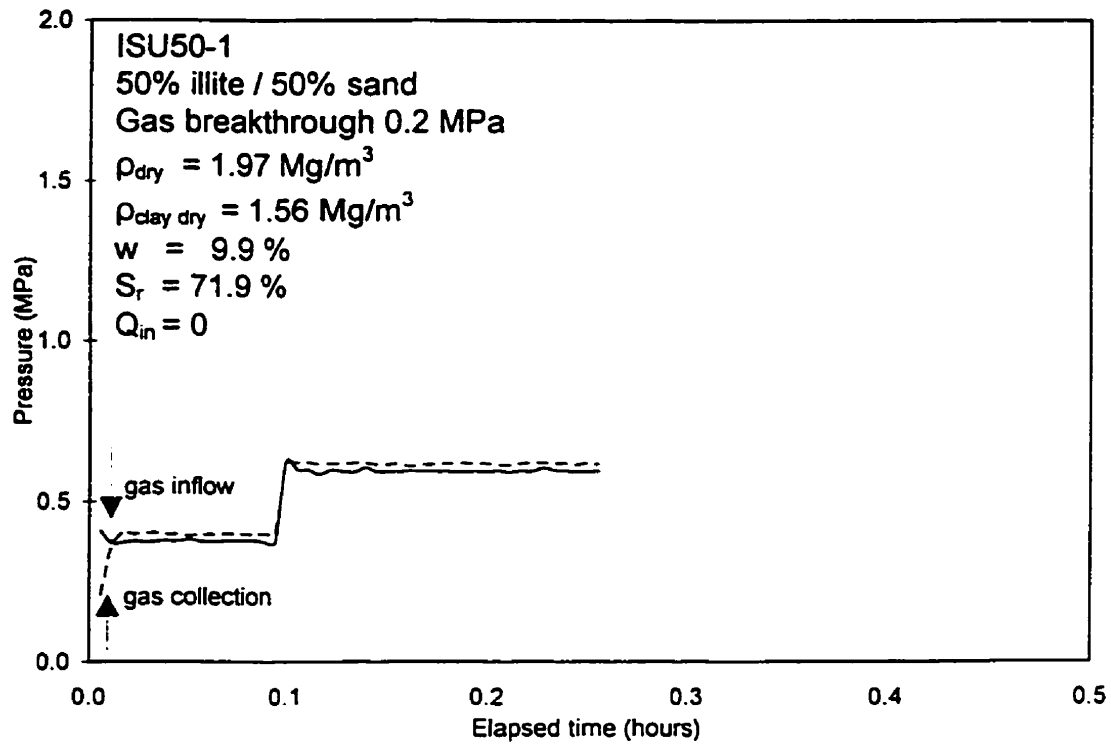


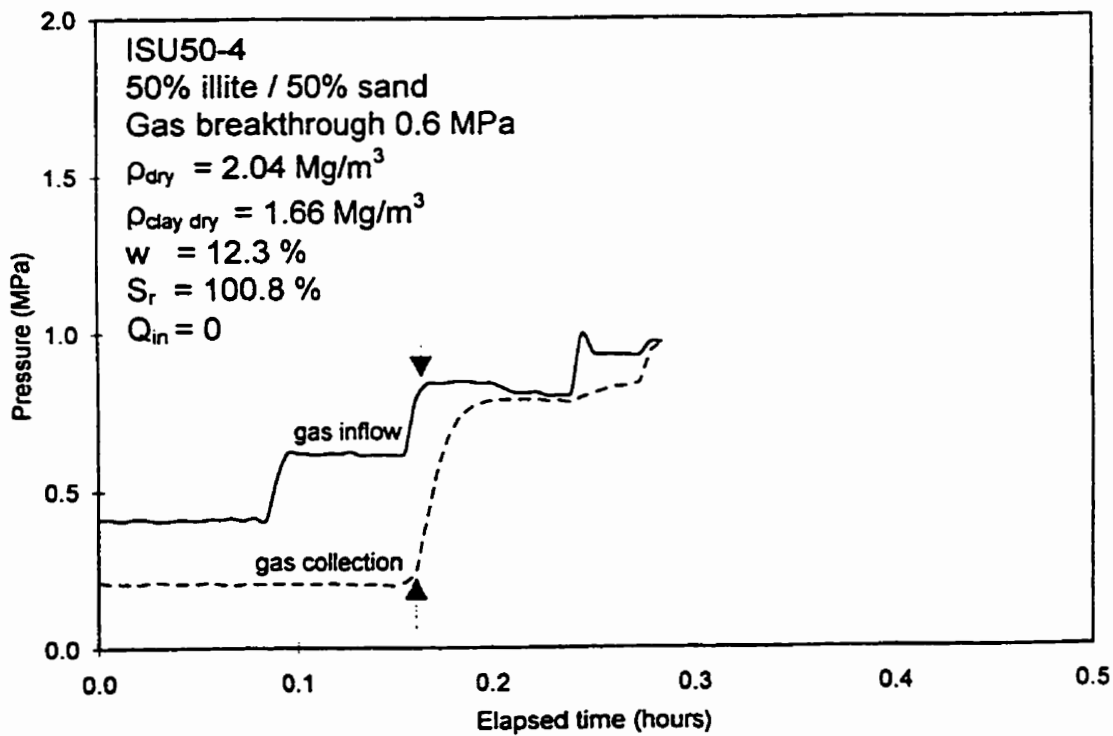
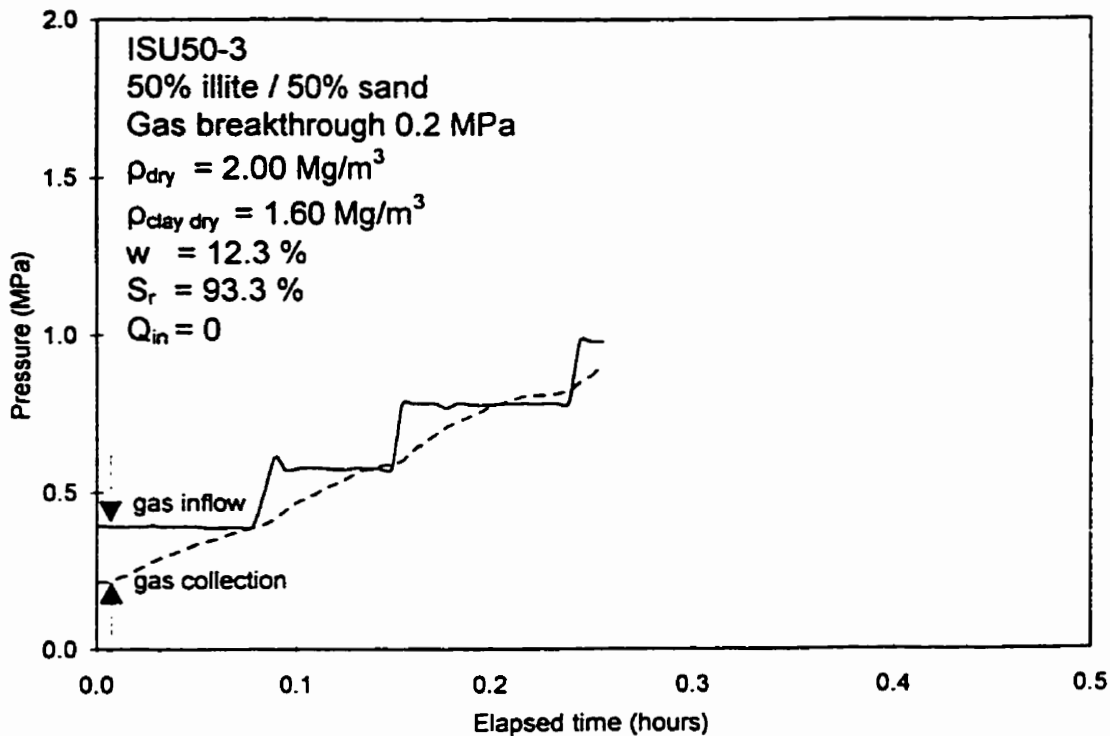


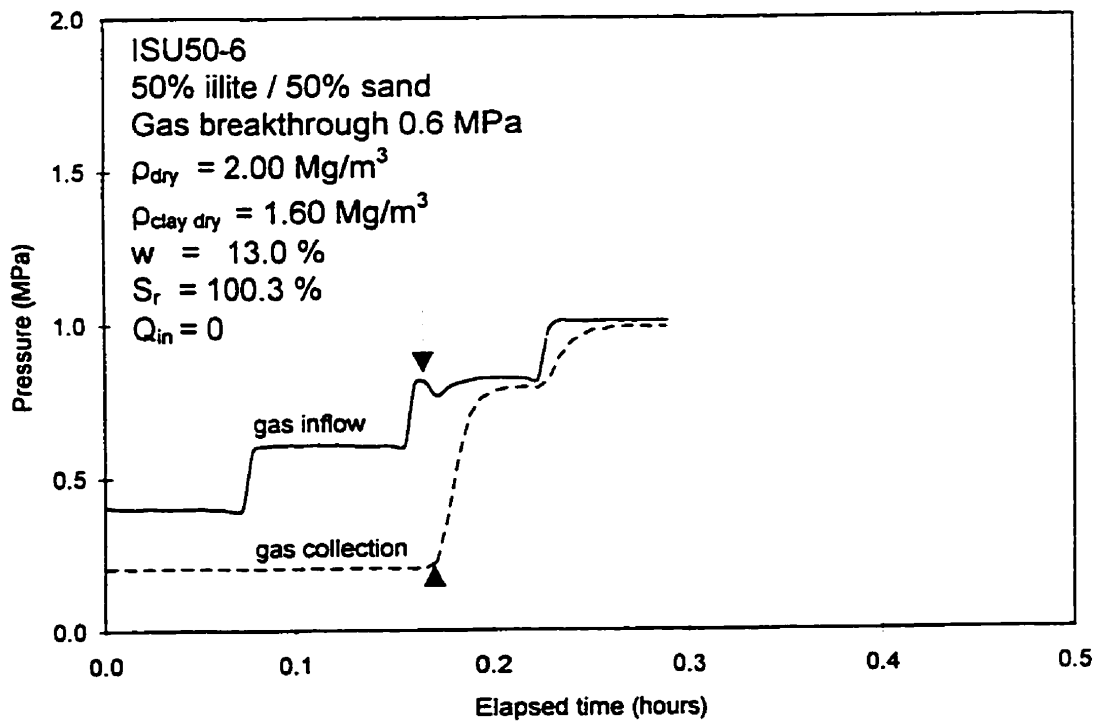
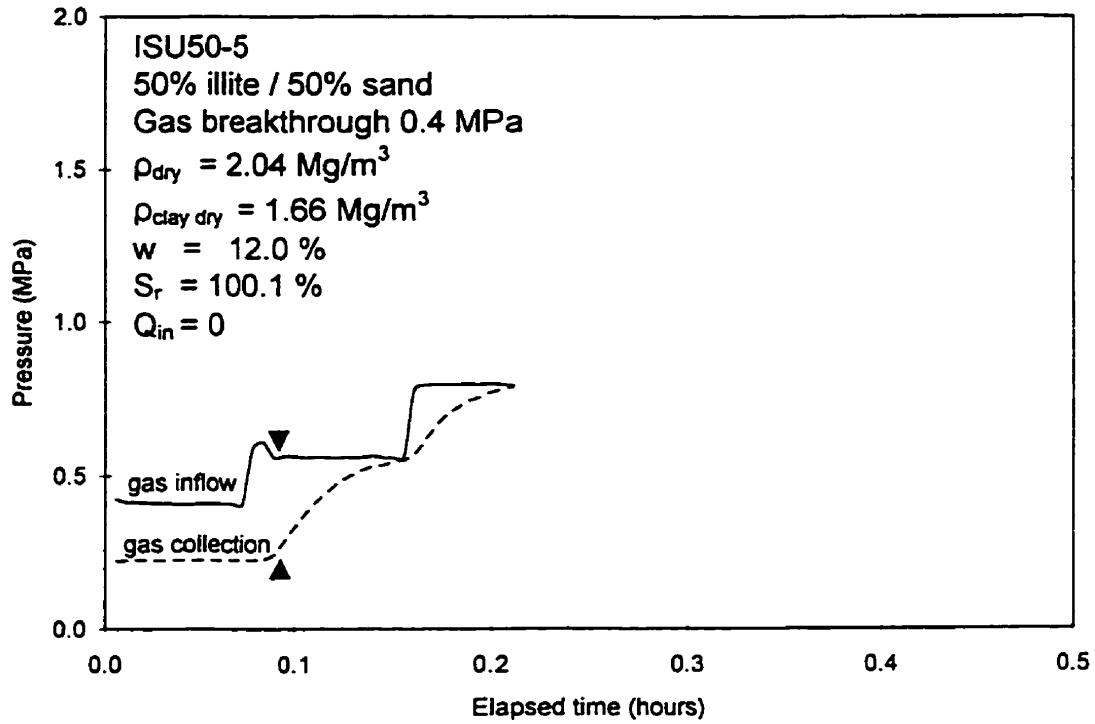


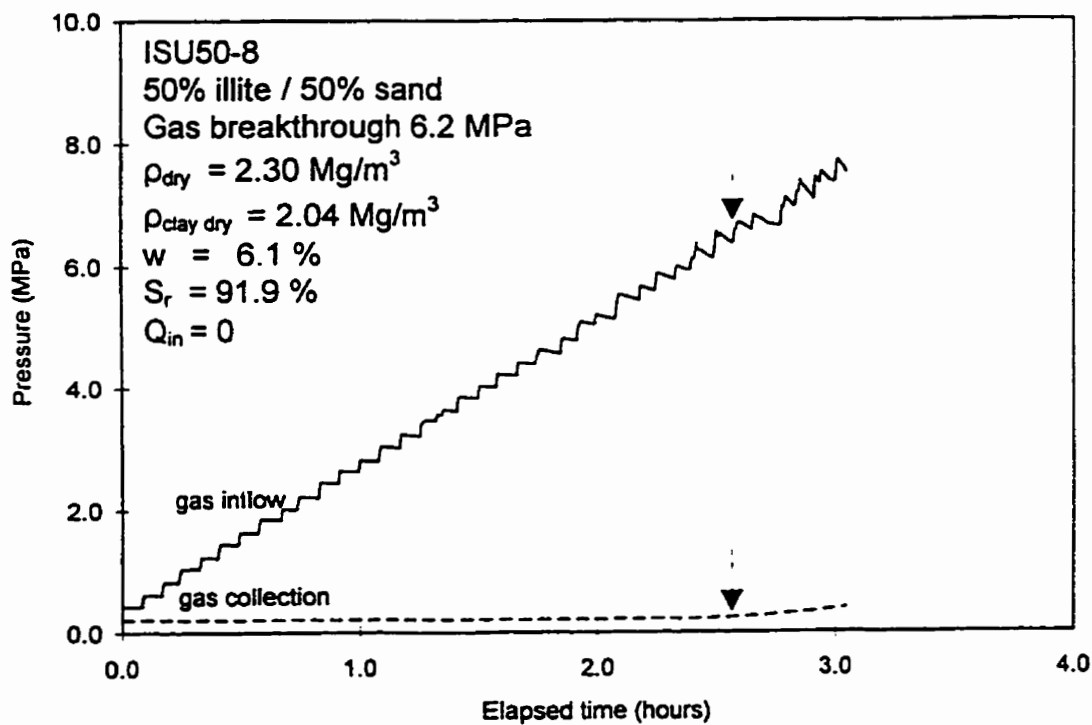
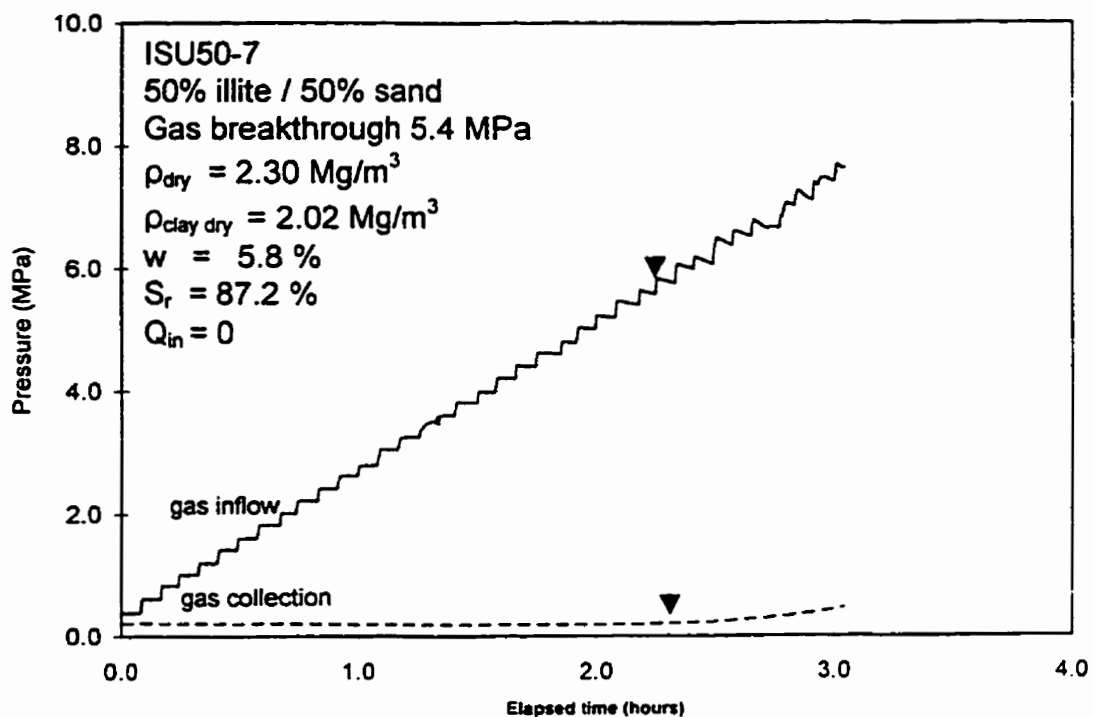


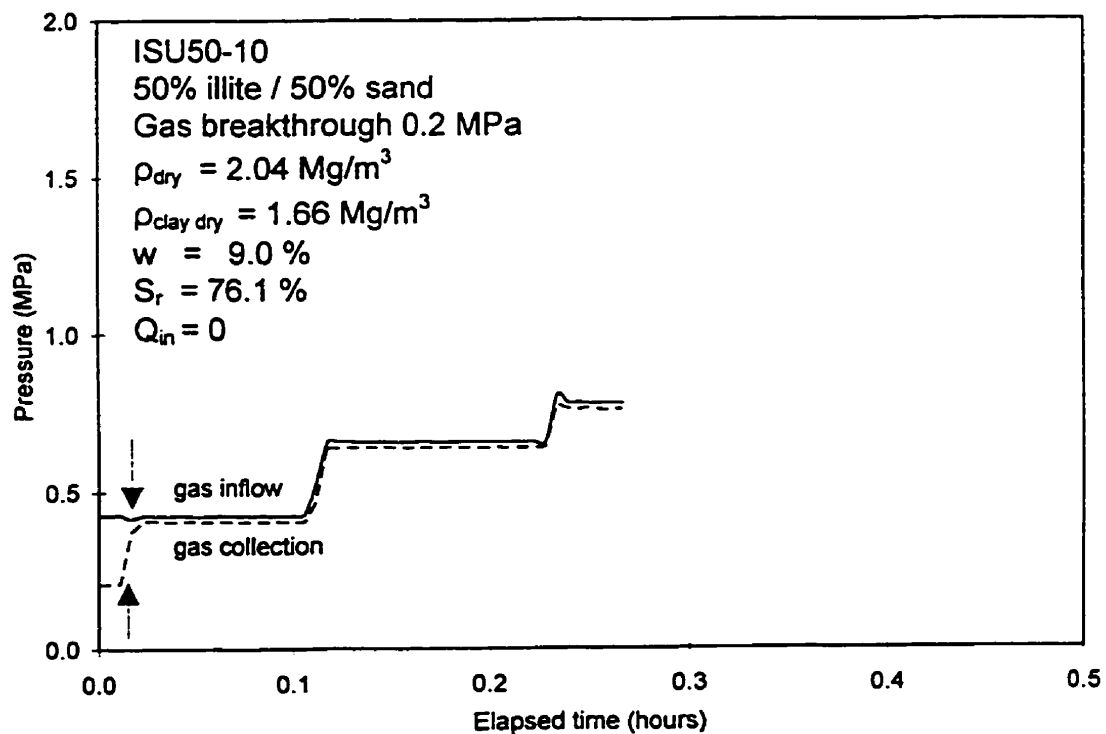
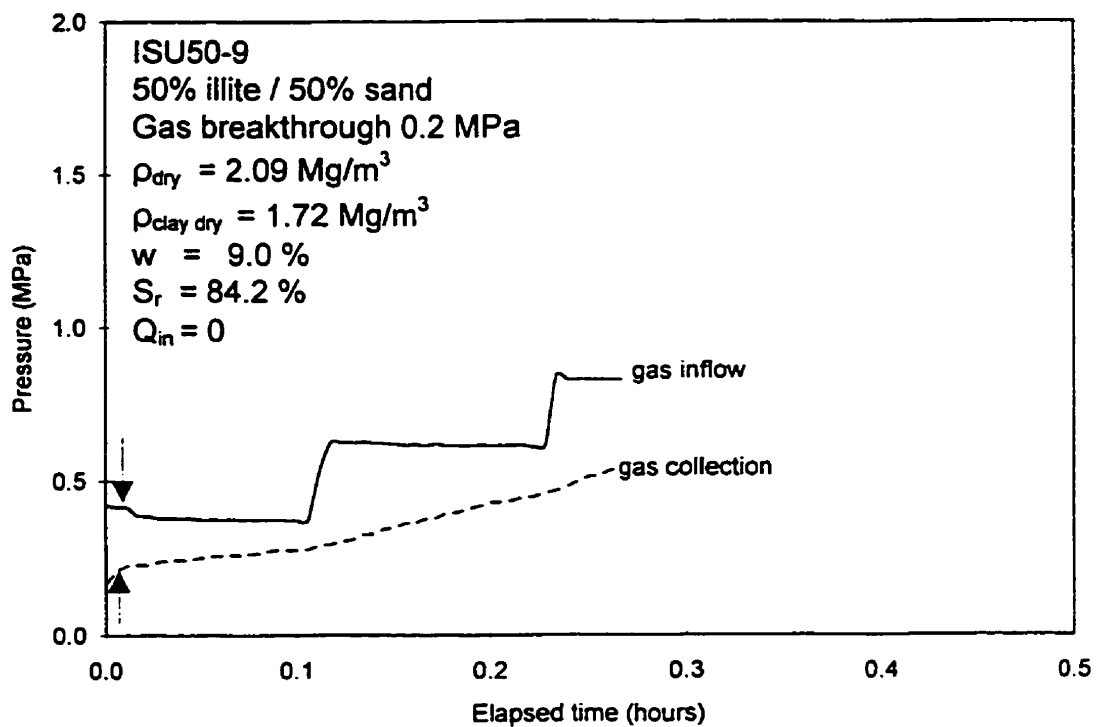


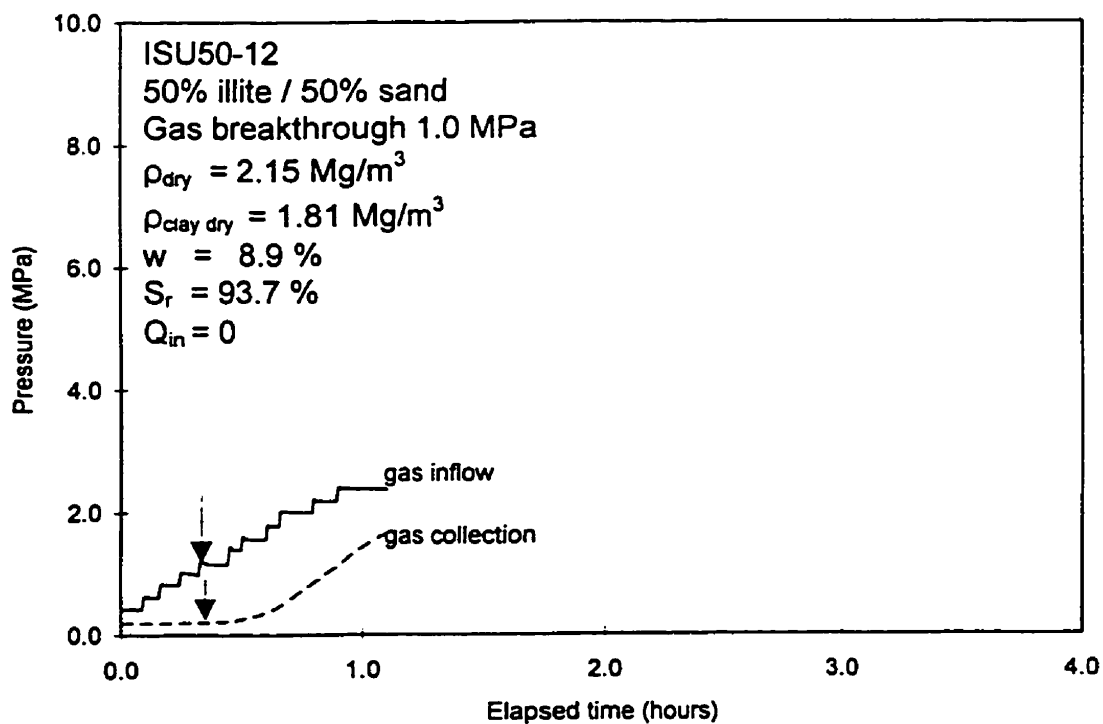
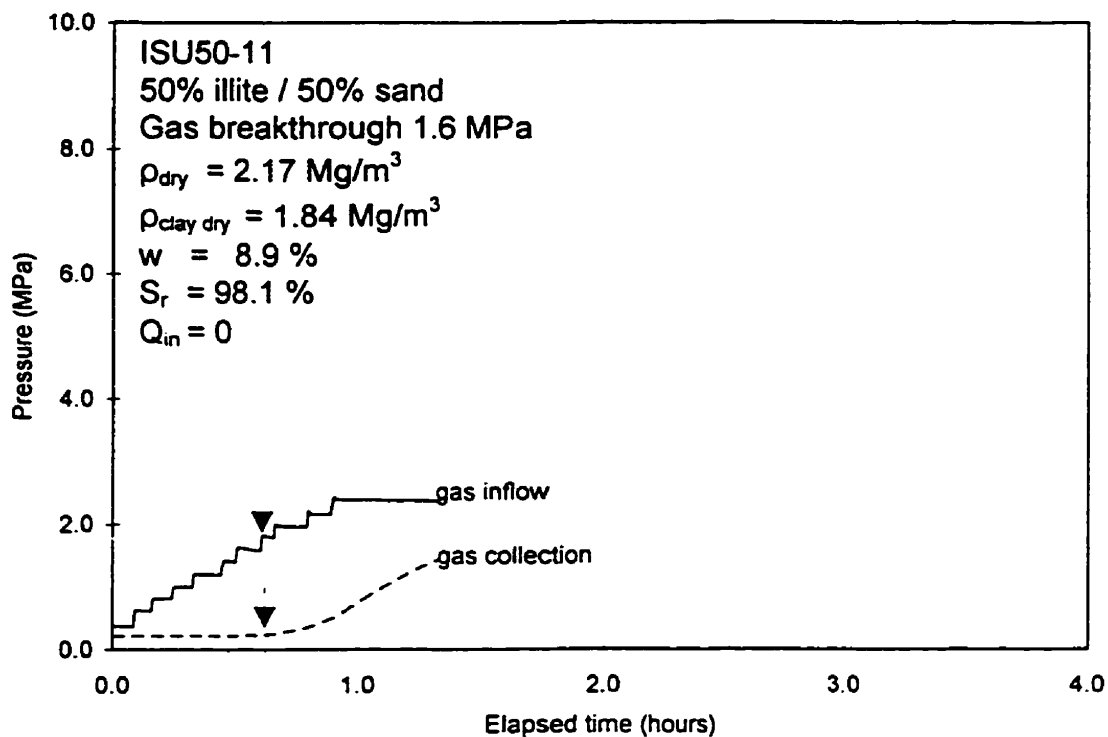


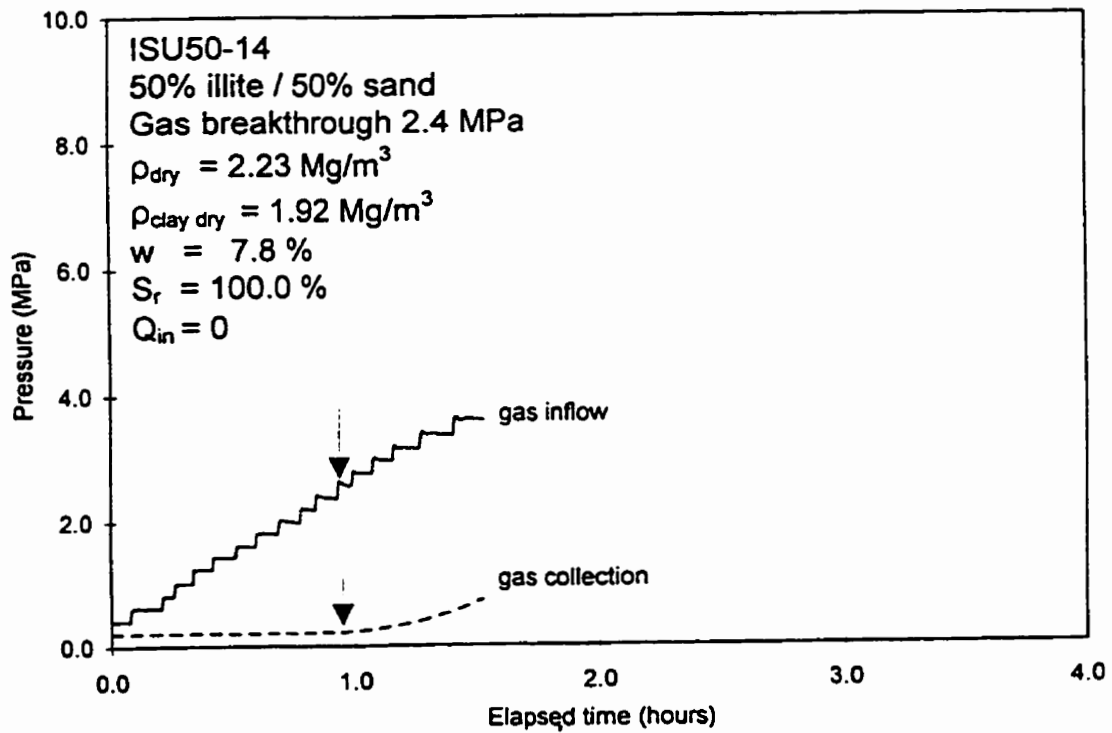
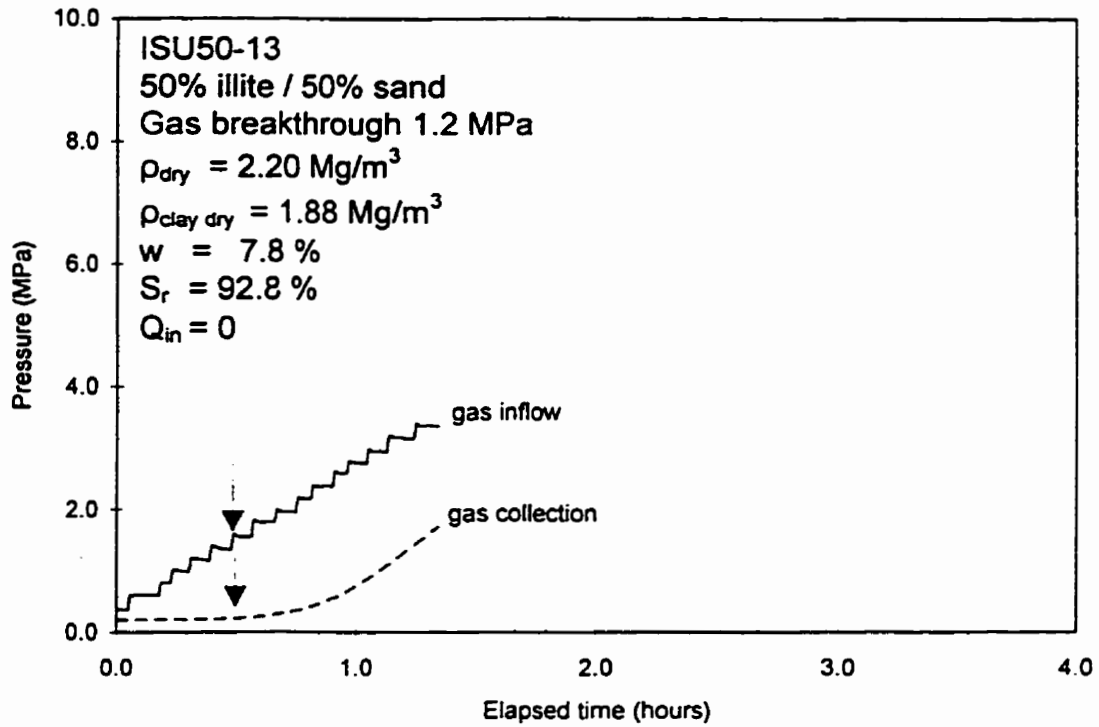


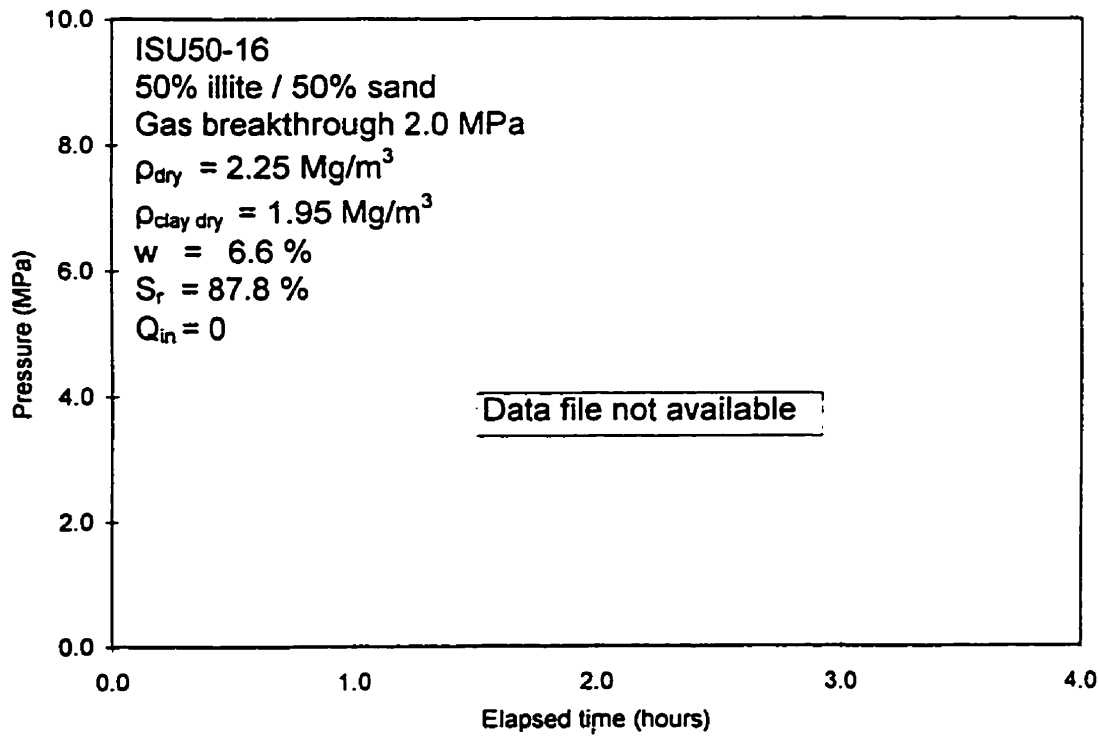
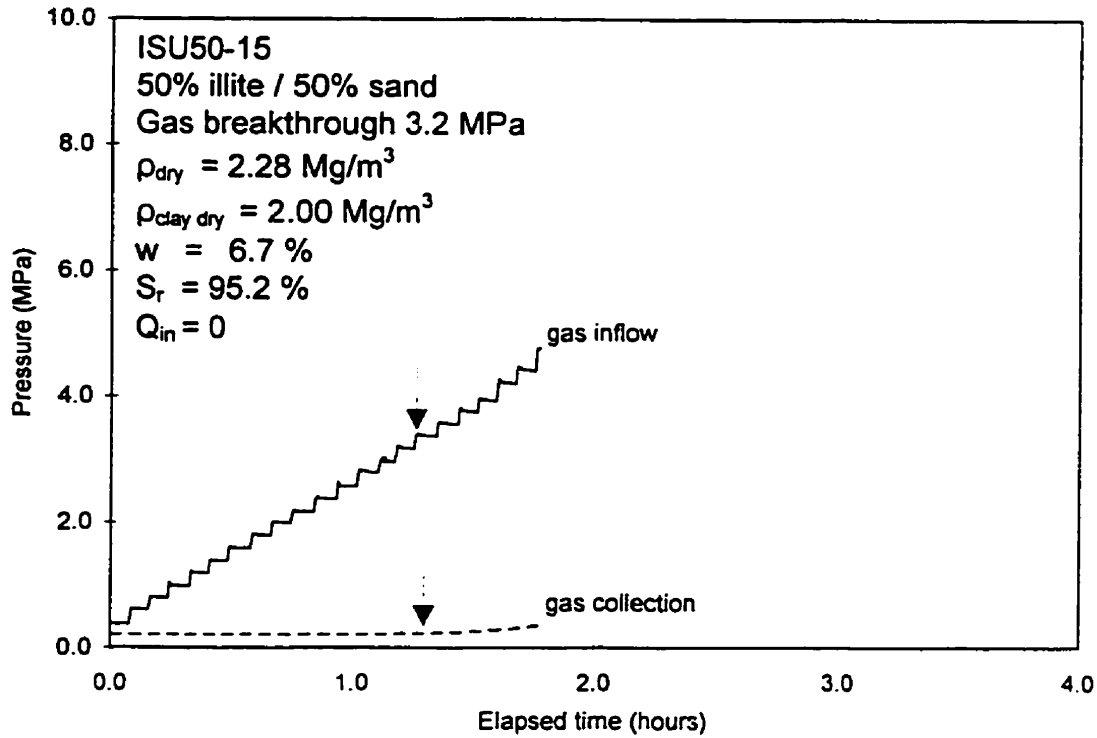


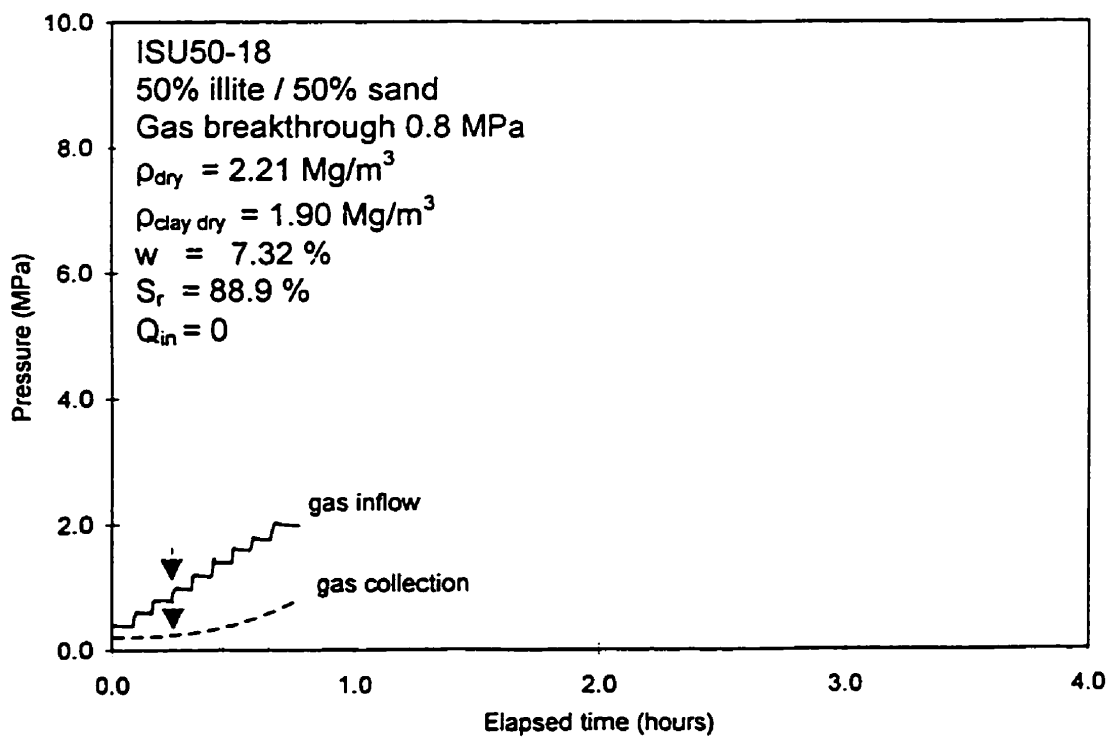
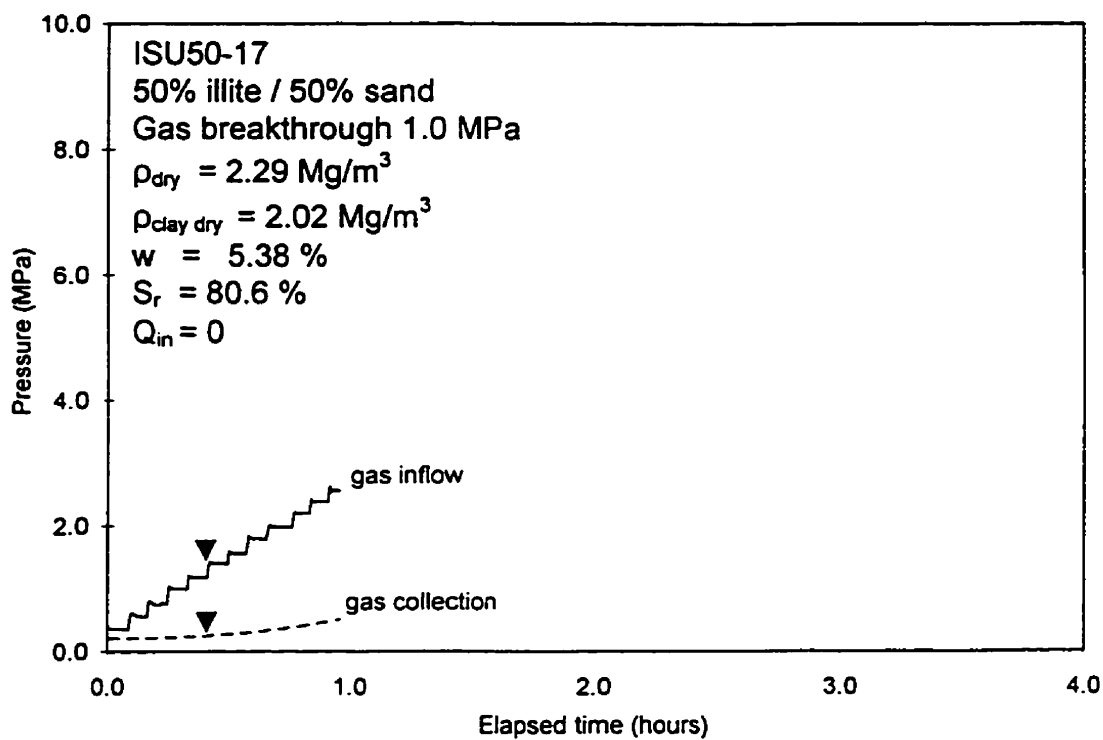


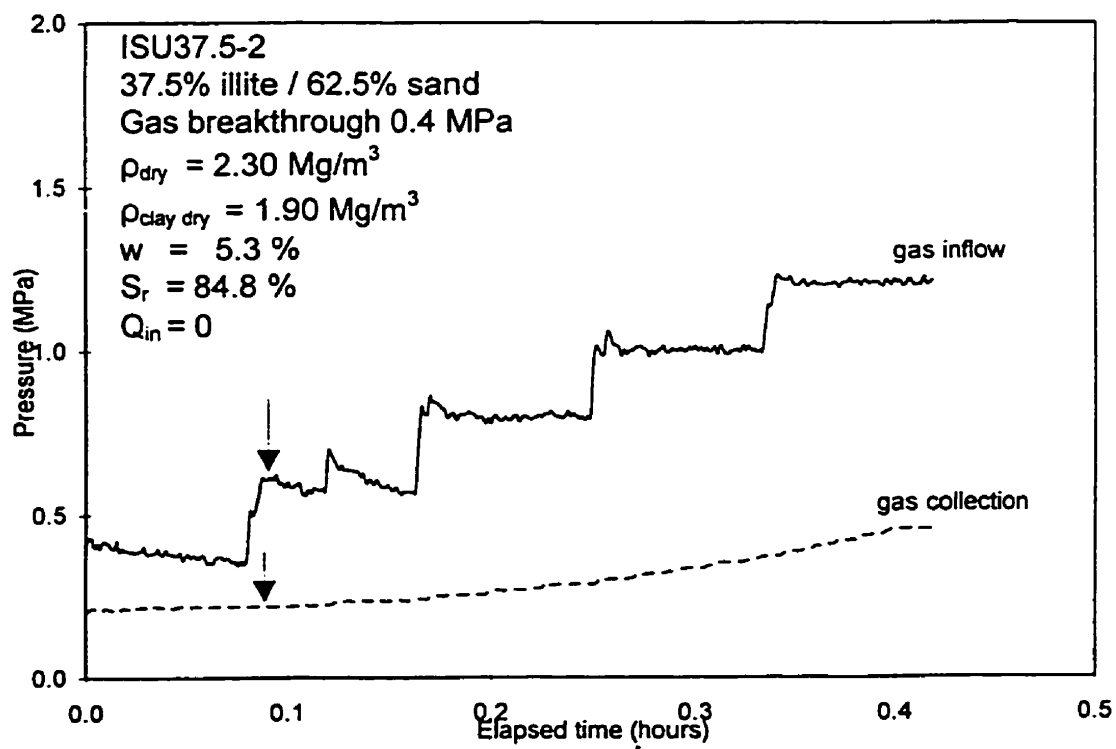
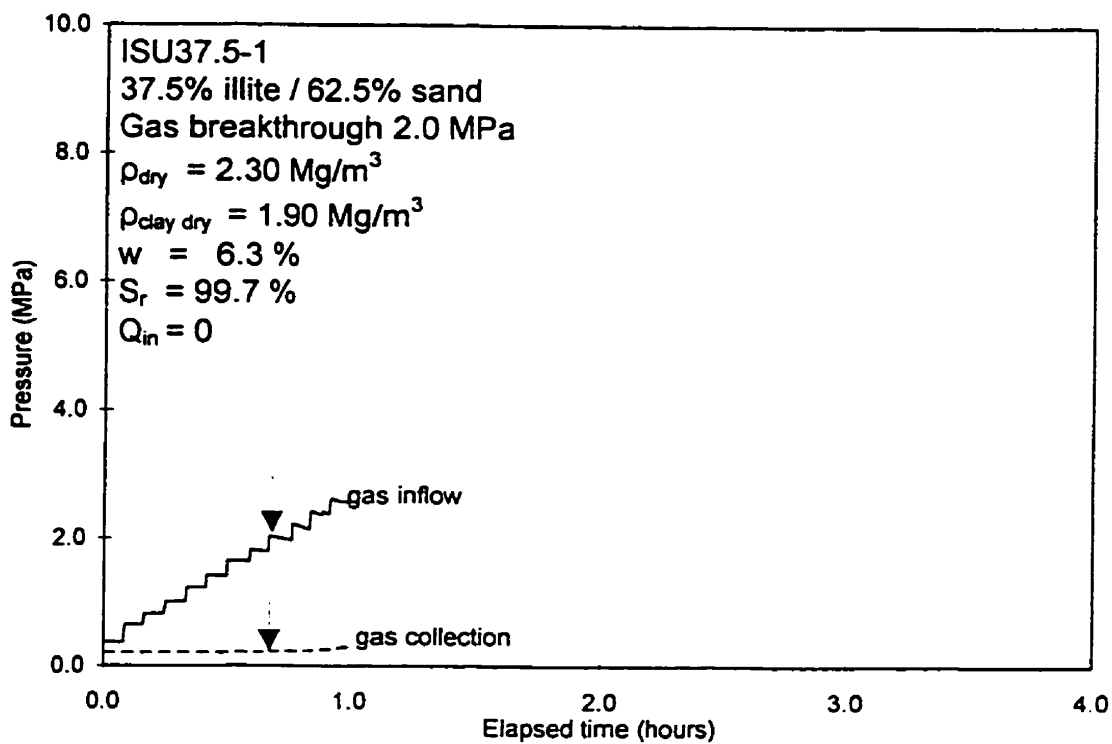


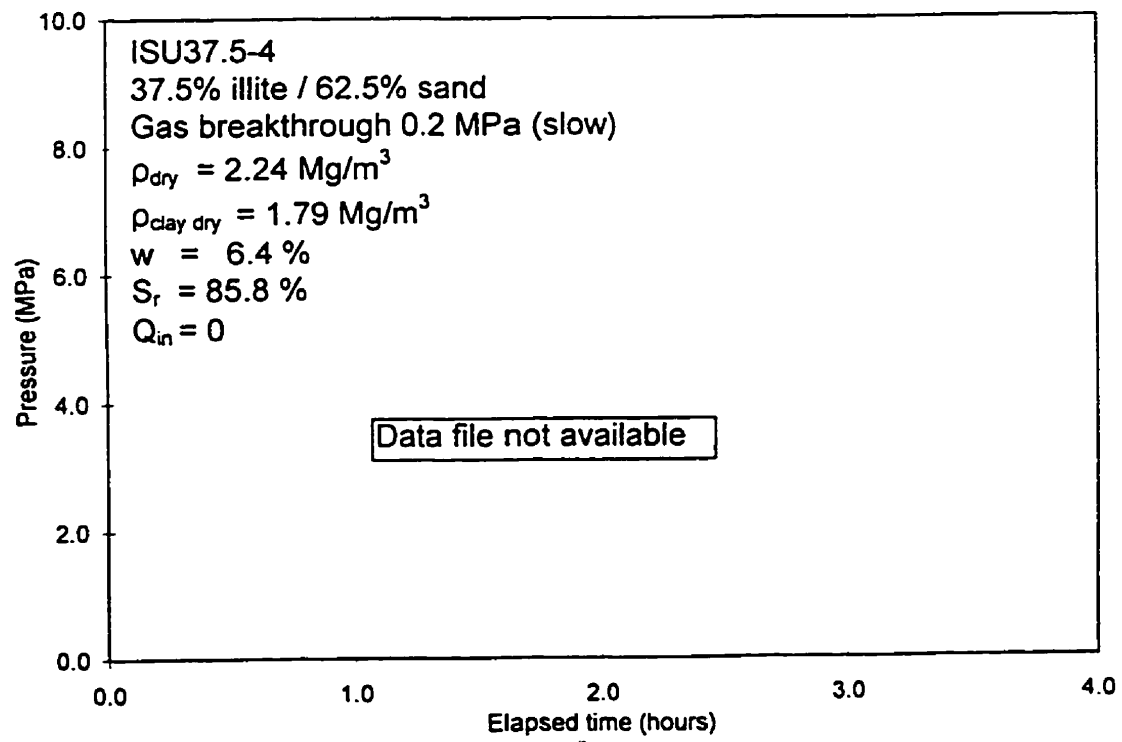
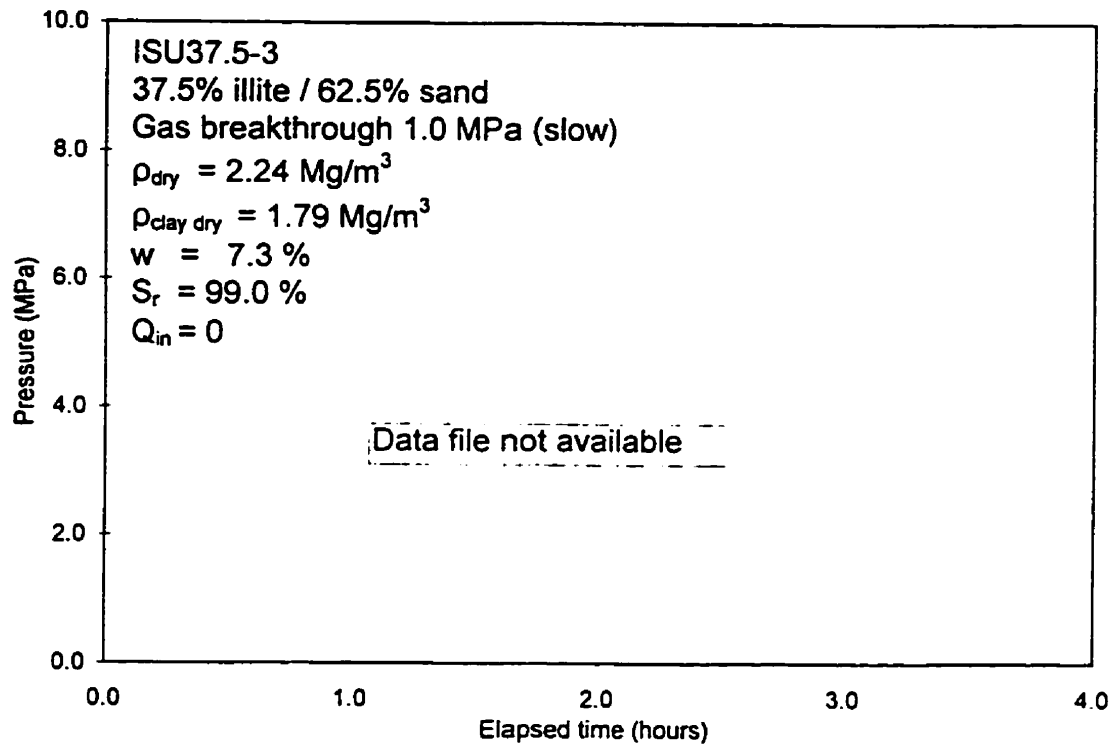


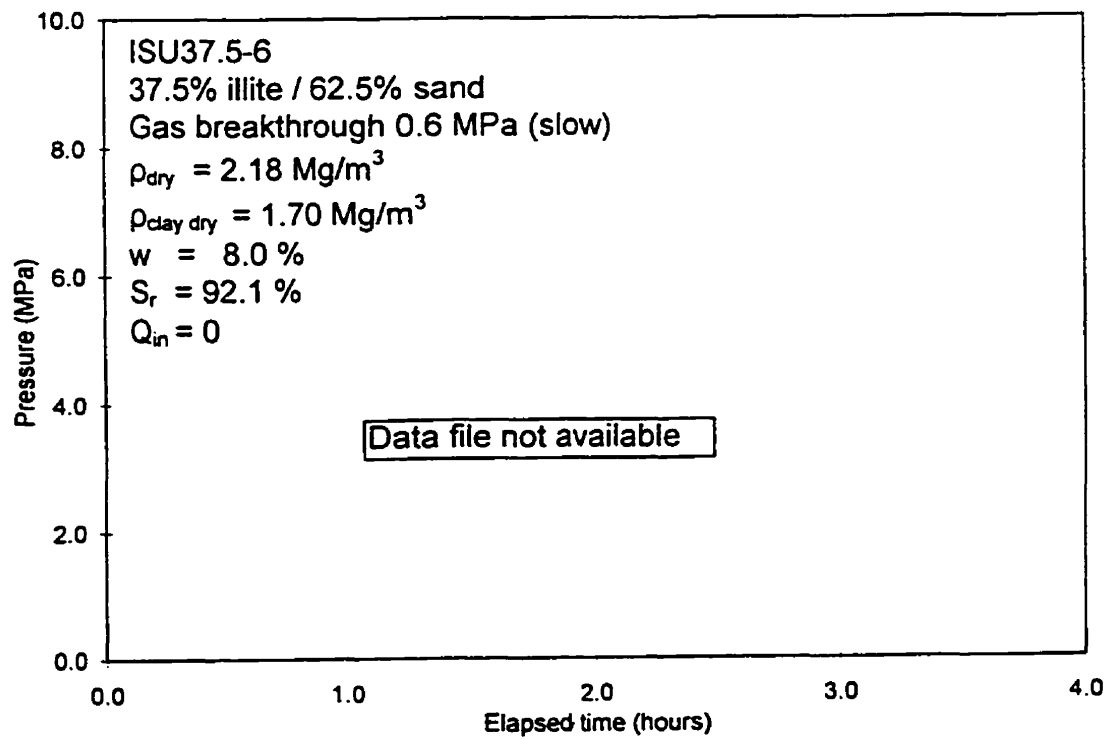
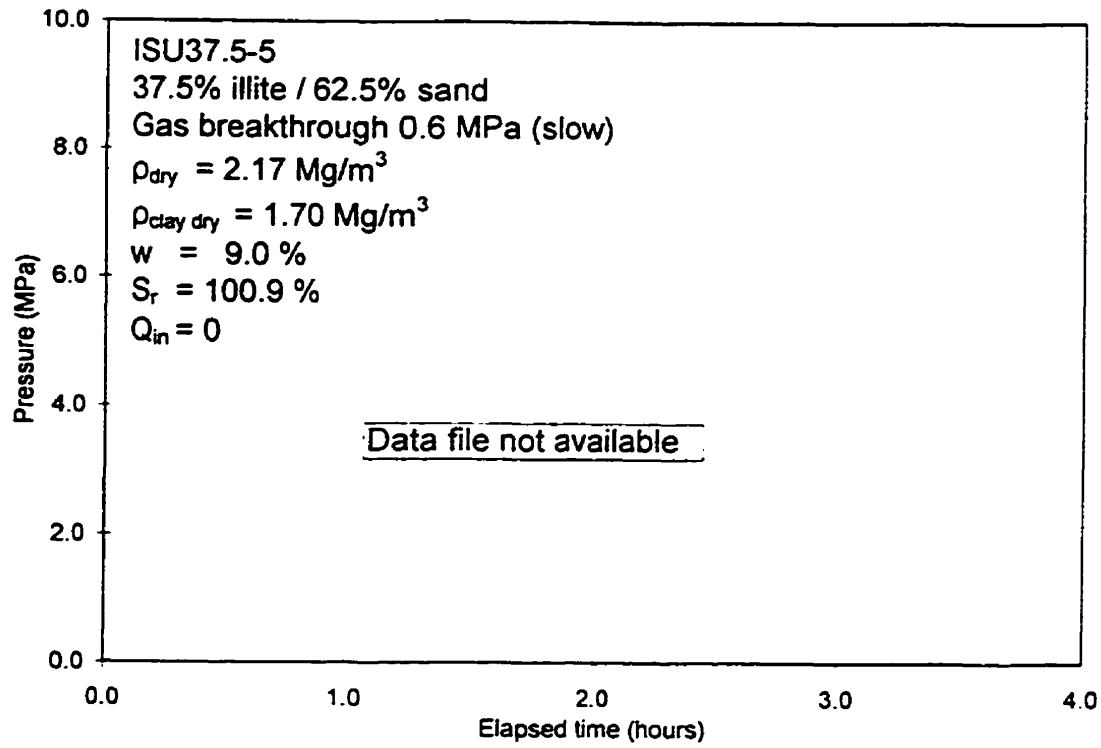


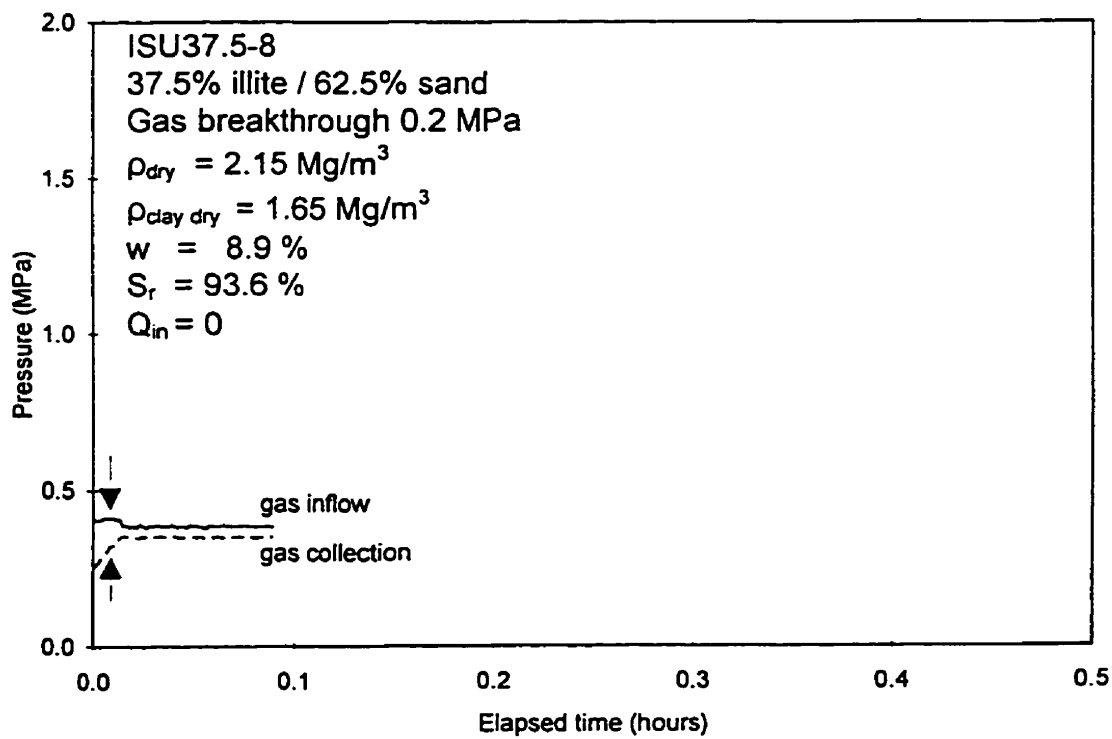
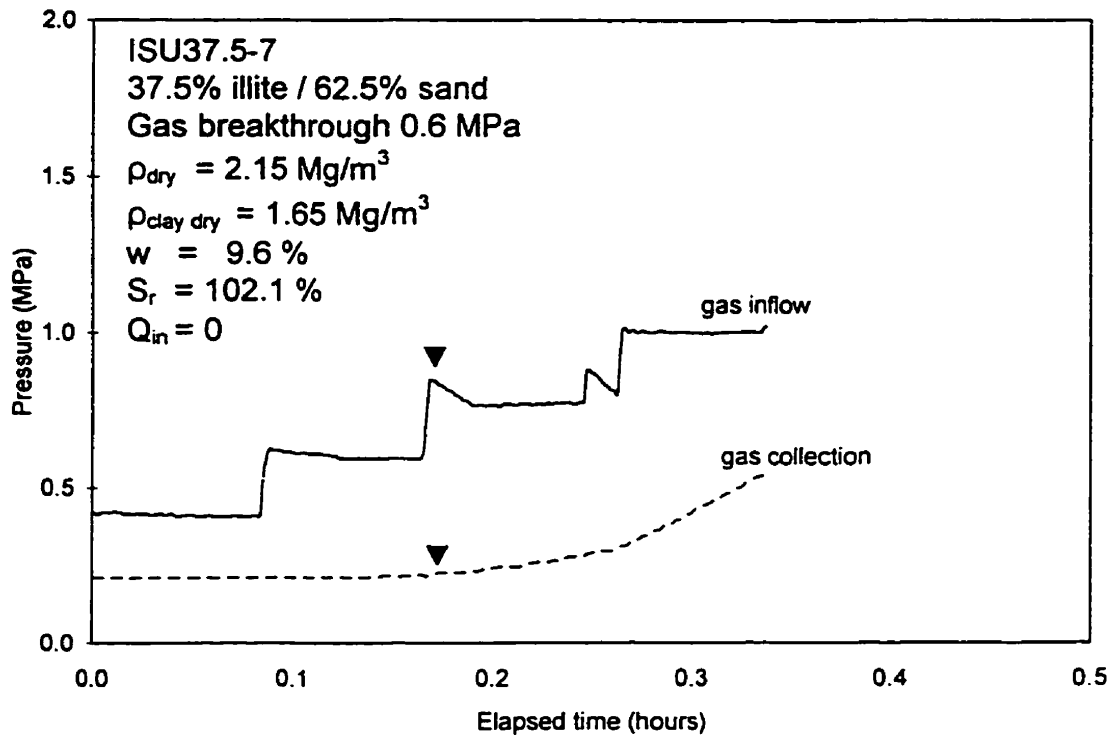


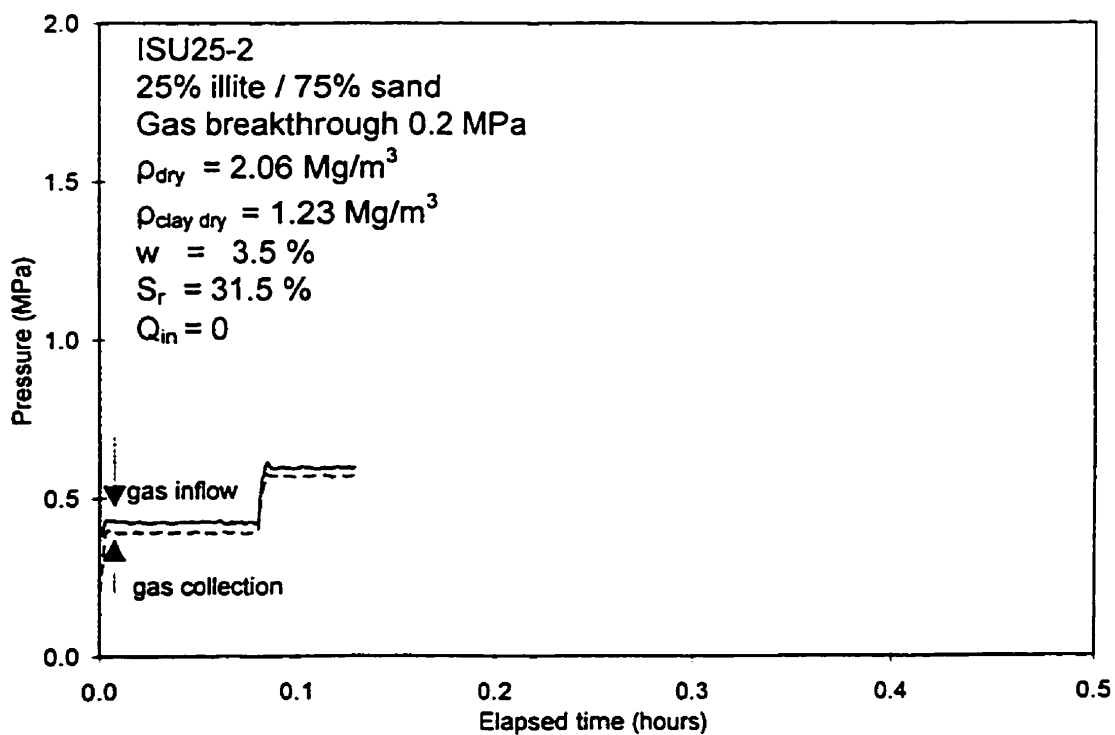
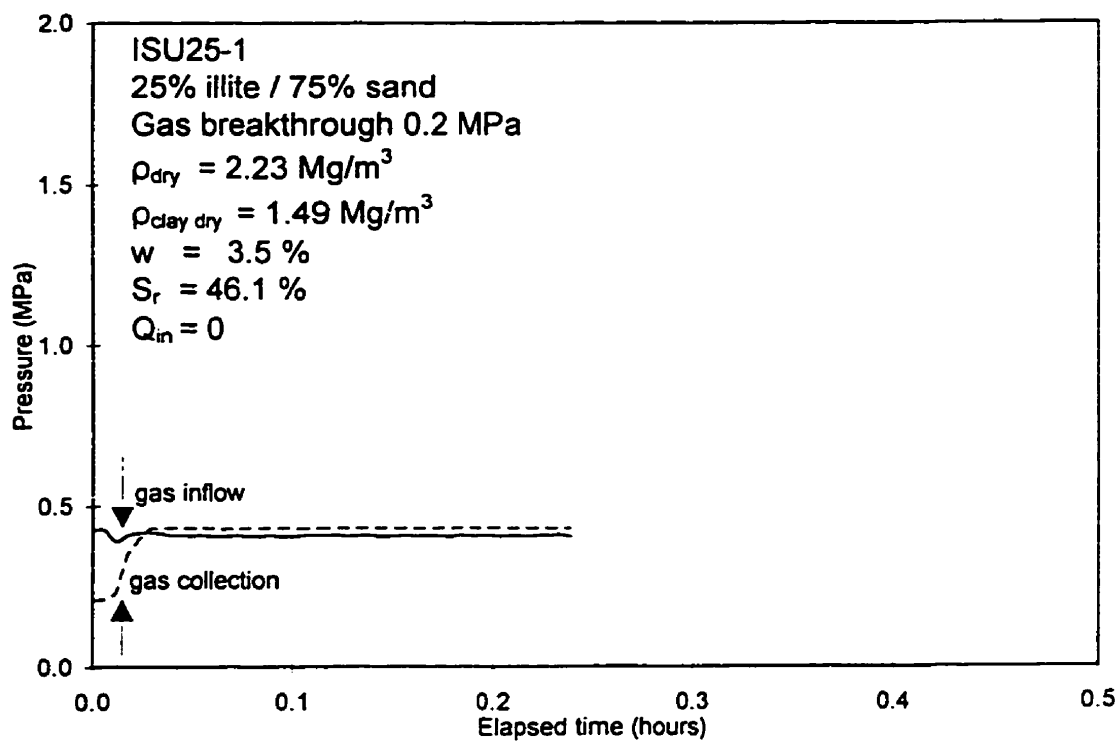


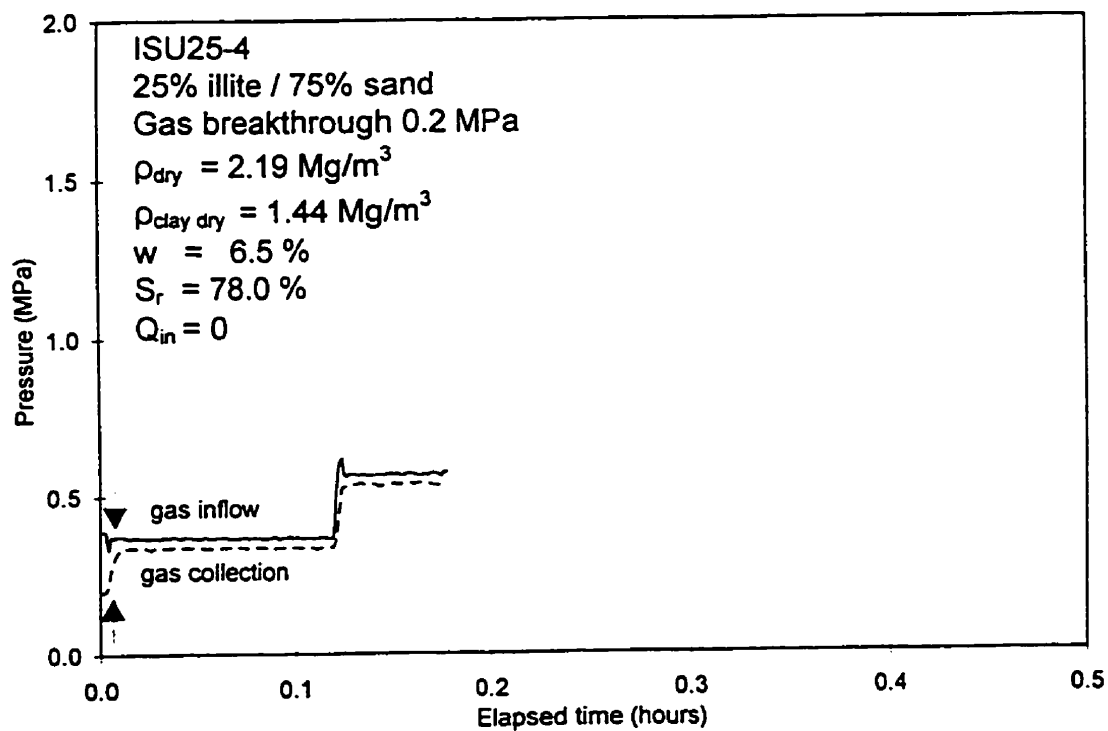
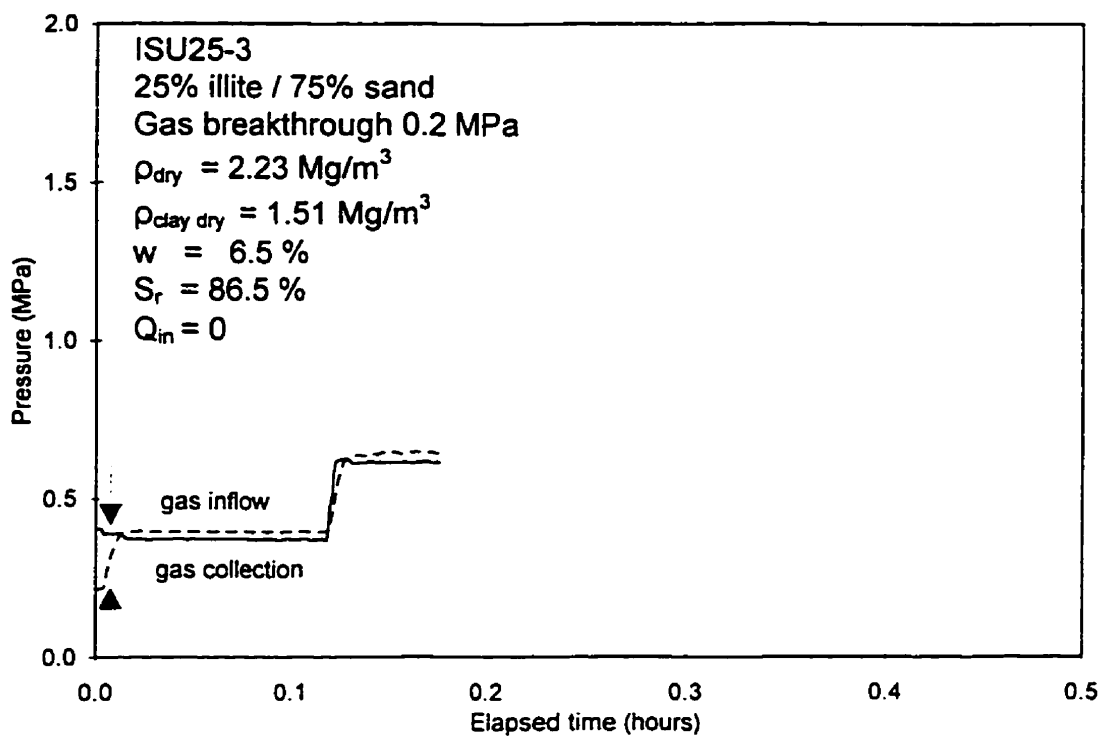


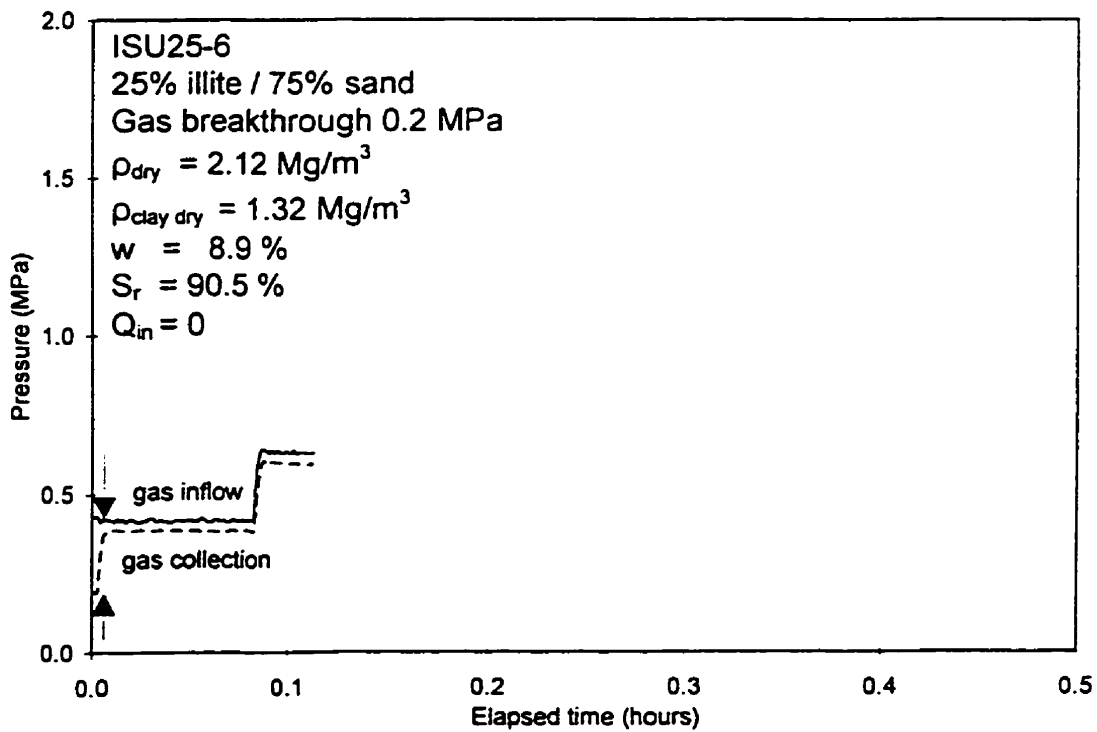
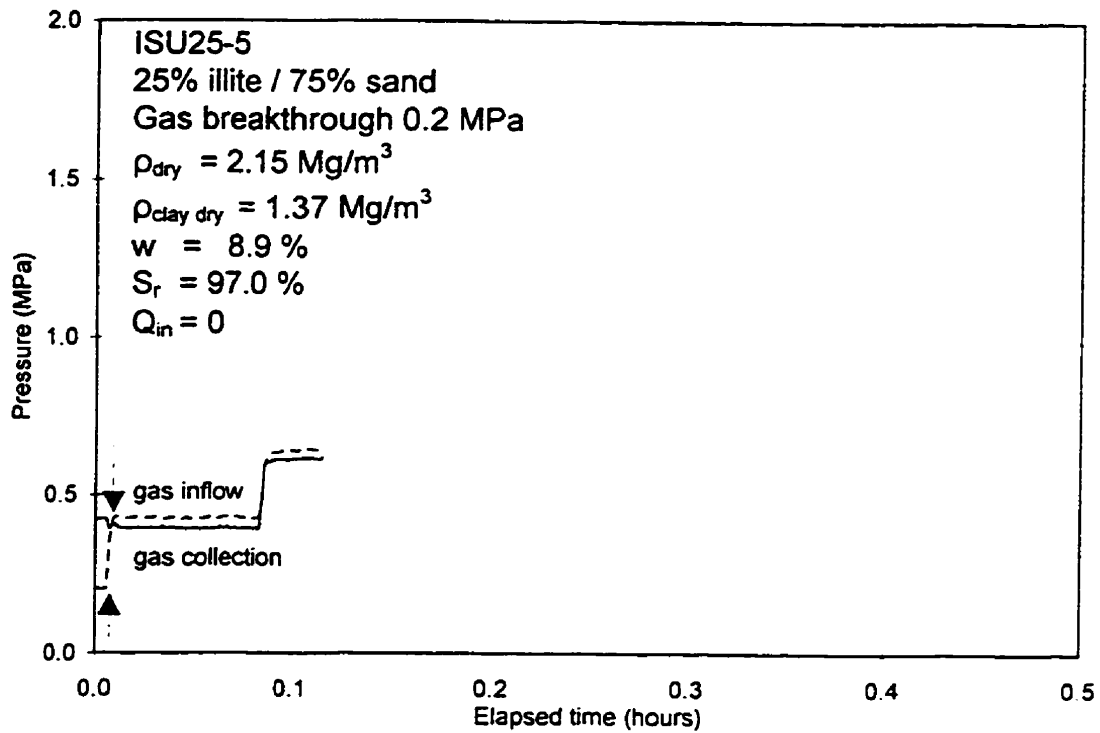


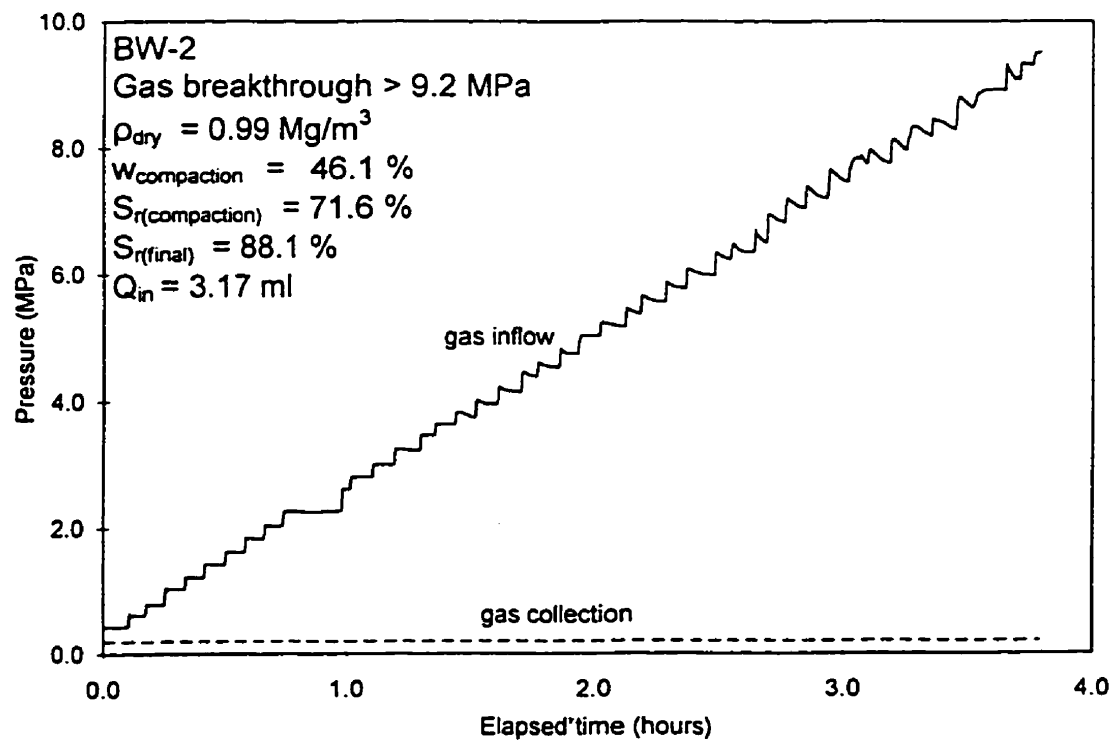
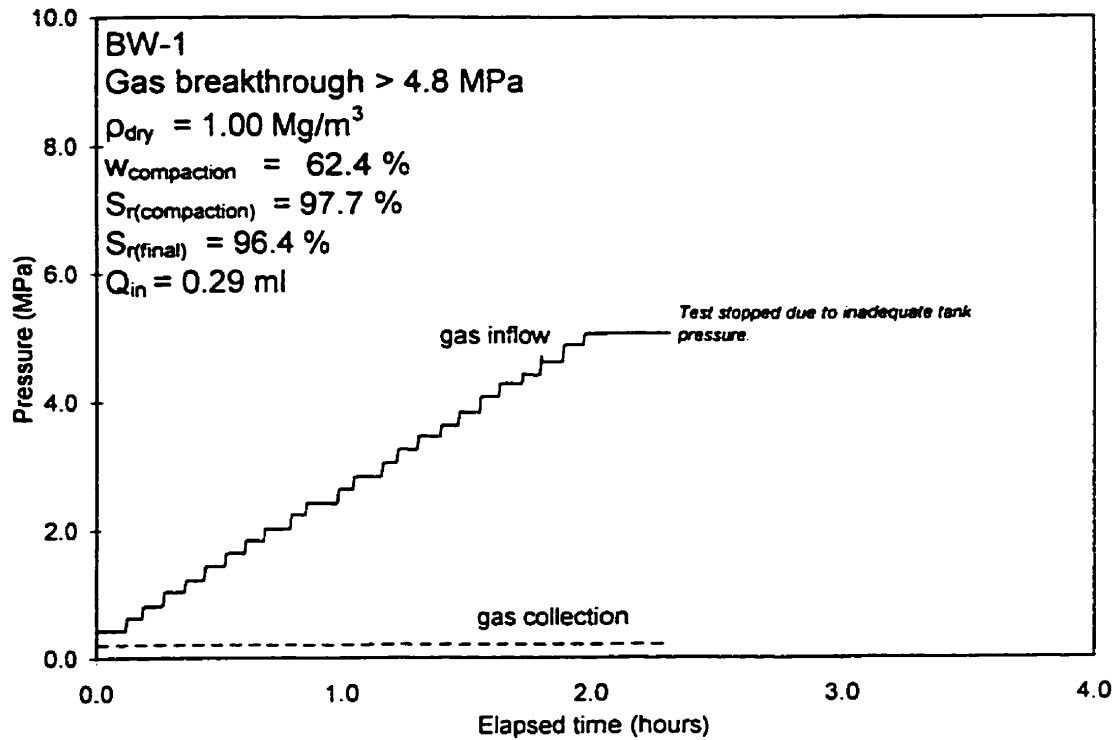


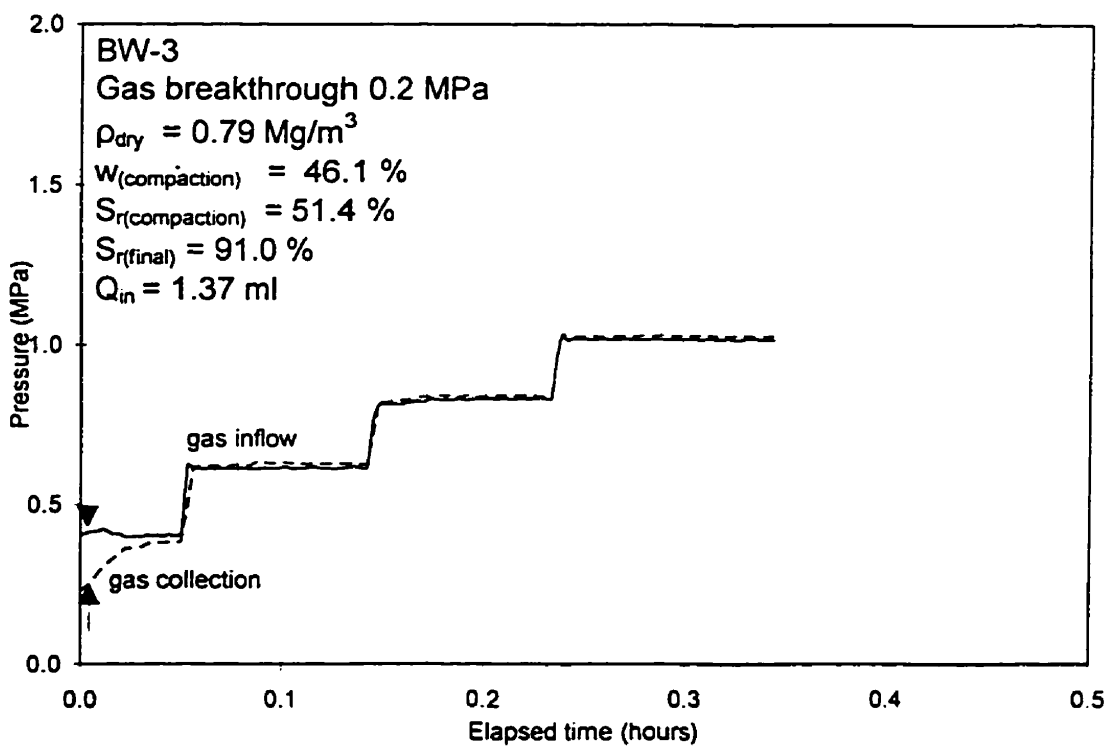
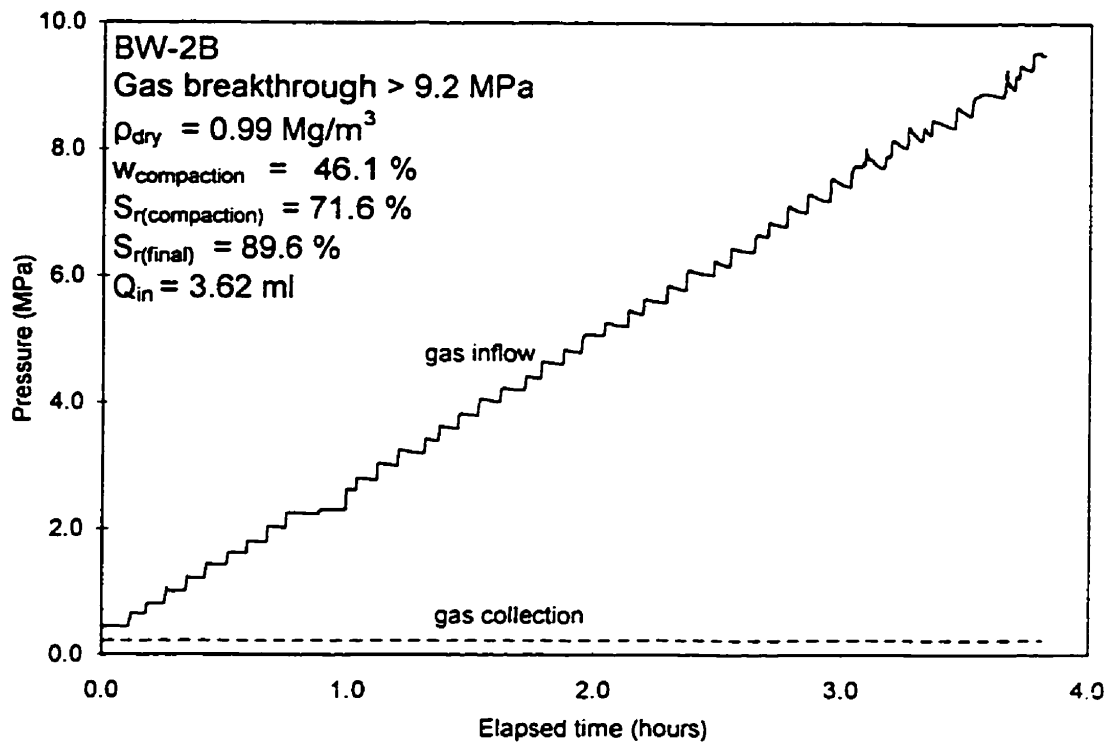


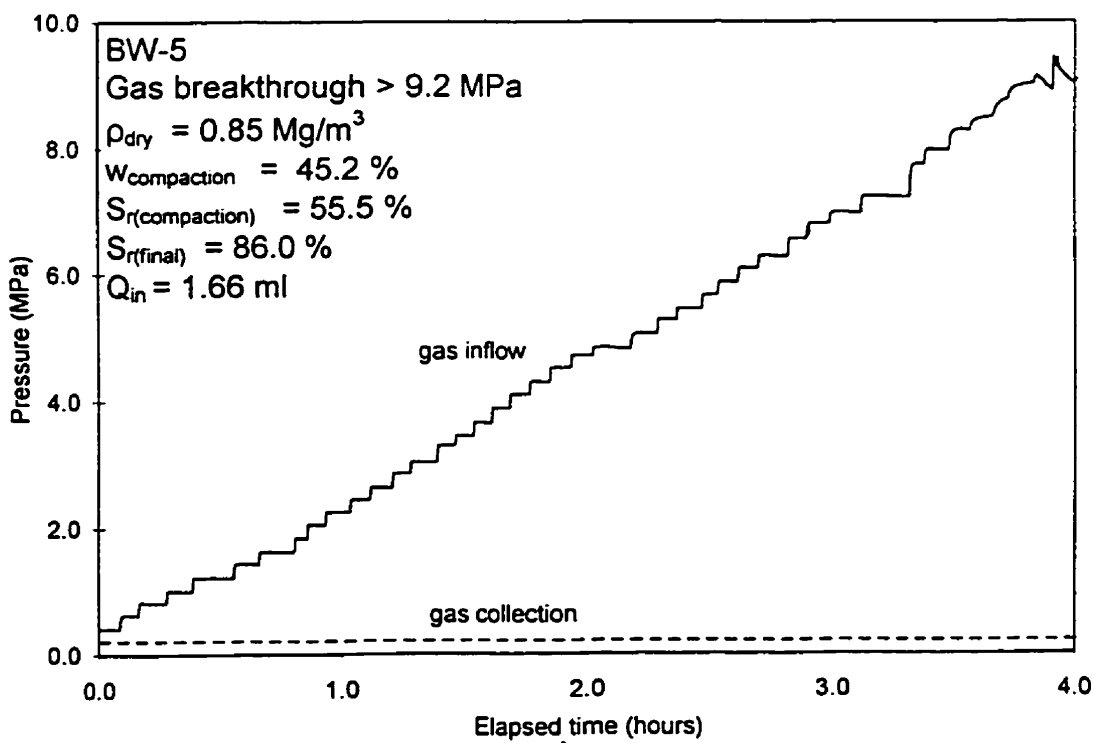
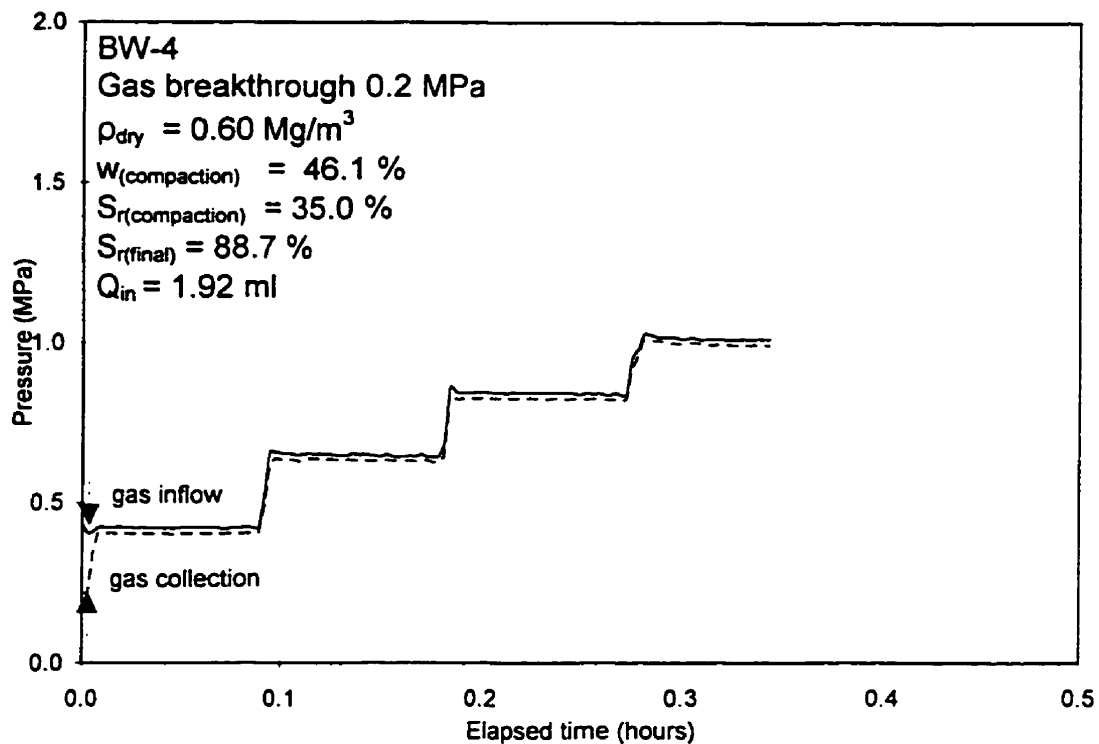


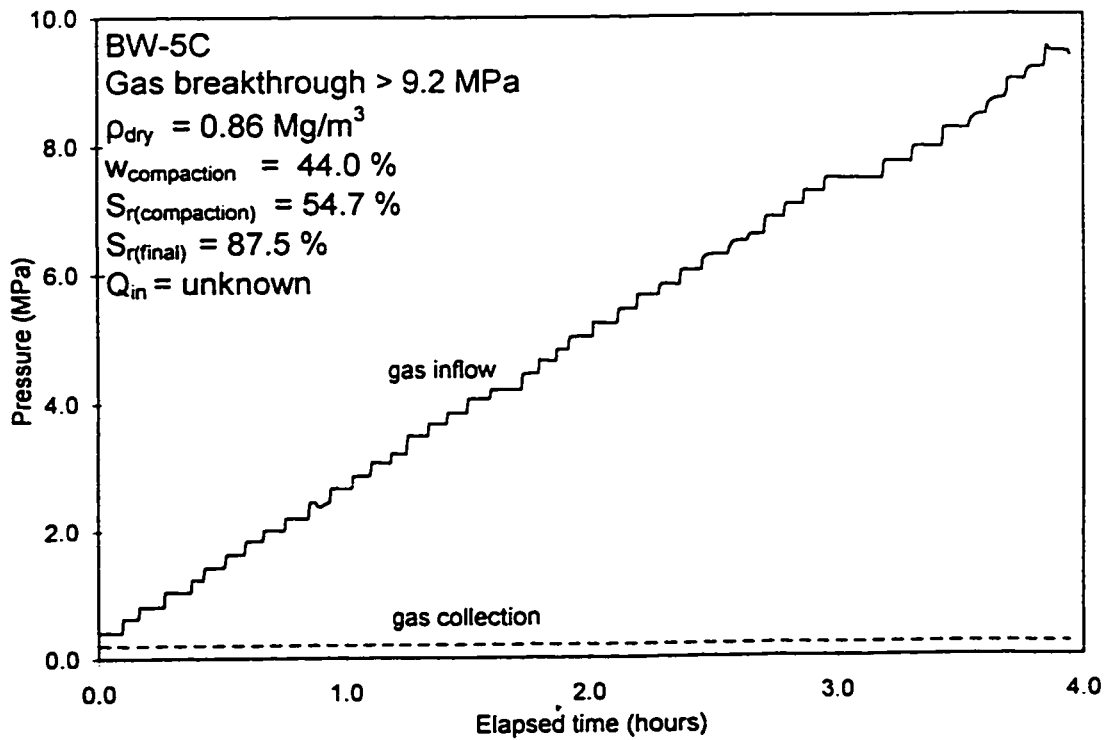
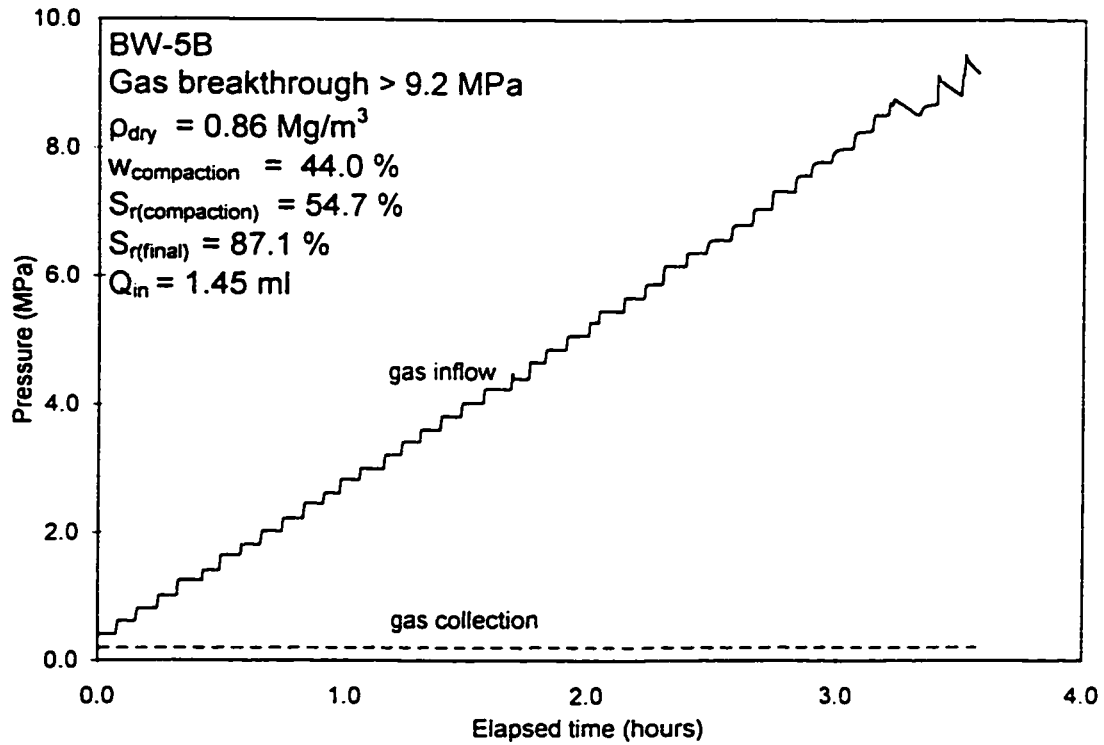


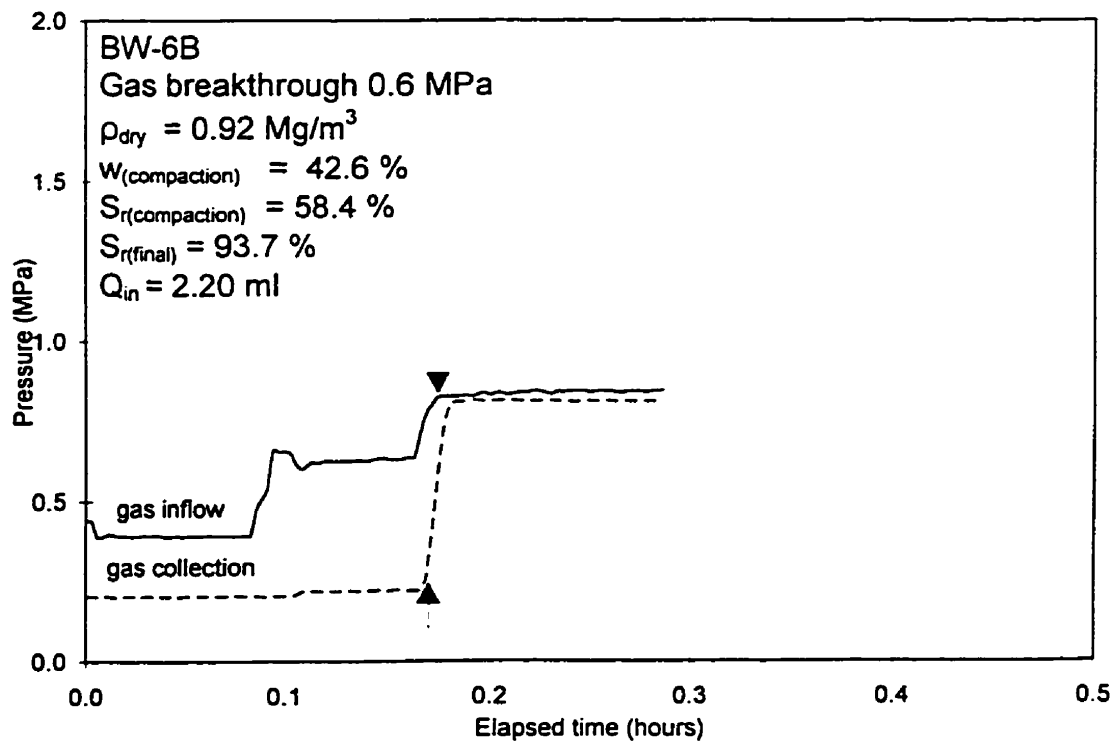
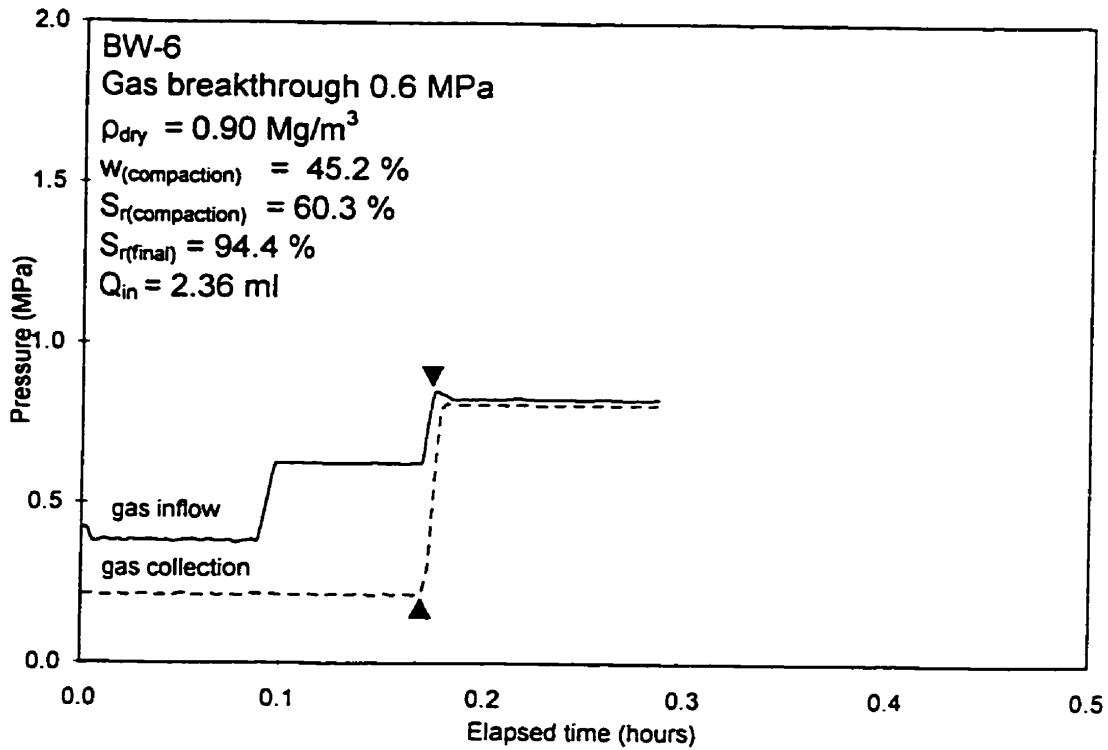


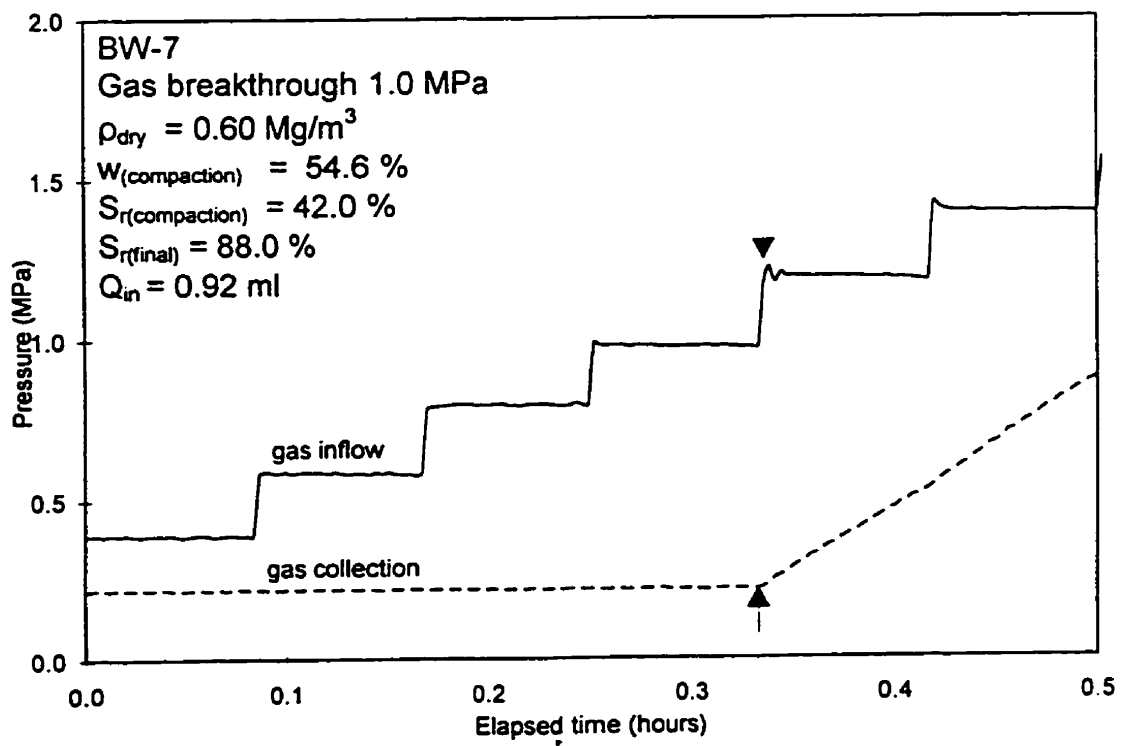
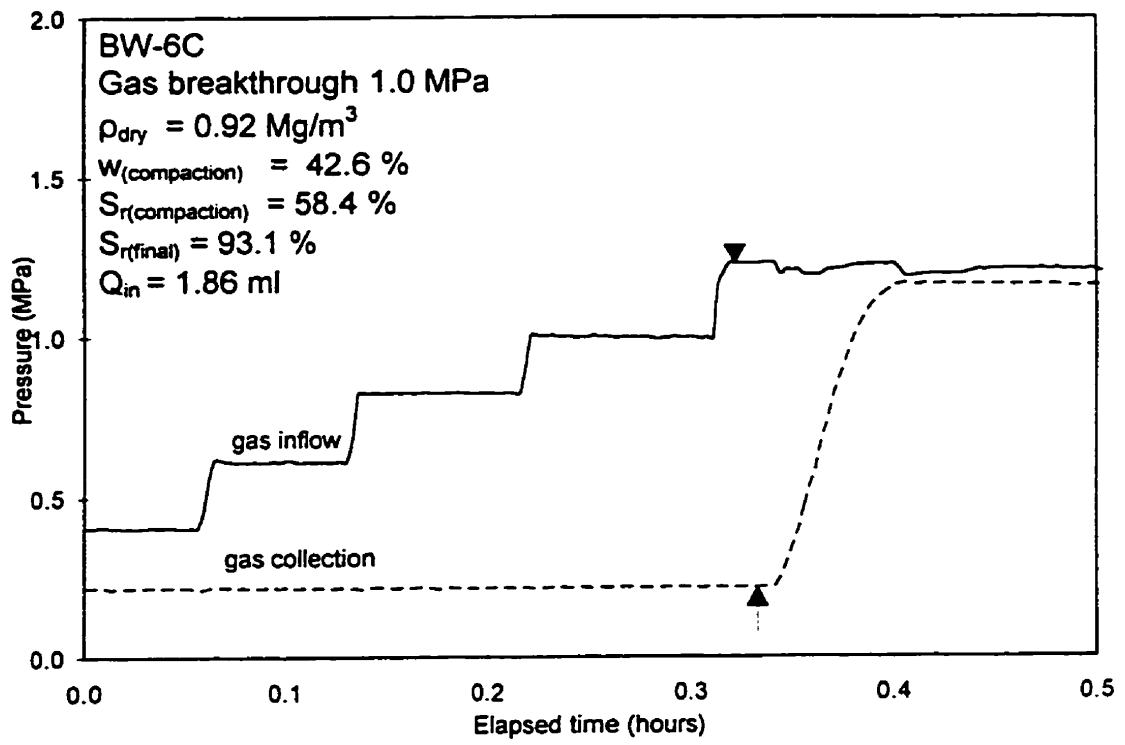


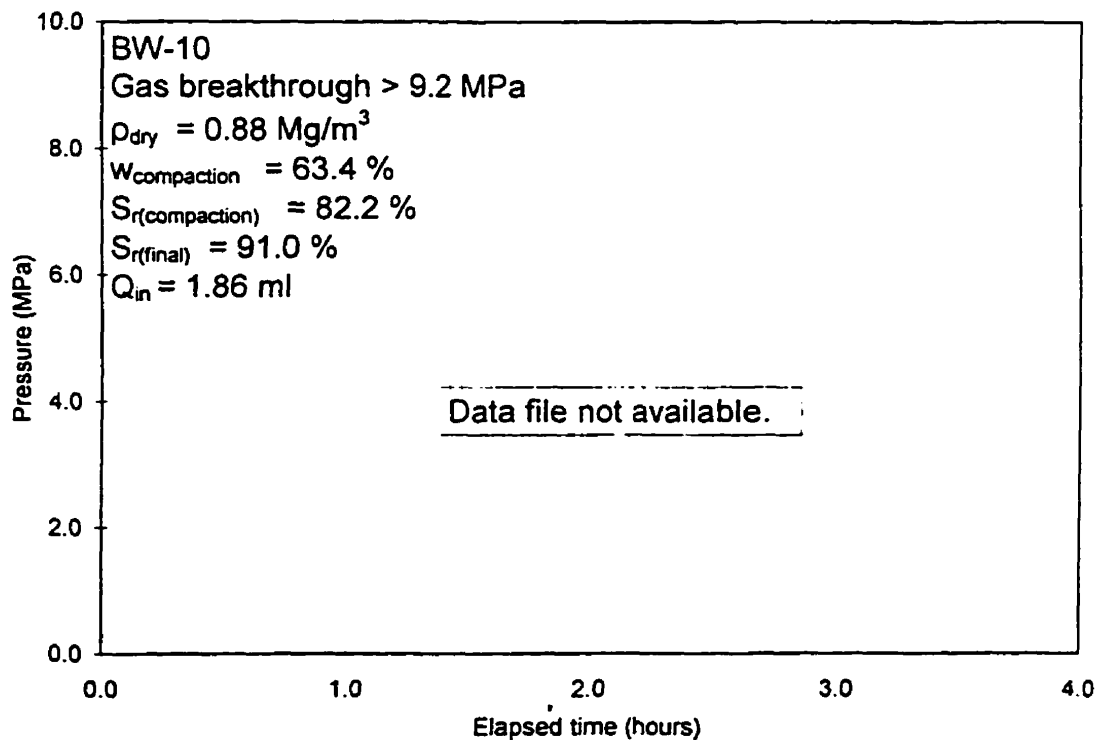
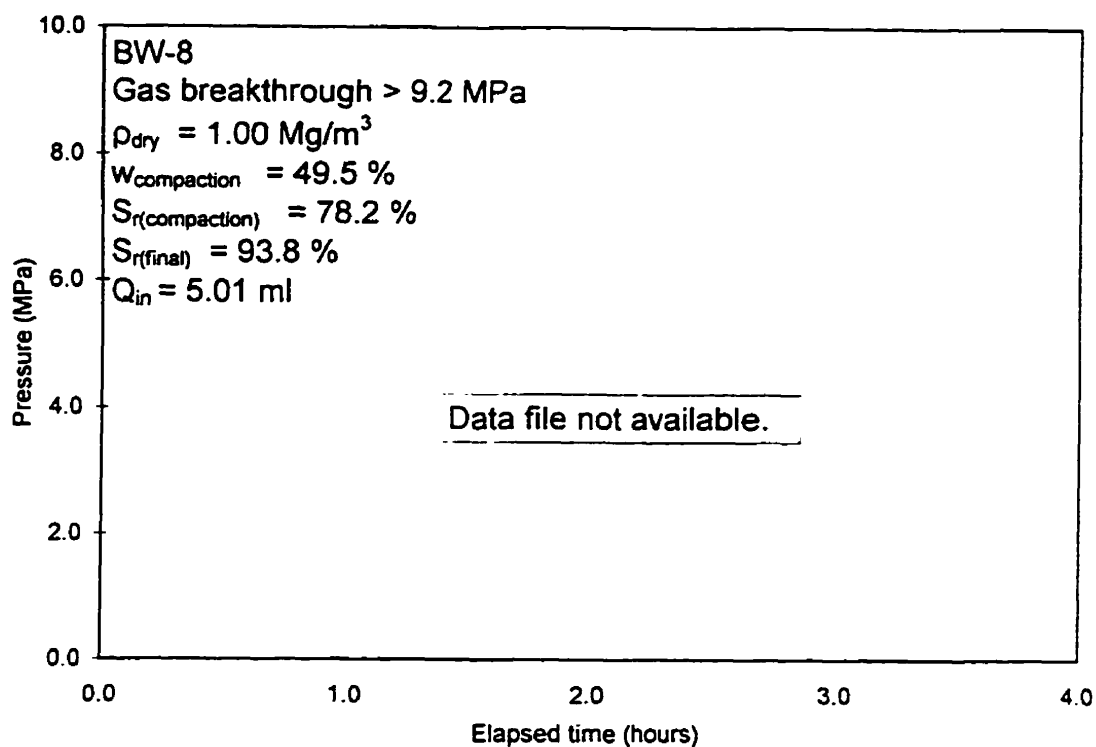


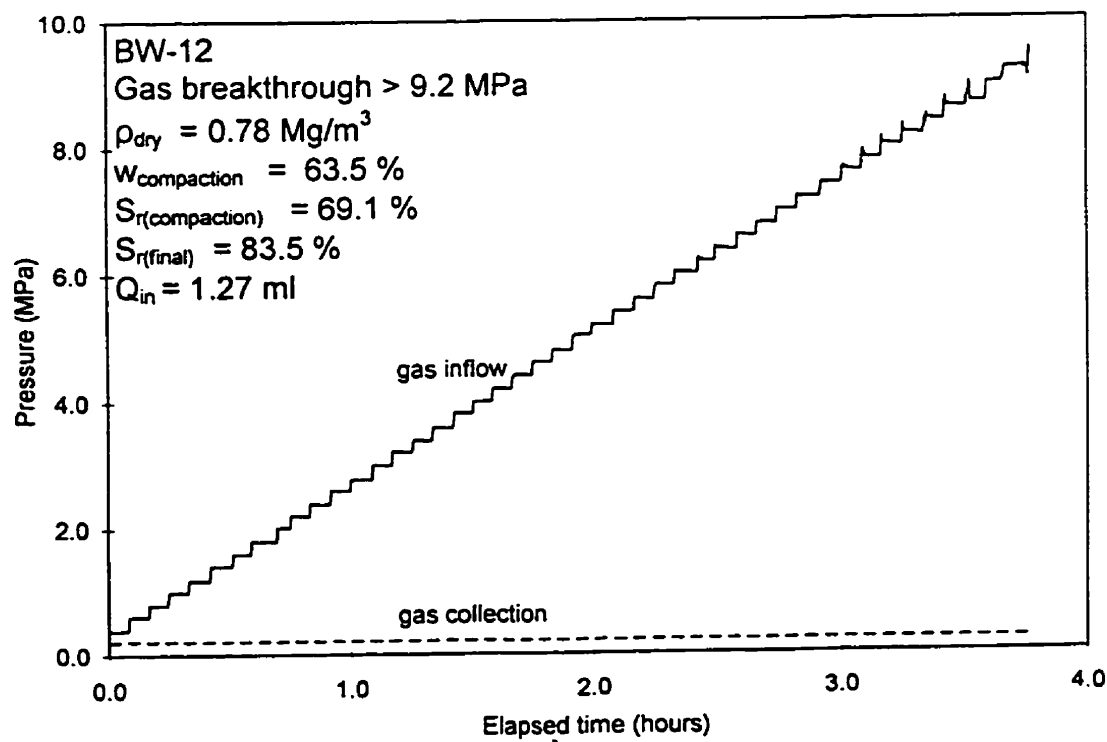
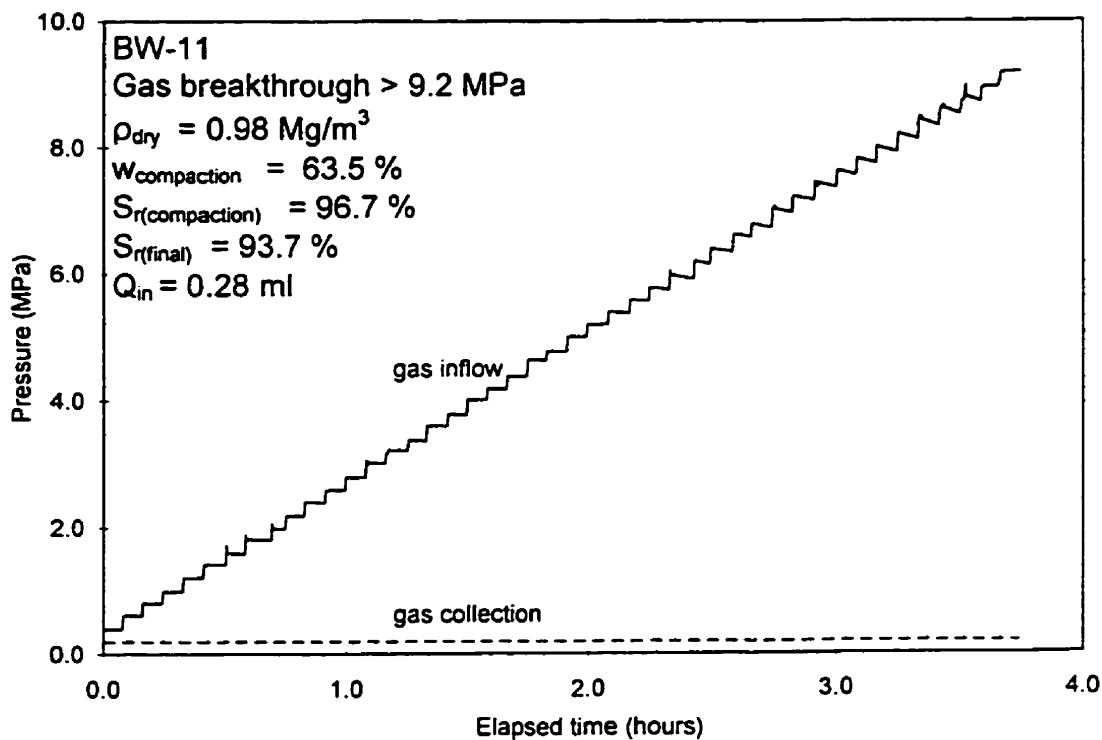


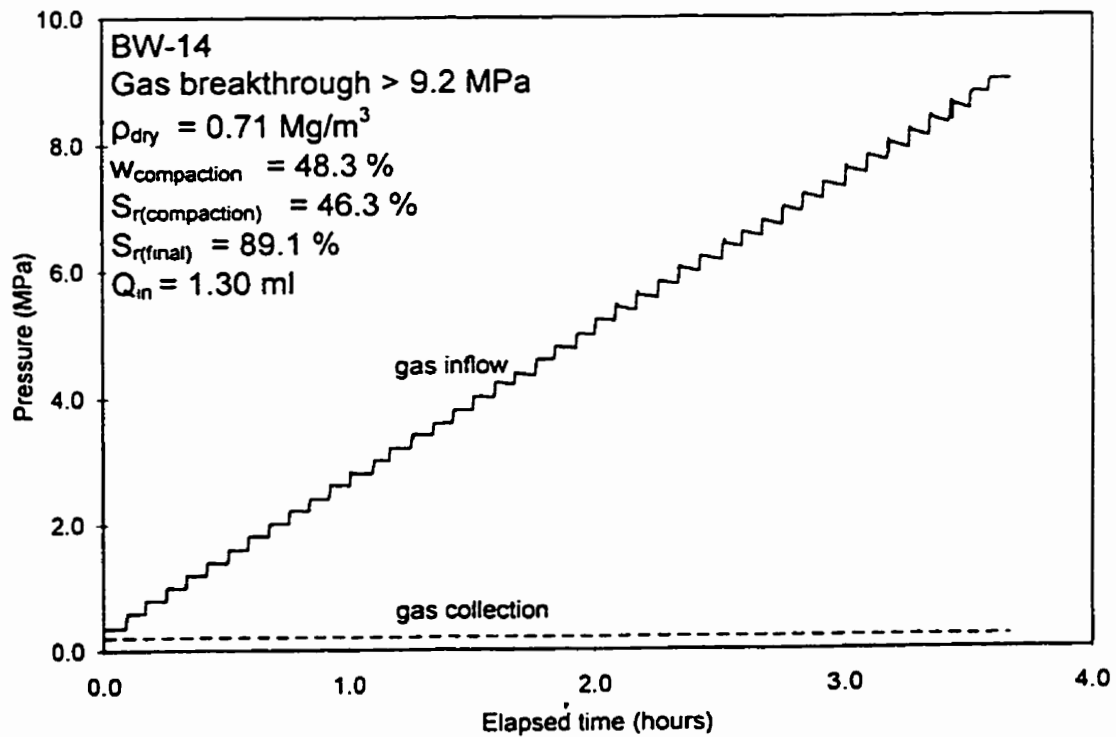
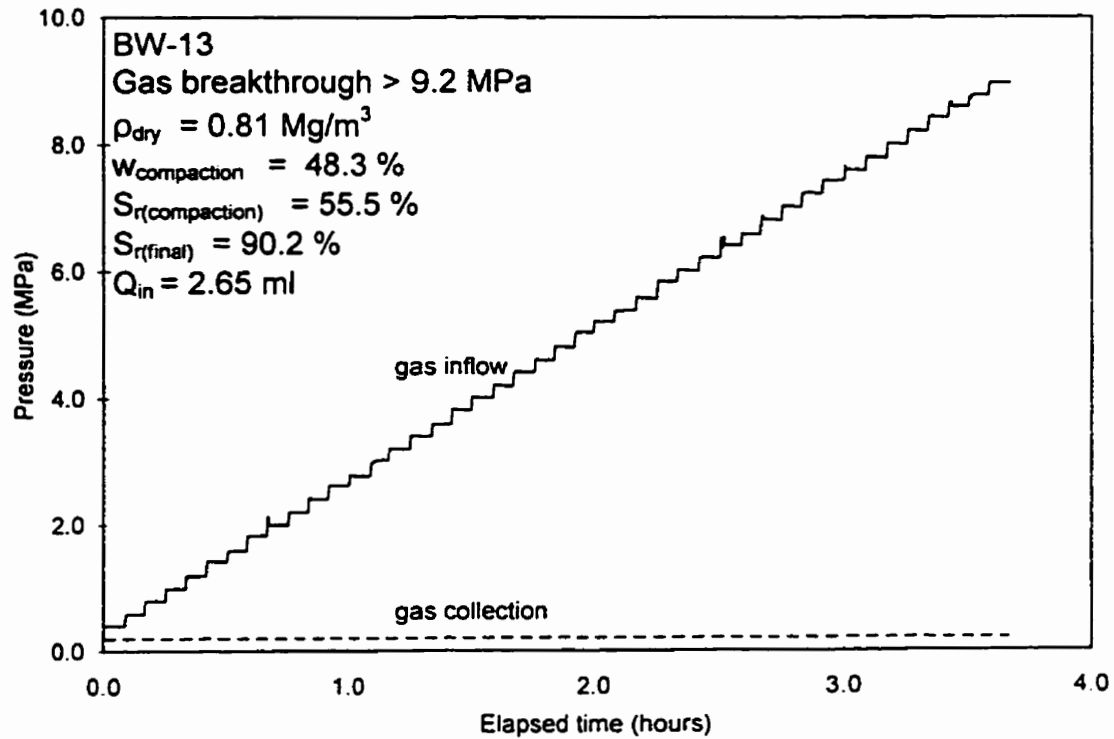


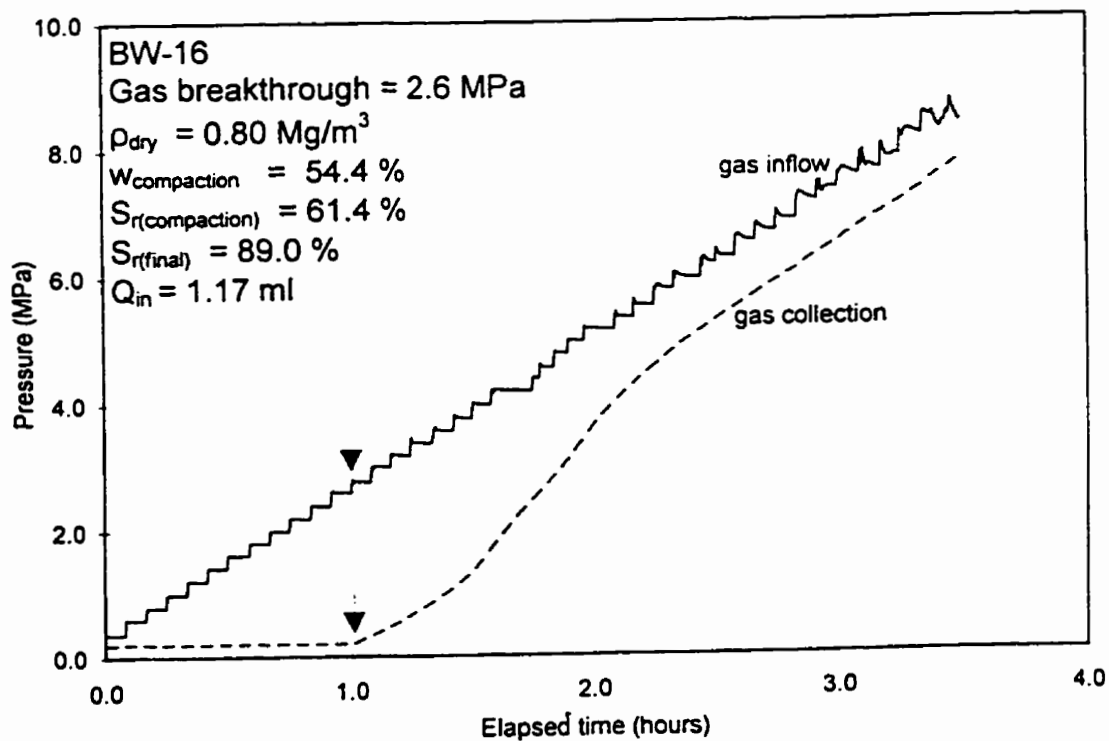
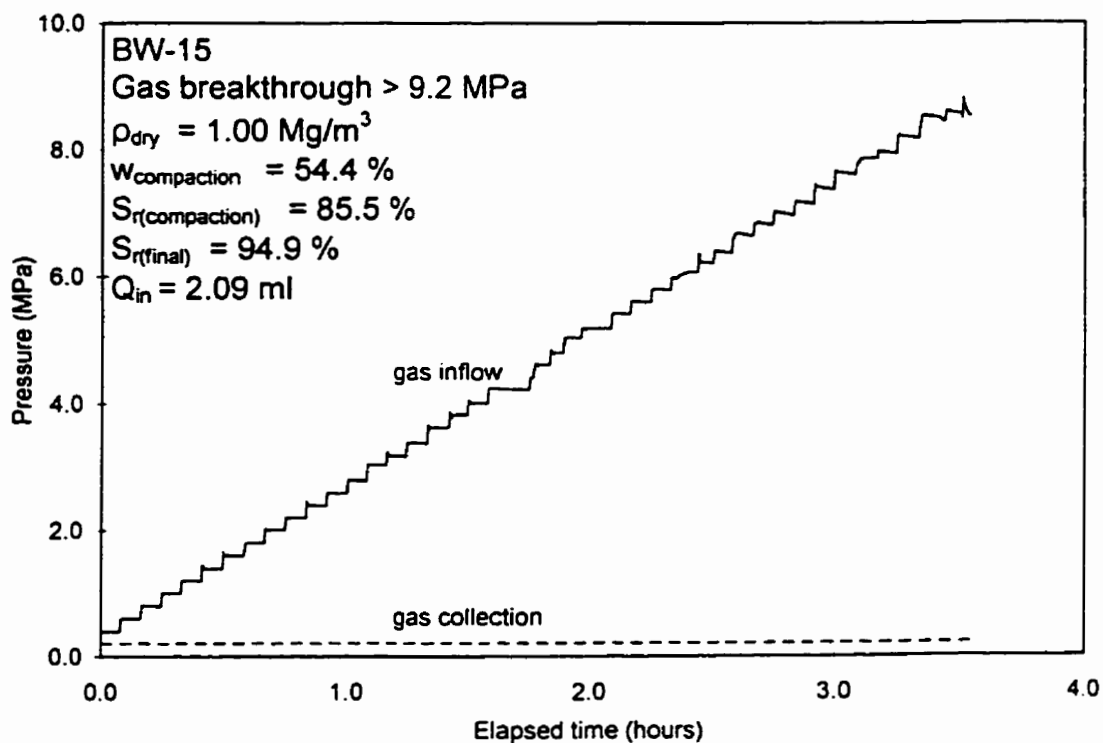


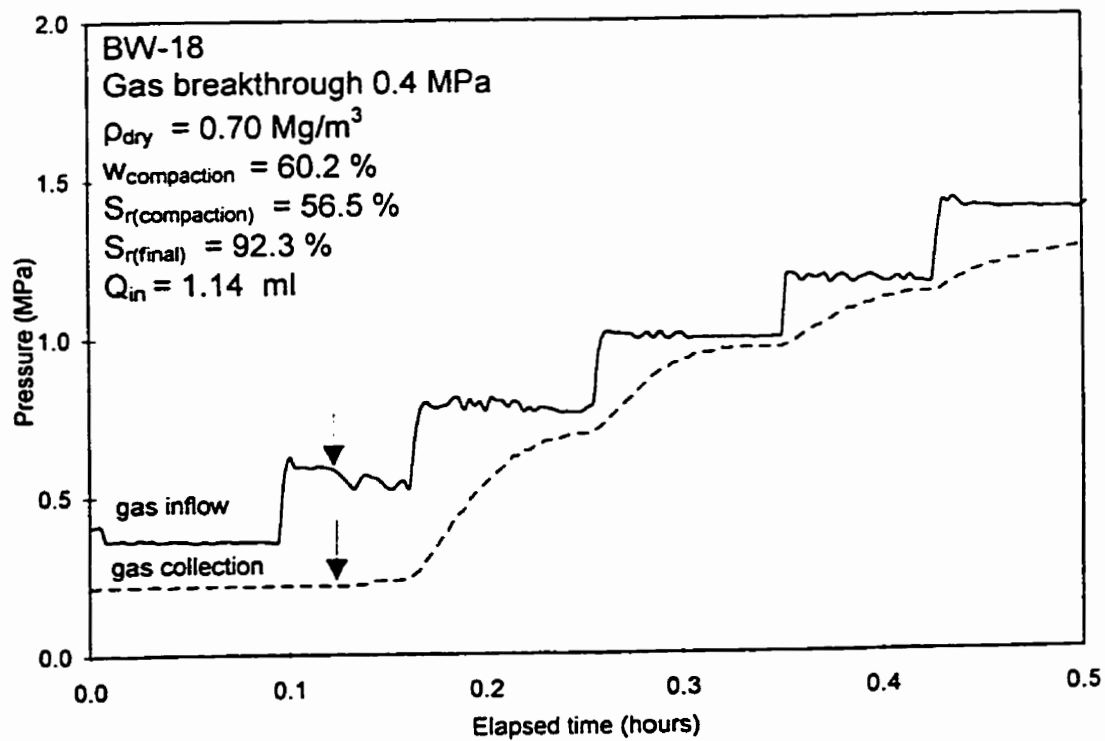
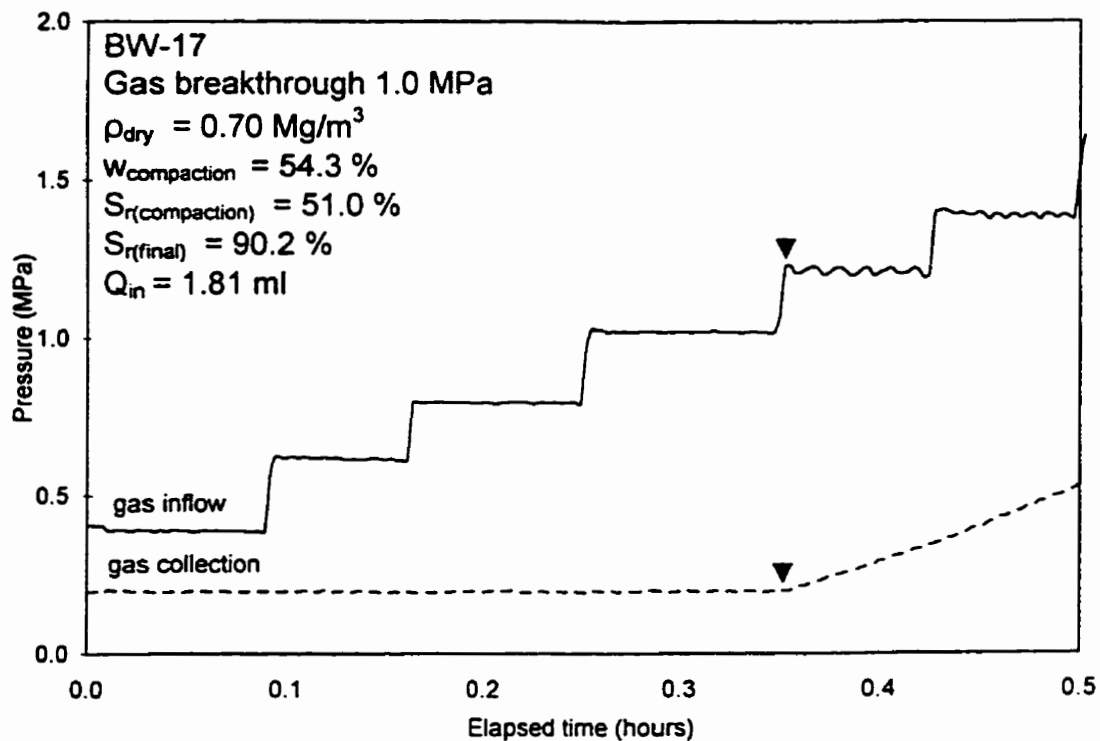


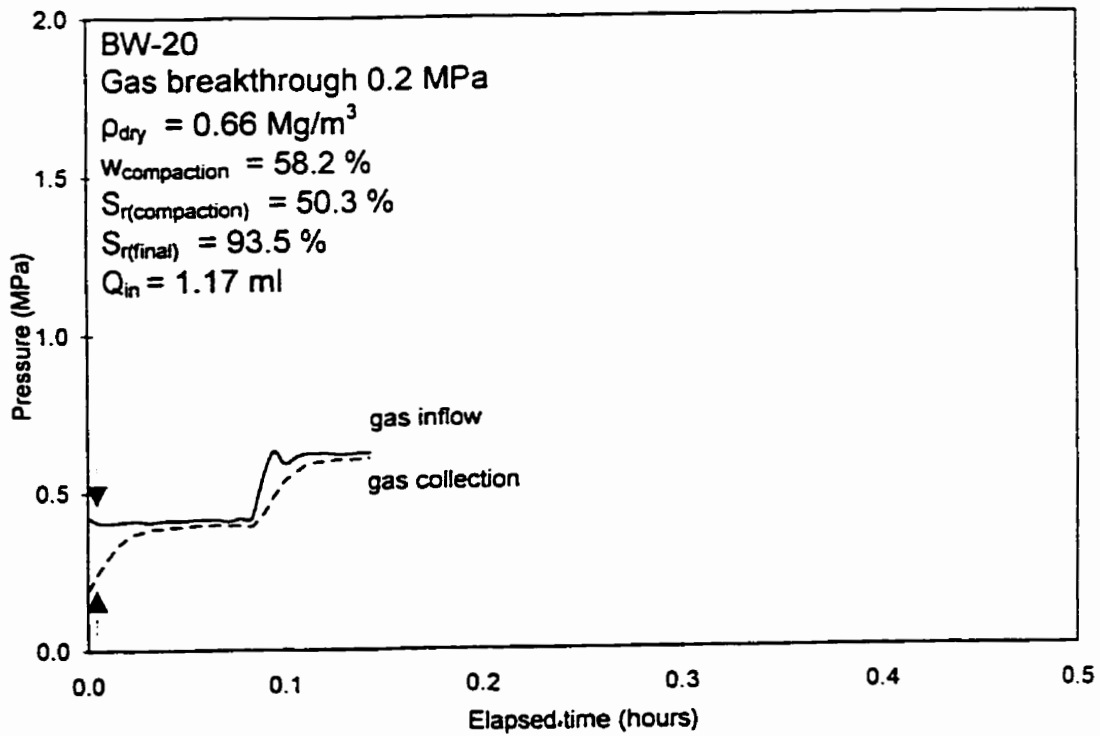
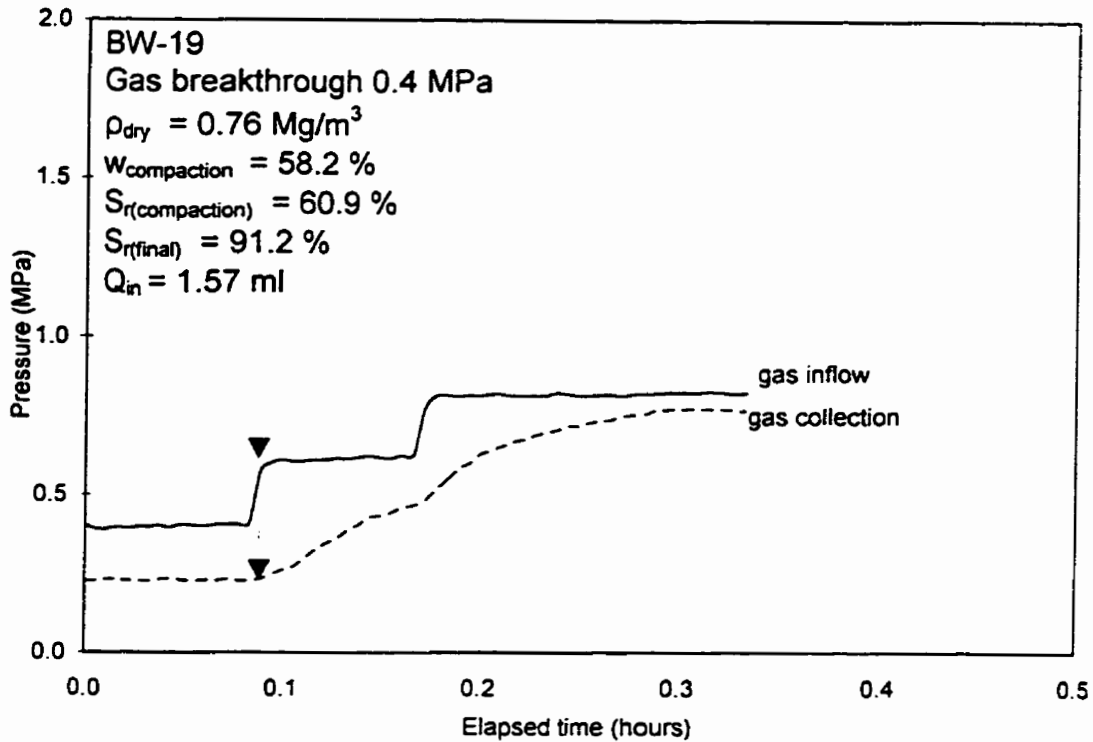


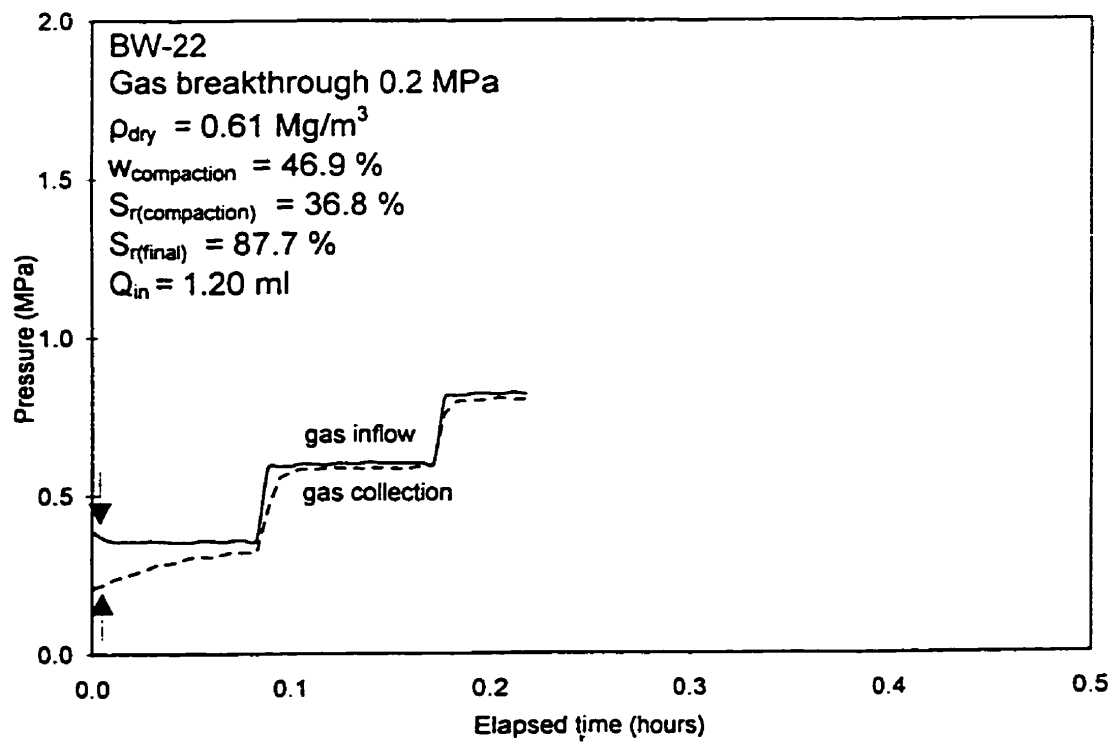
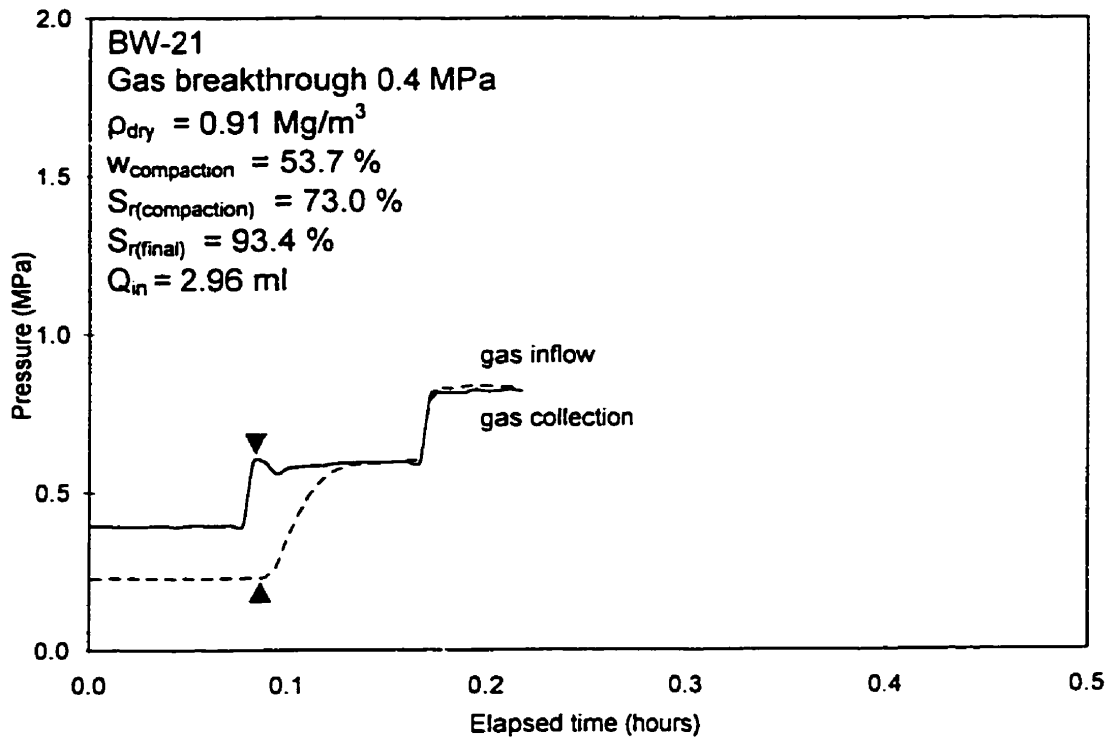


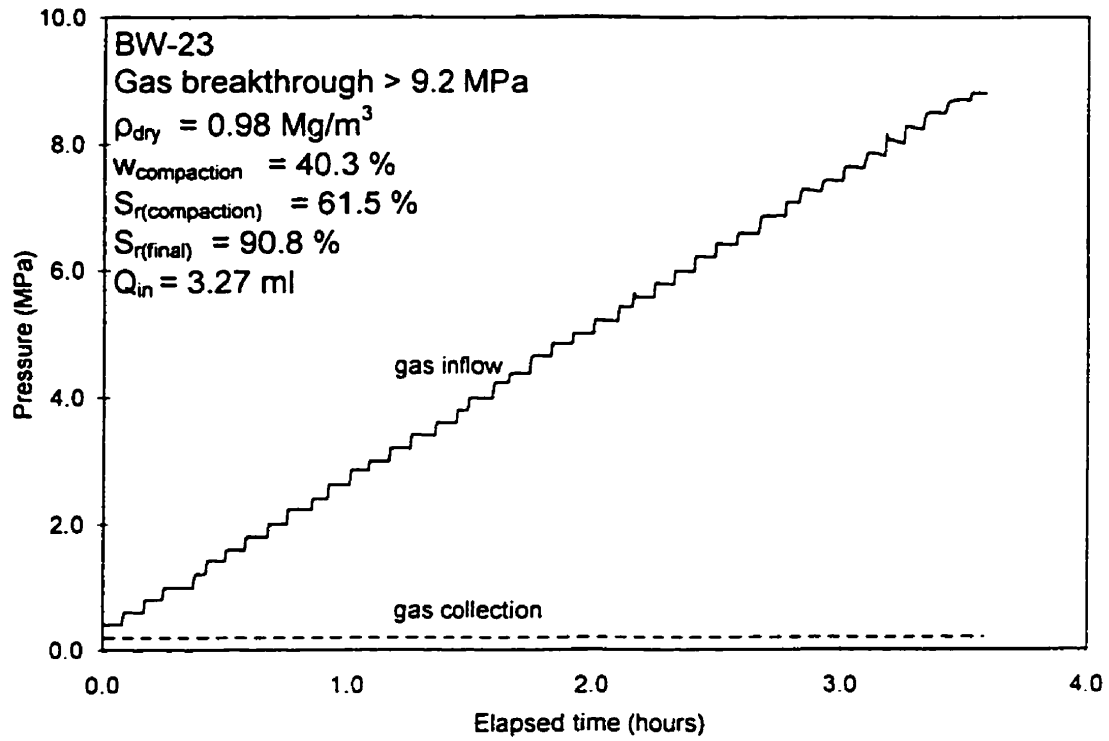


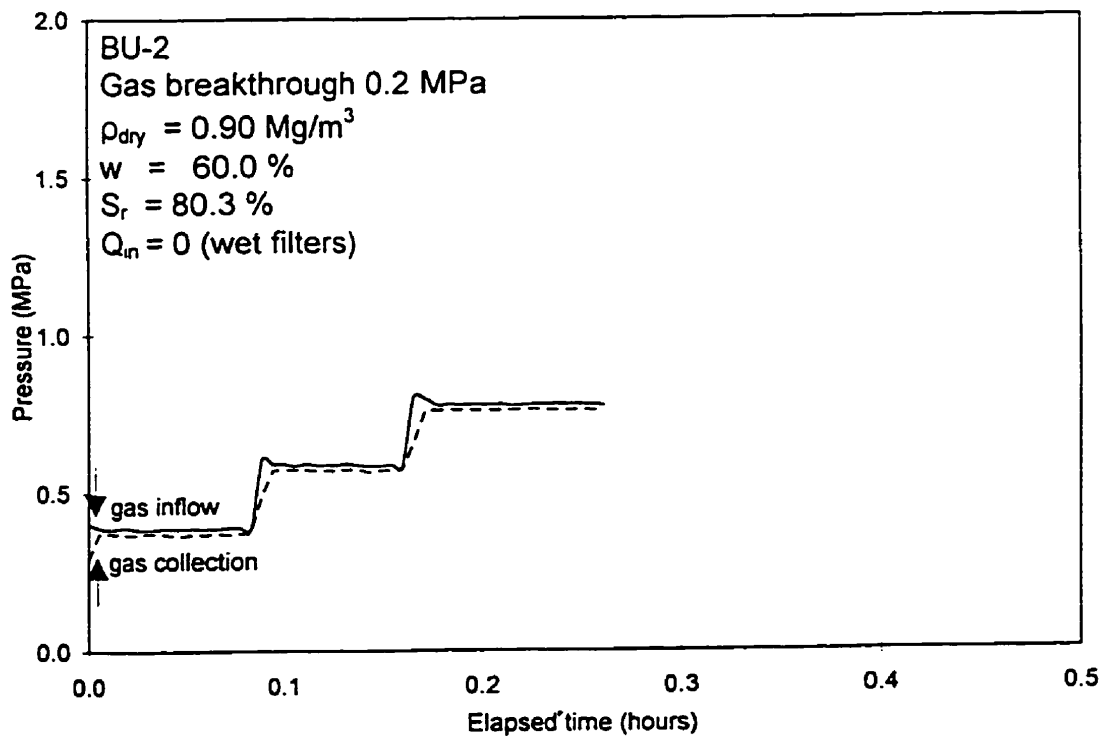
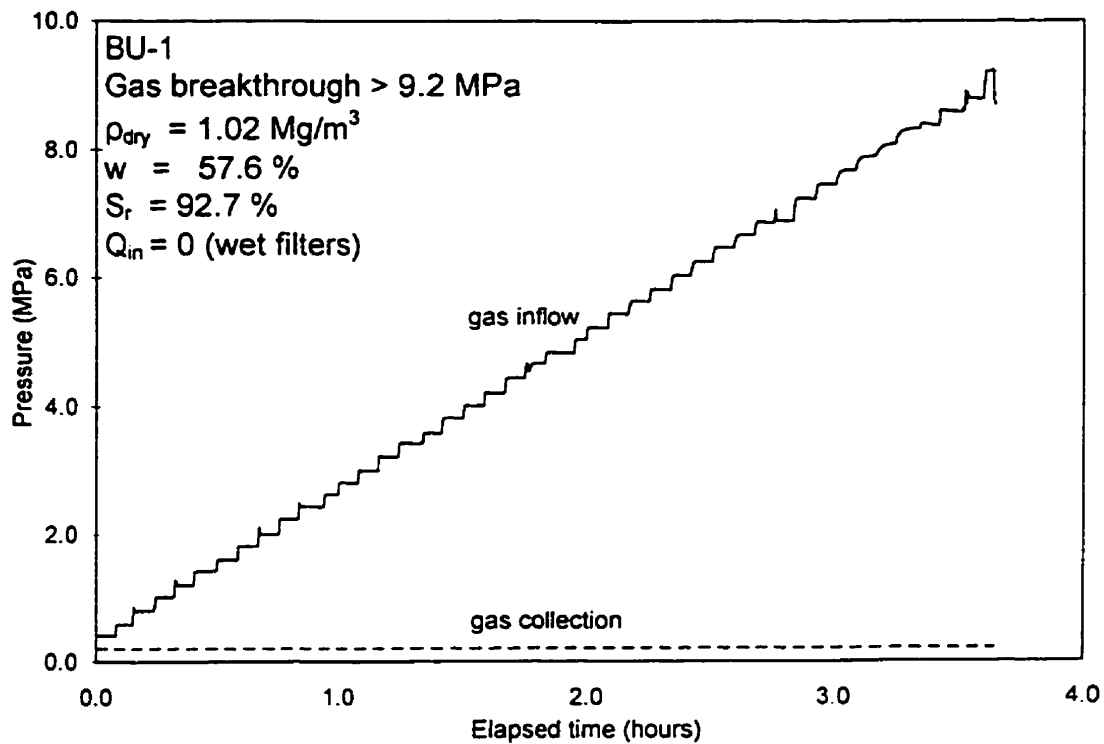


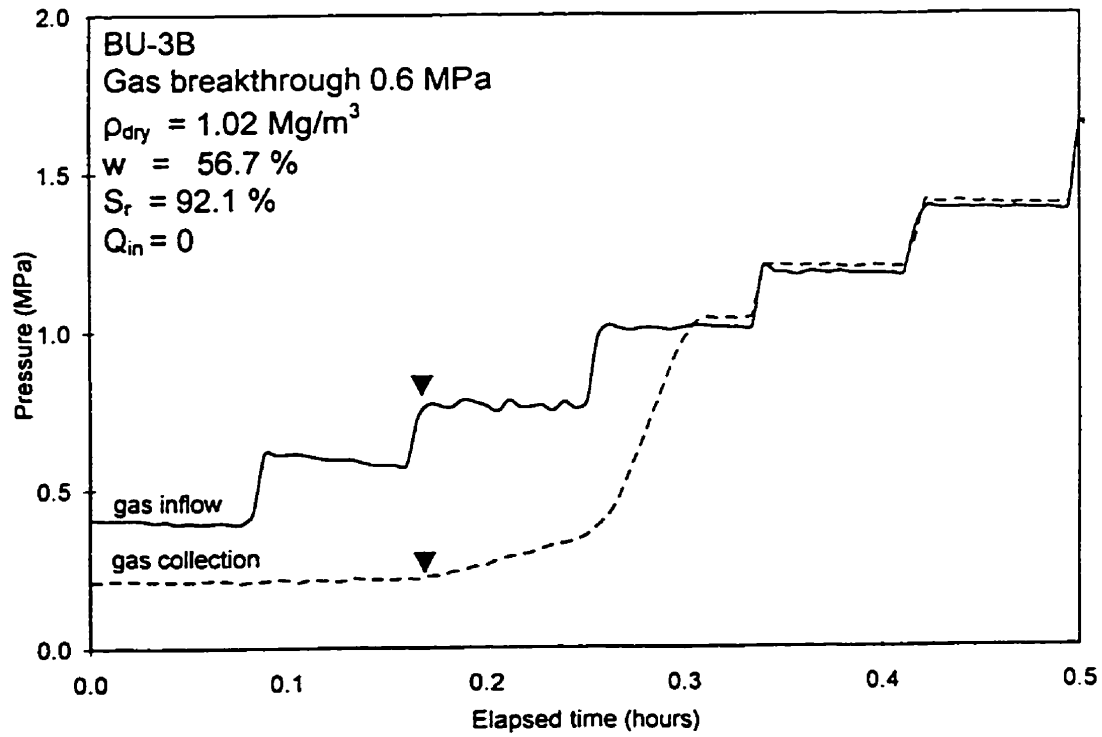
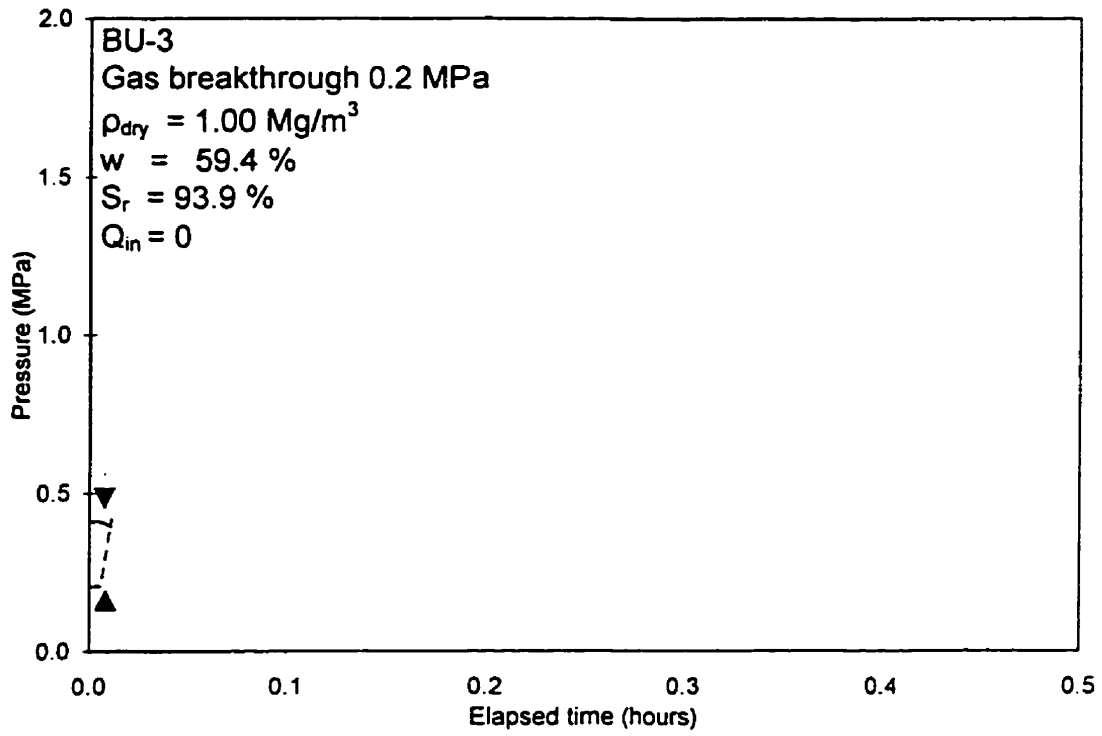


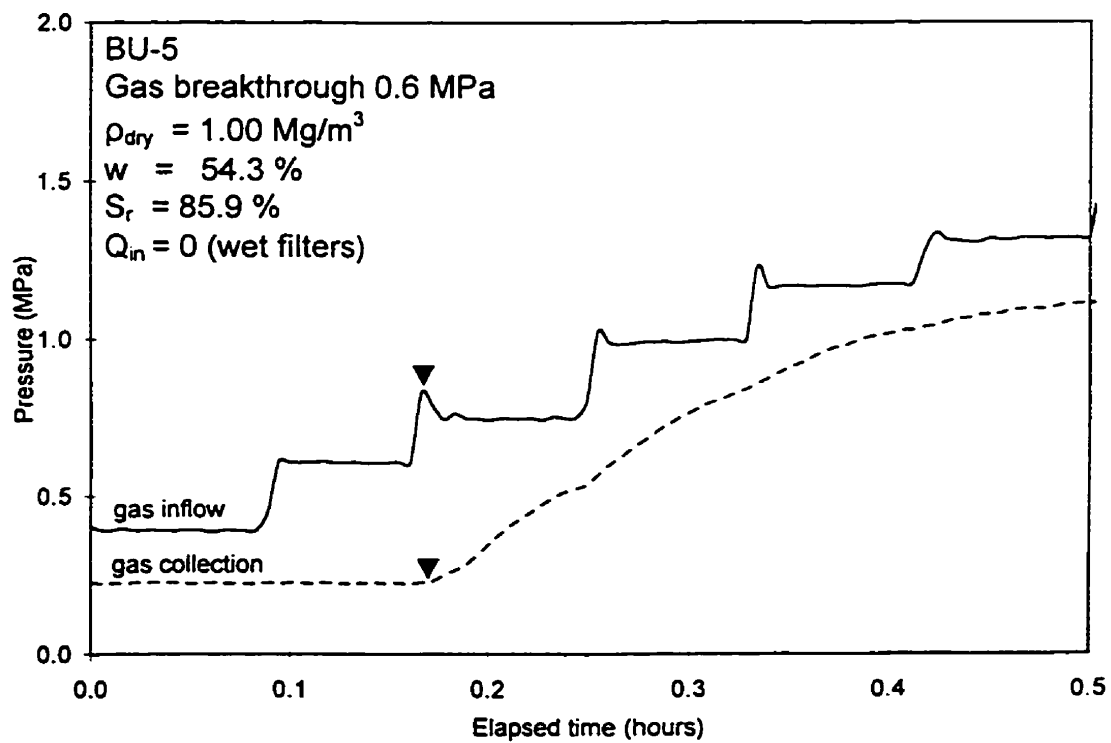
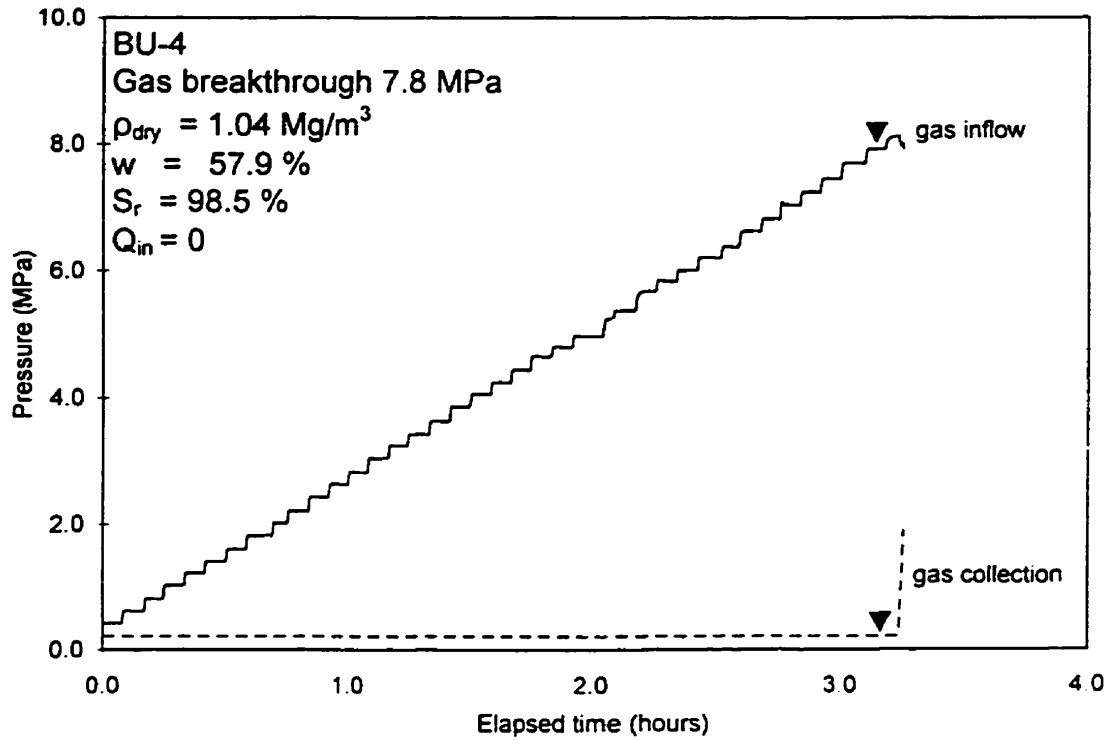


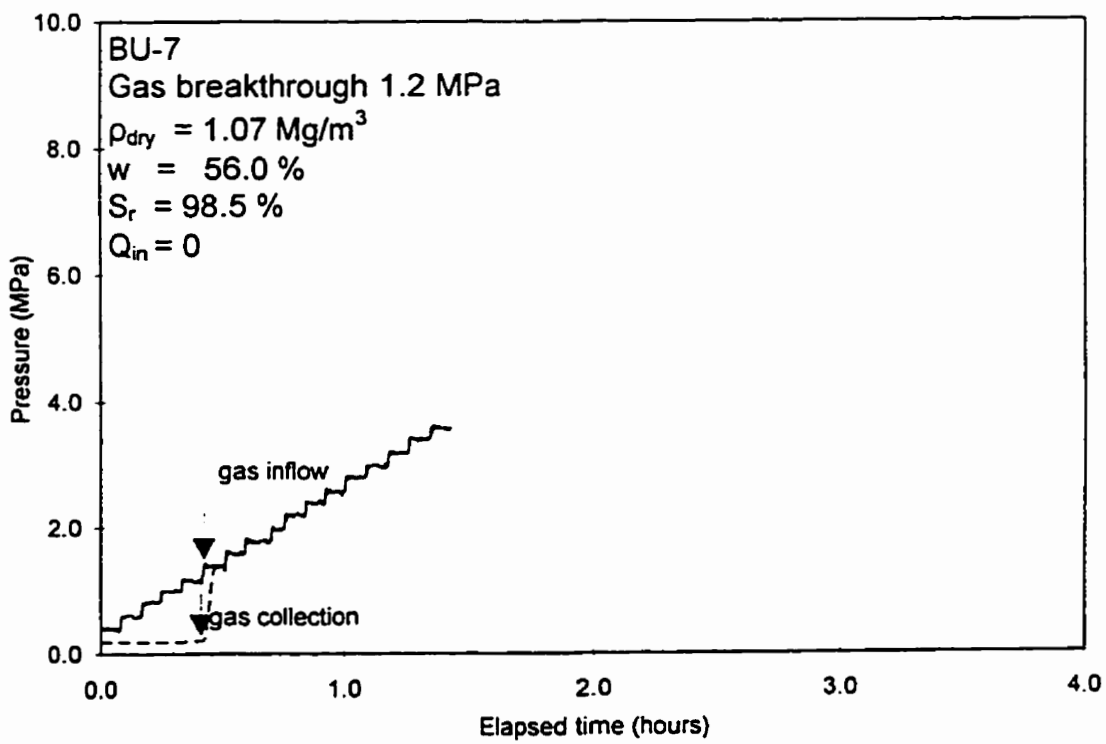
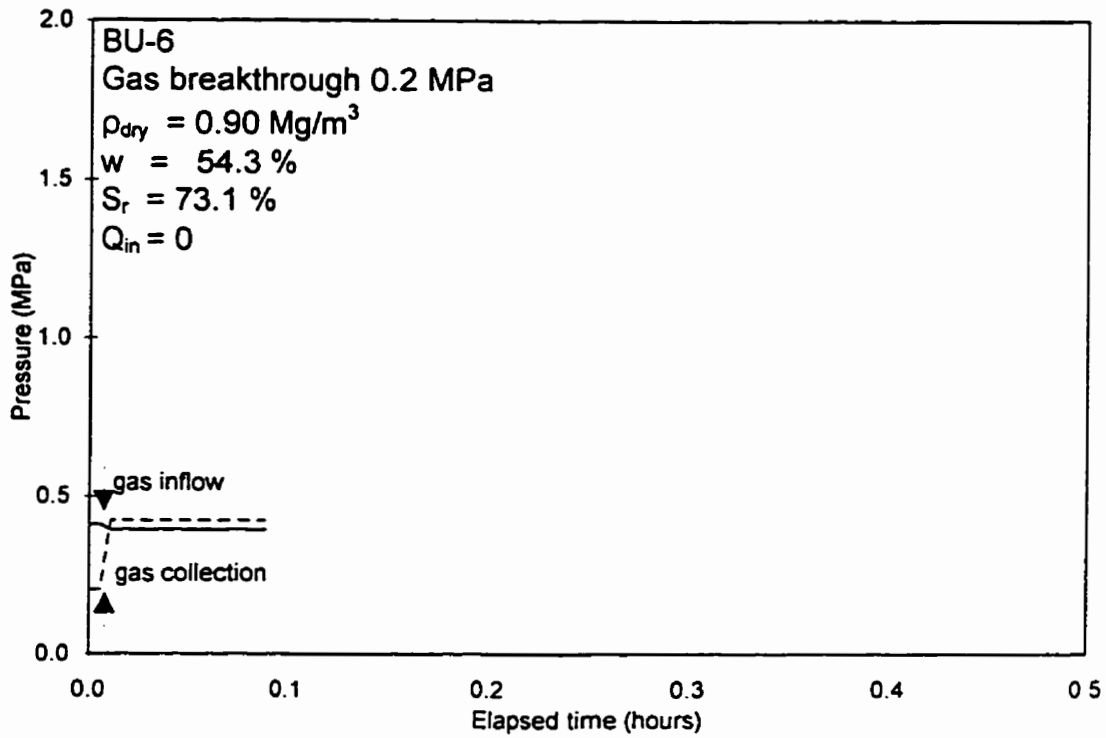


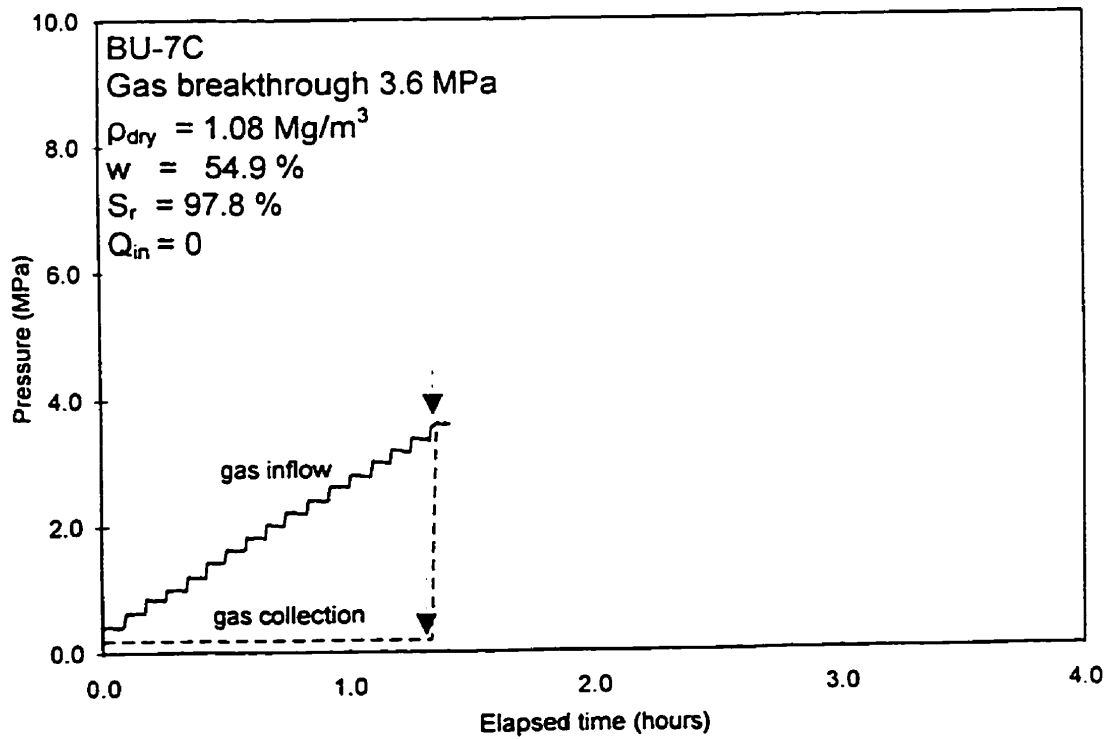
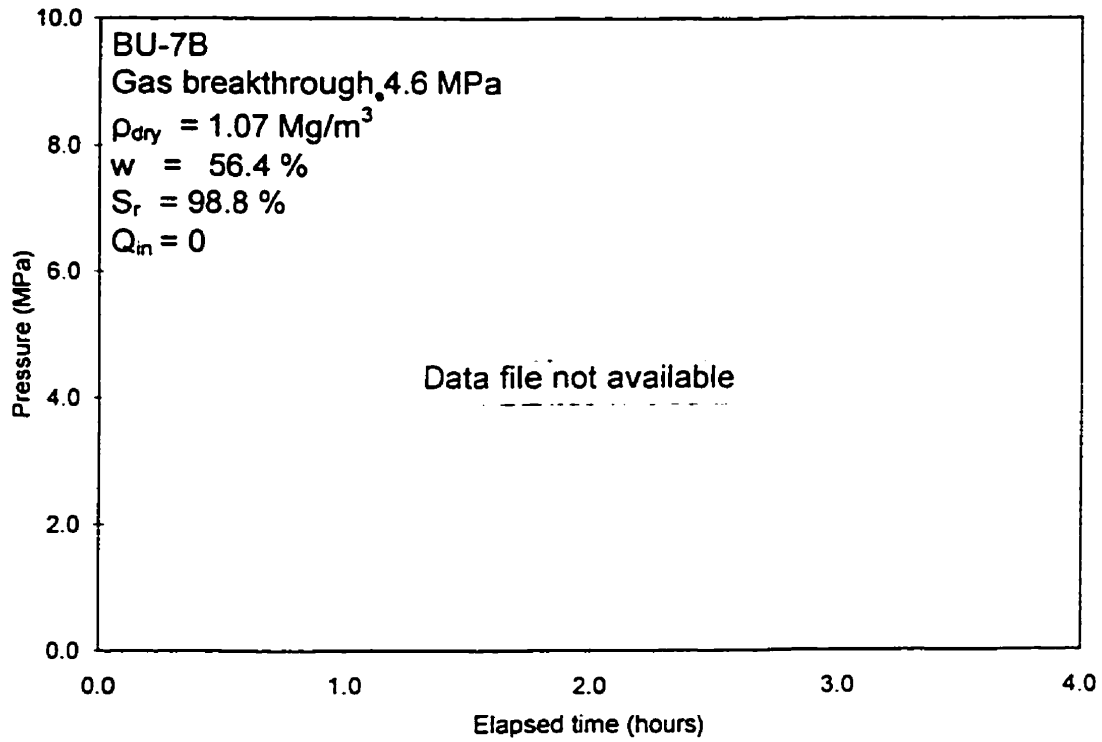


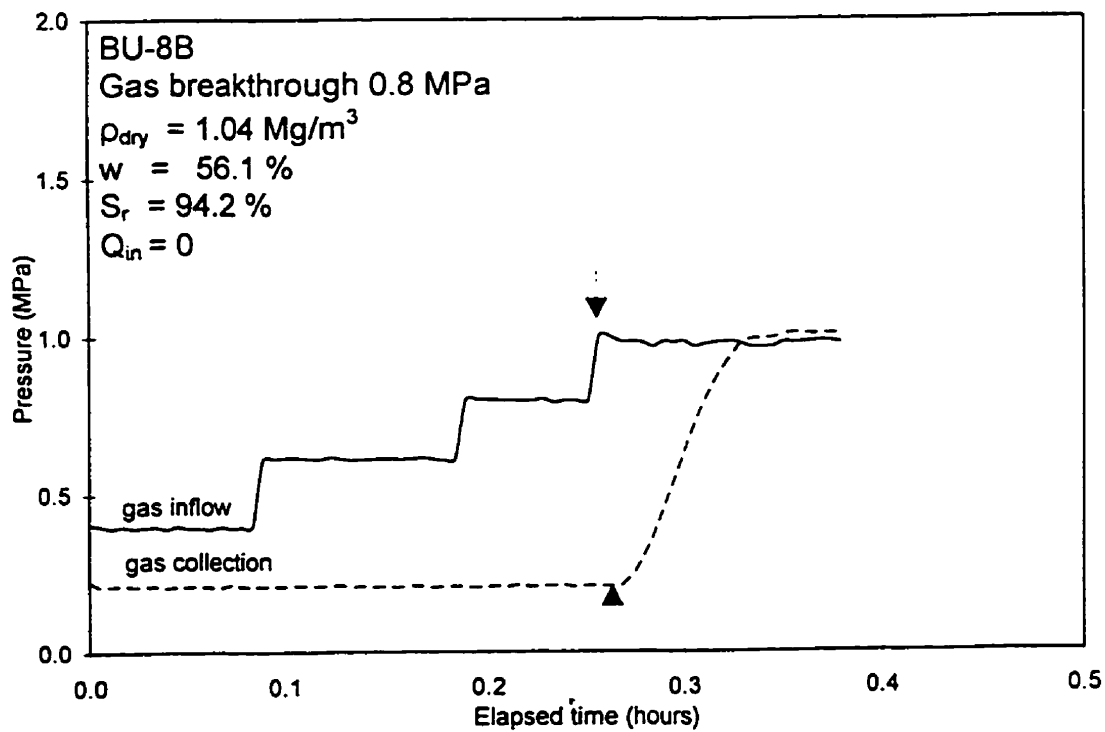
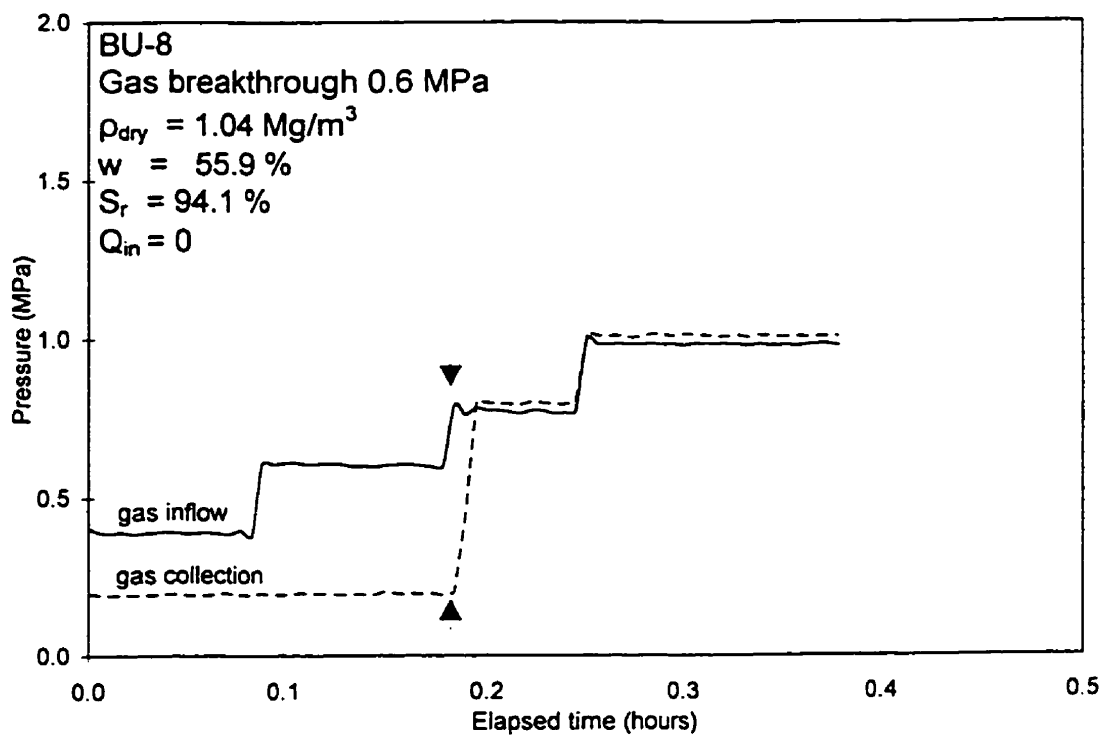


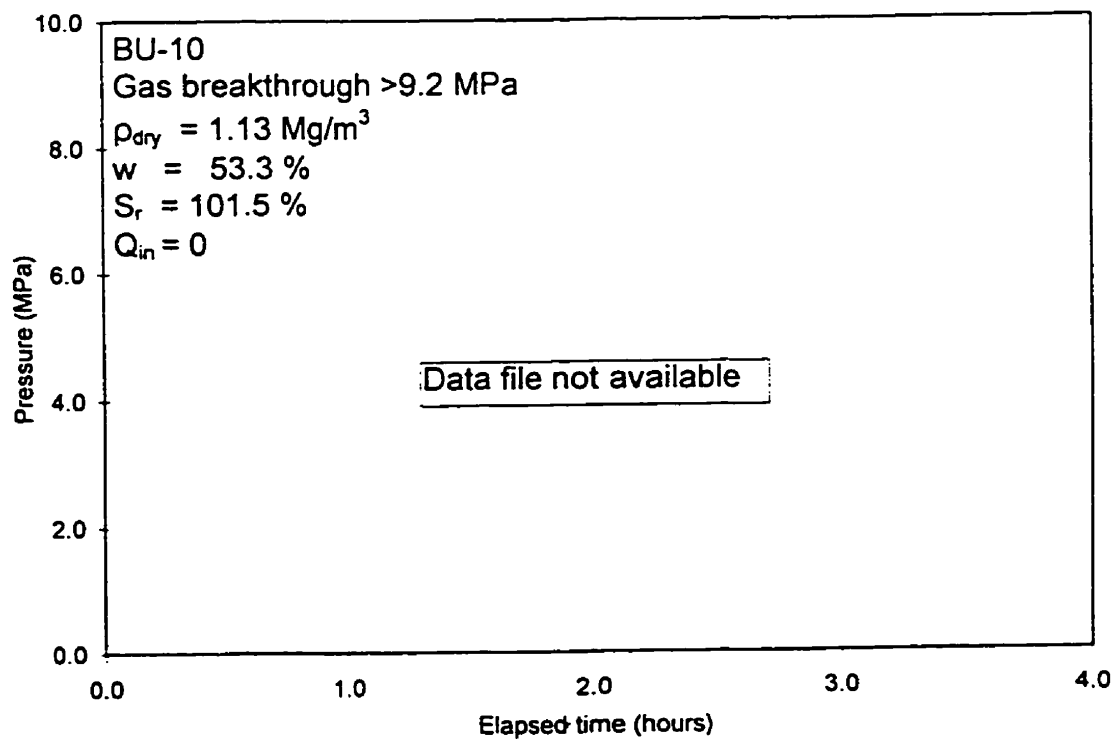
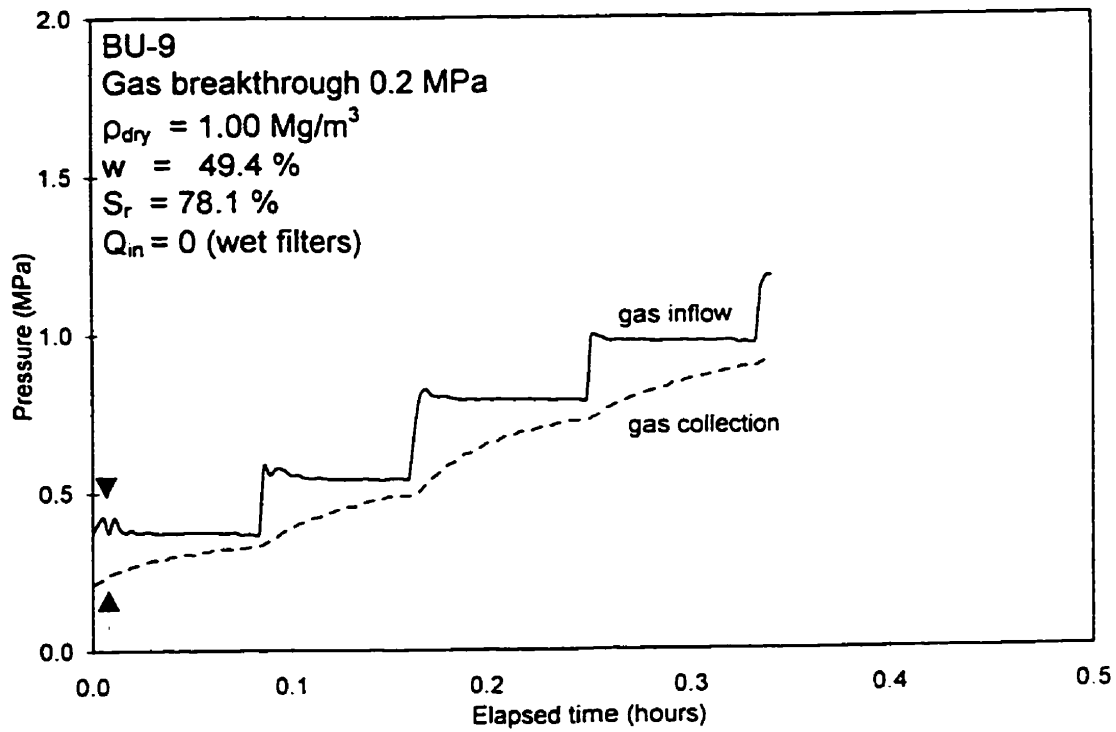


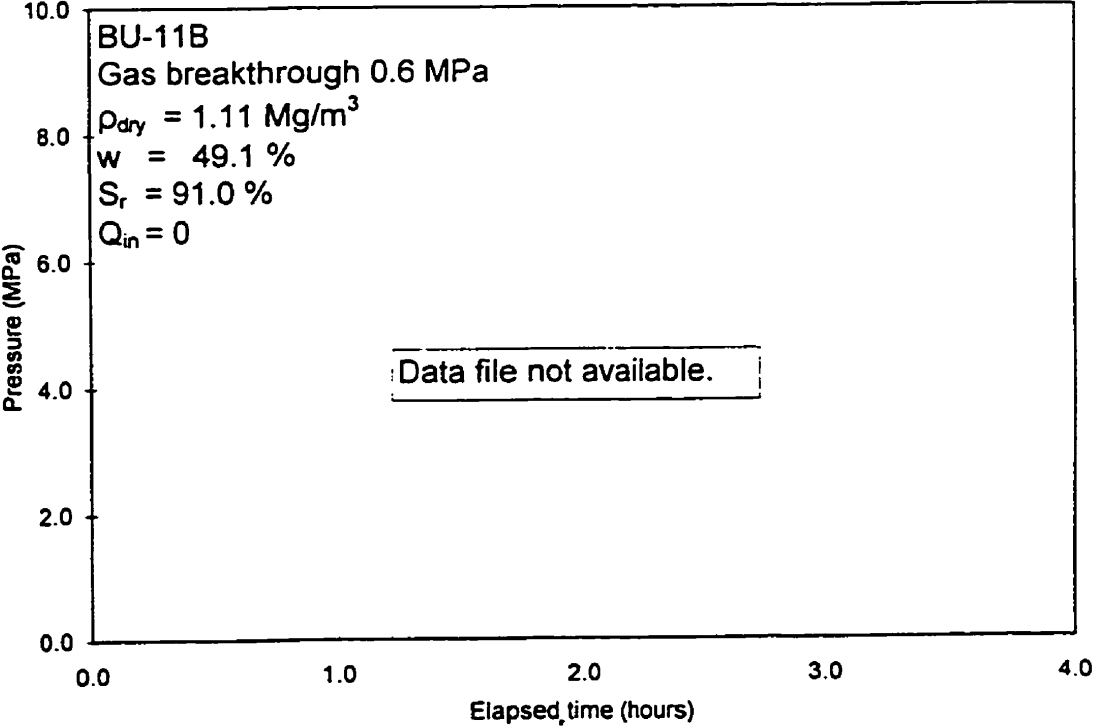
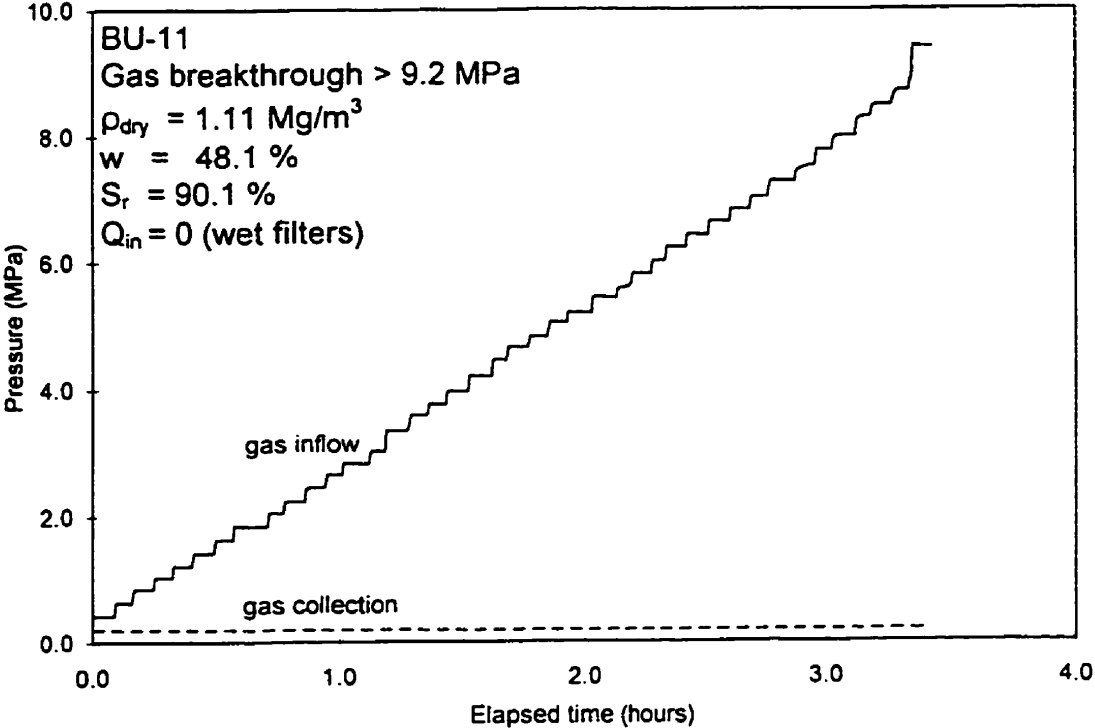


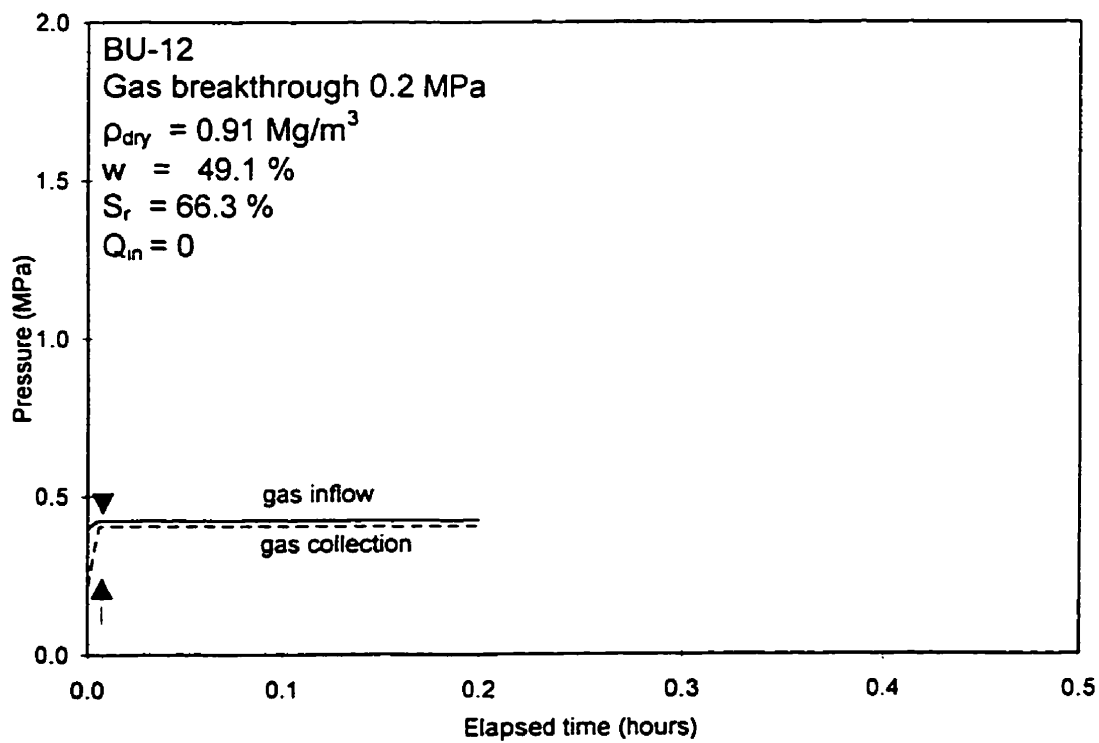
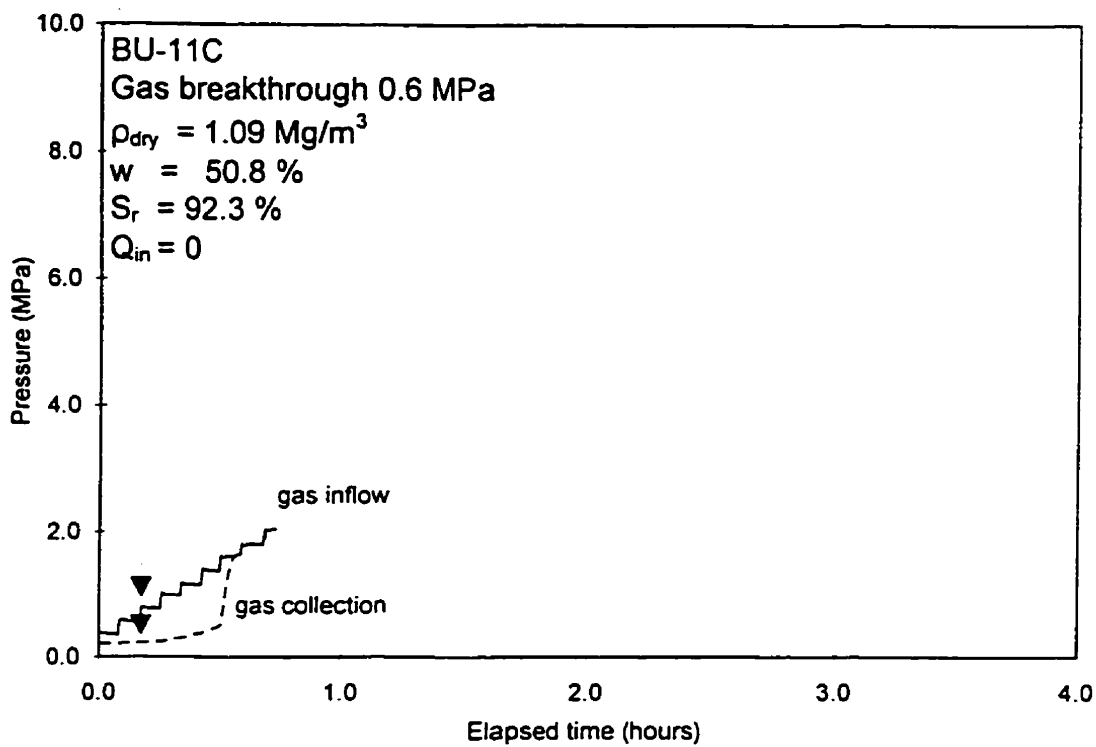


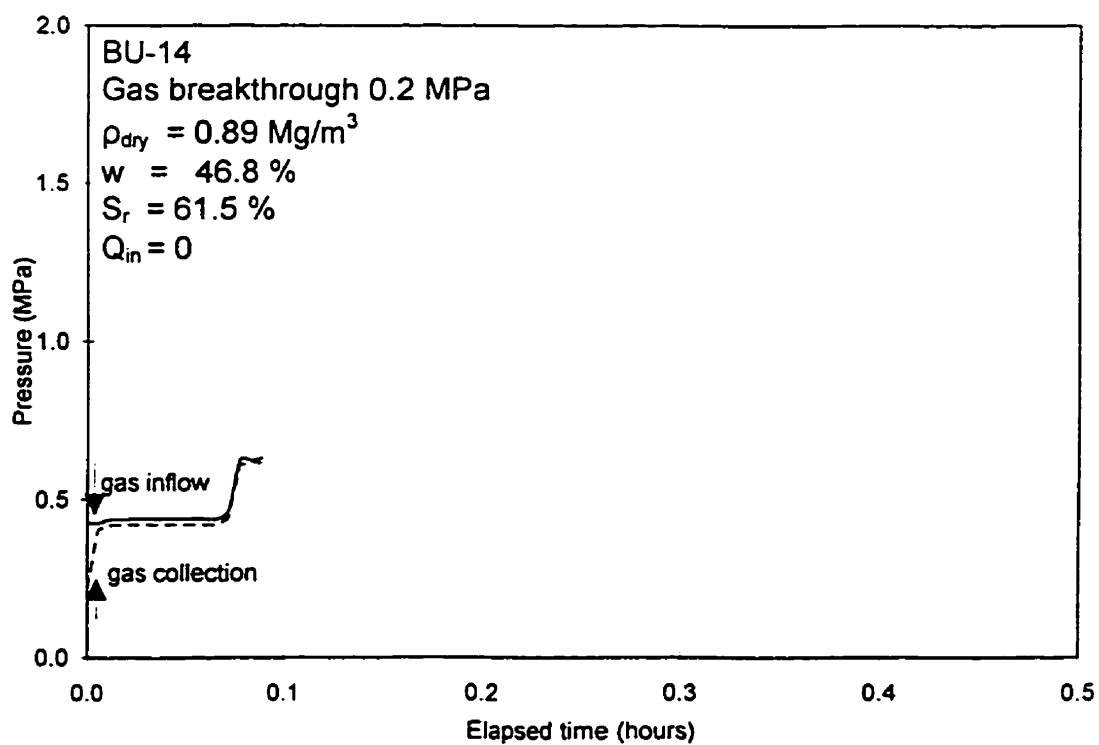
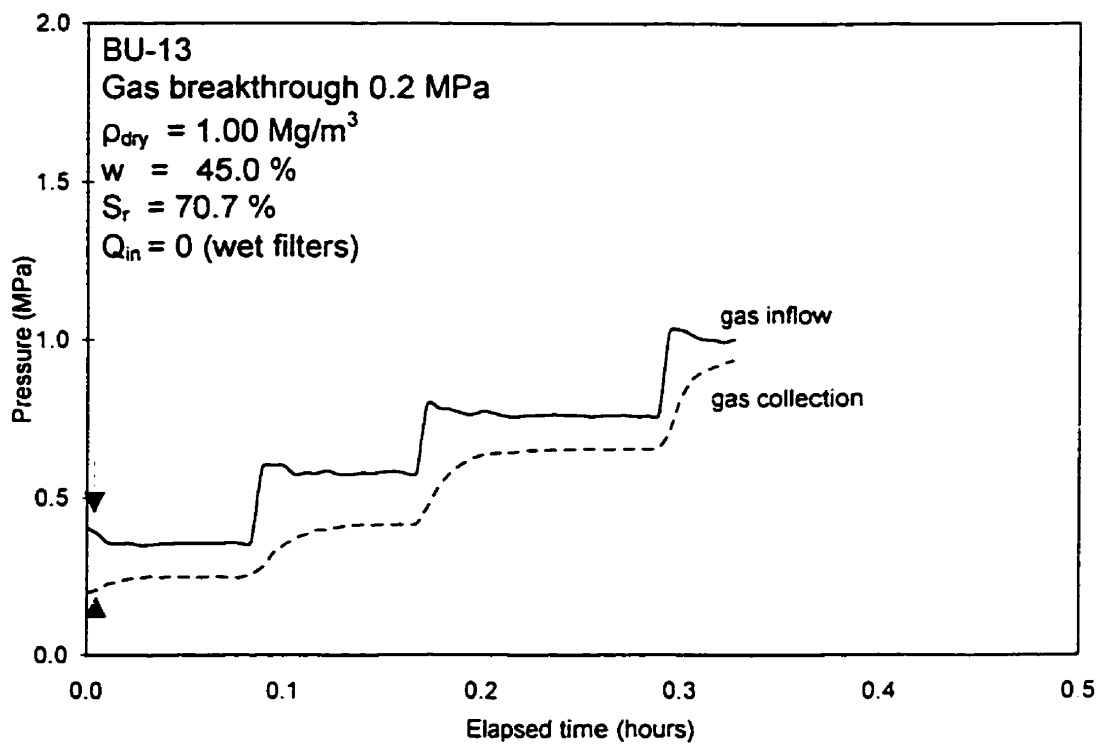


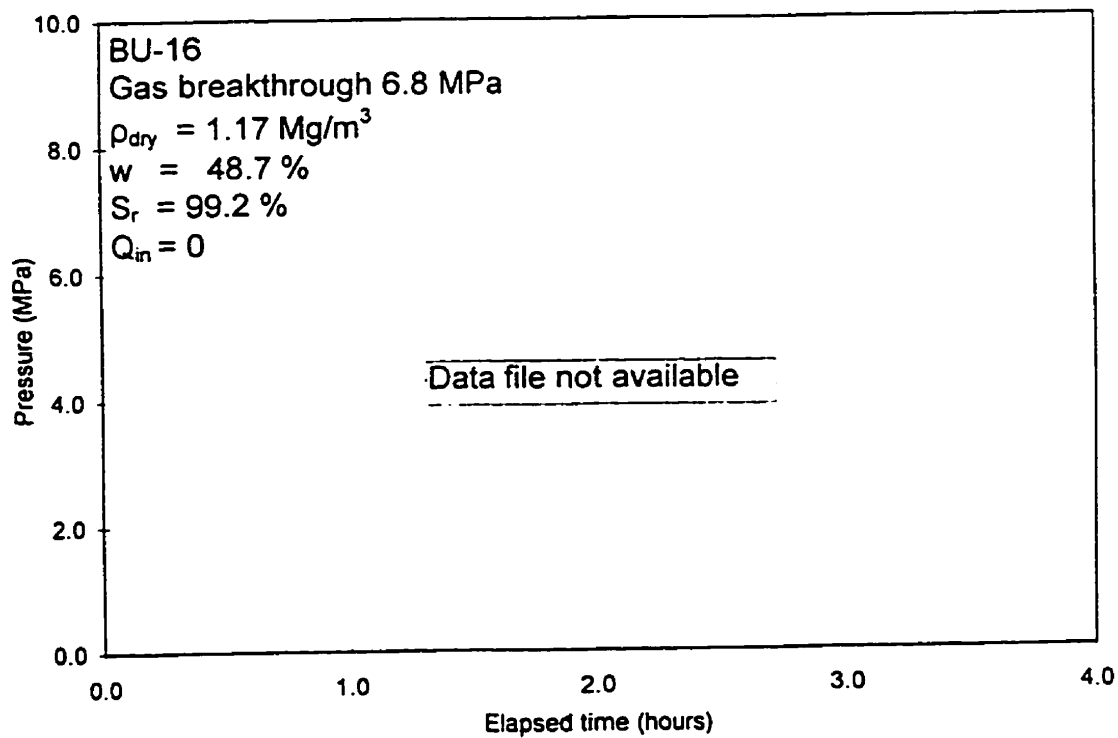
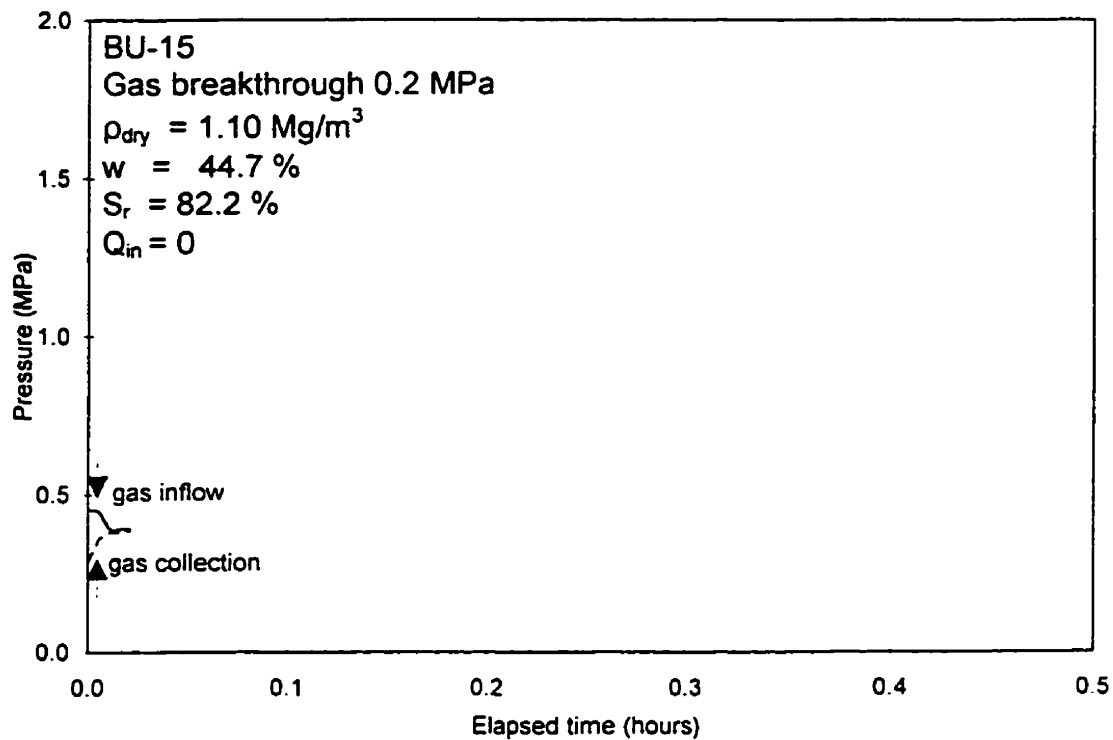


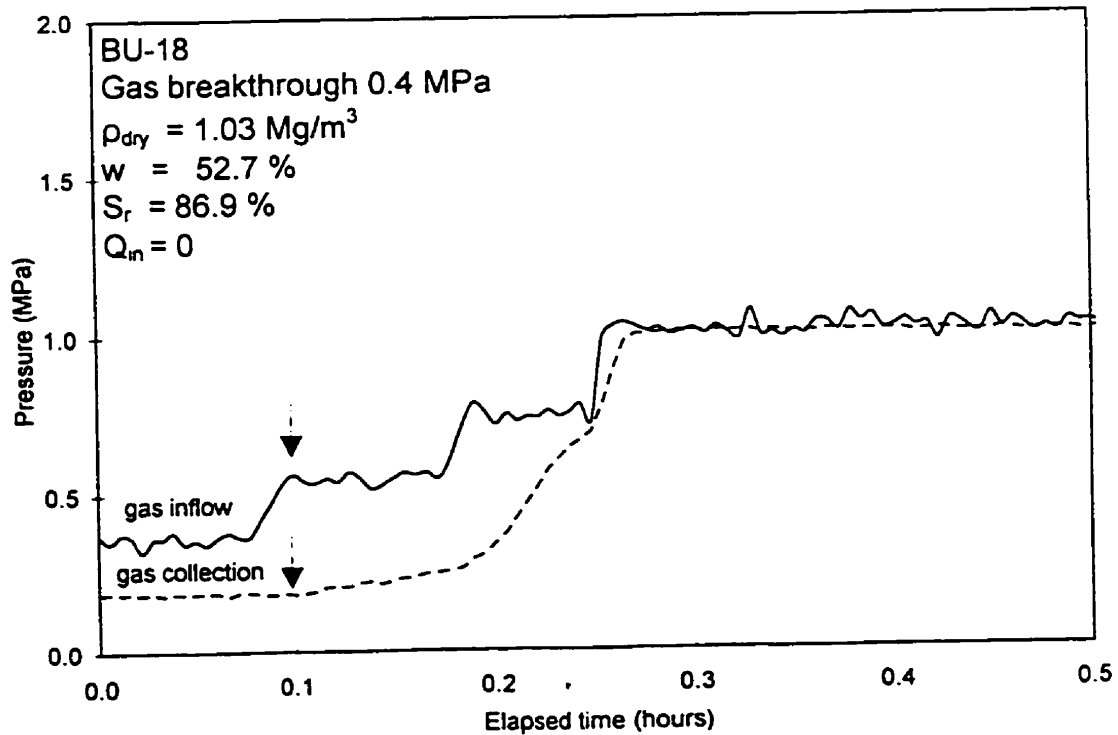
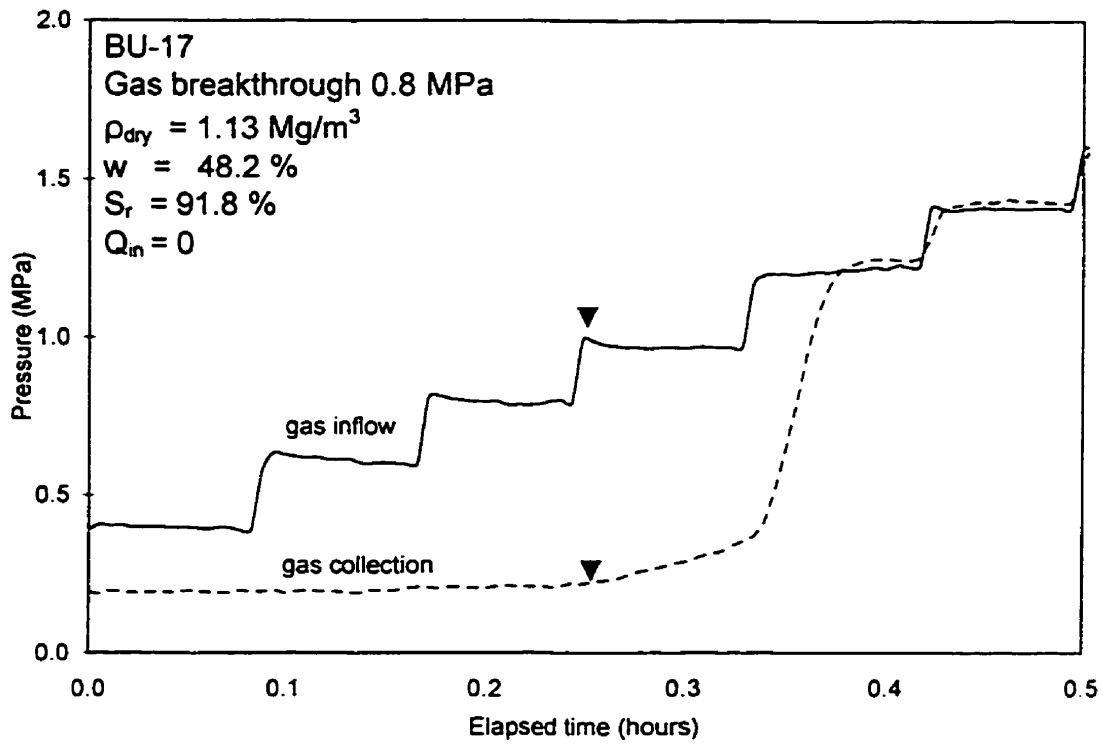


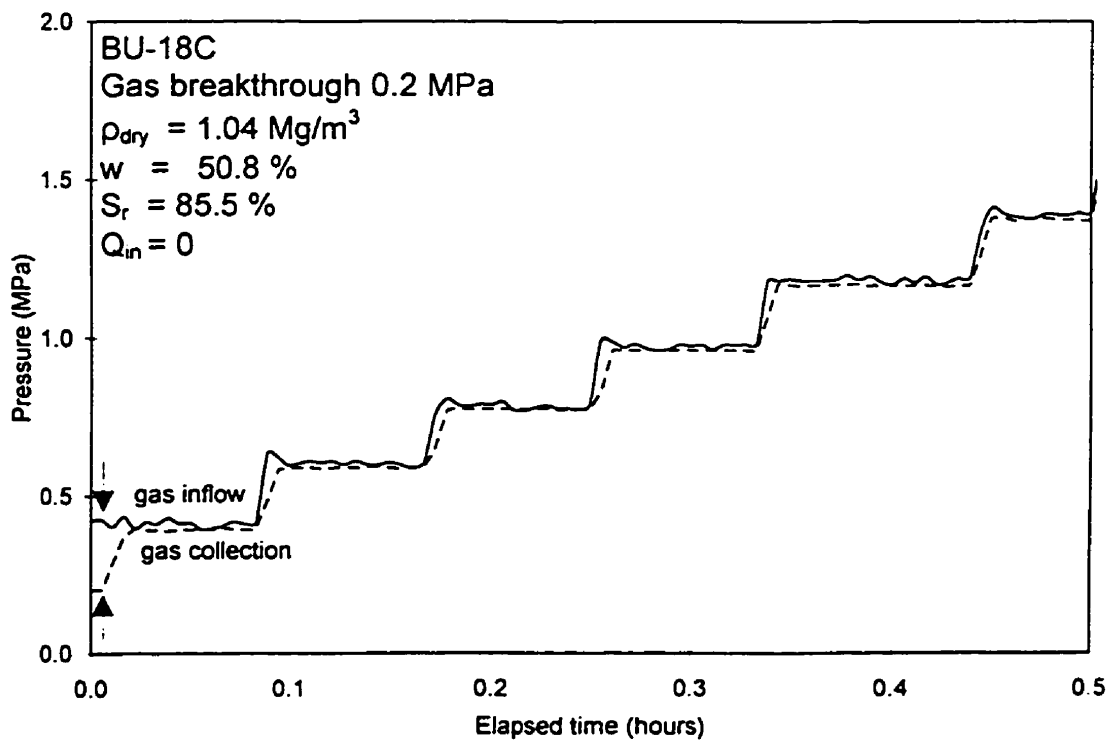
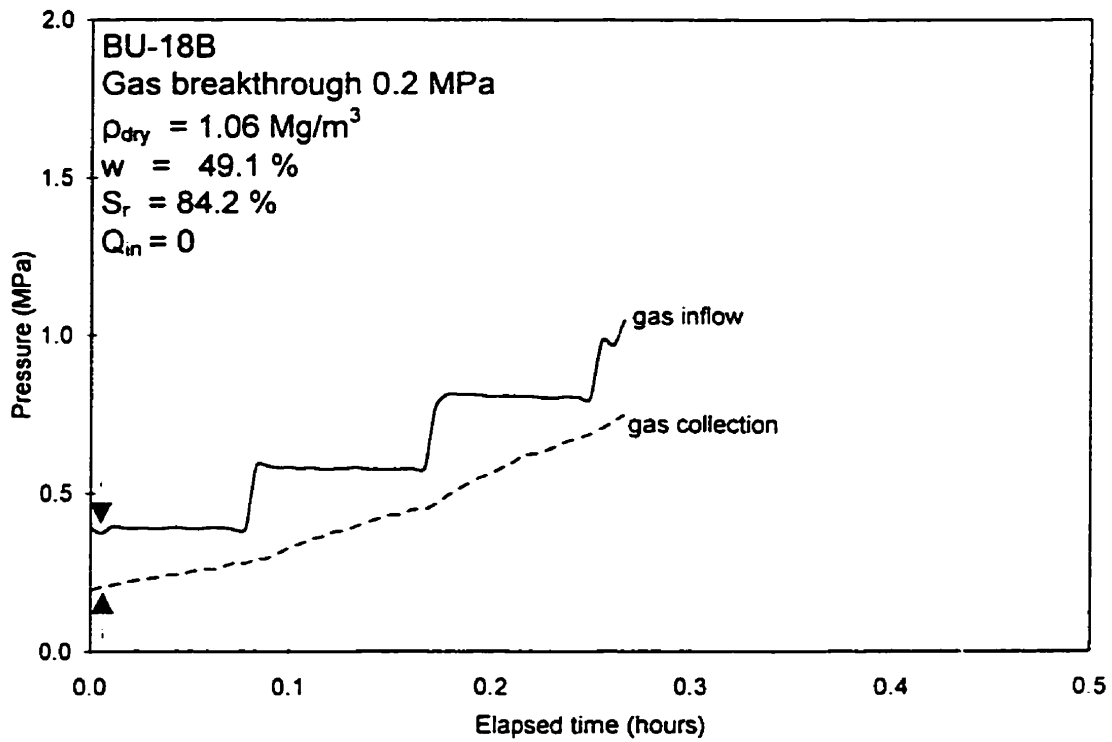


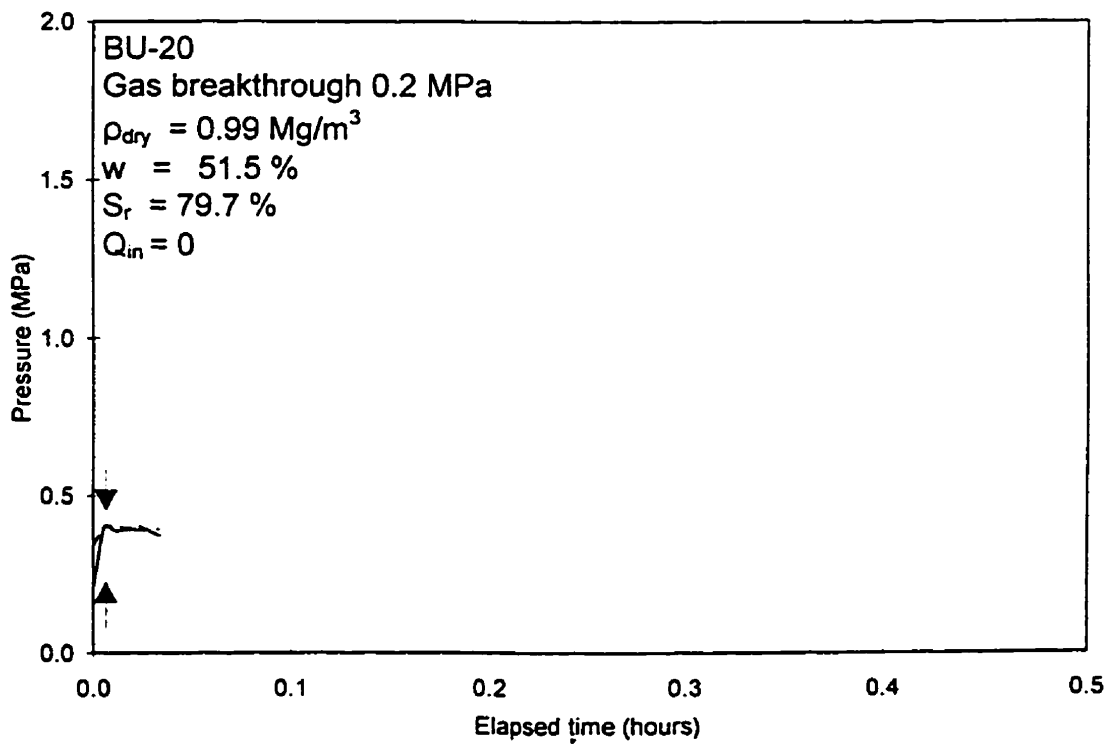
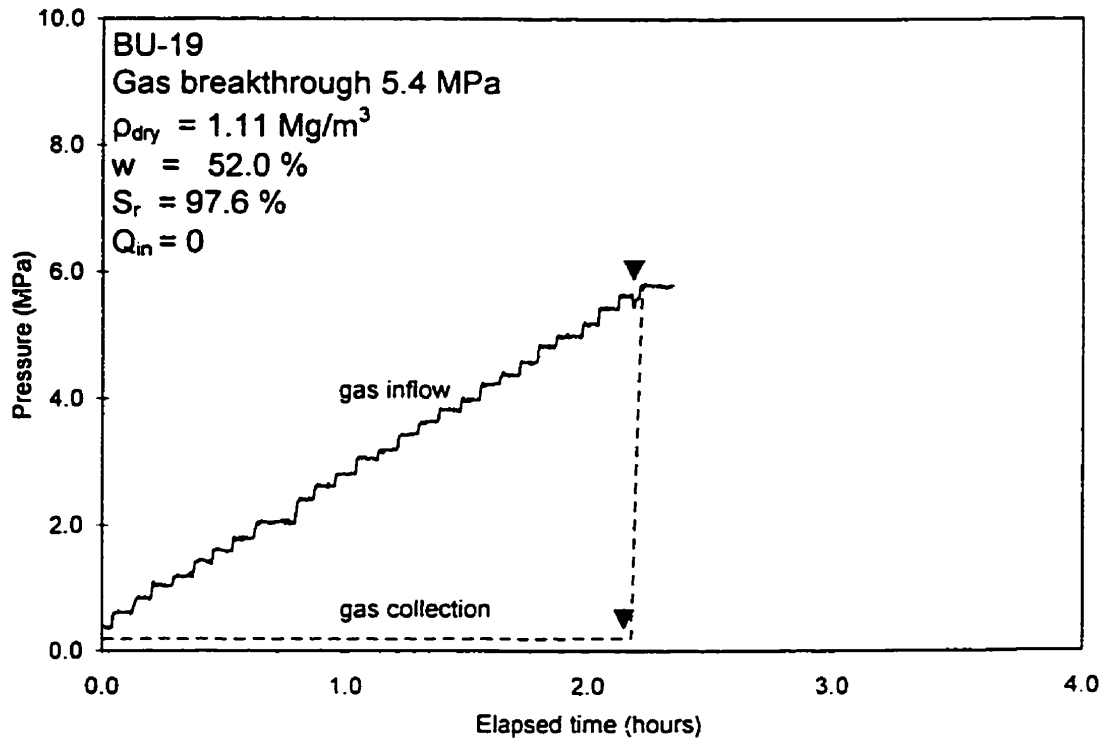


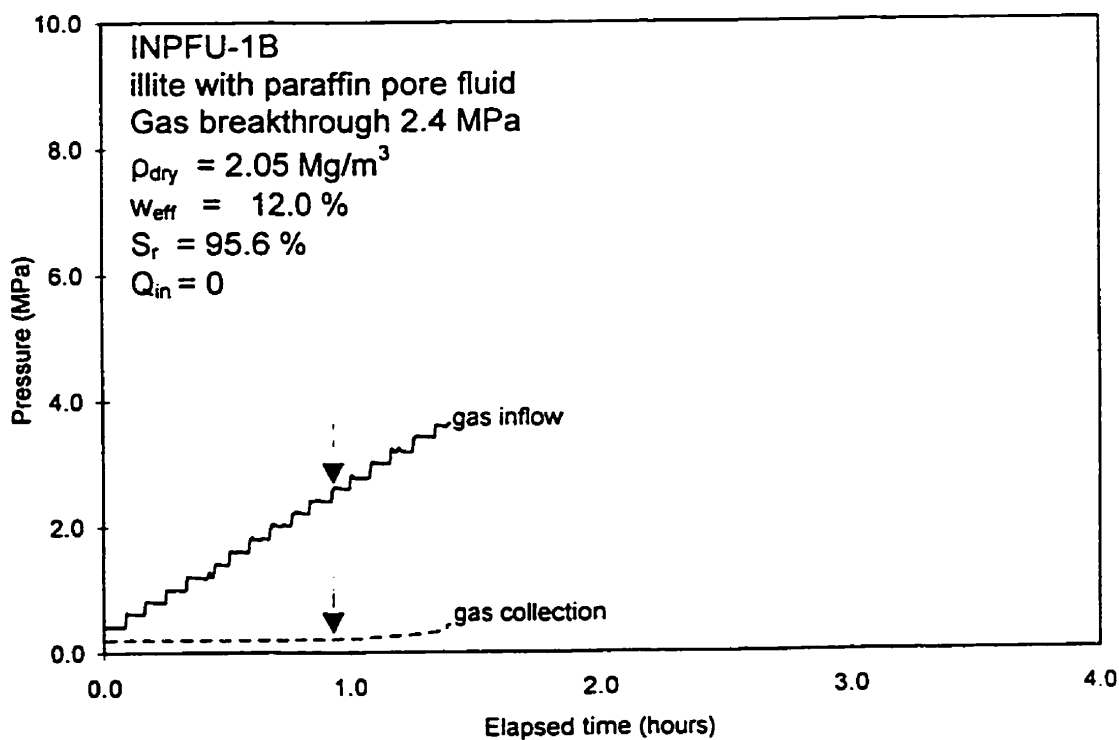
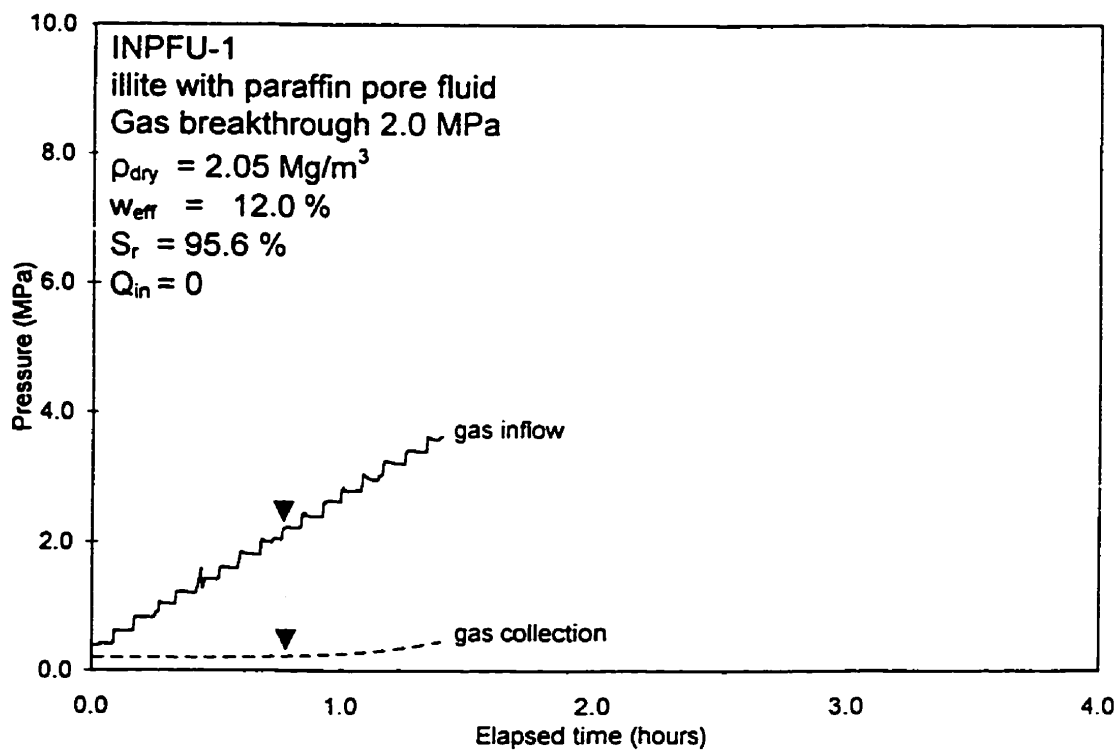


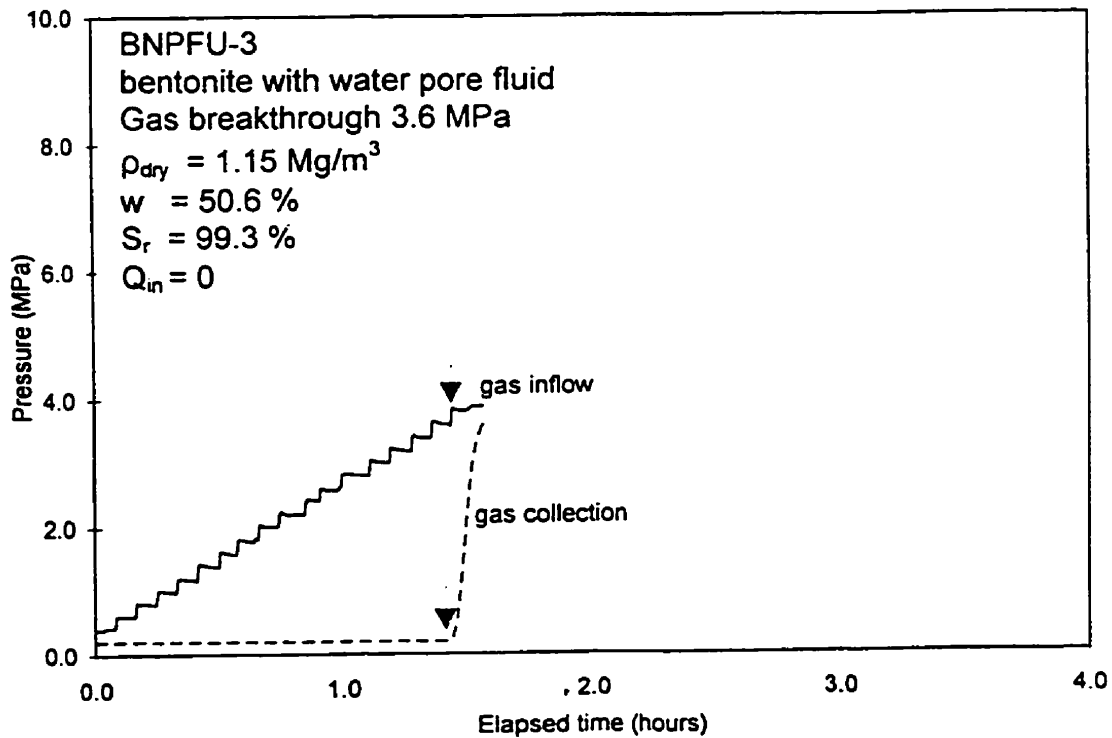
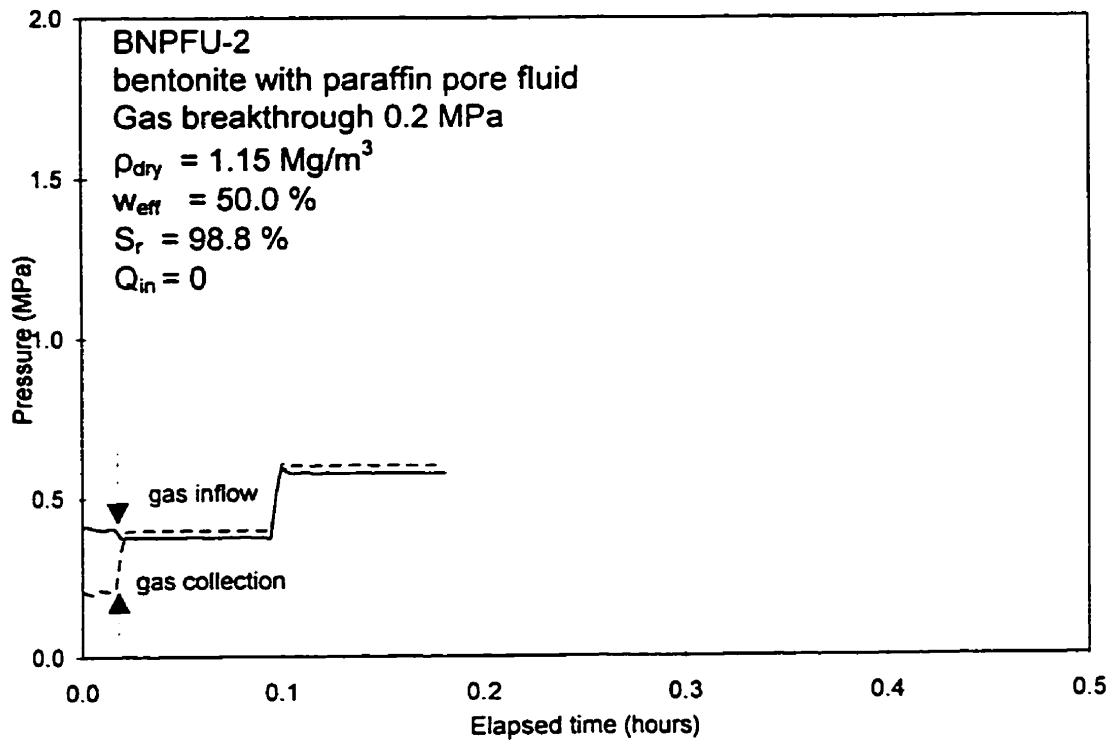


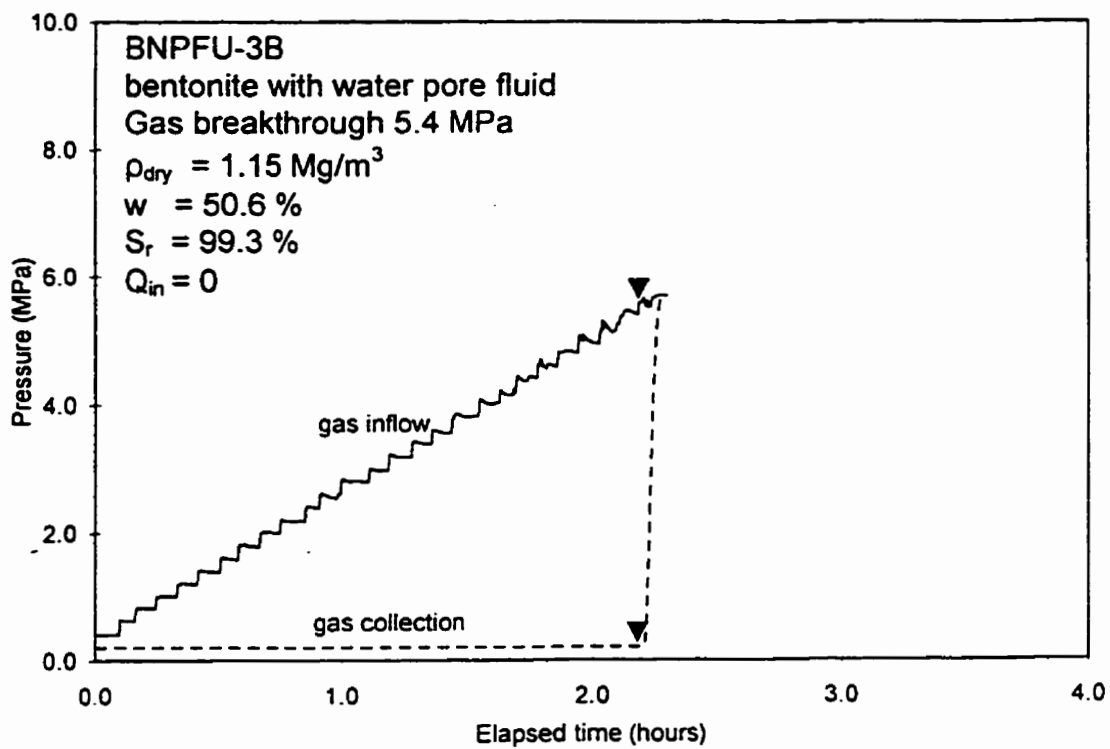


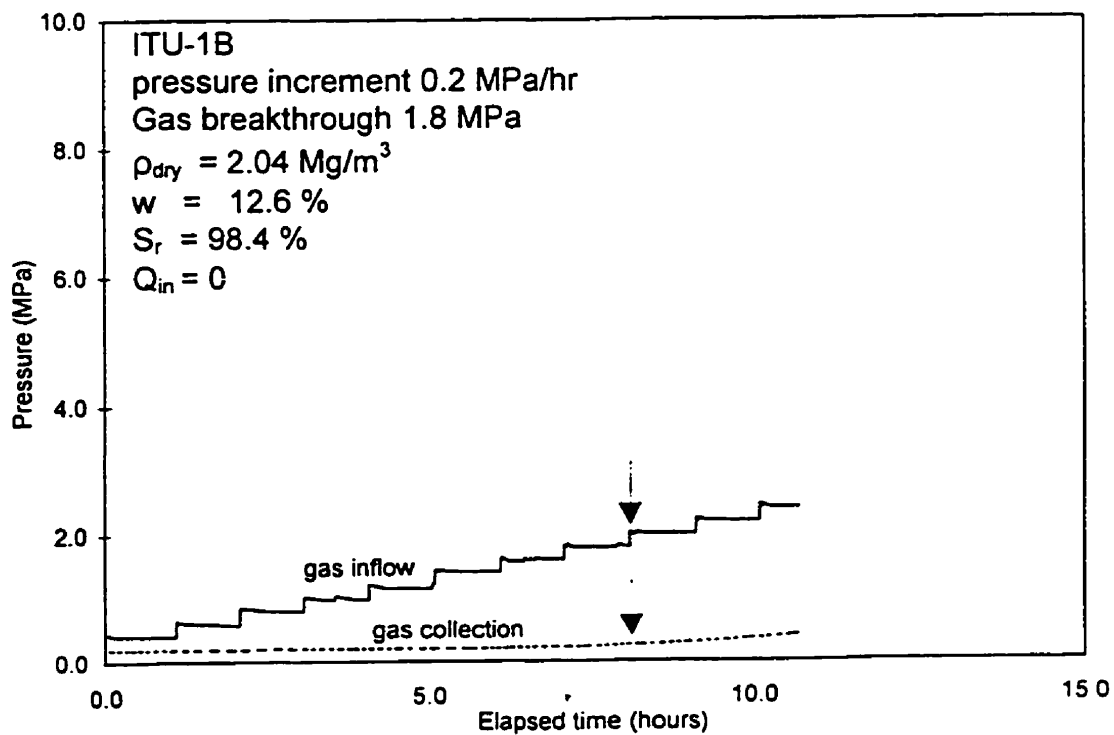
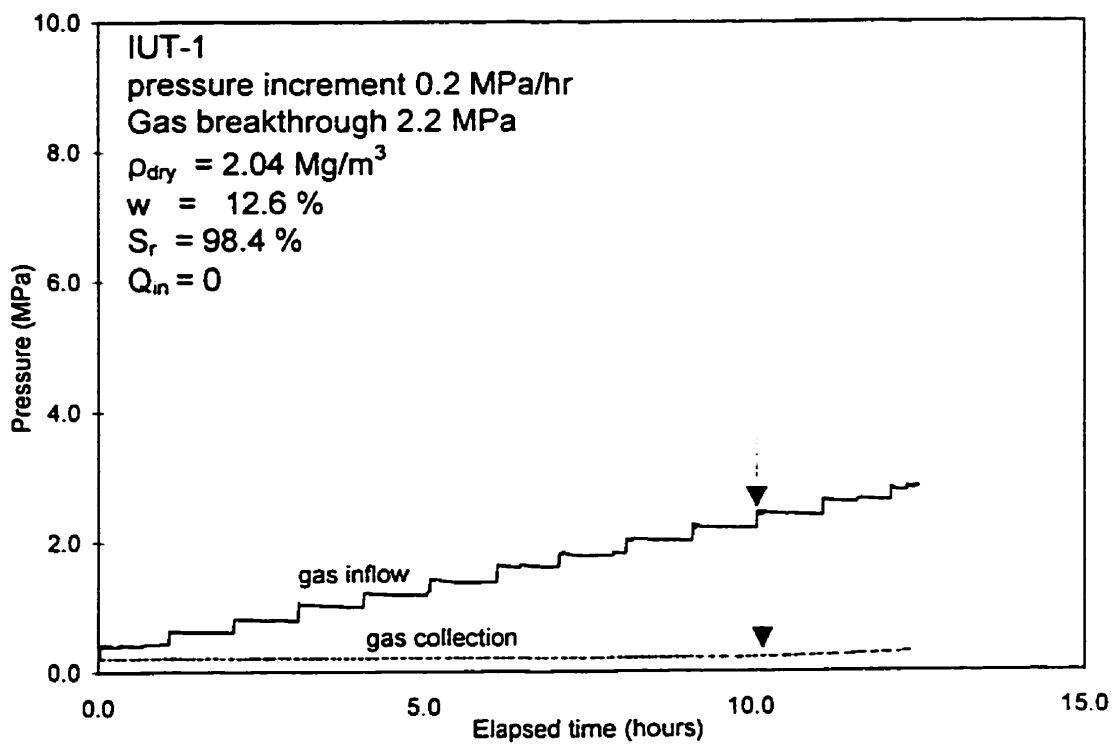


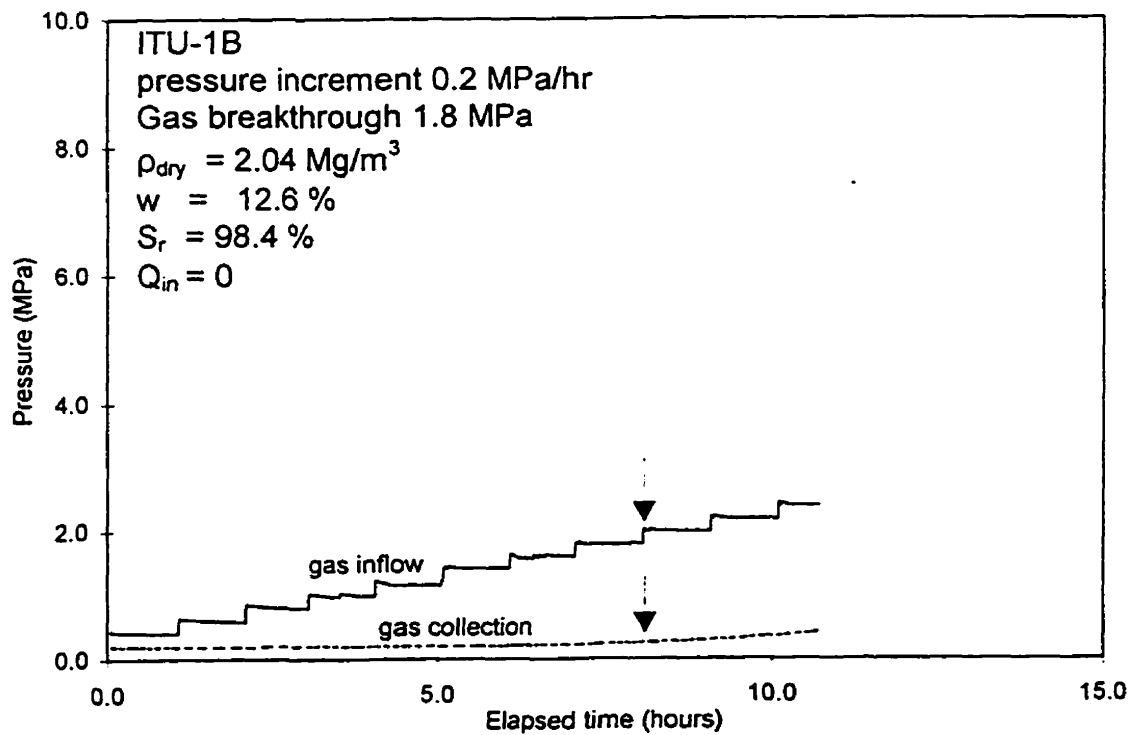
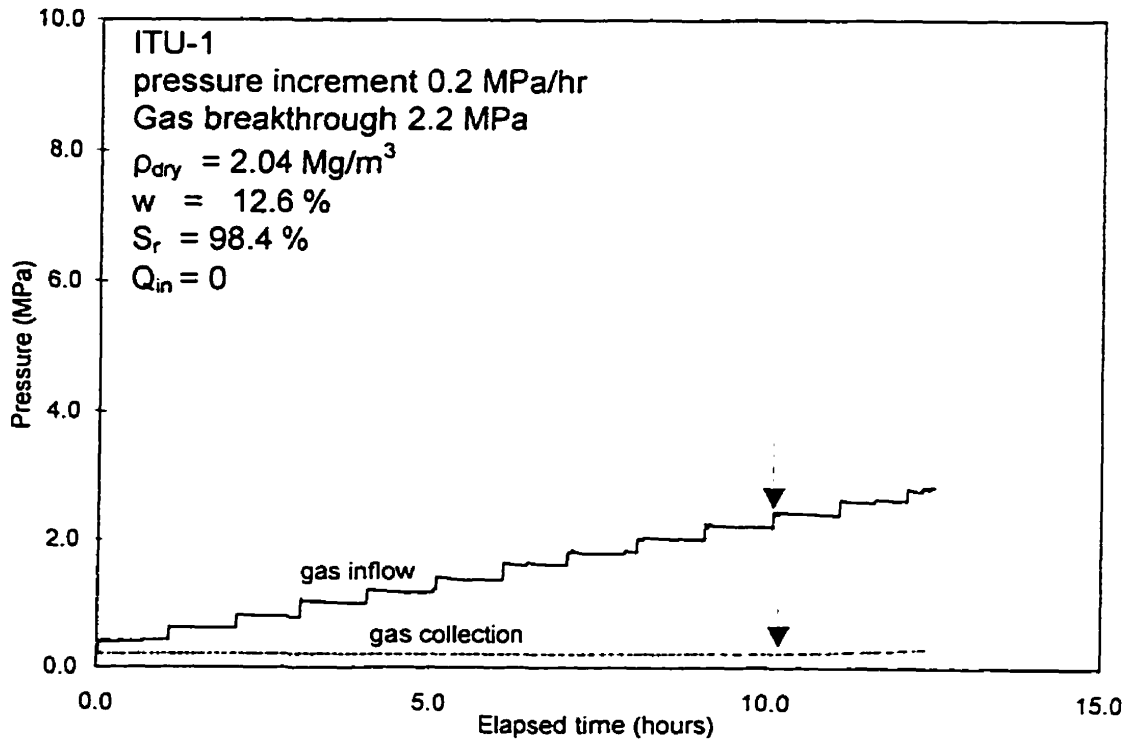


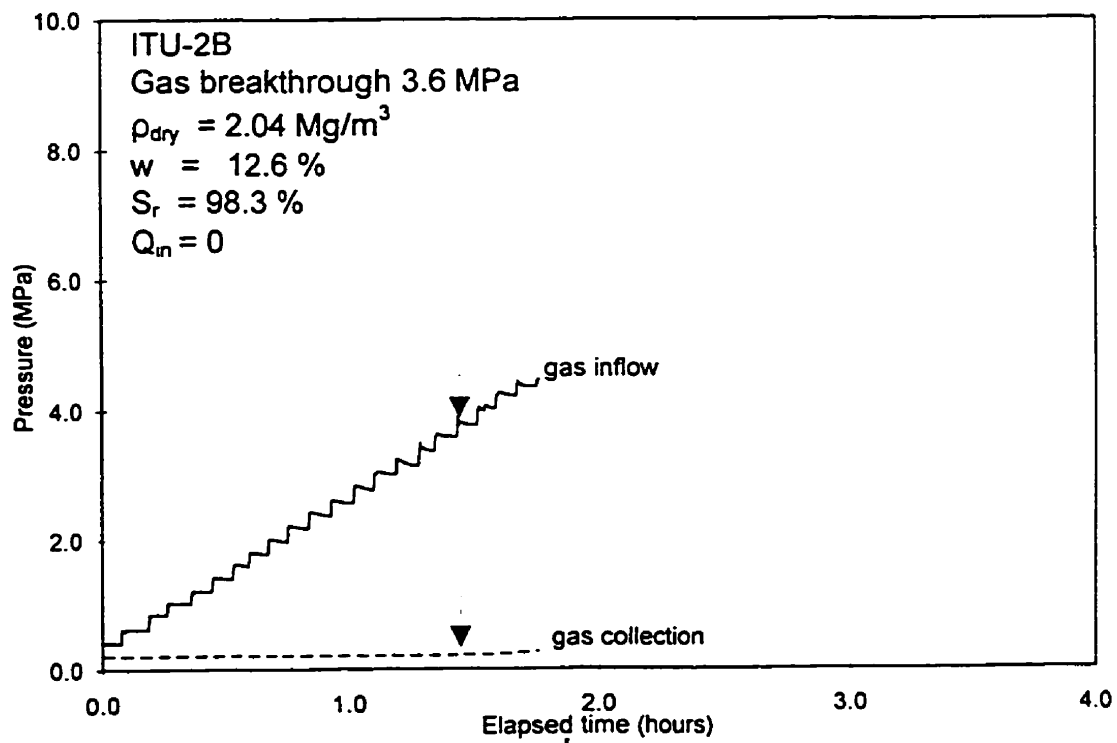
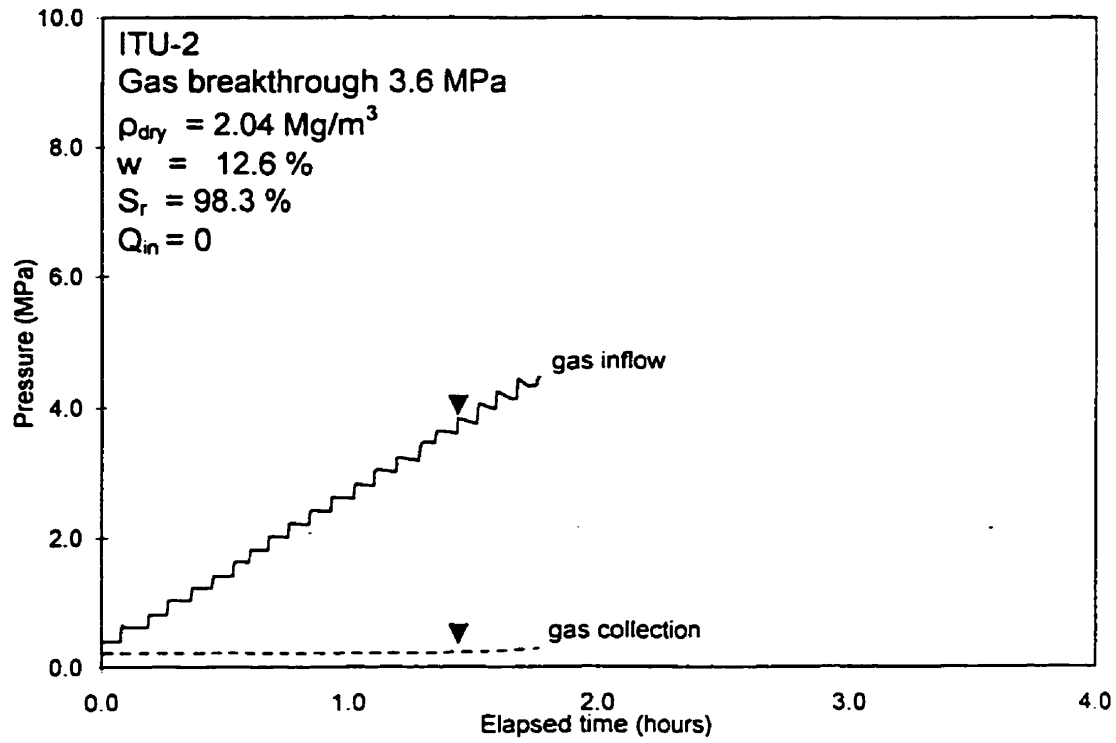


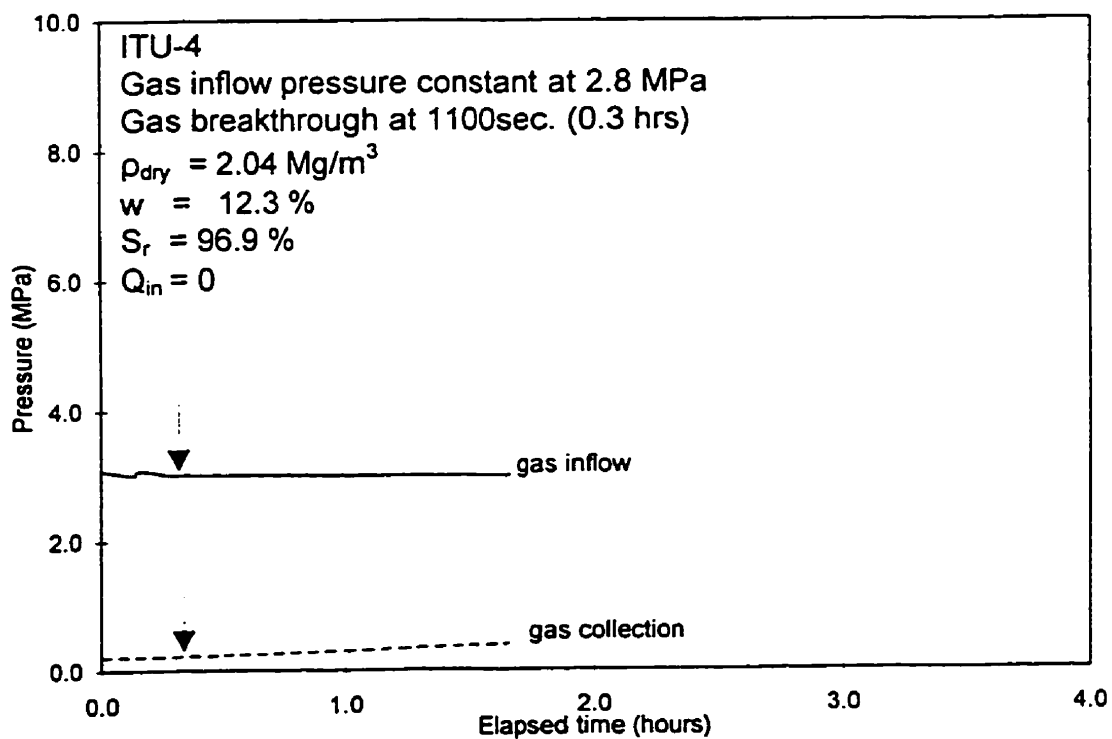
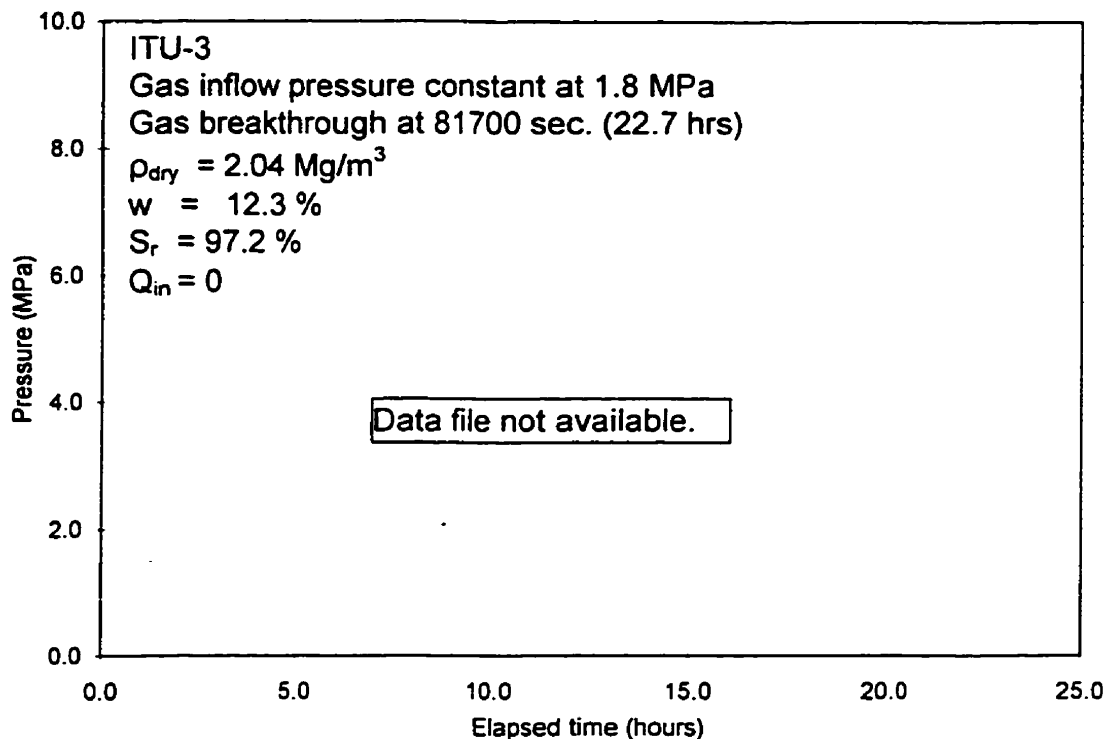


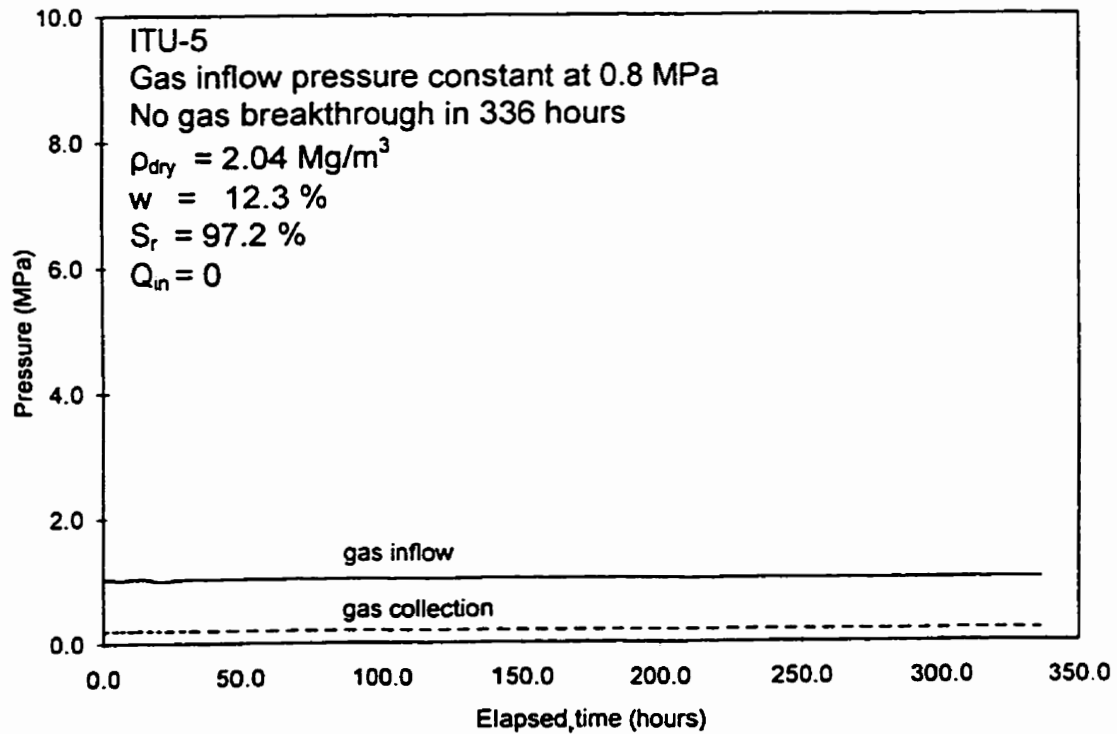
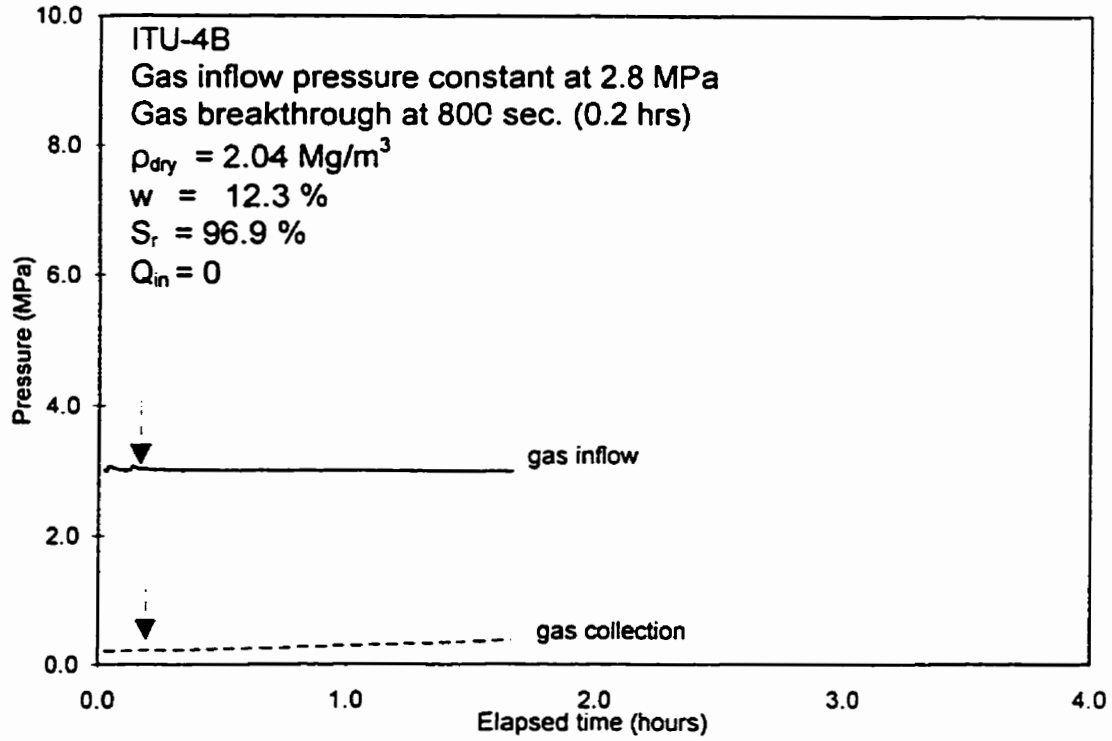












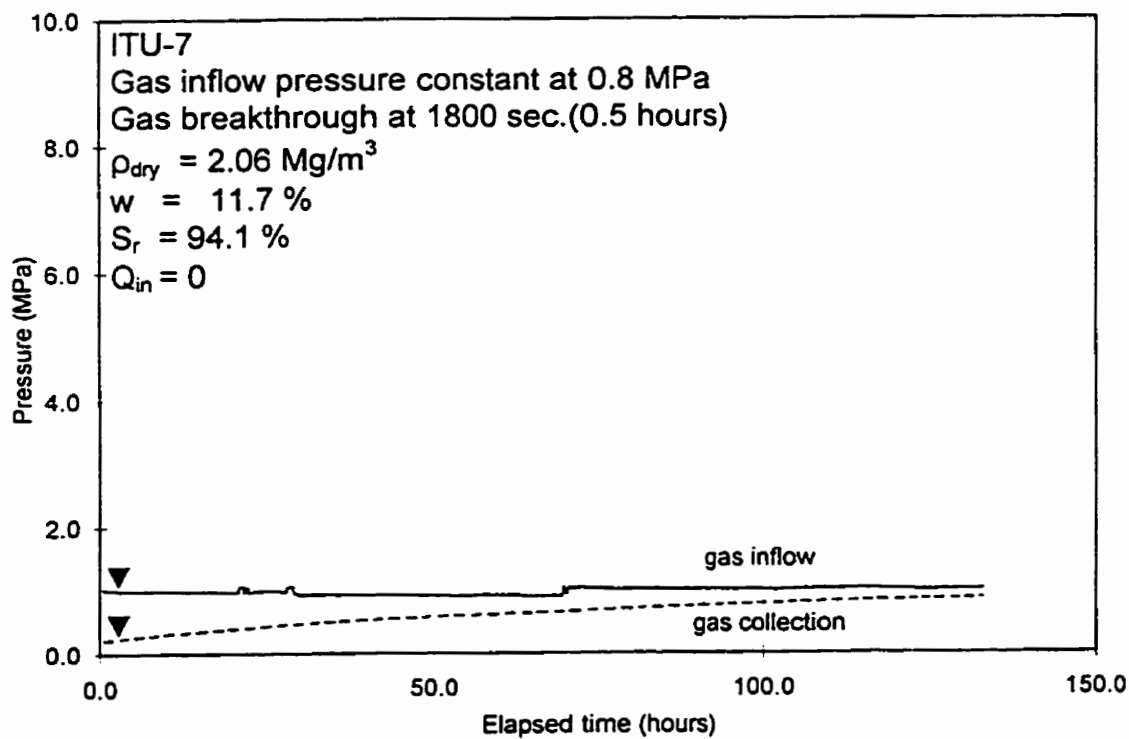
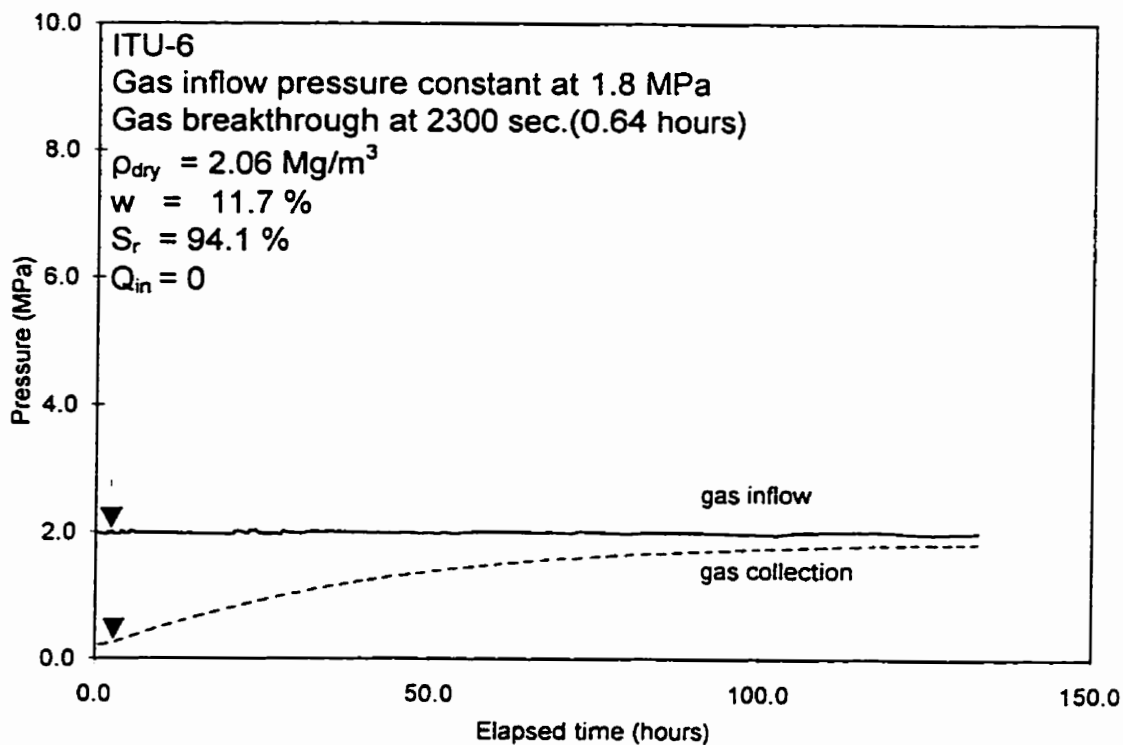
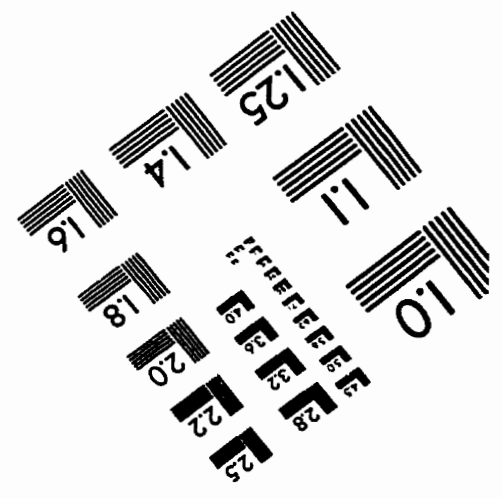
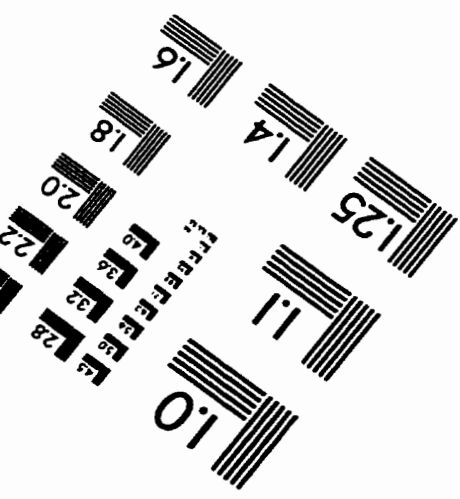
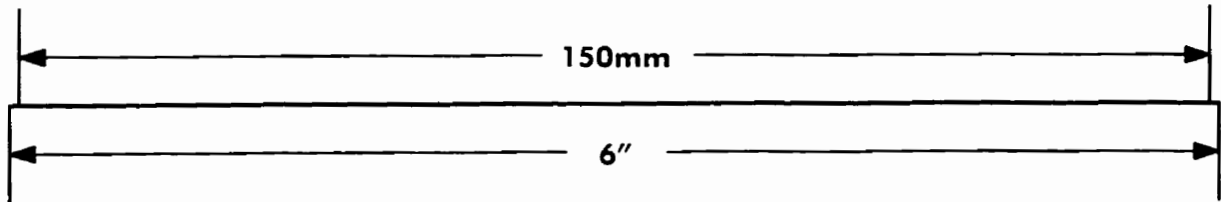
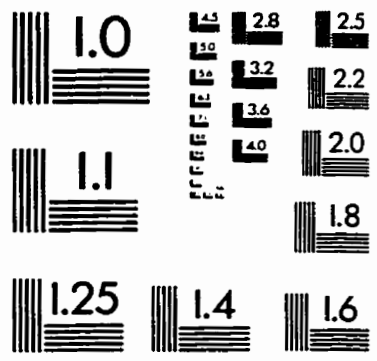
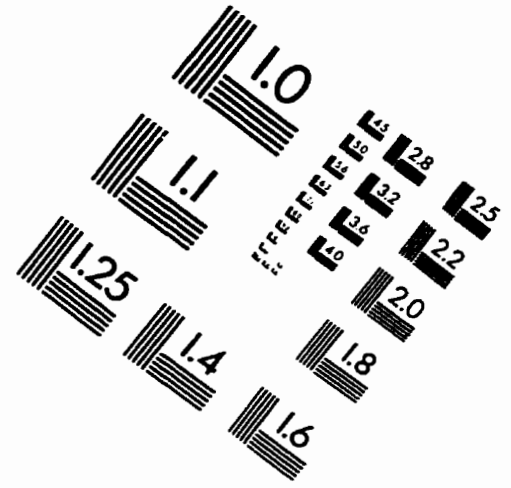
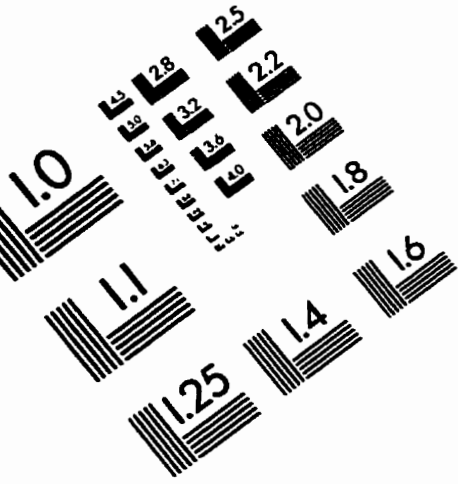


IMAGE EVALUATION TEST TARGET (QA-3)



APPLIED IMAGE . Inc
 1653 East Main Street
 Rochester, NY 14609 USA
 Phone: 716/482-0300
 Fax: 716/288-5989

© 1993, Applied Image, Inc.. All Rights Reserved